Membrane distillation

Author:
Schofield, Richard William

Publication Date:
1989

DOI:

License:

MEMBRANE DISTILLATION

Submitted as partial fulfillment of
the requirements for
the degree of

Doctor of Philosophy

by

Richard William Schofield

in

The School of Chemical Engineering
and Industrial Chemistry

at

The University of New South Wales

1989

CERTIFICATE OF ORIGINALITY

I hereby declare that this thesis is my own work and that, to the best of my knowledge and belief, it contains no material previously published or written by another person, nor material which to a substantial extent has been accepted for the award of any degree or diploma of a University or other institute of higher learning, except where due acknowledgement is made in the text.

R.W. Schofield

ABSTRACT

Membrane distillation was investigated to determine the potential of the process. Emphasis was placed on direct contact membrane distillation of aqueous solutions of non-volatile solutes. Theory was developed to describe heat and mass transfer in the feed, permeate and membrane regions. Heat transfer, gas permeation, membrane mass transfer and feed solute mass transfer were studied experimentally. Process considerations were investigated in a pilot plant study.

Film heat transfer was found to limit the process in most applications. A realistic maximum for the overall film heat transfer coefficient was identified as 5000 W/m^2K. Gas permeation through microporous membranes was successfully described by a novel semi-empirical equation based on combined Knudsen and Poiseuille flow. The removal of air from the membrane pores (deaeration) was found to greatly increase membrane permeabilities, reduce heat losses by conduction across the membrane to less than 10%, and reduce the tendency for membrane wetting. A realistic maximum flux was identified as 200 kg/m^2h. The presence of solute in the feed was found to reduce flux slightly through vapour pressure reduction and increased viscosity (decreased film heat transfer).

Close packed hollow fibre membrane distillation modules with laminar flow of the feed and permeate and low pressures in the liquid streams were found to give near optimum performance. Advantages included near maximum heat transfer and flux, reduced heat losses, reduced tendency for wetting, and flexibility of operation between high flux and high energy recovery.

ACKNOWLEDGEMENTS

PUBLICATIONS AND PRESENTATIONS

Publications

Schofield, R.W., Fane, A.G. and Fell, C.J.D., "Membrane Distillation - A Novel Evaporative Process", Proc. 13th Australasian Chemical Engineering Conference, Perth, August, 1985

Schofield, R.W., Fane, A.G. and Fell, C.J.D., "Heat and Mass Transfer in Membrane Distillation", Journal of Membrane Science, 33 (1987) 299-313.

Fane, A.G., Schofield, R.W., and Fell, C.J.D., "The Efficient use of Energy in Membrane Distillation", Desalination, 64 (1987) 231-243.

Fell, C.J.D., Schofield, R.W., and Fane, A.G., "Membrane Distillation and Pervaporation as Alternatives to Conventional Distillation and Absorption Processes", Institution of Chemical Engineers Symposium Series No. 104, 1987, A371-A383.

Schofield, R.W., Fane, A.G. and Fell, C.J.D., "Gas and Vapour Transport Through Microporous Membranes. I. Knudsen-Poiseuille Transition", submitted Journal of Membrane Science, 1988.

Schofield, R.W., Fane, A.G. and Fell, C.J.D., "Gas and Vapour Transport Through Microporous Membranes. II. Membrane Distillation", submitted Journal of Membrane Science, 1988.

Presentations

"Membrane Distillation - A Novel Evaporative Process", 13th Australasian Chemical Engineering Conference, Perth, Australia, August, 1985.

"Heat and Mass Transfer in Membrane Distillation", Workshop on Membrane Distillation, Rome, Italy, May 1986.

"The Efficient use of Energy in Membrane Distillation", 3rd World Congress on Desalination and Water Reuse, Cannes, France, September 1987.

"Transport Processes in Membrane Distillation", US-Europe Symposium on Advanced Membrane Science and Technology, Ravello, Italy, October 1988.

Table
of
Contents

Chapter 1

Introduction

CHAPTER 1: INTRODUCTION

Over the past few decades, membrane separation processes have made substantial impacts in the fields of science and technology. Processes such as reverse osmosis, ultrafiltration and microfiltration are now recognised as standard unit operations in the process industries. Dialysis has found widespread use in medical applications, and electrodialysis is now a standard technique for deionising water. There are many other membrane processes, however, that are still in the research and development phase, and are virtually unknown outside of membrane laboratories. Membrane distillation falls into this category.

The emergence of membrane technology has coincided with the arrival of two major global problems, namely water pollution and fossil fuel depletion. These problems have lead to an increased interest in technologies for purifying water utilizing renewable or alternative energy sources. Membrane distillation is one such technology.

Over the past twenty years, membrane distillation has received both academic and commercial interest as a process for desalination utilizing low grade thermal energy. However, despite the soundness of the concept, the process has been slow to gain acceptance. Competing technologies such as reverse osmosis and flash distillation have so far withstood the challenges of membrane distillation for a section of the lucrative desalination market. This has lead to the study of other applications for membrane distillation, including the concentration of aqueous solutions, and the separation of dilute ethanol solutions. Meanwhile, the quest for a competitive membrane distillation desalination process continues.

Future trends appear to be in favour of membrane distillation. The
problems of water pollution and fossil fuel depletion show no sign of
abating, while membrane technology is continually maturing. The time is
approaching   when   membrane   distillation   can   compete with other
technologies for the production of pure water.

1.1 MEMBRANE DISTILLATION CONCEPTS

Membrane distillation is unique among the membrane processes, and so has
many novel concepts associated with it. This section introduces the
concepts that are necessary for a full understanding of the material in
this thesis.

1.1.1 Membrane Distillation

A membrane is a thin film that forms an "... active or passive barrier
to the transport of matter between phases adjacent to it" [1.1].
Distillation is a process whereby components are separated from a
solution on the basis of their volatility. Membrane Distillation (MD) is
a process where a thin film (membrane) allows the exchange of volatile
components between two solutions, while preventing mixing of the liquid
streams. This is achieved by separating the two solutions with a dry,
porous, gas permeable film that has the ability to prevent liquids from
entering its porous structure. For the purposes of this study, MD can be
defined more specifically to include only aqueous solutions and
hydrophobic porous membranes, as this is the only system for which the
concept has been technically displayed.

The concept of MD in its basic form is illustrated in figure 1.1. A warm
aqueous solution (feed) contacts one side of a hydrophobic, microporous
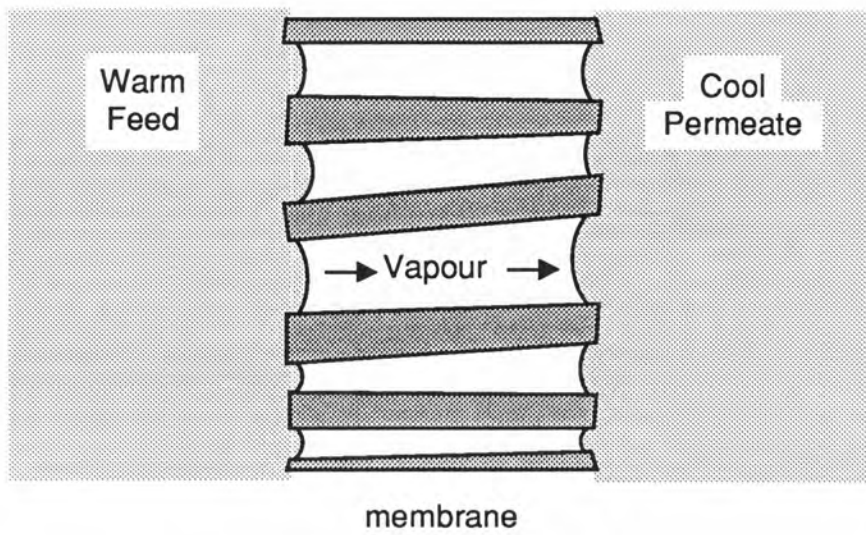
Figure 1.1 Membrane Distillation Concept.

membrane, and cool distilled water (permeate) contacts the other. The membrane, due to its hydrophobic nature, remains internally dry. As the vapour pressure of water is higher for the warm feed than for the cool permeate, there is a driving force for water vapour flux across the membrane. Water evaporates from the feed, permeates across the membrane, and condenses into the permeate stream.

If there are no volatile solutes in the feed, the permeate will be pure water. As the basis of separation is volatility, solute species such as dissolved ions and molecules, macromolecules, bacteria, colloids and particulates will all be retained. If the feed contains volatile solutes, for example low concentrations of organics, these will pass across the membrane with the water vapour. At steady state, MD will produce a permeate equivalent to a single stage fractional distillation, as the membrane is relatively nonselective between gaseous species.

As MD involves a phase change, the latent heat of vaporisation must be supplied to the evaporating surface, and is recovered at the condensing surface. Although this makes MD an energy intensive process, the bulk of the energy required is in the form of thermal energy. Typically, MD would be operated with feed temperatures ranging from 60 to 90 °C, allowing the use of energy sources such as solar energy and waste heat from industry.

1.1.2 Transport Process

Much of this study is devoted to quantifying the various heat and mass transfer processes relevant to MD. This section introduces the four major heat and mass transfer considerations. The concepts introduced here are developed in more detail in the following chapters.

The main interest in MD is the flux of water vapour. The transport processes that control the permeation of water vapour across the membrane are more complex than they initially appear. Just as the evaporating surface is a barrier to non-volatile liquids, the condensing surface is a barrier to non-condensable gases. Air trapped within the membrane pores can only leave through the condensing interface at the rate at which it can dissolve in water. Thus in most MD systems, there is a substantial partial pressure of air within the membrane. It is the combined effect of this air and the structure of the porous membrane that controls the permeation of water vapour. The partial pressure of air within the membrane can be reduced by deaeration, either by externally deaerating the feed and/or permeate, or by reducing the liquid stream pressures within the MD module.

The fact that there is a temperature difference across the membrane means that there is a driving force for thermal conduction across the membrane. This conduction occurs through both the solid (membrane) and gas (air and water vapour) phases. Sufficient heat must be supplied to the membrane surface to provide both the latent heat of vaporisation and the heat transfer by conduction. Heat conducted across the membrane can be considered as a heat loss, as it does not contribute to water vapour flux. Typically, the heat loss by conduction is 10 to 40% of the total heat input.

The transport of heat to and from the membrane surfaces depends on the type of module used to perform MD. For example, if tubular membranes are used, a hot feed stream and a cool permeate stream may flow counter-currently in a shell and tube module, with heat transfer behaviour similar to a shell and tube heat exchanger. If flat sheet membranes are used, heat may be supplied and removed by jacketting the system with

heating and cooling water compartments. The basic approach to describing liquid phase heat transfer is through film heat transfer coefficients. Systems may be designed with either turbulent or laminar flow of the fluids bounding the membrane, with the main design objective being high heat transfer.

The fact that MD removes the solvent from a solution means that there is a tendency for solute to build up at the membrane surface. This can effect the performance of MD, however in most applications the effect is far less than it is in, for example, filtration processes.

1.1.3 MD Membranes

The major requirement of MD membranes is that they be hydrophobic, thus forming a barrier to aqueous phases. Commercially available hydrophobic membranes include polypropylene (PP), polyvinylidene difluoride (PVDF) and polytetrafluoro ethylene (PTFE). The second major consideration for MD membranes is the pore size. The larger the pore size, the less the force that is required for liquid water to invade the pore space, hence the higher the risk of wetting the membrane. If the pore size is too small, however, the membrane permeability will be low, resulting in low fluxes. A reasonable trade-off between these two considerations suggests that MD pore sizes should be in the range 0.1 to 0.5 μm. Membranes in this pore size range are referred to as microporous.

Most commercially available hydrophobic, microporous membranes have porosities in the range 60 to 80%, and thicknesses in the range 50 to 200 μm. Some are supported on a woven or matted support matrix to provide strength. Most microporous membranes are classified as isotropic, meaning that the pore geometry is the same across the entire

membrane. An electron microscope photograph of an MD membrane cross-section is shown in Appendix A, figure A.1, showing that this is not strictly true. For example, for a 75% porous membrane, the porosity may vary from 70% on one side to 80% on the other. The pore size may also vary across the membrane. It is common to report a pore size distribution, as shown in figure 1.2. While the issue of pore size determination is beyond the scope of this discussion, it is important to appreciate both that there is a range of pore sizes within any membrane, and that the measured pore size is dependent on the measuring technique. The manufacturers specification should only be regarded as a nominal pore size.

MD membranes are available in both flat sheet and tubular form. For the purposes of this study, tubular membranes will be divided into two classes referred to as "tubular" and "hollow fibre". The distinction is that under typical MD operating conditions, flow through a tubular membrane will be turbulent, while flow through a hollow fibre membrane will be laminar. Typical operating conditions for MD would be 50 kPa pressure drop along a 0.5 m tube or fibre. Typically, a membrane with a diameter greater than 1 mm would be considered tubular, while a 0.3 mm diameter membrane would be classed as a hollow fibre. Systems in the transition between tubes and fibres would be undesireable as they could alternate between laminar and turbulent flow.

1.1.4 Membrane Wetting

The major requirement of MD membranes is that they prevent the passage of liquid water. If liquid water enters the membrane pores, the process stops, and the membrane simply behaves as a microfiltration membrane. The invasion of liquid water into the pores is referred to as "wetting"
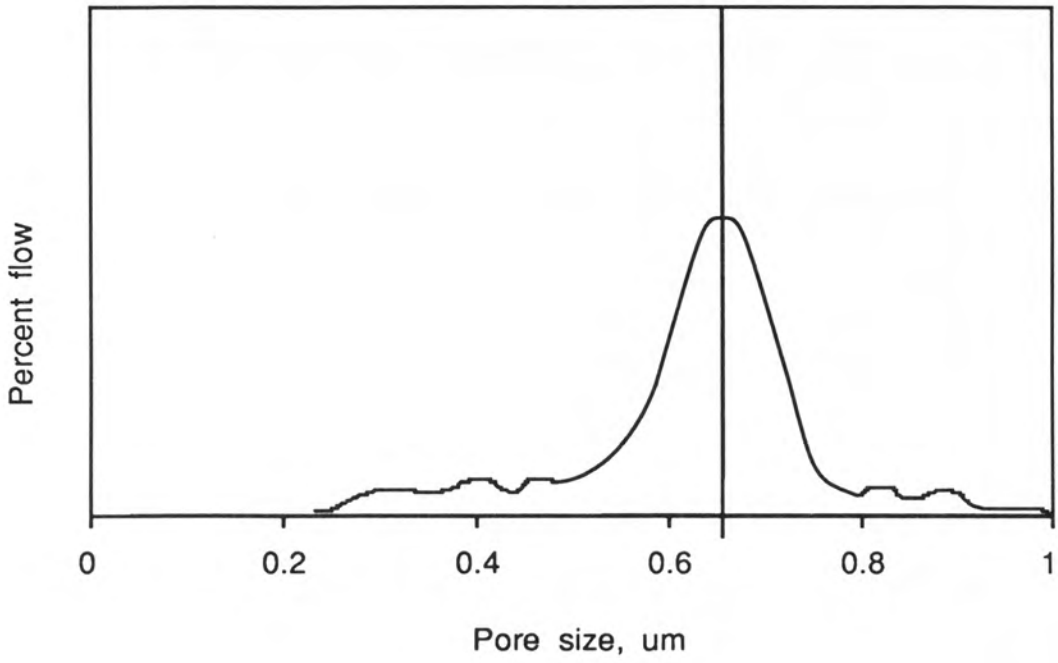
Figure 1.2 : Pore size distribution for a Durapore 0.45 um PVDF membrane measured by Coulter Porometer.

of the membrane. Wetting can provide a direct path for solute to diffuse into the permeate, reducing permeate purity.

The tendency for membrane wetting is increased by the presence of surfactants or organics in the feed, or by high solute concentrations. If wetting occurs over a small fraction of the membrane area, operation can continue provided the permeate pressure is slightly higher than the feed pressure. Under these conditions, the bulk flow of permeate back through the wet pores will prevent contamination of the permeate with the feed. Provided the back-flux of permeate is much less than the vapour flux, system performance will not be greatly affected. The tendency for membrane wetting can be reduced by operating with low pressures in the liquid phases.

Wetting can be combatted by cleaning and drying the membranes. This can result in total recovery of the initial membrane performance. In an industrial context, a periodic cleaning cycle may be necessary. The period between cycles may be a few hours for complex systems, or more than one month for simple, clean systems.

1.1.5 Variations of MD

The process described in section 1.1.1 is classified as "Direct Contact MD". Some variations of MD are described below, with additional details included in Appendix B.

The most common variation of MD is "gas-gap MD". In this process, the permeate condenses on a cooled surface that is separated from a sheet membrane by a thin air-filled channel. The feed is usually heated within the module by an adjacent heating fluid channel. The concept is

illustrated in figure 1.3. The major reason for developing this variation of MD was to minimise the heat loss by conduction across the membrane. The air gap is intended to act as an insulating layer. The disadvantage of this system is that the air gap increases the permeation path of the water vapour, thus reducing flux. From an industrial viewpoint, gas-gap MD has the advantage that the heat transfer surfaces are incorporated in the MD module, eliminating external heat exchangers. From a design viewpoint, however, this eliminates heat transfer area as an independent variable, as it is constrained to be equal to the membrane area.

Other variations of MD include "low pressure MD", where the permeating vapour is removed under vacuum, and condensed in an external unit, and "sweeping gas MD" where the permeating vapour is removed in an inert gas stream and condensed externally. These concepts are also illustrated in figure 1.3.

1.1.6 Applications

MD is a process that removes water from aqueous solutions. The product can be either the permeate or the concentrated solution. A major application of MD is desalination. The fact that salt water does not contain volatile solutes means that the permeate purity will be high. MD is able to concentrate salt solutions up to near saturation, yielding water recoveries in excess of 90%. MD is equally well suited to other non-volatile solutes such as sugar.

Other applications for MD include the concentration of complex aqueous solutions. Feeds that contain dissolved ions, macromolecules, colloids and even low concentrations of organics can be processed by MD.

Direct contact MD

Gas gap MD

External condenser

Sweeping gas MD

Vacuum condenser

Low pressure MD

Feed   Permeate   Vapour   Coolant
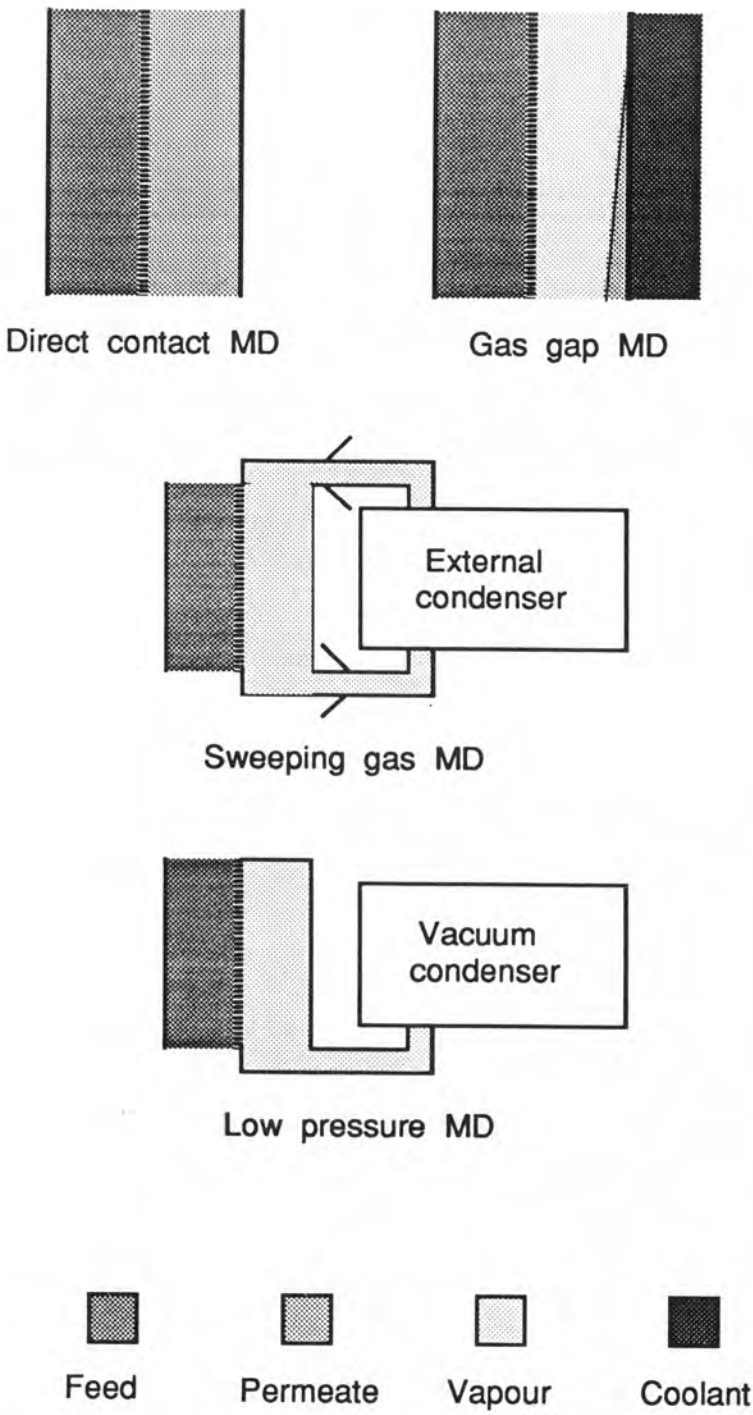
Figure 1.3 : Variations of MD

Potential applications include concentrating fruit juices, milk and industrial waste waters. MD can also be used for the separation of ethanol from water, when low concentrations are present. An example of this application is the removal of ethanol from fermentation broths.

1.2 PREVIOUS WORK

Membrane distillation is a relatively immature technology. It has found limited industrial acceptance and has been poorly represented in the literature. This is surprising, as the concept is more than 20 years old. The following historical development outlines the major steps in arriving at a process that is now on the brink of industrial feasibility.

An early form of MD was proposed by Bodell in 1963 [1.2,1.3]. The membranes used in Bodell's process were microporous, hydrophobic capillary tubes fabricated from silicone rubber. The outer surface of the tubes was contacted with a warm aqueous solution. Water vapour passing through the membrane pores was entrained in an air stream (sweeping gas MD), and transported to an external condenser. The process was proposed primarily for the production of distilled water.

Direct contact MD was first proposed by Weyl [1.4] in 1964. His PTFE membranes were crude by today's standards, having a thickness of 3mm and a porosity of 42%. Weyl claimed good agreement between diffusion theory and experimental flux for his system, however details were not published. Weyl's patent also included a method of recovering the latent heat of vaporisation. This involved transfering heat from the permeate to a lower temperature feed through a non-permeable heat transfer film. In a system that will be refered to here as "multiple effect MD", a

stack (or spiral) of membranes separated by heat transfer films, allowed the latent heat to be used many times. This concept is illustrated in figure 1.4.

The first published work on MD was by Findley [1.5] in 1967. Findley examined many membrane materials, including various papers and plastics, glass fibres and diatomaceous earth, using teflon, silicones and water repellants to achieve hydrophobicity. He gained an appreciation of the importance of air trapped within the membrane, heat loss by conduction, and high temperature operation. Findleys conclusion was that the process could become feasible if "low cost, high temperature, long-life membranes with desireable characteristics" could be developed. This was not achieved until the 1980s, however further developments were made in MD during the interim.

During the late 1960s and '70s, Rodgers [1.6,1.7,1.8] continued developing the multiple effect system proposed by Weyl. His work resulted in a novel and interesting application for MD. He found that a stacked multiple effect system could be modified to behave like a distillation column. In 1971 [1.9], Rodgers patented an MD process for the separation of D_2O from H_2O. Conventionally, heavy water distillation was performed in a 60m high, 40 stage column, yielding 2% recovery with a holdup of 75 days [1.9]. Rodgers claimed that with a 0.02m high, 50 stage membrane column (or stack), he could achieve 75% recovery of D_2O with a holdup of 6 to 7 hours. Despite the amazing claims, no further reference is made to this process in the literature.

In the late 1970s, Cheng [1.10,1.11] addressed the problem of membrane wetting. He suggested that wetting occurs due to the effect of dissolved salt in the feed, which changes the hydrophobic nature of the membrane
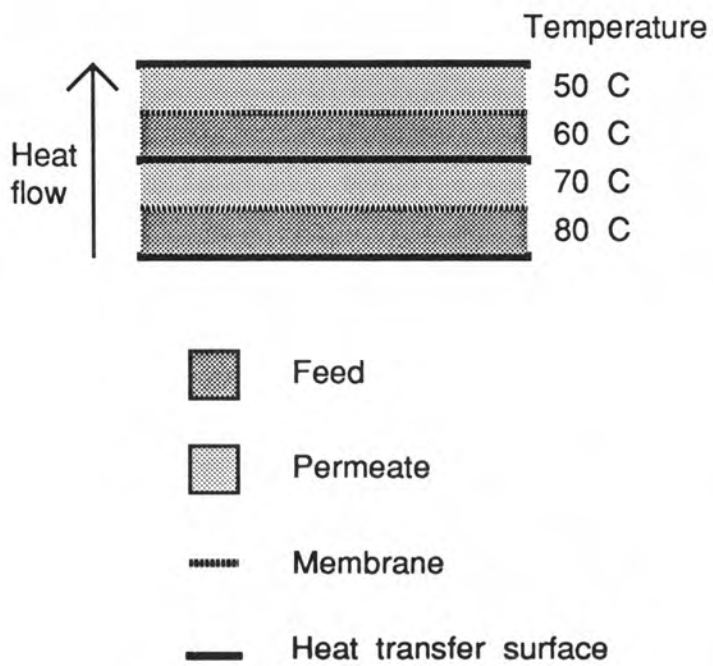
Figure 1.4 : Multiple effect MD

at the liquid/vapour interface. He claimed that at the convex (into the membrane) liquid/gas interface, surface tension effects caused uneven evaporation, resulting in precipitation of salt on the membrane walls, rendering them hydrophilic. Cheng's approach to combatting this phenomenon was to clad the hydrophobic membrane with a hydrophilic membrane having a smaller pore size. The interfacial surface curvature would then become concave (out of the membrane), being controlled by the hydrophilic membrane. Cheng claimed success with his system, however this approach has not been adopted by others. The main objection is the added heat and mass transfer resistance of the hydrophilic layer.

The 1980s saw the re-emergence of MD. Membrane manufacturing techniques had advanced to a stage where the economics were favourable for the development of MD. In 1982, Gore (USA) [1.12] published details of the Gore-Tex™ MD system, based on expanded PTFE membranes. In this system, latent heat was recovered from the permeate to preheat the feed, and the linear system was wrapped in a spiral providing compact modules. Gore claimed energy recoveries as high as 95%, with a possible trade-off between energy recovery and productivity. After several years developing the system to the stage of commercial production, the technology was abandoned. The major problems with the system involved poor heat transfer as a result of inadequate understanding of the transport processes.

In 1984, Schneider and van Gassell (West Germany) [1.13] published details of the Enka MD system. Their system was based on turbulent flow in tubular polypropylene membranes in counter-current shell and tube modules. This system will be discussed in chapter 8. Enka investigated flux enhancement by deaeration achieved by both the reduction of solution pressures and the vacuum removal of noncondensible gases from

the pore space. They had reasonable success predicting fluxes with a Knudsen diffusion model incorporating adjustable parameters to account for deaeration. Enka studied various membrane tube dimensions, feed flow rates and temperatures, and concluded that MD could be competitive with multiple effect evaporation for the production of boiler feed water. Now, five years later, their system has been offered commercially with limited acceptance.

Also in 1984, Drioli et. al. (Italy) [1.14] published results of their research in MD. This initial study addressed fundamental aspects such as flux/temperature and flux/concentration relationships, as well as flux decline and membrane fouling and wetting. Their experimental system was not well designed from a heat transfer viewpoint, however this situation was improved in later studies.

1985 saw the publication of four papers on MD in the proceedings of the Second World Congress on Desalination and Water Re-Use. This was the first indication that MD was attracting global attention. Sarti et. al. (Italy) [1.15] gave results from a theoretical and experimental study of direct contact MD. Their theory was based on the vapour pressure of solutions, and the molecular diffusion of water vapour through a stationary film of air. However their experimental sheet membrane apparatus had extremely bad heat transfer characteristics, making it difficult to draw meaningful conclusions.

Andersson et. al. (Sweden) [1.16] published results for field testing of their gas-gap system. Their commercial system was based on modules built up of cassettes forming feed, permeate, heating water and cooling water channels. The system has more recently been tested in pilot plant studies utilizing the waste heat from diesel powered electricity

generators. As with the Enka system, the Swedish National Development Co. system has had limited commercial success.

Jönsson et. al. (Sweden) [1.17] published results of a theoretical study of the gas-gap system. They developed appropriate theory for the gas-gap case, and examined the effect of varying membrane and air gap thicknesses. They concluded that a thin air gap could reduce heat loss significantly, while only reducing the flux slightly.

Hanbury and Hodgkies (Scotland) [1.18] published an assessment of the Gore-tex system, based on laboratory results. They concluded that the Gore-tex system was not economically viable, however their conclusion was based on an incorrect calculation. After a reassessment, they later concluded that the process could be viable, however there were doubts about its suitability for long term applications.

In May 1986, the "Workshop on Membrane Distillation" was held in Rome, Italy. This was the first occassion to bring together all people with an interested in MD. Details of the eight papers presented at the workshop are given below. As a result of the workshop, a document was prepared standardizing terminology for MD. This document is reproduced in Appendix B.

Kimura (Japan) [1.19] reported results from studying both fundamental aspects and applications for gas-gap MD using PTFE membranes. Experiments were conducted with various acid, base and salt solutions, as well as fruit juices, milk, sugar and gelatin. Kimura presented a detailed theoretical analysis based on the molecular diffusion of water vapour through still air at atmospheric pressure, accounting for latent heat, and sensible heat transfer in all phases. This analysis was used

both to interpret results and to optimise module design. Even with an optimised module design, the conclusion was that gas-gap MD is generally only attractive when a source of waste heat is available.

Sarti (Italy, unpublished) presented much of the work from his previous paper [1.15] as well as some preliminary results for separating ethanol and water. He found that ethanol concentrations higher than 8% lead to wetting of the membrane, and suggested that maintaining a diffusion gap could prevent contamination of the permeate with the feed.

Ripperger (West Germany, unpublished) presented results for the Enka system, many of which had already been published [1.13]. New results for long term tests showed that membrane fouling causes around 20% flux decline over one year. This can be combatted by cleaning and drying every 2 to 12 months. No biological fouling was detected at feed temperatures above 90 °C. Preliminary tests were reported for the concentration of apple juice, with membrane wetting occurring at high concentrations. An economic analysis indicated that for plants larger than 50 tonnes per hour, multiple effect evaporation was more economic than MD.

Kjellander (Sweden, unpublished) presented work from a previous paper [1.16]. Latest production figures indicated distilled water costs of around $2/tonne.

Johnson (Australia, unpublished) presented some preliminary results for an adaptation of MD called "osmotic distillation", a proprietry process of Syrinx Research Inc. The process, which couples MD with reverse osmosis, can be used for water production or concentrating aqueous solutions. Initial production figures were given for concentrating milk.

Franken (The Netherlands) [1.20] presented work on membrane wetting criteria for organic/aqueous systems. His results for various membranes showed maximum allowable ethanol concentrations of 20 to 40%. Due to the inability of theory to predict wetting behaviour, he described a simple experimental technique for determining maximum organics concentrations.

Calabro (Italy) [1.21] presented results for MD of sucrose and salt solutions. She used a linear relationship between flux and vapour pressure difference to describe experimental results. The results showed that MD could concentrate electrolyte and non-electrolyte solutions to very high concentrations, while maintaining a high purity permeate.

The eighth presentation at the "Workshop on Membrane Distillation" [1.22] detailed preliminary findings from this study, most of which make up chapter 4 of this thesis.

In 1987, Gostoli (Italy) [1.23] published a study continuing on from Sarti's work [1.15]. Here he compared previous results for direct contact MD with results for gas-gap MD, concluding that the same basic equations could describe both processes. The low fluxes reported for both systems suggest that the module designs were far from optimum.

In 1988, Schneider (West Germany) [1.24] published work continuing on from the Enka study [1.13]. The major new contribution of this study was recognition of the need to improve heat transfer on the shell side of shell and tube modules. Schneider suggested the use of woven, twisted and braided tube bundles to provide uniform flow distribution and high turbulence on the shell side. The overall conclusion was that MD was still not competitive for large scale desalination, but may find

specialty applications for the production of high purity water utilizing waste heat.

In September 1988, Franken (The Netherlands) [1.25] submitted his Ph.D thesis at the University of Twente. Titled "Membrane Distillation - A New Approach Using Composite Membranes", it introduced a hybrid process combining MD with pervaporation for the separation of ethanol and water. Basically, a dense pervaporation membrane is coated onto an MD membrane. The pervaporation layer provides selectivity to water over ethanol, and the MD layer replaces the usual pervaporation vacuum/condenser system. Fluxes of 1 kg/m^{2}h with selectivities of up to 30 were reported.

In summary, this review of the literature has shown that over the past 25 years, MD systems have been developed based on tubular membranes, flat sheet membranes, spiral modules and gas-gap devices, however no system has proved particularly successful in the commercial arena. Many applications have been investigated, showing that the technology is capable of a wide range of duties, however from an economic viewpoint, the process is not quite competitive with alternative technologies. The theoretical developments have been disjointed, with no study conducting a full optimisation of the process to determine its full potential.

1.3 THIS STUDY

1.3.1 Scope

The broad aim of this study was to examine the fundamental aspects of heat and mass transfer in MD to assess the potential and limitations of the process, and to determine which system can best fulfil this potential. Attention was focussed on direct contact MD of aqueous

solutions of non-volatile solutes using commercially available membranes, as this encompasses the major applications of MD. Reference is made to variations of MD and other applications where appropriate.

The approach used was to examine heat transfer, gas phase mass transfer and solute mass transfer independently, to determine the controlling parameters for the process. Emphasis was placed on maximising flux, and minimising the inefficiencies associated with heat loss by conduction across the membrane and temperature polarisation. The controlling parameters were found to be liquid film heat transfer and membrane permeability. Maximum targets were identified for these parameters, and systems were designed to approach these maxima.

The knowledge gained in the parametric study was applied in a preliminary pilot plant study. Production results were used to indicate the costs and performances of industrial MD facilities.

The major finding was that deaerated hollow fibre MD systems with laminar flow of the feed and permeate can provide near optimum heat and mass transfer performance. Added advantages of this system are reduced heat loss by conduction, reduced tendency for membrane wetting, and flexibility of operation.

1.3.2 Chapter Summaries

Chapter 2 develops the fundamental heat and mass transfer equations relevant to direct contact MD. Aspects of heat transfer covered include vaporisation and condensation, film heat transfer, thermal conduction across the membrane and combined heat and mass transfer. Mass transfer theory covers gas permeation mechanisms, vapour pressure reduction, and

concentration polarisation. The theory behind membrane wetting is
discussed briefly.

Chapter 3 examines the suitability of various membrane modules for MD.
Design considerations are given for cross flow cells and shell and tube
modules, and details are given of the various modules used in this
study.

Chapter 4 is a study of heat transfer in MD. The relative importance of
film heat transfer, latent heat transfer and conduction across the
membrane is examined. Methods are given for estimating and measuring
film heat transfer coefficients for various MD module designs. Film heat
transfer was found to limit the process in many situations. A maximum
realistic target for the overall film heat transfer coefficient was
found to be 5000 W/m^2K.

Chapter 5 examines gas permeation through microporous   membranes.
Experiments were conducted with various gases to allow prediction of
water vapour fluxes through totally deaerated MD membranes. Data were
correlated using a novel semi-empirical equation based on combined
Knudsen and Poiseuille flow.

In chapter 6, the results from chapter 5 are extended to predict the
flux of water vapour through both aerated and deaerated MD membranes.
Experimental results support the theory, and display the benefits of
deaeration. Deaeration by lowering liquid pressures is found to increase
flux, decrease heat loss by conduction, and may reduce the tendency for
membrane wetting. The increase in membrane permeability by deaeration
makes the process film heat transfer limited in most situations.

Chapter 7 deals with flux reduction caused by solute in the feed. The effects of vapour pressure reduction and concentration polarisation are compared with the effects of changing transport properties. Vapour pressure reduction is found to be the major cause of flux reduction for salt solutions, while increased viscosity (decreased film heat transfer) has the major effect for sugar solutions. In most applications, the flux reduction by solute is relatively small.

Chapter 8 gives the results of a pilot plant study on MD. Two modules are examined, based on hollow fibre polypropylene membranes. Production results and computer modelling lead to predictions of system performance for industrial cases. Tests conducted with salt water and an industrial waste water display the suitability of MD for these two applications.

Chapter 9 gives the conclusions for this study, as well as recommendations for future work.

Appendix A includes photographs of some of the membranes, modules and equipment used in this study. Appendix B contains a report on terminology for membrane distillation. Appendix C includes details of computer modelling used in this study.

1.4 REFERENCES

[1.1]   Gekas, V., "Terminology for Pressure Driven Membrane Operations", European Society for Membrane Science and Technology, June 1986.

[1.2]   Bodell, B.R., "Silicone Rubber Vapour Diffusion in Saline Water Distillation", U.S. Patent Application Ser. No. 285032, 1963.

[1.3]   Bodell, B.R., "Distillation of Saline Water Using Silicone Rubber Membranes", United States Patent US 3,361,645, 1968.

[1.4]   Weyl, P.K., "Recovery of Demineralised Water from Saline Waters", United States Patent US 3,340,186, 1967.

[1.5]   Findley, M.E., "Vaporization Through Porous Membranes", Ind. Eng. Chem. Proc. Des. Dev., 6 (1967) 226-230.

[1.6]   Rodgers, F.A., "Distillation Under Hydrostatic Pressure with Vapour Permeable Membranes", United States Patent US 3,406,096, 1968.

[1.7]   Rodgers, F.A., "Stacked Microporous Vapour Permeable Membrane Distillation System", United States Patent US 3,650,905, 1972.

[1.8]   Rodgers, F.A., "Distillation System Using Microporous Stack", United States Patent US 3,896,004, 1975.

[1.9]   Rodgers, F.A., "Apparatus for Increasing the Concentration of a Less Volatile Liquid Fraction in a Mixture of Liquids", United States Patent US 3,562,116, 1971.

[1.10] Cheng, D.Y., "Method and Apparatus for Distillation", United States Patent US 4,265,713, 1981

[1.11] Cheng, D.Y. and Wiersma, S.J., "Composite Membrane for a Membrane Distillation System", United States Patent US 4,316,772, 1982

[1.12] Gore, D.W., "Gore-Tex Membrane Distillation", Proc. 10th Ann.

       Conv. Water Supply Improvement Assoc., Honolulu, July 1982.

[1.13] Schneider, K., van Gassel, T.S., "Membrandestillation", Chem.Ing.

       Tech., 56 (1984) 514-521.

[1.14] Drioli, E., Chlubek, N. and Punzo, A., "Studio sui Processi a

       Membrana Condotti sotto Gradiente Termico", La Chimica e

       l'Industria 66 (1984) 147-152.

[1.15] Sarti, G.C., et.al., Low Energy Desalination Process using

       Hydrophobic Membranes", Desalination, 56 (1985) 277-287.

[1.16] Andersson, S.-I., Kjellander, N., and Rodesjo, B., "Design and

       Field Tests of a New Membrane Distillation Desalination Process",

       Desalination, 56 (1985) 345-354.

[1.17] Jönsson, A.-S., Wimmerstedt, R. and Harrysson, A.-C., "Membrane

       Distillation - A Theoretical Study of Evaporation Through Micro-

       porous Membranes", Desalination, 56 (1985) 237-250.

[1.18] Hanbury, W.T. and Hodgkiess, T., "Membrane Distillation - An

       Assessment", Desalination 56 (1985) 287-297.

[1.19] Kimura, S., Nakao, S. and Shimatani, S., "Transport Phenomena in

       Membrane Distillation", J. Membrane Science, 33 (1987) 285-298.

[1.20] Franken, A.C.M. et. al., "Wetting Criteria for the Applicability

       of Membrane Distillation", J Membrane Science, 33 (1987) 315-328.

[1.21] Drioli, E., Wu, Y. and Calabro, V., "Membrane Distillation in the
       Treatment of Aqueous Solutions", J. Mem. Sci., 33 (1987) 277-284.

[1.22] Schofield, R.W., Fane, A.G. and Fell, C.J.D., "Heat and Mass
       Transfer in Membrane Distillation", J. Membrane Science, 33
       (1987) 299-313.

[1.23] Gostoli, C., Sarti, G.C. and Matulli, S., "Low Temperature
       Distillation Through Microporous Membranes", Separation Science
       and Technology, 22(2&3) (1987) 855-872.

[1.24] Schneider, K. et. al., "Membranes and Modules for Transmembrane
       Distillation", J. Membrane Science, 39(1) (1988) 25-42.

[1.25] Franken, A.C.M., "Membrane Distillation - A New Approach Using
       Composite Membranes", Ph.D. Thesis (1988), University of Twente,
       The Netherlands.

Chapter 2

Theory

CHAPTER 2: THEORY

Theory applicable to MD includes heat transfer in the solid, liquid and gas phases, mass transfer in the liquid and gas phases, phase equilibrium, and water entry pressure. This chapter develops the fundamental theory applicable to direct contact membrane distillation. Additional theory is developed in other chapters dealing with specific aspects of MD.

MD is both a mass transfer and a heat transfer process. The fact that there is a phase change means that the latent heat of vaporisation must be supplied to one side of the membrane, and removed from the other. The occurrence of simultaneous heat and mass transfer in the liquid and gas phases suggests that a theoretical analysis will be complex [2.1,2.2]. It transpires, however, that the coupling of heat and mass transfer is not strong.

In the liquid phase (feed), the flux of water from the liquid boundary layer into the membrane only alters the film heat transfer coefficient by around 1%, as will be shown in section 2.1.3. In chapter 7, solute mass transfer is found to have only a small effect on flux, hence the effects of thermal gradients in the boundary layer on solute mass transfer can effectively be ignored. Thus, in the liquid phase, heat and mass transfer can be considered independently.

In the gas phase, mass flux results in convective heat transfer within the membrane, and temperature gradients within the membrane have an effect on gas permeation. The effects of heat and mass transfer coupling within the membrane are discussed in sections 2.1 and 2.2. It must be appreciated, however, that transport equations describing heat and mass

fluxes within the membrane are only approximate. In section 1.1, pore size and porosity were shown to vary across the membrane. It would be expected that the errors incurred by evaluating transport properties at the average membrane temperature would be no greater than the error from assuming an average pore size and porosity. This emphasises the need to measure transport properties in situ wherever possible.

In this study, heat and mass transfer equations were derived separately, with the appropriate equations being combined to provide an MD flux relationship.

2.1 HEAT TRANSFER

In MD, the occurrence of a phase change from liquid to vapour on one side of the membrane, and back to liquid on the other side can lead to high heat transfer rates. A typical temperature profile across an MD system is shown in figure 2.1. Heat transfer from the feed solution to the membrane interface must be sufficient to supply the latent heat of vaporisation as well as the sensible heat transported across the membrane due to the trans-membrane temperature gradient. The transfer of water vapour across the membrane can be considered as a heat transfer process, as latent heat is consumed at the higher temperature interface, and liberated at the lower temperature interface. Thus an MD system is governed by four interacting heat transfer processes, as shown in figure 2.2 where an electrical analog is used to visualise the heat transfer. Heat is transported to the membrane interface by means of a film heat transfer coefficient, h_f, where the subscript f refers to the feed. Similarly, heat is removed by the permeate subject to the film heat transfer coefficient h_p. This heat passes across the membrane by two parallel paths, namely vaporisation and conduction, as described by the
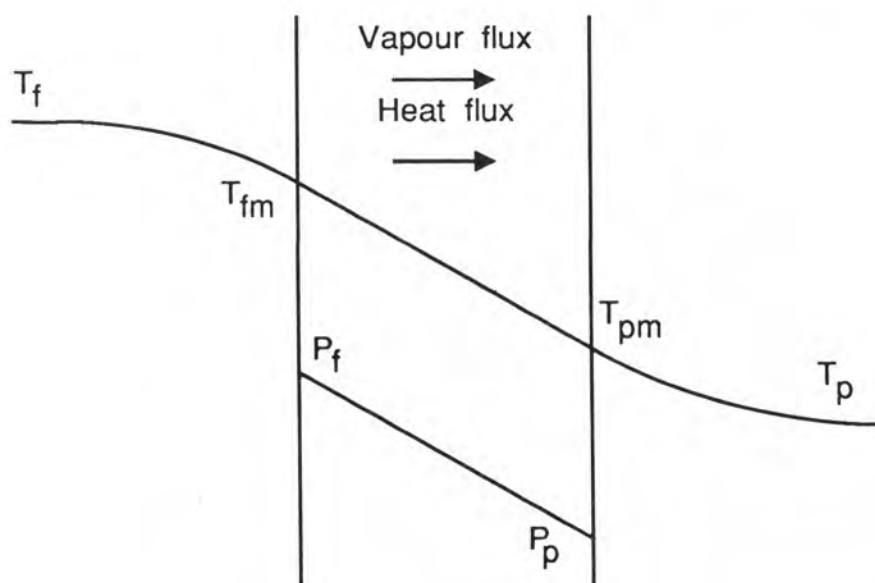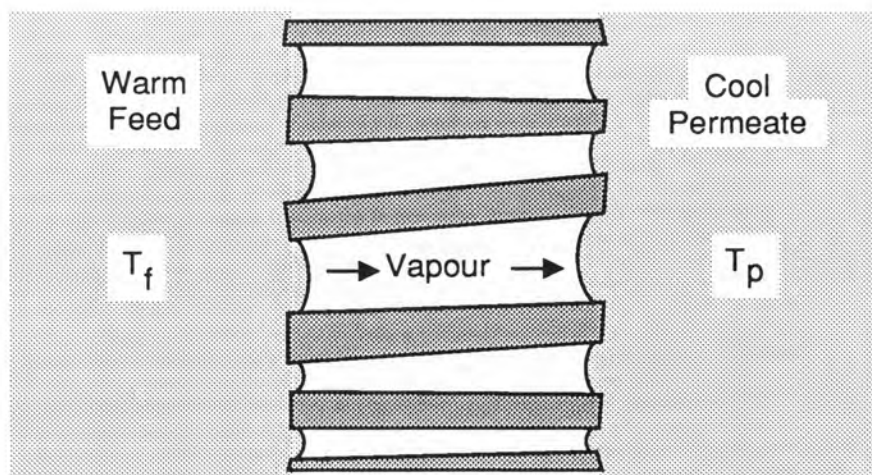
Figure 2.1 : Membrane distillation temperature profile.
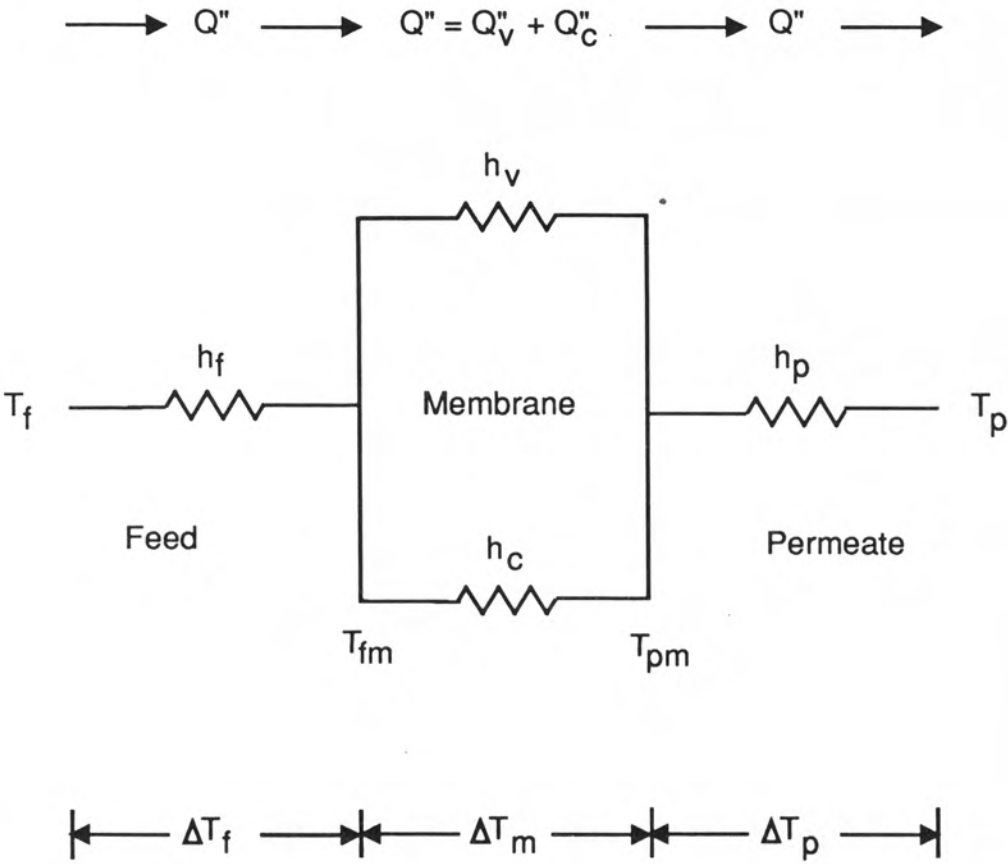
Figure 2.2 : Heat transfer paths in MD.

two heat transfer coefficients h_v and h_c respectively. Theoretical
expressions for each of these heat transfer coefficients are developed
below.

2.1.1 Vaporisation and Condensation

The essence of membrane distillation is the vaporisation of water,
permeation of the water vapour across the membrane, and condensation of
the permeate. Viewing the process from within the membrane, a vapour
pressure gradient results in the transport of gaseous water molecules
from one side of the membrane to the other. However viewing the process
from outside the membrane, a temperature gradient results in the
transfer of heat (and mass) across the membrane. The physical property
that   reconciles   these   different   views   is   the   latent heat of
vaporisation. To illustrate this, consider the most basic expression for
vapour flux across the membrane.

$$J = C \; \Delta P \tag{2.1}$$

where J is the mass flux and ΔP is the water vapour pressure drop. C is
a form of membrane gas permeability, which depends on pressure,
temperature, pore geometry and the level of air within the membrane, as
discussed in section 2.2. Equation (2.1) describes MD as viewed from
within the membrane. The mass flux, J, can be converted to a heat flux,
Q''_v, by multiplying by the latent heat of vaporisation, ΔH_v, giving

$$Q''_v = C \; \Delta H_v \; \Delta P \tag{2.2}$$

For the case where the feed does not contain solute (chapters 4 and 6),
the pressure driving force can be converted to a temperature driving

force using the approximation $dP/dT \approx \Delta P/\Delta T_m$, giving

$$Q''_v = C \frac{dP}{dT} \Delta H_v \Delta T_m \qquad (2.3)$$

which may be rewritten

$$Q''_v = h_v \Delta T_m \qquad (2.4)$$

where $h_v = C \frac{dP}{dT} \Delta H_v$

The approximation $dP/dT \approx \Delta P/\Delta T$ gives less than 1% error for $\Delta T_m < 10$ °C, which is usually the case. For the case where there is a substantial level of solute in the feed, this substitution cannot be made (see chapter 7).

Equation (2.4) describes MD as viewed from outside the membrane. In other words, the mass flux of water vapour across the membrane can be described in terms of a heat flux caused by a temperature gradient. The coefficient h_v is the heat transfer equivalent of the membrane permeability.

Evaluation of the vapour heat transfer coefficient, h_v, requires knowledge of the latent heat of vaporisation, ΔH_v, and the slope of the vapour pressure curve, dP/dT. The latent heat of vaporisation for water varies slightly with temperature, being 2.40×10^6 J/kg at 40 °C, and 2.31×10^6 J/kg at 80 °C [2.3].

The vapour pressure of water, P, can be calculated from an equation of state, such as the Antoine equation [2.4]

$$P = \exp (23.238 - 3841/(T-45)) \qquad (2.5)$$

where T is the temperature in degrees K, and P is in Pa. Figure 2.3
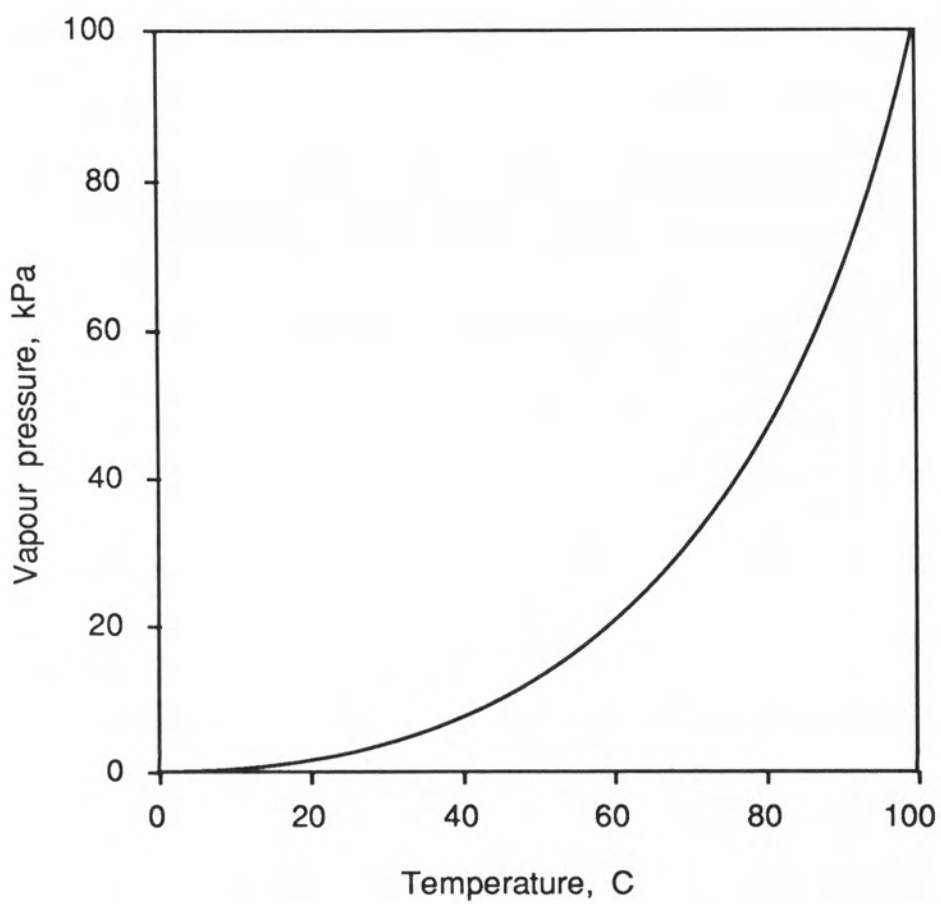
Figure 2.3 : Water vapour pressure curve.

shows the relationship between water vapour pressure and temperature over the range 0 to 100 °C. It is evident that the slope of the vapour pressure curve increases exponentially with temperature, and hence so does the vapour heat transfer coefficient. Accordingly, higher fluxes are achieved at higher operating temperatures. The slope of the vapour pressure curve can be calculated using the Clausius-Clapeyron equation [2.5].

$$\frac{dP}{dT} = \frac{MP\Delta H_v}{RT^2} \qquad\qquad (2.6)$$

where M is the molecular weight [kg/mol] and R is the gas constant [J/molK].

The relationship between vapour pressure and temperature is dependent on solute concentration. The presence of solute causes a lowering of the vapour pressure, which is a colligative property. For dilute (ideal) solutions of non-volatile solutes, the solution vapour pressure may be written [2.6]

$$P = (1-x)\ P° \qquad\qquad (2.7)$$

where P° is the vapour pressure of pure water at that temperature, and x is the mole fraction of solute. A more elaborate treatment of vapour pressure reduction will be given in section 2.2 and chapter 7. (Note, the approximation $dP/dT \approx \Delta P/\Delta T_m$ in equation (2.3) cannot be used when vapour pressure reduction is significant.)

2.1.2 Sensible Heat Transfer

The presence of a temperature gradient across the membrane causes the

transfer of sensible heat. This is virtually independent of the latent heat transfer, and can be considered as a parallel path, as indicated by h_c in figure 2.2. The three mechanisms of sensible heat transfer are conduction, convection and radiation. In this application, radiation is negligible due to the low temperatures involved.

Within an MD membrane, the mean free path of the gas molecules is similar to the pore size. This means that a water molecule is as likely to collide with a pore wall as it is to collide with another molecule. This intimate contact between gas and membrane allows the assumption that the gas and polymer are at the same temperature at any point through the membrane. Hence the polymer and the gas (comprising of water vapour and air) can be considered as a composite material. Accordingly, the thermal conductivity, k, can be calculated as

$$k_m = \epsilon k_g + (1-\epsilon)k_s \qquad\qquad (2.8)$$

where ϵ is the membrane porosity (typically 0.75), and the subscripts m, g, and s refer to the membrane, gas and solid respectively. The thermal conductivity of a gas is independent of pressure in the range of interest, however it does vary with temperature. An equimolar mixture of air and water vapour has a conductivity of $k_g = 0.0235$ W/mK at 40 °C and 0.0265 W/mK at 80 °C [2.7]. The thermal conductivity of polypropylene is $k_s = 0.14$ W/mK, while PVDF and PTFE have conductivities of 0.24 W/mK [2.8]. Thus most MD membranes would have a composite conductivity of $k_m = 0.05$ to 0.08 W/mK, with 60 to 80% of conduction occurring in the solid phase. In chapter 4, equation (2.8) was tested experimentally with good agreement.

The heat transfer by conduction across the membrane is given by the

equation

$$Q''_c = k_m \, \Delta T_m / \delta \qquad\qquad (2.9)$$

$$\equiv h_c \, \Delta T_m$$

where δ is the membrane thickness. Typically, the heat transfer by conduction is 10 to 40% of the total heat transfer (conduction plus vapour) across the membrane. Heat transfer by conduction is a heat loss, and should be minimised in the interest of energy efficiency.

Within the membrane, there is a mass flux of water vapour with a negative temperature gradient in the direction of flow. This gives rise to convective heat transfer. The amount of convective heat transfer depends on the mass flux and the heat capacity of the vapour. At 80 °C, the heat capacity of water vapour is 2100 J/kgK [2.7]. The relative importance of convection and conduction can be assessed by means of the Peclet number,

$$Pe = \frac{J \, C_p \, \delta}{k_m} \qquad\qquad (2.10)$$

which is the ratio of convective to conductive heat transfer. Assuming a typical value of $k_m/\delta = 500$ W/m^{2}K, Peclet numbers can be calculated for typical high and low flux values. At a flux of $J = 50$ kg/m^{2}h, Pe = 0.06, and at $J = 5$ kg/m^{2}h, Pe = 0.006. Thus the heat transfer by convection is typically 0.6 to 6% of the heat transfer by conduction. A Peclet number of 0.06 (at high flux) indicates that convective heat transfer may be significant. In chapter 4, however, the fractional heat loss by conduction is shown to be low (10 to 20%) at high fluxes. Thus the convective heat transfer would be negligible compared to the total heat

transfer. This means that convective heat transfer in the gas phase can effectively be ignored, and sensible heat transfer can be described by the conduction heat transfer coefficient in equation (2.9).

Sufficient heat must be supplied to the membrane surface to provide the latent heat requirements as well as the heat loss by conduction across the membrane. These heat flows can be added linearly [2.2] to give the total heat flux

$$Q'' = Q''_v + Q''_c$$

$$= (h_c + h_v)\, \Delta T_m \qquad\qquad (2.11)$$

Typical heat fluxes observed in MD are in the range 2000 to 30000 W/m^2.

2.1.3 Liquid Film Heat Transfer

The need to supply heat to one side of the membrane and remove heat from the other side requires temperature gradients in the liquid films bounding the membrane. This is referred to as "Temperature Polarisation", which will be discussed in chapter 4. A temperature profile for MD is depicted in figure 2.1, showing such temperature gradients. If the temperature drops across the liquid films are a significant portion of the total temperature drop, the system is said to exhibit bad temperature polarisation.

Heat transfer to and from the membrane is described by the two film heat transfer coefficients h_f and h_p, as shown in figure 2.2. The magnitude of these coefficients is dependent on the membrane module geometry and the fluid flow characteristics.

The equation for heat flux in the liquid boundary layers is simply

$$Q'' = h_f \ (T_f - T_{fm}) = h_p \ (T_{pm} - T_p) \qquad (2.12)$$

For the experimental studies described in chapters 4 and 6, the film heat transfer coefficients were approximately equal on either side of the membrane. This meant that they could be combined in an overall film heat transfer coefficient, h, where

$$h = (1/h_f + 1/h_p)^{-1} \qquad (2.13)$$

allowing equation (2.12) to be written

$$Q'' = h \ (\Delta T_b - \Delta T_m) \qquad (2.14)$$

where ΔT_b is the bulk temperature difference, and ΔT_m is the trans-membrane temperature difference. For the case where h_f and h_p are equal, the average membrane temperature is equal to the average temperature of the bulk streams.

For the case where h_f and h_p are not equal, the temperature difference between the bulk and the interface on the feed side can be calculated by solving equations (2.11) and (2.12), giving

$$\Delta T_f = \Delta T_b \ \frac{1/h_f}{1/(h_v + h_c) + 1/h_f + 1/h_p} \qquad (2.15)$$

The same equation may be used for the temperature drop on the permeate side by interchanging the subscripts f and p.

Methods of evaluating film heat transfer coefficients for various MD

configurations will be detailed in chapter 4. Conventional film heat transfer theory is applicable, despite the occurrence of simultaneous mass transfer. The effect of mass flux from the boundary layer into the membrane can be described by a convective heat transfer term. The ratio of this convective term to conduction within the laminar boundary layer can again be evaluated using the Peclet number (equation (2.10)). The thermal conductivity of water at 60 °C is k = 0.65 W/mK, and the heat capacity is C_p = 4180 J/kgK. For a boundary layer thickness of 100 μm (which is high [2.7]), and a flux of 50 kg/m^{2}h, the Peclet number is Pe = 0.01, indicating that the contribution of this convective term is negligible.

The presence of solute in the feed can have a significant effect on film heat transfer, through the dependence of transport properties on solute concentration. This will be discussed in chapter 7.

2.2 MASS TRANSFER

Mass transfer in MD occurs by convective and diffusive transport of water vapour across the microporous membrane. The driving force for mass transfer is the difference in water vapour pressure on either side of the membrane. Resistance to mass transfer comes from both the membrane structure, and the presence of air trapped within the membrane. Solute in the feed also affects mass transfer through vapour pressure reduction and concentration polarisation. The theory behind these concepts is developed below.

2.2.1 Gas Permeation Models

The three gas permeation models relevant to MD are molecular diffusion,

Knudsen diffusion, and Poiseuille flow. These three mechanisms are illustrated in figure 2.4, and are discussed below.

In most situations, the dominant mechanism of water vapour flux across MD membranes is molecular diffusion through the air trapped within the membrane. Air enters the system as dissolved air in the feed and establishes a steady state partial pressure within the membrane pores. This air is continually removed by dissolving in the distillate (or feed), however the solubility is so low (typically 10 ppm) that the air flux is negligible compared to the water flux. For example, the permeate production rate (flux × area) is typically between 1 and 5% of the feed and permeate recirculation rates. The capacity of the permeate to dissolve air, however, is only 0.001% (10 ppm) of the permeate recirculation rate, hence the flux of water vapour is at least 1000 times the flux of air. Accordingly, the air establishes a pressure gradient opposing the flux of water vapour. The negligible flux of air means that for theoretical purposes, the air can be considered as a stationary film.

The equation for steady-state diffusion of water through a stationary film of air is [2.9]

$$J = \frac{1}{P_{aM}} \frac{DPM}{RT} \frac{\Delta P}{\delta} \qquad (2.16)$$

where P_{aM} is the logarithmic mean pressure of air, and D is the binary diffusion coefficient. For the case of diffusion through isotropic porous materials, the effective diffusion coefficient is $D_{eff} = D\epsilon/\chi$ [2.9], accounting for the membrane porosity, ϵ, and tortuosity, χ. It should be remembered that porosity may vary across the membrane, and that an average value is normally used. The tortuosity, χ, is often
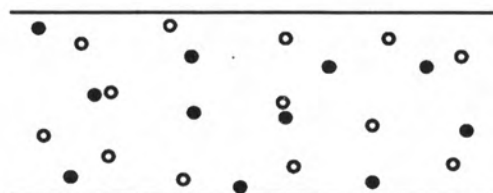
Figure 2.4 : Three gas permeation mechanisms.

determined   by   fitting   an   equation   such   as   equation   (2.16)   to
experimental results. The value of χ usually lies between 1 and 4. In
chapter 6, χ=2 was found to give good agreement between experimental and
predicted results.

Equation (2.16) can be simplified by replacing the logarithmic mean air
pressure with the geometric mean air pressure. This simplification is
reasonable provided the ratio of downstream to upstream air pressure is
less than 2 (4% error). At low pressures of air this is not the case,
however at low pressures of air molecular diffusion is not the
controlling mechanism (see chapter 6), hence the simplification can be
tolerated. The molecular diffusion equation can therefore be written

$$ J = \frac{1}{P_a} \; \frac{\epsilon}{\chi\delta} \; \frac{DPM}{RT} \; \Delta P \qquad\qquad (2.17) $$

$$ \equiv \frac{d}{P_a} \; \Delta P $$

where P_a is the geometric mean pressure of air, and **d** accounts for the
diffusion coefficient and membrane pore geometry. The parameter **d** is
not pressure dependent, as the product of D and P is a constant at low
pressures. The diffusion coefficient, D, is dependent on temperature to
the power 2.3 [2.1] making **d** dependent on $T^{1.3}$. Most MD systems operate
with an average membrane temperature between 310 and 350 K. If D is
evaluated at 330 K, the error in **d** over the temperature range of
interest is only 5%.

Equation (2.17) is not sufficient to model MD fluxes under all
conditions, as it predicts infinite flux for a totally deaerated
membrane. Clearly this is not the case. As the partial pressure of air
is decreased, the resistance imposed by the microporous structure

becomes increasingly important.

The mechanism of water vapour flux through a deaerated MD membrane depends on the mean free path of the water molecules relative to the membrane pore size. If the mean free path of the gas is much less than the pore size, then the dominant flux mechanism is viscous or Poiseuille flow. If the mean free path is much greater than the pore size, then Knudsen diffusion is the dominant mechanism [2.10]. These mechanisms are illustrated in figure 2.4. The mean free path of water vapour at 25 kPa and 25°C is 0.18 μm, compared to pore sizes of 0.1 to 0.5 μm for microporous membranes. This implies that water vapour flux through deaerated MD membranes falls in the transition region between Knudsen diffusion and Poiseuille flow.

A third mechanism encountered in gas permeation is surface diffusion, whereby gas molecules adsorb on the membrane walls and diffuse under a pressure gradient. This mechanism would not be expected for water vapour permeation through hydrophobic materials for the following reason. If linear temperature and pressure gradients are assumed across the membrane, then the water vapour is below its dew point temperature (see figure 2.3) at any point across the membrane. Condensation will not occur, however, unless there is a nucleating surface. If there was an adsorbed layer of water molecules on the pore walls, this would provide a surface for condensation, and membrane wetting would occur.

Knudsen diffusion is a gas flux mechanism whereby gas molecules under a pressure gradient pass across a porous structure by a series of molecule/wall collisions. For gas permeation through an isotropic, microporous membrane the Knudsen diffusion equation may be written [2.11]

$$J = \frac{2}{3} \frac{r\epsilon}{\chi} \left\{ \frac{8RT}{\pi M} \right\}^{\frac{1}{2}} \frac{M}{RT} \frac{\Delta P}{\delta} \tag{2.18}$$

where r is the pore radius, and $(8RT/\pi M)^{\frac{1}{2}}$ is the mean molecular speed.

The Poiseuille flow model describes viscous flow of a gas through a porous structure. For flow through a microporous membrane, the Poiseuille flow equation may be written

$$J = \frac{1}{8} \frac{r^2\epsilon}{\chi} \frac{1}{\eta} \frac{MP}{RT} \frac{\Delta P}{\delta} \tag{2.19}$$

where η is the viscosity of the gas.

There are many models in the literature for describing the Knudsen/Poiseuille transition region. Most of these involve a combination of equations (2.18) and (2.19), however some, such as the "Dusty Gas" model [2.11], were derived independently. A review of these models is given in chapter 5, where the issue of gas permeation is addressed in more detail.

For this study, a semi-empirical equation was formulated to describe the Knudsen/Poiseuille transition region. Emphasis was placed on simplicity, as well as recognisable physical significance of the adjustable parameters. Inspection of equations (2.18) and (2.19) revealed that in Knudsen diffusion, $J \propto \Delta P$, while in Poiseuille flow, $J \propto P\Delta P$. This lead to the equation

$$J = a\wp^b \, \Delta P \tag{2.20}$$

$$0 \le b \le 1$$

where $\wp$ = dimensionless pressure = P/P_{ref}

a = Membrane permeation constant

b = fraction of permeability arising from viscous effects

= 0 for Knudsen diffusion

= 1 for Poiseuille flow

The reference pressure, P_{ref}, is a typical or average water vapour pressure for the system, for example 25 kPa for low temperature MD. The membrane permeation constant, **a**, is simply the proportionality between flux and pressure drop at the reference pressure. The exponent, **b**, indicates the extent to which viscous effects control the process. For example, if Knudsen diffusion is slightly dominant, **b** may have a value of 0.3. The derivation of equation (2.20) is given in chapter 5.

Equation (2.17) is applicable to aerated MD systems, while equation (2.20) applies to fully deaerated systems. For partially deaerated systems, as would often be the case, a combination of the two mechanisms is required. As the two mechanisms are essentially independent, the approach used here is to add the resistances imposed by both models, giving

$$J = \left\{ \frac{1}{a\wp^b} + \frac{P_a}{d} \right\}^{-1} \Delta P \tag{2.21}$$

Thus three parameters, **a**, **b** and **d**, are required to predict MD fluxes at any air pressure, P_a, remembering that $\wp$ and ΔP refer to water vapour pressures only.

2.2.2 Solute Effects

In many membrane processes, the concentration of solute in the feed dictates the system performance. This is not the case in MD. For the purposes of this discussion, only non-volatile solutes in the feed will be considered.

The major effect that feed solute has in MD is to reduce the vapour pressure at the evaporating surface. Vapour pressure reduction is a colligative property, and for dilute solutions obeys Raoult's law [2.6]

$$P = (1-x) \ P^\circ \tag{2.7}$$

where x is the mole fraction of solute and P° is the vapour pressure of pure water at that temperature. Vapour pressure reduction by solute means that if the trans-membrane temperature difference is less than a threshold temperature, ΔT_{th}, then flux will be from the permeate to the feed. The threshold temperature can be calculated by solving equations (2.6) and (2.7), giving

$$\Delta T_{th} = \frac{RT^2}{M \Delta H_v} \frac{x}{1-x} \tag{2.22}$$

For example, according to equation (2.22), a 1 M (5.6 wt%) salt solution at 60 °C has $\Delta T_{th} = 0.4$ °C. (N.B. deviation from ideality (see chapter 7) increases this value to around 0.7 °C.) Thus threshold temperature differences become important at high concentrations when low driving forces are used.

For concentrated solutions, equation (2.7) does not hold, and vapour pressures must be determined from experimental results or published

data. As an example, the vapour pressures of NaCl solutions are
discussed in chapter 7.

As with other membrane processes, concentration polarisation results in
the wall (or interfacial) concentration being higher than the bulk
concentration. The film model for concentration polarisation (using MD
notation) is [2.12]

$$J = \rho \, k_s \, \ln \, (c_{fm}/c_f) \qquad\qquad (2.23)$$

where ρ is the density of water, k_s is the solute mass transfer
coefficient in the feed, and c_{fm} and c_f are the concentrations of solute
at the interface and in the bulk feed respectively.

The presence of solute in the feed also alters the fluid dynamics
through density and viscosity, and influences heat transfer through
thermal conductivity and heat capacity. In some situations, these
effects are greater than the vapour pressure reduction, as will be
discussed in chapter 7.

2.3 COMBINED HEAT AND MASS TRANSFER

For most applications of MD, combination of the heat and mass transfer
equations is sufficiently complex to justify computer modelling and
iterative solutions, rather than direct solution of the equations.
Computer modelling of MD systems is discussed in Appendix C. For the
system studied in chapter 6, however, direct solution was possible as
the feed and permeate film heat transfer coefficients were equal, and
there was no solute in the feed. For this simplified case, the heat and
mass transfer equations can be combined to give

$$J = \frac{h_v}{\Delta H_v} \frac{h}{h_v + h_c + h} (T_f - T_p) \qquad (2.24)$$

where $h = (1/h_f + 1/h_p)^{-1} \equiv h_f/2$

$$h_v = \Delta H_v \frac{dP}{dT} \left\{ \frac{1}{a\rho^b} + \frac{P_a}{d} \right\}^{-1}$$

$$h_c = (\epsilon k_g + (1-\epsilon)k_s) / \delta$$

In chapter 4, this equation was further simplified, as the focus of attention was heat transfer. For this purpose, h_v was simplified to

$$h_v = \Delta H_v \, C \, \frac{dP}{dT} \qquad (2.25)$$

This was found to give reasonable accuracy for the fully aerated system used in chapter 4.

2.4   WATER ENTRY PRESSURE

The essence of MD is that the membrane allows the passage of gases and vapours, but prevents the passage of liquids. This utilizes the fact that some polymers are hydrophobic, for example polypropylene, polyvinylidene difluoride (PVDF), and polytetrafluoro ethylene (PTFE). For a microporous, hydrophobic membrane, the pressure needed to force liquid water into the dry membrane can be calculated from the capillary equation

$$P_{liq} - P_{gas} = \frac{2 \, \sigma \, \cos \theta}{r} \qquad (2.26)$$

where σ is the liquid surface tension, and θ is the contact angle. This is illustrated in figure 2.5. For most commercial microporous
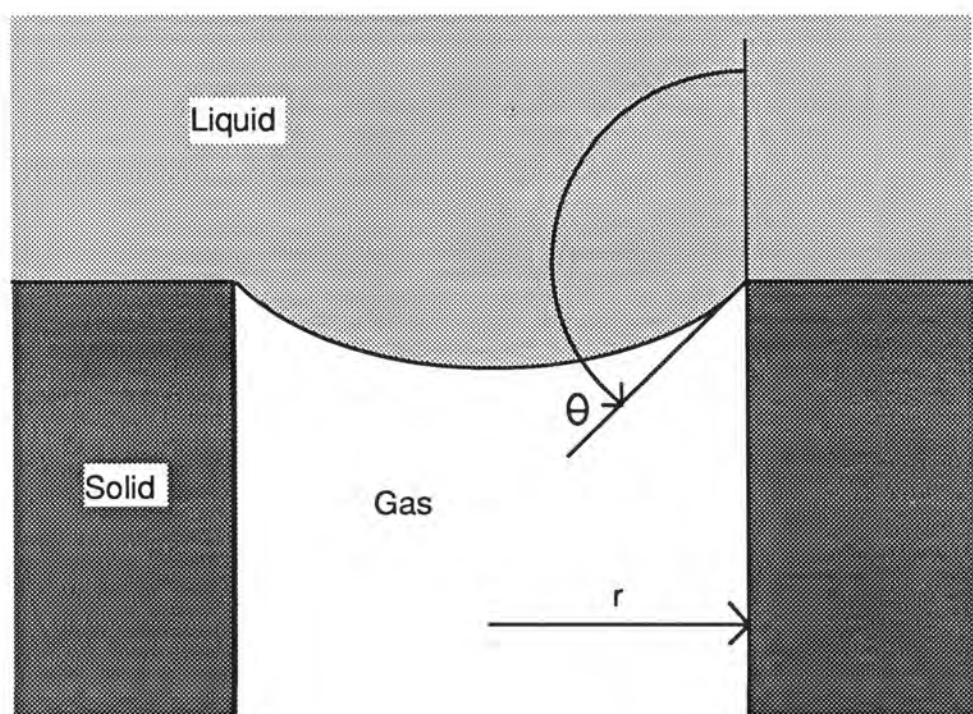
Figure 2.5 : Water entry pressure concept.

hydrophobic membranes, the water entry pressure is above 200 kPa.

In practice, the water entry pressure evaluated from equation (2.25) is not appropriate. The presence of surfactants in low concentrations, or organics in low to medium concentrations [2.13] will reduce the contact angle leading to membrane wetting. Salts in high concentrations have also been observed to have an effect. The phenomenon of membrane wetting has not been studied fully, however some evidence and discussion is given in chapter 7.

2.5 NOTATION

a   Membrane permeability constant $[kg \ m^{-2} \ s^{-1} \ Pa^{-1}]$

b   Exponent defined in equation (2.20) [-]

c   Concentration $[kg \ m^{-3}]$

C   Membrane mass transfer constant $[kg \ m^{-2} \ s^{-1} \ Pa^{-1}]$

C_p Heat capacity $[J \ kg^{-1} \ K^{-1}]$

d   Membrane molecular diffusion constant $[kg \ m^{-2} \ s^{-1}]$

D   Diffusion coefficient $[m^2 \ s^{-1}]$

h   (Overall film) Heat transfer coefficient $[W \ m^{-2} \ K^{-1}]$

ΔH_v Latent heat of vaporisation $[J \ kg^{-1}]$

J   Mass flux through membrane $[kg \ m^{-2} \ s^{-1}]$

k   Thermal conductivity $[W \ m^{-1} \ K^{-1}]$

k_s Solute mass transfer coefficient $[m \ s^{-1}]$

M   Gas molecular weight $[kg \ mol^{-1}]$

P   Water vapour pressure [Pa]

P_a Partial pressure of air [Pa]

Pe   Peclet number [-]

P°   Vapour pressure of pure water [Pa]

ΔP Water vapour pressure drop across membrane [Pa]

$\wp$ Dimensionless pressure $= P/P_{ref}$ [-]

Q'' Heat flux [W m^{-2}]

r   Pore radius [m]

R   Gas constant [J mol^{-1} K^{-1}]

T   Temperature [K,°C]

x   Mole fraction of solute [-]

δ Membrane thickness [m]

ϵ Membrane porosity [-]

η Gas viscosity [Pa s]

θ Contact angle [Rad]

ρ Density [kg m^{-3}]

σ Surface tension [N m^{-1}]

χ Membrane tortuosity [-]

Subscripts

a   Air

b   Bulk

c   Conduction

f   Feed

g   Gas

liq   Liquid

m   Membrane

M   Logarithmic mean

p   Permeate

s   Solid

th   Threshold

v   Vapour

2.6 REFERENCES

[2.1] Bird, R.B., Stewart, W.E. and Lightfoot, E.N., "Transport Phenomena", Wiley & Sons, New York, 1960.

[2.2] Treybal, R.E., "Mass Transfer Operations", 2nd ed., McGraw-Hill, 1968.

[2.3] Weast, R.C. (ed.), "Handbook of Chemistry and Physics", 57th ed., CRC Press, Cleveland, Ohio.

[2.4] Foust, A.S., et. al. "Principles of Unit Operations", 2nd ed., Wiley & Sons, New York, 1980.

[2.5] Smith, J.M., and van Ness, H.C., "Introduction to Chemical Engineering Thermodynamics", 3rd ed., McGraw-Hill, 1975.

[2.6] Barrow, G.M., "Physical Chemistry", 2nd ed., McGraw-Hill, 1966.

[2.7] Holman, J.P., "Heat Transfer", 5th ed., McGraw-Hill, 1981.

[2.8] Perry, R.H. and Chilton, C.H., "Chemical Engineer's Handbook", 5th ed., McGraw-Hill, 1974.

[2.9] Sherwood, T.K., Pigford, R.L., and Wilke, C.R., "Mass Transfer", McGraw-Hill, New York, 1975.

[2.10] Present, R.D., "The Kinetic Theory of Gases", McGraw-Hill, 1958.

[2.11] Evans, R.B., Watson, G.M., Mason, E.A., "Gaseous Diffusion in Porous Media. II. Effect of Pressure Gradient", J. Chem. Phys., 36(7) (1962) 1894-1902.

[2.12] Porter, M.C., "Concentration Polarisation with Membrane Ultrafiltration", Ind. Eng. Chem. Prod. Res. Develop., 11(3) (1972) 234-248.

[2.13] Franken, A.C.M., "Membrane Distillation - A New Approach Using Composite Membranes", Ph.D. Thesis (1988), University of Twente, The Netherlands.

Chapter 3

Experimental Modules

CHAPTER 3: EXPERIMENTAL MODULES

Membrane distillation is unlike any other membrane process. The need to
supply heat to one side of the membrane and remove heat from the other
side requires high heat transfer coefficients in the liquid films
bounding the membrane. If these film heat transfer coefficients are low,
an experimental study of MD is dominated by temperature polarisation,
and yields little information on the membrane-controlled aspects of the
process. This chapter examines the suitability of "standard" membrane
cells for MD experiments, and explains the designs of the sheet membrane
and hollow fibre membrane modules used throughout this study.

3.1 STANDARD EXPERIMENTAL MEMBRANE MODULES

Membrane processes such as reverse osmosis, ultrafiltration and dialysis
have been studied in the laboratory for several decades. Experimental
membrane apparatuses have evolved to suit the needs of each individual
study, and several standard designs have dominated due to their balance
of simplicity and effectiveness. Early work done on membrane
distillation used modifications of these standard membrane cells,
however in most cases they were found to be inappropriate. The merits of
stirred cells, cross flow cells and shell and tube modules are discussed
below.

3.1.1 Stirred Cells

The standard sheet membrane cell for the filtration processes is the
stirred cell. In its basic form it consists of a cylindrical cell with a
porous membrane support and a magnetic stirrer, as shown in figure 3.1.
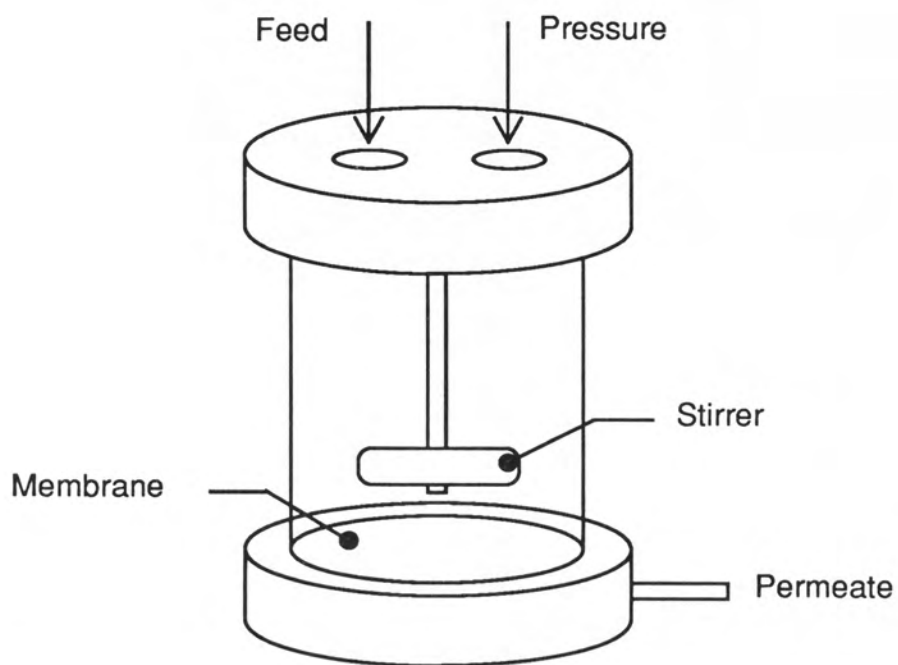The cell is fully or partly filled with the feed solution, and is

Figure 3.1 : Stirred Cell.

pressurised with compressed gas. The magnetic stirrer provides shear at the membrane surface to control cake build-up and concentration polarisation. The permeate is collected beneath the porous support.

Some early experiments in MD were done with stirred cells, however an obvious modification was required. The need for fluid shear on either side of the membrane required the use of two semi-cells, each with its own stirrer. The hot and cold solutions were either heated in situ, or in external apparatus. The stirred cell MD apparatus had two major problems. Firstly, the membrane was unsupported, hence the volume in each semi-cell was not fixed, complicating flux measurement. A more important problem, however, was that stirred cells do not provide sufficient shear rates to give adequate heat transfer.

Film heat transfer coefficients for stirred cells have been estimated, as detailed in chapter 4. The results show that even at high stirrer speeds, the individual film heat transfer coefficients are low (typically less than 2000 W/m^2K). Sarti [3.1] reported that in unstirred cell experiments, the flux was five times higher when the hot solution was in the bottom semi-cell than in the top. This suggests that unforced convection, for example by roll cells, played a major part in the heat transfer. In this study, stirred cells were not used for MD experiments.

3.1.2 Cross Flow Cells

A second class of experimental sheet membrane cells is the cross flow cell. In this apparatus, the membrane is exposed to a shear field by flowing fluid across the membrane surface. The concept is illustrated in Figure 3.2. Generally, the feed is recirculated, and the shear rate is varied by adjusting the channel height and feed flow rate. This makes it
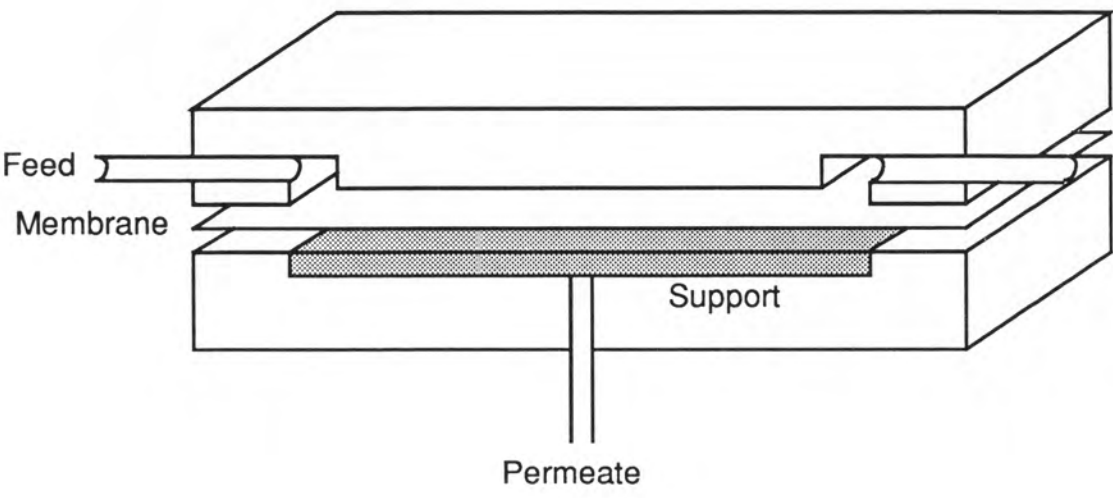
Figure 3.2 : Cross flow cell.

easy to achieve either turbulent or laminar flow.

As with the stirred cell, the basic cross flow cell only addresses one side of the membrane. Unlike the stirred cell, however, the cross flow cell cannot be operated with two semi-cells and an unsupported membrane. Such a system is unstable as it is impossible to balance the pressures on either side of the membrane.

The cross flow cell concept can be modified to suit MD. Four appropriate semi-cell designs are shown in figure 3.3. In semi-cell A, the feed is recirculated and heated/cooled prior to entering the module. In semi-cell B the same occurs, however there is a rigid support for the membrane. A thin sheet of sintered stainless steel with a 50 μm pore size and 35 % porosity is ideal for this task, as the conductivity of the metal reduces the temperature drop across the support. Semi-cell C is jacketed with a heating/cooling fluid compartment. Provided the flow rate of the heating/cooling fluid is high, this eliminates temperature gradients in the direction of feed flow. Semi-cell D is the same, however with a porous support or spacer material, and no recirculation of the feed/permeate. If the porous spacer is removed from semi-cell D, this becomes the laboratory equivalent of the early Gore-tex [3.2] system, which has been studied independently in the laboratory [3.3] with a membrane cell made up of A and D semi-cells.

The various semi-cells in figure 3.3 can be mixed and matched depending on the requirements. The jacketted cells simplify interpretation of results by eliminating temperature gradients in the direction of flow, however they add an extra source of temperature polarisation. In this study, a combination of cells A and D has been used to study concentration polarisation effects, while various configurations of C
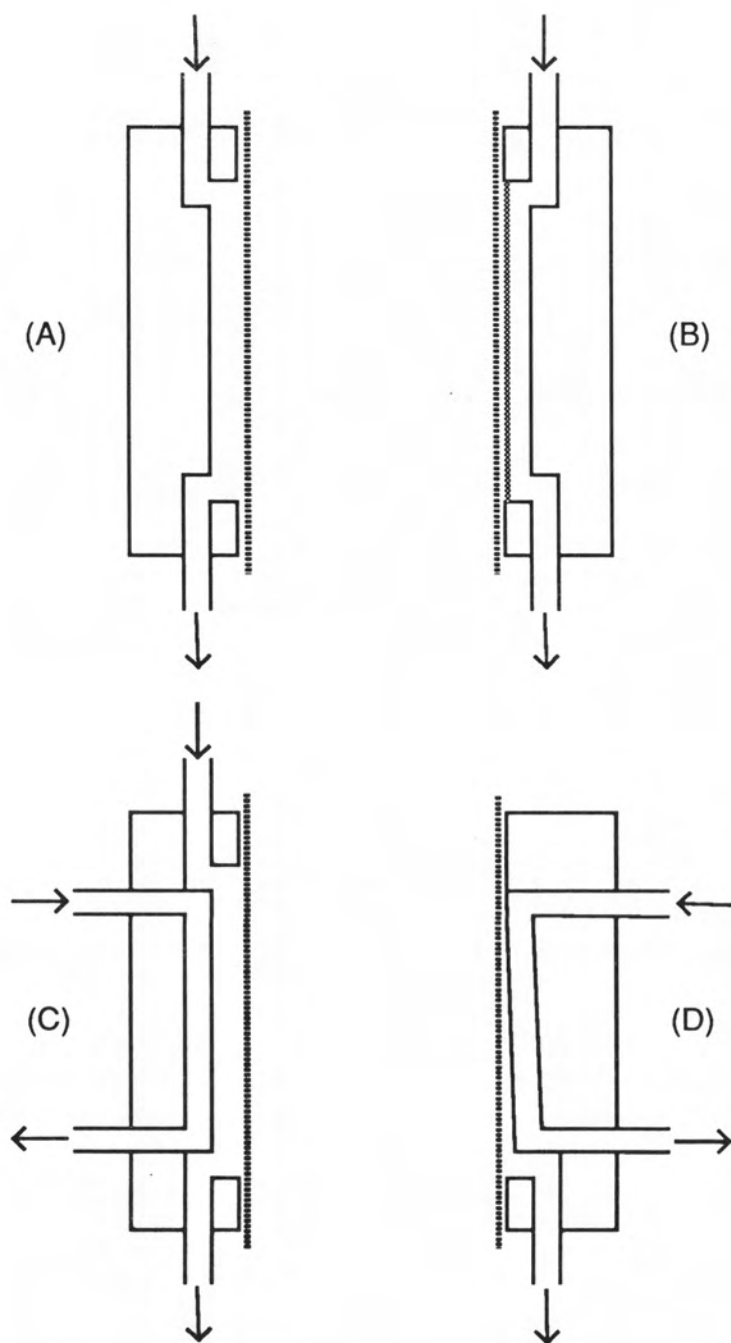
Figure 3.3 : Variations of cross flow cells.

and D have been used for studying membrane permeabilities and other MD transport processes.

3.1.3   Shell and Tube Modules

The standard membrane apparatus for studying hollow fibre or tubular membranes is the shell and tube module. This is similar in design to the shell and tube heat exchanger, and is shown in figure 3.4. Tubular membranes have an advantage over sheet membranes in that they do not require a support. In an industrial situation this means that higher temperature polarisation coefficients can be achieved with tubular membranes than with sheet membranes, as will be detailed in chapter 4. In the laboratory, however, tubular membranes have the disadvantage that they cannot be easily replaced in a module. Most sheet membrane apparatuses allow for membrane replacement, while most tubular membrane modules are limited to the life time of the membrane.

The requirements of a shell and tube module for MD are different from those for other membrane processes. The major difference is the need for high shear rates on either side of the membrane. In general, the tube side has excellent flow characteristics, as the fluid flow is evenly distributed among the fibres within the bundle. Problems are encountered, however, in achieving even flow distribution on the shell side.

The major cause of poor flow characteristics on the shell side is channelling. This occurs when the fibres have sufficient mobility to open up a clear channel along the length of the module. If this occurs, most of the feed flows along the channel and never comes into contact with the membrane. One method of reducing channelling is to plait or
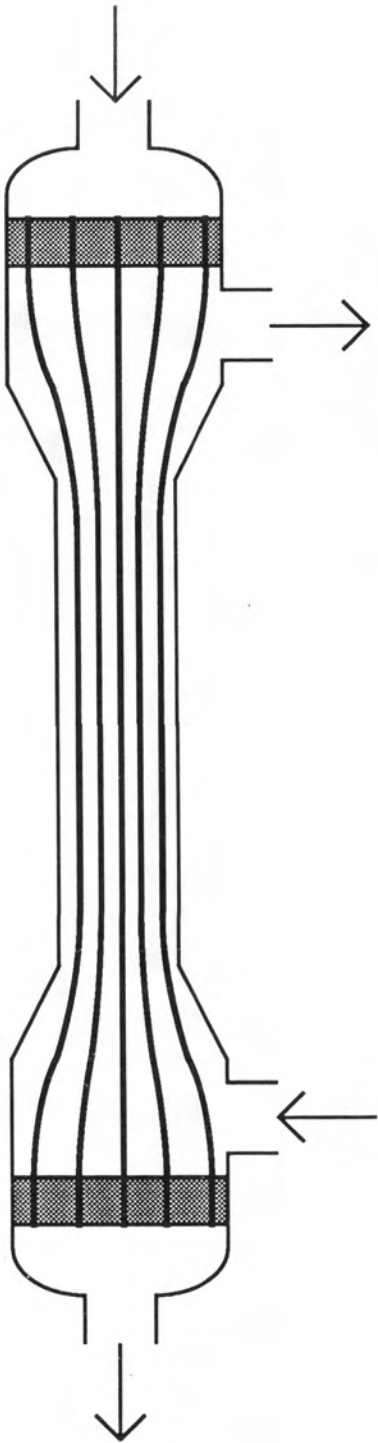
Figure 3.4 : Shell and tube module

braid or weave the fibres to reduce their mobility [3.4]. This not only prevents chanelling, but induces turbulence to counter temperature polarisation. Another method of preventing channelling is to pack the fibres tightly into the shell. If the fibres have an appropriate ratio of inside to outside diameter, the hydraulic diameter will be the same on either side of the membrane resulting in good shell side fluid dynamics, as shown in figure 3.5. This effect can be achieved with minor modifications to most commercial shell and tube modules. The module ends remain the same, while the tubular section of the shell is reduced in diameter until the fibres are tightly packed. The fibres must be sufficiently splayed at the ends of the module to allow easy fluid access to the entire tube bundle.

Shell and tube modules are not well suited to small scale laboratory experiments. The need to recirculate both feed and permeate means that flux must be determined by incremental changes in the feed or permeate reservoir volumes. Also permeate composition cannot be analysed directly, as it is continually mixed with the recirculated volume. In contrast, in a jacketted sheet membrane apparatus, as shown in figure 3.3 (D), permeate flux is directly measured by the permeate leaving the module. Hence, in this study, tubular membranes were not used for studying the fundamental aspects of MD. The use of hollow fibre membranes in the pilot plant study will be discussed in chapter 8. In the following section, details are given of a laboratory scale hollow fibre MD module that allows replacement of the membranes and variation of the shell side flow cross-section.

Good shell side
fluid dynamics

Poor shell side
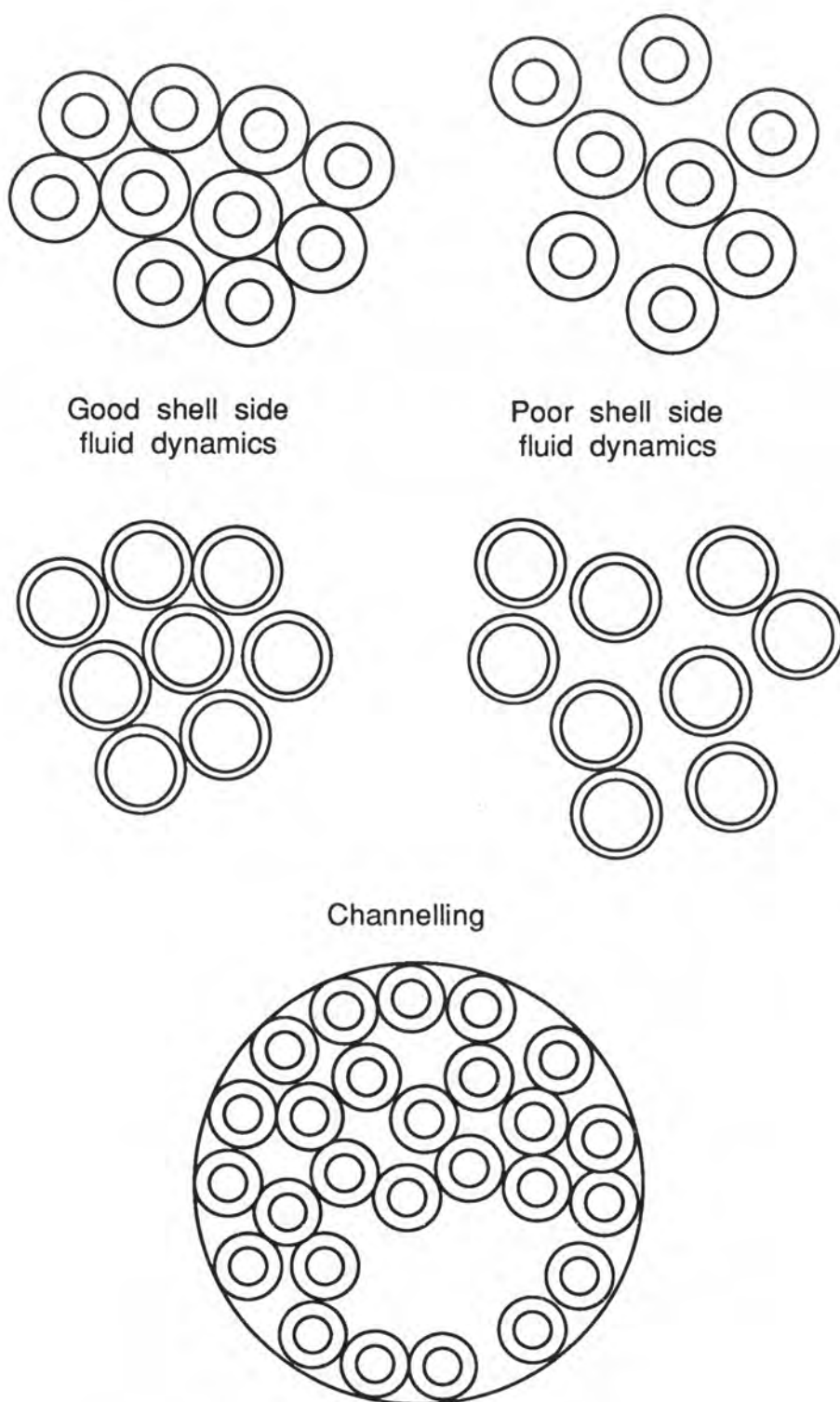fluid dynamics

Channelling

Figure 3.5 : Flow around tube bundles

3.2 EXPERIMENTAL MD MODULES USED IN THIS STUDY

The experimental MD cell used for studying membrane transport properties is depicted in figure 3.6. Basically, the cell is a cylindrical jacketted cross flow cell, with the major design objectives being to minimise temperature polarisation, and to provide an even temperature over the entire surface of the membrane. The operation of the cell is as follows. The membrane is bounded on either side by a thin film of feed or permeate. These liquid films are in turn bounded by thin stainless steel walls which are heated or cooled by jets of heating or cooling water. Feed flow is only sufficient to prevent solute build-up, and the permeate may be either recirculated or dead-end. In the latter case the rate at which permeate leaves the cell determines the flux.

The feed and permeate flow channels are specifically designed to minimise temperature polarisation. The basic concept is to minimise the gap between the stainless steel walls and the membrane. This gap is controlled by a suitable spacer material. For experiments done with concentrated solutions as the feed, a non-woven polyester support material with a thickness of 100 μm was used for the spacer. For experiments done with water as the feed, one or more layers of hydrophilic tissue were used for the spacer. An identical spacer was used on the permeate side for the sake of symmetry. To ensure that the feed has easy access to the entire membrane surface, concentric grooves emanate from a single radial groove as shown in figure 3.6. This is also shown in a photograph in Appendix A, figure A.2. This flow distribution network ensures that feed must only permeate along 1 mm of the spacer material to reach any part of the membrane surface. The dimensions of the grooves are such that only a small percentage of the membrane area is exposed to these localised regions of higher temperature
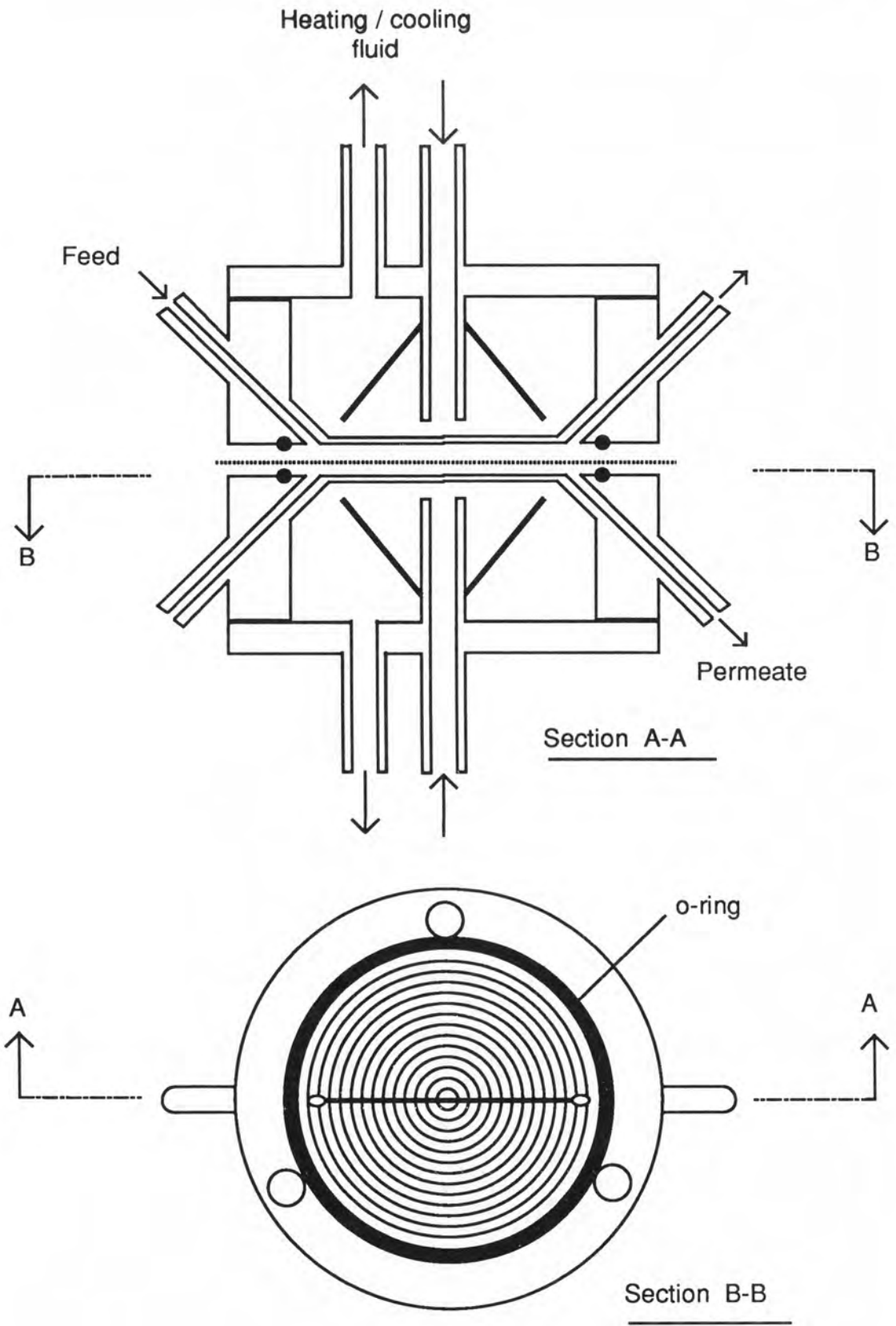
Heating / cooling
fluid

Feed

Permeate

Section A-A

o-ring

A   A

B   B

Section B-B

Figure 3.6 : Sheet MD cell (actual size).

Flow in the heating and cooling jackets is designed to provide even heat transfer over the entire area of the membrane. A jet of fluid is aimed at the centre of the cylindrical cell. Conical baffles ensure that the fluid radiates to the circumference of the cell before returning to the thermostated reservoir. The observation that a 50% reduction in the heating fluid flow rate gives no detectible drop in flux indicates that heat transfer in the heating and cooling fluids does not limit the process. A quantitative appraisal of temperature polarisation in this module is given in chapter 4.

A second MD cell was used for the study of solute effects in MD. The major design criteria for this cell were to minimise temperature polarisation on the permeate side of the membrane, and to provide well defined flow characteristics on the feed side. The cell used is shown in figure 3.7. The operation of the cell is as follows. The recirculated feed is heated prior to entering the cell. Headers, or distribution channels, ensure that the feed flow is evenly distributed across the width of the membrane. The channel height and width are adjusted by inserting different gaskets, and the feed flow rate is adjusted to give the desired Reynolds number. Permeate condenses on a stainless steel plate which is cooled by recirculating cooling water. A thin layer of spacer material, for example tissue, allows permeate to flow to the central exit tube. Turbulence promoters in the cooling water channel ensure high heat transfer rates. The module dimensions are given in chapter 7.

A third MD module was designed to study tubular and hollow fibre membranes. The design criteria were to allow replacement of the membranes, and variation of the shell side flow cross-section. The module design is shown in figure 3.8, and a photograph is included in
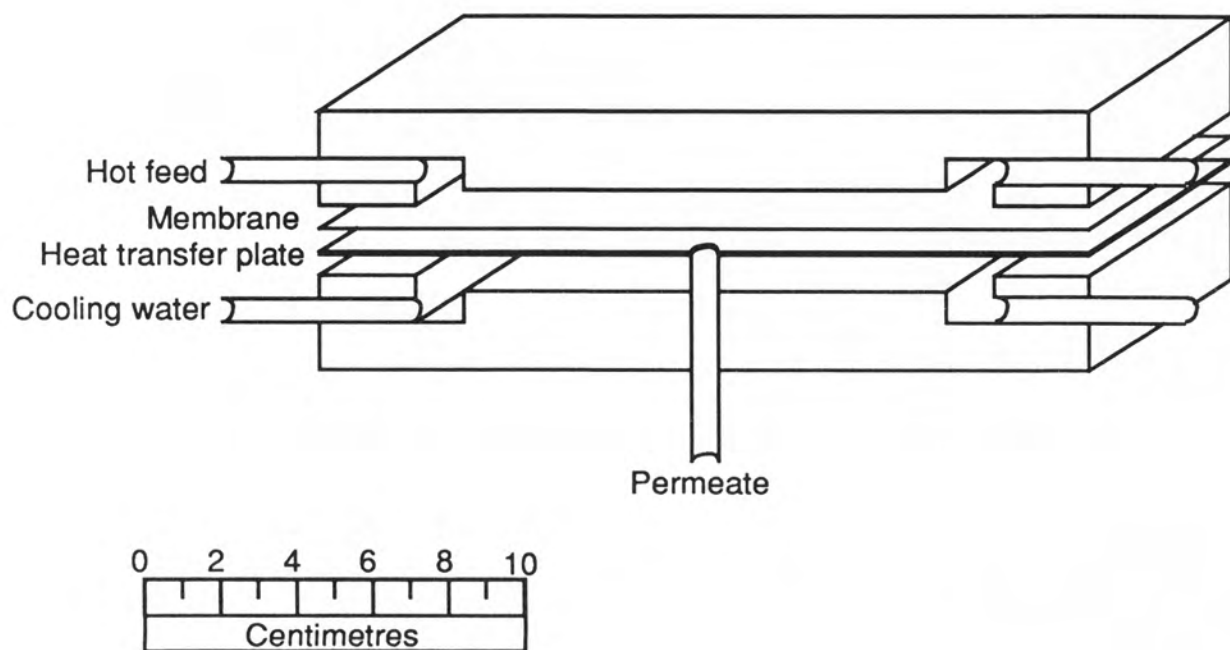
Figure 3.7 : Cross flow MD cell.
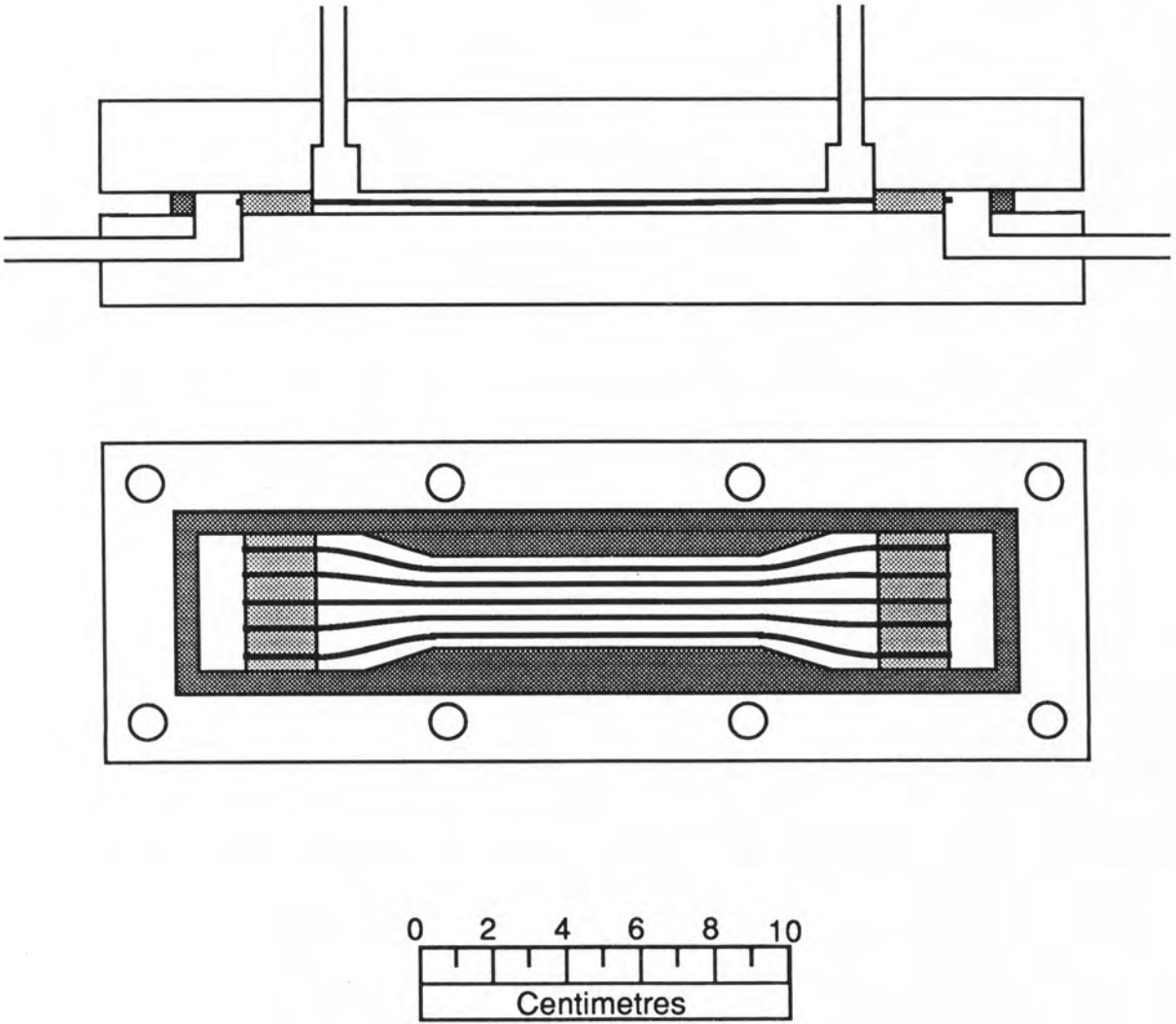
Figure 3.8 : Cross flow hollow fibre membrane cell.

Appendix A, figure A.3. In its usual operation, the feed flows down the
fibre lumen, while permeate is recirculated through the shell. A rubber
gasket separates the two halves of the cell, and   determines   the   shell
side width and thickness. The membrane fibres are "potted" at either end
using, for example, silicone rubber. Silicone rubber   will   bond
reasonably well to the rubber gasket, but not to the cell walls, hence
the gasket can be removed complete with the potted fibres. Modifications
can   then be made to the gasket to increase or decrease the channel
width, with all else remaining equal. Thus   the   effect   of   shell   side
packing density can be studied. When desired, the membranes, with or
without the gasket, can be removed and replaced. This apparatus is also
suited to the study of braided or woven membrane configurations.

The   module   shown   in figure 3.8 is constructed of poly(methyl
methacrylate) (perspex or plexiglass) to allow visual inspection of the
fibres during operation. Thus the presence of channelling can be
detected. This material limits its operation to 60 - 70 °C. For higher
temperature studies, an alternative material must be used.

3.3 REFERENCES

[3.1]   Sarti, G.C., et.al., "Low Energy Desalination Process using
        Hydrophobic Membranes", Desalination, 56 (1985) 277-287.

[3.2]   Gore, D.W., "Gore-Tex Membrane Distillation", Proc. 10th Ann.
        Conv. Water Supply Improvement Assoc., Honolulu, July 1982.

[3.3]   Hanbury, W. and Hodgkiess, T., "Membrane Distillation - an
        Assessment", Desalination, 56 (1985) 287-298.

[3.4] Schneider, K. et. al., "Membranes and Modules for Transmembrane

       Distillation", Journal of Membrane Science, 39(1) (1988) 25-42.

Chapter 4

Heat
Transfer
in
Membrane
Distillation

CHAPTER 4: HEAT TRANSFER IN MEMBRANE DISTILLATION

Membrane distillation is a process largely controlled by heat transfer. In chapter 2, fundamental aspects of heat transfer were discussed, and equations were developed that are generally applicable to MD. The emphasis in this chapter is on the engineering aspects of heat transfer. Equations are developed for determining heat transfer coefficients from experimental results, for predicting the performance of various module designs, and for assessing the energy efficiency of MD systems. An experimental study quantifies the heat transfer processes that dominate MD, leading to a better understanding of the capabilities and limitations of MD.

4.1 THEORY

4.1.1 Fundamental Heat Transfer Theory

In chapter 2, heat transfer processes in MD were depicted using an electrical analog. This representation is reproduced in figure 4.1. Basically, film heat transfer coefficients, h_f and h_p, describe heat flows to and from the evaporating and condensing surfaces, while vapour and conduction heat transfer coefficients, h_v and h_c, describe the heat transfer associated with vapour flux and conduction across the membrane.

In section 2.3, heat transfer equations were combined with the mass transfer equation

$$J = C \; \Delta P \hspace{6cm} (4.1)$$

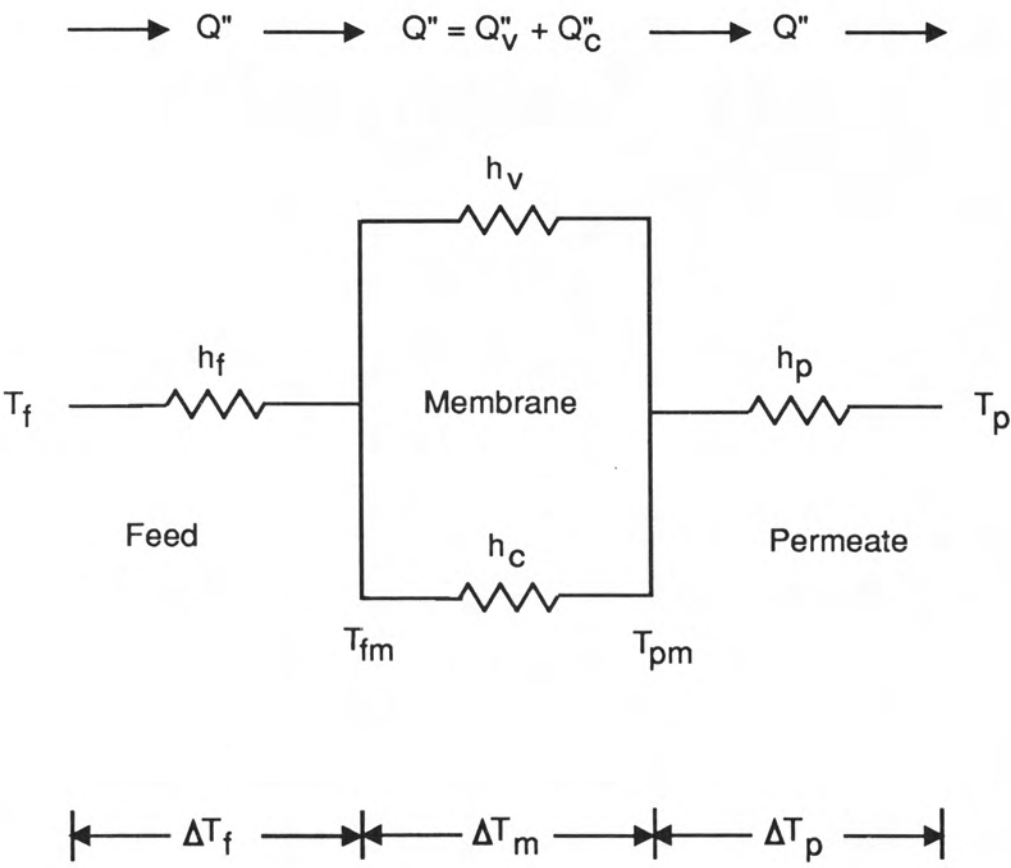While more elaborate mass transfer equations were derived in section

Figure 4.1 : Heat transfer paths in MD.

2.2, equation (4.1) was adequate for this study on heat transfer. The combined heat and mass transfer equation is

$$J = \frac{h_v}{\Delta H_v} \; \frac{h}{h_v + h_c + h} \; \Delta T_b \qquad (4.2)$$

$$\text{where} \quad h = (1/h_f + 1/h_p)^{-1} = h_f/2 \qquad (4.3)$$

$$h_v = J \, \Delta H_v \; / \; \Delta T_m = C \, \frac{dP}{dT} \, \Delta H_v \qquad (4.4)$$

$$h_c = k_m \; / \; \delta = (\epsilon k_g + (1-\epsilon)k_s) \; / \; \delta \qquad (4.5)$$

Equation (4.4) is valid for the the case where there is no solute in the feed, allowing the approximation that $\Delta P/\Delta T_m \approx dP/dT$ evaluated at the average membrane temperature. Equation (4.3) assumes that the feed and permeate heat transfer coefficients are equal, which, for this study, is justified as follows. For the jacketted cross-flow cell used (see section 3.2), the feed (or permeate) heat transfer coefficient had contributions from a jet of recirculated heating (or cooling) water, a stainless steel sheet, and a thin laminar film of feed (or permeate). Early experiments showed that reducing the heating (or cooling) water flow rate by 50% resulted in no detectable drop in flux, suggesting that the heat transfer coefficients were controlled by the thermal conductivities of the stainless steel and liquid films. The conductivity of water only varies by 5% over the temperature range 40 to 80 °C [4.1], and the conductivity of stainless steel is essentially constant over this range. Thus, for the symmetrical apparatus, the feed and permeate heat transfer coefficients were approximately equal, allowing their combination in an overall film heat transfer coefficient, $h=h_f/2$. The average membrane temperature for this case is equal to the average of the heating and cooling water temperatures, allowing the calculation of dP/dT in equation (4.4), using equations (2.5) and (2.6).

Equation (4.2) can be used to show, graphically, the effect that the film heat transfer coefficient has on flux. For a membrane with a permeability of $C = 5 \times 10^{-7}$ kg/m^{2}sPa (see section 4.4), with a constant bulk temperature difference of 10 °C, figure 4.2 shows flux as a function of average temperature for several film heat transfer coefficients. It can be seen that with low heat transfer coefficients, there is little reward for operating at high temperatures, as the process quickly becomes heat transfer limited. With high heat transfer coefficients, however, flux increases exponentially with operating temperature.

To aid in interpreting experimental results, equation (4.2) can be rearranged to give

$$\frac{\Delta T_b}{J \, \Delta H_v} = \frac{1}{dP/dT} \, \frac{1}{C \, \Delta H_v} \left\{ 1 + \frac{k_m/\delta}{h} \right\} + \frac{1}{h} \qquad (4.6)$$

In MD experiments, it is usual to report fluxes for various bulk feed and permeate temperatures. For each operating condition, dP/dT can be calculated at the average membrane temperature. For the range of operating temperatures, $\Delta T_b/J\Delta H_v$ can be plotted against $1/(dP/dT)$, with the intercept yielding h, and C being calculable from the slope. Thus both the heat transfer characteristics of the apparatus, h, and the mass transfer characteristics of the membrane, C, may be determined. This procedure requires an estimate of the membrane conductivity, k_m, which can be calculated from equation (4.5). This equation is tested experimentally in section 4.4.

4.1.2 Temperature Polarisation

The concept of the temperature gradients in the liquid films reducing
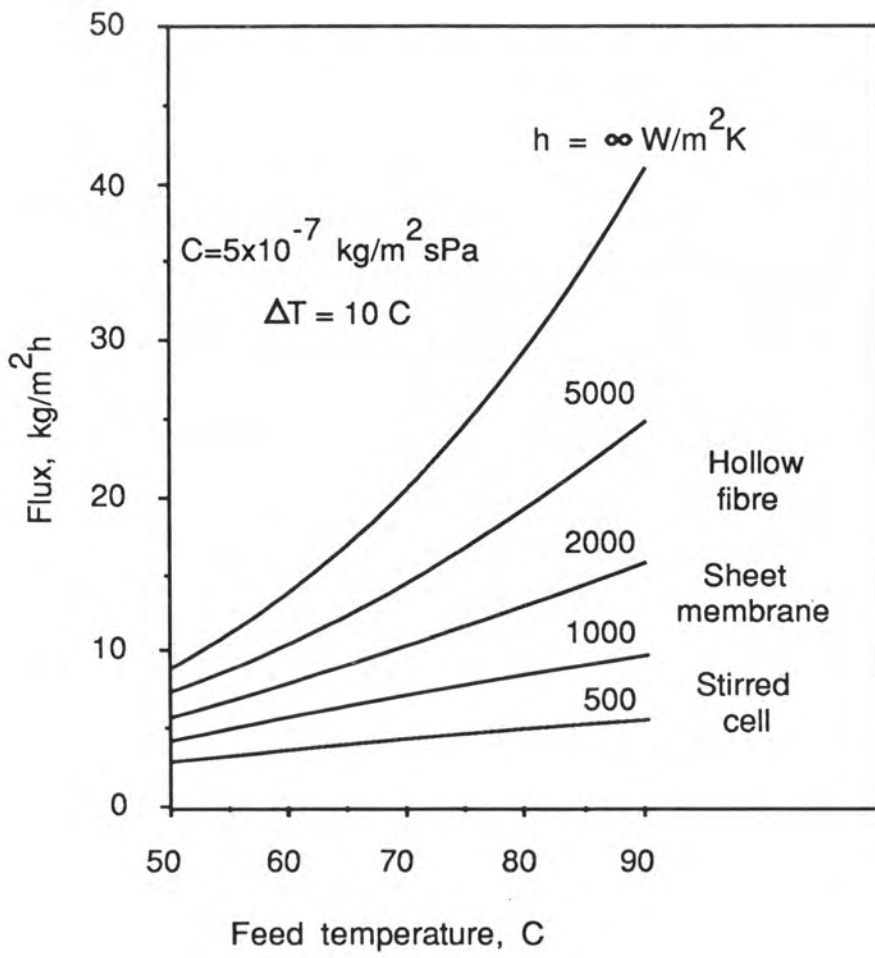
Figure 4.2 : Effect of film heat transfer coefficient
and temperature on flux.

the driving force in MD is referred to as "Temperature Polarisation".
Although this term is not strictly correct, it owes its origins to the
similarity with concentration polarisation observed in other membrane
processes. Temperature polarisation can be quantified by means of a
temperature polarisation coefficient, TPC, defined as the fraction of
the overall driving force that contributes to the trans-membrane driving
force.

$$TPC = \frac{(T_{fm} - T_{pm})}{(T_f - T_p)} \equiv \frac{\Delta T_m}{\Delta T_b} \qquad (4.7)$$

From equations (2.11) and (2.14), the temperature polarisation
coefficient can be written in terms of the various heat transfer
coefficients

$$TPC = \frac{h}{h_v + h_c + h} \qquad (4.8)$$

Note that the temperature polarisation coefficient lies between zero and
one, however in practice, TPC is rarely greater than 0.8, due to the
relative magnitudes of h_v, h_c and h. If the value of TPC is low, it
means that the process is limited by heat transfer in the liquid films,
while if TPC is high the process is limited by the permeability of the
membrane. In a well designed system, the value of TPC should be between
0.4 and 0.7. The temperature polarisation coefficient is not a constant
for any given system. The value of TPC decreases with increasing average
temperature, through the dP/dT dependence of h_v. For instance, for
counter-current flow in a shell and tube module, TPC may be 0.5 at the
hot end, and 0.7 at the cold end.

It can be seen now that equation (4.2) simply states that flux =
permeability × driving force, where h_v is the heat transfer equivalent

of the membrane permeability, ΔT_b is the overall driving force, and ΔH_v converts the mass flux to a heat flux. The remaining term in equation (4.2) is an expression for the temperature polarisation coefficient, which when multiplied by ΔT_b, gives the membrane driving force, ΔT_m.

4.1.3 Prediction of Film Heat Transfer Coefficients

In many situations it is not convenient to measure film heat transfer coefficients. For the purposes of module design and appraisal, it is more convenient to estimate h_f and h_p from heat transfer theory. In section 2.1, it was shown that film heat transfer in MD is not greatly affected by the simultaneous mass transfer associated with flux, hence conventional heat transfer theory is appropriate.

For many flow geometries and regimes, it is possible to estimate the film heat transfer coefficient via a correlation for the dimensionless Nusselt number, Nu, defined as

$$Nu = hX/k \qquad\qquad (4.9)$$

where k is the thermal conductivity of the fluid, and X is a characteristic length. The Nusselt number is usually correlated against the dimensionless Reynolds and Prandtl numbers, where $Re = \rho v X/\mu$, and $Pr = C_p \mu/k$. While such correlations can lead to errors of up to 25% in the Nusselt number [4.1], they provide a useful basis for comparing designs and predicting system performance.

For fully developed turbulent flow in smooth tubes, Dittus and Boelter recommend the correlation [4.1]

$$Nu = 0.023 \ Re^{0.8} \ Pr^{n} \tag{4.10}$$

where   n = 0.4   for heating

= 0.3   for cooling

where the characteristic length, X, is the tube diameter, d. The properties in this equation are evaluated at the bulk fluid temperature. Equation (4.10) is valid for Prandtl numbers between 0.6 and 100 (Pr=3.0 for water at 60 °C) with moderate temperature differences between the wall and the bulk fluid. For large temperature differences across the boundary layer, Sieder and Tate recommend [4.1]

$$Nu = 0.027 \ Re^{0.8} \ Pr^{0.33} \ (\mu/\mu_{m})^{0.14} \tag{4.11}$$

where μ_{m} is the fluid viscosity evaluated at the membrane wall temperature. Equations (4.10) and (4.11) are valid for fully developed turbulent flow. In the entrance region, where flow is not developed, Nusselt recommends [4.1]

$$Nu = 0.036 \ Re^{0.8} \ Pr^{0.33} \ (d/L)^{0.055} \tag{4.12}$$

for   10 < L/d < 400

where L/d is the ratio of length along the tube to the diameter. For a 1 mm i.d. tube, equation (4.9) is valid for the first 400 mm of the tube. It should be noted, however, that equations (4.11) and (4.12) are approximately equal for 100 < L/d < 400, for which case $0.036(d/L)^{0.055}$ = 0.027 ± 0.001.

For non-circular cross-sections in turbulent flow [4.2], the same

correlations can be applied by using the hydraulic diameter, d_h, as the
characteristic length, where

$$d_h = 4A/p \qquad\qquad (4.13)$$

where A is the cross-section for flow, and p is the wetted perimeter.
For circular cross-sections, equation (4.13) yields the tube diameter.
Equation (4.13) can be used when calculating heat transfer coefficients
on the shell side of tubular membrane bundles, or in channel flow.

Heat transfer coefficients for laminar flow in hollow fibres can also be
calculated from Nusselt numbers. For laminar tube flow, Sieder and Tate
[4.1] recommend

$$Nu = 1.86 \; (Re \; Pr)^{0.33} \; (d/L)^{0.33} \; (\mu/\mu_m)^{0.14} \qquad\qquad (4.14)$$

for   Re Pr d/L > 10

Equation (4.14) is only valid for developing laminar flow, such as in
the entrance region. For example, for flow of water at 60 °C through a
0.3 mm fibre at Re = 200, (Re Pr d/L) = 10 at L=18 mm. Hence equation
(4.14) may only be used for the first 18mm of the fibre. The remainder
of the fibre is in fully developed laminar flow, and the Nusselt number
is essentially constant. In fully developed laminar flow, the Nusselt
number is independent of flow rate, depending only on the flow geometry
and boundary conditions [4.3].

For various cross-sectional shapes, laminar Nusselt numbers are
available for several different boundary conditions. Shah and London
[4.3] suggest that for counter flow heat exchange through conductive

walls the appropriate boundary conditions are constant wall heat flux along the tube, and constant wall temperature around the circumference at any point. The wall heat flux may vary along the tube in MD, however for the example given above with a 0.3 mm fibre at Re = 200, if the wall heat flux changes by 2 fold over a 50 mm length, the Nusselt number only changes by 3% [4.3].

Figure 4.3 provides a list of Nusselt numbers for various cross-sections [4.1,4.3]. (Note, reference [4.1] misreports values from reference [4.3].) The hydraulic diameter for each geometry is also listed for use in equation (4.9).

Little information is available on Nusselt numbers applicable to laminar flow along the shell side of hollow fibres. (Note, shell side mass transfer in hollow fibre contactors has been studied by Yang and Cussler [4.4].) With reference to figure 4.4, the gaps between fibres can be visualised as combinations of triangles and rectangles with curved sides. Inspection of the Nusselt numbers in figure 4.3 suggests an appropriate value may be $Nu \approx 5$ for shell side heat transfer. This ignores the ends of the module where the fibres are splayed, and turbulent crossflow occurs. The length of splayed fibres should be minimised in module design. In general, heat transfer coefficients on the shell side are lower than on the tube side.

The hydraulic diameter for shell side flow may be calculated from the fractional void space on the shell side, α. Ignoring the ends of the module where the fibres are splayed, the shell side voidage is

$$\alpha = (\pi r_s^2 - n\pi r_o^2) / \pi r_s^2 \qquad (4.15)$$
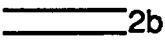
Shape	Nu	d_h
$\triangle$ s	3.11	$s/\sqrt{3}$
$\square$ s	3.61	s
$\square$ s 2s	4.12	4s/3
$\bigcirc$ r	4.36	2r
$\rule{}{}$ 2b	8.24	4b

Figure 4.3 : Nusselt number and hydraulic diameter for various laminar flow geometries.

Good shell side
fluid dynamics

Poor shell side
fluid dynamics
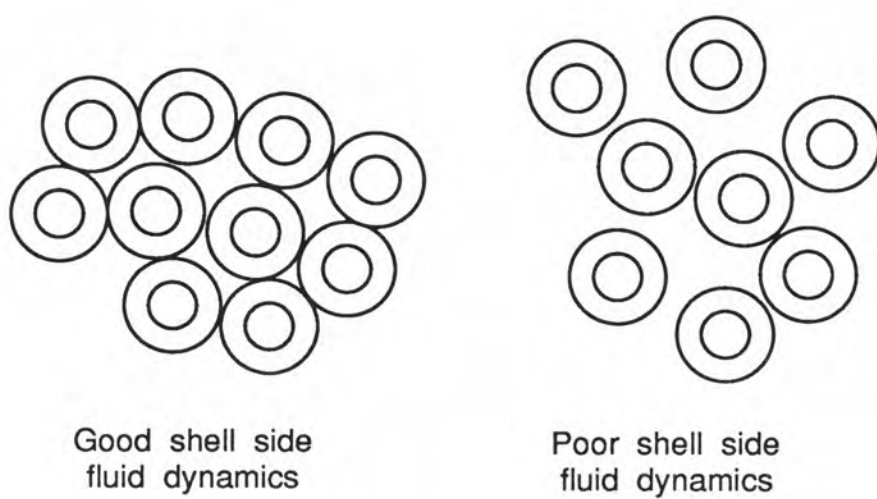
Channelling
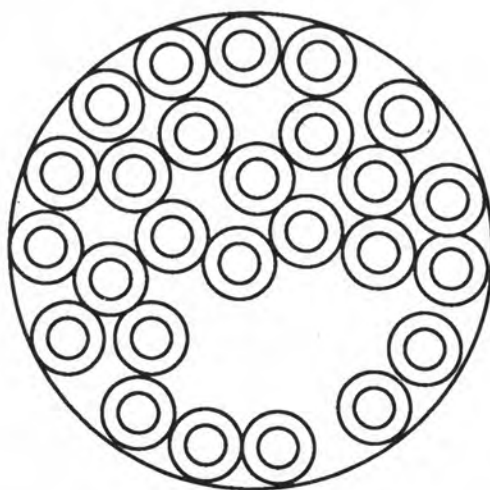
Figure 4.4 : Flow around hollow fibre bundles.

The subscripts s and o refer to the shell and the outside of the fibres respectively, and n is the number of fibres. Ignoring the inside of the shell in the wetted perimeter, the hydraulic diameter, defined in equation (4.13), becomes

$$d_h = 4 \ (\pi r_s{}^2 - n\pi r_o{}^2) \ / \ 2\pi r_o n$$

$$= 2 \ r_o \ \alpha/(1-\alpha) \tag{4.16}$$

The theoretical minimum α for parallel cylinders is around 0.1, however in practice, with hollow fibre membranes, it is difficult to obtain $\alpha < 0.5$, due to misalignment of the fibres.

With tubular and hollow fibre membranes, the membrane area is based on the inside area of the tubes, as this would normally be the feed side (the higher heat transfer coefficient should be used on the high temperature side). The membrane area is greater on the outside of the fibres than on the inside, however contact between the fibres can reduce the effective outside area. For thin-walled tubes ($r_o/r_i<1.5$) it is reasonable to assume equal areas on either side of the membrane, however for thick-walled fibres ($r_o/r_i>1.5$) it may be necessary to increase h_p to account for increased area. If this is not done, estimates of h_p can be considered as conservative.

The most complicated heat transfer situation in MD occurs when a tube bundle is encased loosely in a shell, for example with $\alpha > 0.5$. This leads to channelling, where the fibres move to open up a clear path along the module, as shown in figure 4.4. The bulk of the liquid flow will occur as turbulent flow along the channel (or channels), while the remainder will procede by laminar flow between the fibres. The result is

extremely bad temperature polarisation, low flux, and excessive
recirculation rates. This situation should be avoided in module design,
which will be discussed in chapter 8.

Based on the Colton and Smith [4.5] mass transfer correlation for
stirred cells, using the heat transfer/mass transfer analogy, Nusselt
numbers for stirred cells have been estimated as Nu = 70 at Re = 8000,
and Nu = 150 at Re = 32000, where Re = $\rho \omega r^2 / \mu$. The uncertainties of
these estimates may be as high as 50%, however as stirred cells are not
recommended for MD, a more precise treatment is not warranted.

In some MD configurations, the heating fluid and feed solution are
separated by a heat transfer surface, for example a stainless steel
plate. Heat transfer through a conductive plate can be calculated from

$$Q'' = (k/\delta) \, \Delta T \qquad\qquad\qquad (4.17)$$

In such systems, the heat transfer coefficients for the heating fluid,
conducting wall, and feed solution can be combined by adding their
individual resistances. The general equation for combining n heat
transfer coefficients in series is

$$h = \left\{ \sum_{i=1}^{n} \frac{1}{h_i} \right\}^{-1} \qquad\qquad\qquad (4.18)$$

Many MD systems incorporate turbulence promoters in the flow channels to
combat temperature polarisation. In such systems, heat transfer
coefficients are best estimated from experimental results, for example
using equation (4.6).

As gas-gap MD has not been investigated in this study, film heat

transfer coefficients have not been estimated for this case. It is worth
noting, however, that if dropwise condensation occurs on the condensing
surface, the heat transfer coefficients will be high [4.1], while film
condensation may lead to bad temperature polarisation. An accurate
appraisal of heat transfer in gas-gap MD devices must be based on
experimental results.

The combination of a number of heat transfer coefficients using equation
(4.18) may lead to compounding errors. It is appropriate, therefore, to
examine how errors in h affect the accuracy of equation (4.2). Consider
a system where the temperature polarisation coefficient is
$TPC = \Delta T_m / \Delta T_b = 0.5$. From equation (4.8), $h = h_c + h_v$ for this case. An
overestimate of h by 20% will give $TPC = 1.2/(1 + 1.2) = 0.55$, resulting
in an overestimate of ΔT_m by $0.05/0.5 = 10\%$. This, in turn, will lead to
an overestimate of the flux by 10%. This emphasises the need to measure
h wherever possible.

4.2 MODULE APPRAISAL

4.2.1 Estimated Film Heat Transfer Coefficients

Equations presented in the previous section allow the estimation of heat
transfer coefficients for various fluid flow rates and membrane
geometries. These equations can be applied to the various module designs
commonly encountered in MD, to assess the adequacy of heat transfer in
each system.

To illustrate heat transfer appraisal, consider an MD module based on
0.3 mm i.d., 0.6 mm o.d. hollow fibres 0.4 m long, as was used in the
pilot plant study in chapter 8. At 60 °C and a pressure drop of 40 kPa,

the fluid velocity is 0.6 m/s, and the Reynolds number is 380. Hence laminar Nusselt numbers are appropriate and fully developed flow is assumed. For the flow of the hot feed down the lumen (ignoring solute effects), the Nusselt number is 4.36 from figure 4.3. The conductivity is k = 0.65 W/mK and d_h = 0.0003 m, giving h_f = 10000 W/m^{2}K. For flow on the shell side, the Nusselt number is ~5, and for a shell side void fraction of α = 0.6, equation (4.16) gives d_h = 0.0009 m. This gives a heat transfer coefficient of h_p = 3600 W/m^{2}K. The overall film heat transfer coefficient is calculated from the individual coefficients using equation (4.18), giving h = (1/10000 + 1/3600)$^{-1}$ = 2650 W/m^{2}K. As a rule of thumb, if h < 1000 W/m^{2}K, temperature polarisation will be excessive.

Similar calculations were performed for other geometries and flow regimes, and the results for individual film heat transfer coefficients are summarised in Table 4.1, based on the properties of water at 60 °C. For systems where the temperature varies over a wide range along the membrane, heat transfer coefficients may have to be evaluated at several positions along the module, as transport properties vary with temperature. This is particularly important in turbulent systems, where the Nusselt number is dependent on (viscosity)$^{-0.8}$, as viscosity is strongly dependent on temperature.

It is evident from Table 4.1 that tubular and hollow fibre membranes provide excellent film heat transfer coefficients on the tube side, and with small shell side voidages, the shell side heat transfer coefficients are reasonable. It should also be emphasised that in hollow fibre systems with fully developed laminar flow, the film heat transfer coefficient is independent of flow rate [4.3], and is maximised when the flow cross-section is minimised. In tubular systems with turbulent

Table 4.1:   Predicted Film Heat Transfer Coefficients for Various
             Membrane Distillation Systems.

Heat Transfer Geometry	Flow Regime	Nu (-)	d_h (mm)	h_i (W/m^{2}K)
1.0 mm i.d. tube	Re=5000	29	1.0	19000
	Re=3000	19	1.0	12000
	Re=1000	4.4	1.0	2900
1.4 mm o.d. tubes, α=0.6	Re=3000	22	4.2	3300
0.3 mm i.d. fibre	laminar	4.4	0.3	9500
0.6 mm o.d. fibre bundle				
α = 0.4	laminar	~5	0.4	8100
α = 0.6	laminar	~5	0.9	3600
α = 0.8	laminar	~5	2.4	1400
Parallel plates				
2b = 2 mm	Re=5000	29	4.0	4700
2b = 2 mm	laminar	8.2	4.0	1300
2b = 0.5 mm	laminar	8.2	1.0	5300
2b = 0.2 mm	laminar	8.2	0.4	13000
Stirred cell	Re=8000	70	50	800
	Re=32000	150	50	1900
1 mm st. steel plate	-	1	1.0	16300

flow, however, the film heat transfer coefficients are maximised when
the flow rate (turbulence) is maximised.

For sheet membranes, the heat transfer coefficients are generally lower
than for tubes or fibres, except when extremely thin channels are used.
This situation may be improved by using turbulence promoters. It is also
apparent that stirred cells are not suited to MD, as they do not provide
adequate heat transfer.

The results in Table 4.1 suggest appropriate design targets for the
overall film heat transfer coefficient, h. For most geometries,

individual heat transfer coefficients of 3000 to 5000 W/m^2K can be achieved using realistic design parameters, suggesting a realistic design target of h = 2000 W/m^2K. Using extreme design parameters, individual coefficients of over 10000 W/m^2K can be achieved, suggesting a maximum value of h = 5000 W/m^2K.

The results in Table 4.1 can be used to estimate the heat transfer coefficients for proposed MD systems. For example, a jacketted sheet MD system comprising heating and cooling fluids at Re = 5000 in 2 mm channels, 1mm stainless steel heat transfer plates, a 0.5 mm laminar feed channel and a 0.2 mm permeate channel would have 6 heat transfer resistances between the heating and cooling fluids. The overall film heat transfer coefficient would be h = (2/4700 + 2/16300 + 1/5300 + 1/13000)$^{-1}$ = 1200 W/m^2K. The low overall film heat transfer coefficient suggests that turbulence promoters or reduced channel thicknesses may be required for this design.

4.2.2 Measured Film Heat Transfer Coefficients

Equation (4.6) provides a means of analysing experimental or production results to determine the overall film heat transfer coefficient, h, and the membrane permeability, C. It is based on equal feed and permeate heat transfer coefficients, which is a reasonable assumption for a well designed system. To illustrate the use of equation (4.6), consider the results published by Hanbury and Hodgkiess [4.6] for a laboratory analysis of the Gore-tex system. Hanbury correlated his results using the equation $J\Delta H_v/\Delta T_b$ = 4.9 $T_m^{1.17}$ for $30 \leq T_m \leq 70$ °C. A plot of $\Delta T_b/J\Delta H_v$ versus $1/(dP/dT)$ (equation (4.6)) for T_m = 30, 40, 50, 60 and 70 °C is shown in figure 4.5, with the linearity of the graph supporting the equation. The intercept of figure 4.5 is 9.2×10^{-4} m^2K/W, giving
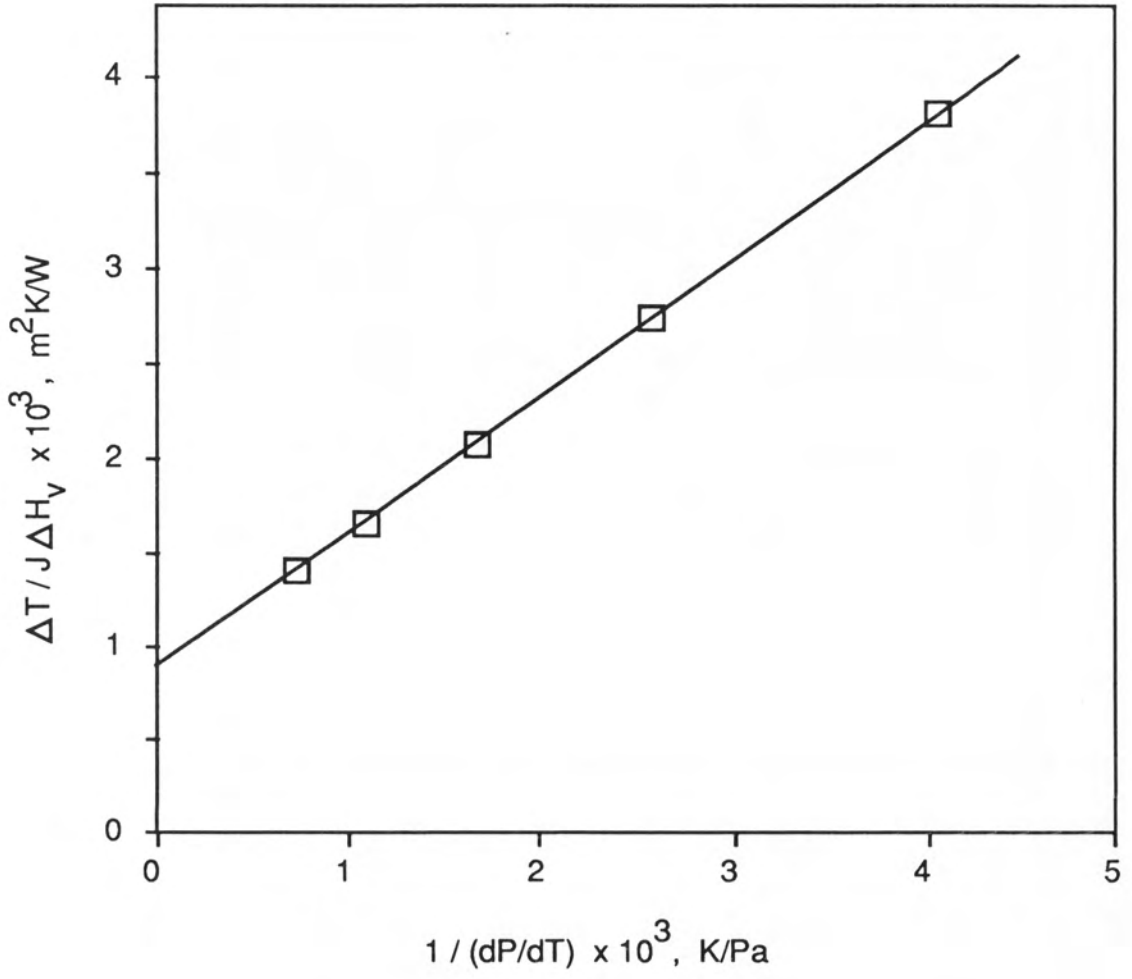
Figure 4.5 : Hanbury's results plotted according to equation (4.6).

h = 1100 W/m^{2}K. The slope of figure 4.5 is 0.71 m^{2}Pa/W. Assuming a value

of h_c = 700 W/m^{2}K for the PTFE membrane, this gives C = 9.6 × 10^{-7}

kg/m^{2}sPa.

In light of the previous discussion, a heat transfer coefficient of

h = 1100 W/m^{2}K shows that Hanbury's experimental system was not well

designed from a heat transfer viewpoint. From equations (4.4) and (4.8)

the temperature polarisation coefficient for this system at 70 °C

would be TPC = 1100 / (3100 + 700 + 1100) = 0.22. The value of C for

Hanbury's system is roughly double the values reported in section 4.4

for this study. This reflects the fact that Gore-tex membranes are often

as thin as 60 μm, compared to thicknesses of 100 to 140 μm for the

membranes used in this study. The fact that C is high for Hanbury's

system, but h is low, suggests that Hanbury has underestimated the

potential of the Gore-tex system.

4.3 EXPERIMENTAL PROGRAM

An experimental study was conducted to examine heat transfer processes

in MD. The major objective was to quantify the heat transfer parameters

for an experimental sheet membrane system, to display the controlling

heat transfer processes under various conditions.

The sheet membrane apparatus used throughout this study is shown in

figure 4.6. The design of the experimental MD cell was detailed in

chapter 3, and its operation is as follows. The membrane was contacted

on either side by a thin film of feed or permeate 0.1 mm thick. These

liquid films were each bounded by thin stainless steel heat transfer

plates. Access to all areas of the membrane surface was facilitated by

fine grooves in the stainless steel plates. A layer of hydrophilic
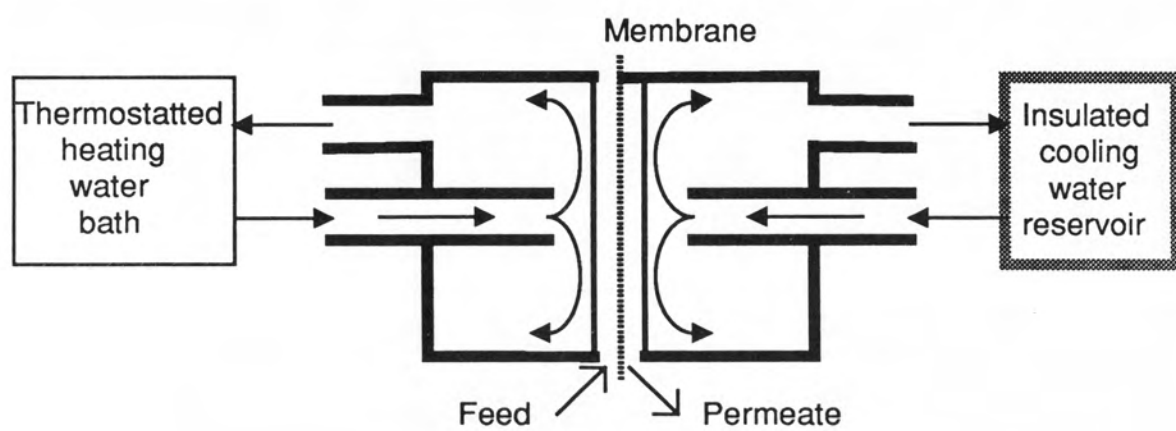
Figure 4.6 : MD apparatus for heat transfer study.

tissue maintained the liquid film thickness at 0.1 mm, while acting as a wick to keep the membrane surfaces wet. The stainless steel plates were heated or cooled by jets of recirculated water. The design of the module was intended to minimise temperature polarisation, and to maintain an even temperature over the entire membrane area.

Initial experiments with constant heating and cooling water temperatures yielded constant fluxes (±5%) over periods of several hours. Fluxes were also found to be reproducible (±5%) with different membrane samples from the same batch. Steady state was observed within 2 minutes of a step change in heating or cooling water temperatures. Throughout this study of heat transfer, distilled water was used as the feed, thus eliminating solute effects.

For the bulk of the experimental study, the apparatus was operated with thermostatted heating water, however the cooling water was recirculated within an insulated reservoir. As heat passed across the membrane, the temperature of the cooling water increased. This rise in cooling water temperature was originally intended to allow an in situ measurement of the total heat flux across the membrane. The heat of vaporisation, calculated from the flux measurement, could then be subtracted yielding the heat transfer by conduction across the membrane. The compounding of experimental errors lead to a 25 % error in the measured membrane conductivity, hence a separate experiment was conducted to study this parameter. Despite this, the remainder of the experiments was conducted using the insulated cooling water reservoir, as this provided a profile of flux versus cooling water temperature for each heating water temperature used.

Heat transfer across the membrane was determined using the same

apparatus, however the tissue paper was removed so that the membrane contacted the stainless steel. The membrane cell was operated without feed or permeate, so that the only heat transfer across the membrane was by conduction across the dry membrane.

Three hydrophobic, microporous sheet membranes were examined in this study. Details of the membranes are summarised in Table 4.2.

Table 4.2: Membranes used in Experimental Study.

Membrane	Enka 0.1	Enka 0.2	Durapore 0.45
Polymer	Polypropylene	Polypropylene	Polyvinylidene difluoride
Pore size*, μm	0.10	0.20	0.45
Thickness, mm	0.10	0.14	0.11
Porosity*	0.75	0.75	0.75

* Manufacturers data

4.4 RESULTS AND DISCUSSION

For the three membranes detailed in Table 4.2, experiments were conducted with heating water temperatures of 60, 70, and 80 °C, with increasing cooling water temperature. For 5 °C increments of cooling water temperature, the flux was determined from the slope of the permeate volume versus time curve. The results were plotted according to equation (4.6) as $\Delta T_b / J \Delta H_v$ versus $1/(dP/dT)$. For the three membranes, the results are shown in figures 4.7, 4.8 and 4.9.

The linearity of the three graphs in figures 4.7 to 4.9 supports the form of equation (4.6) for average temperatures ranging from 40 to 75
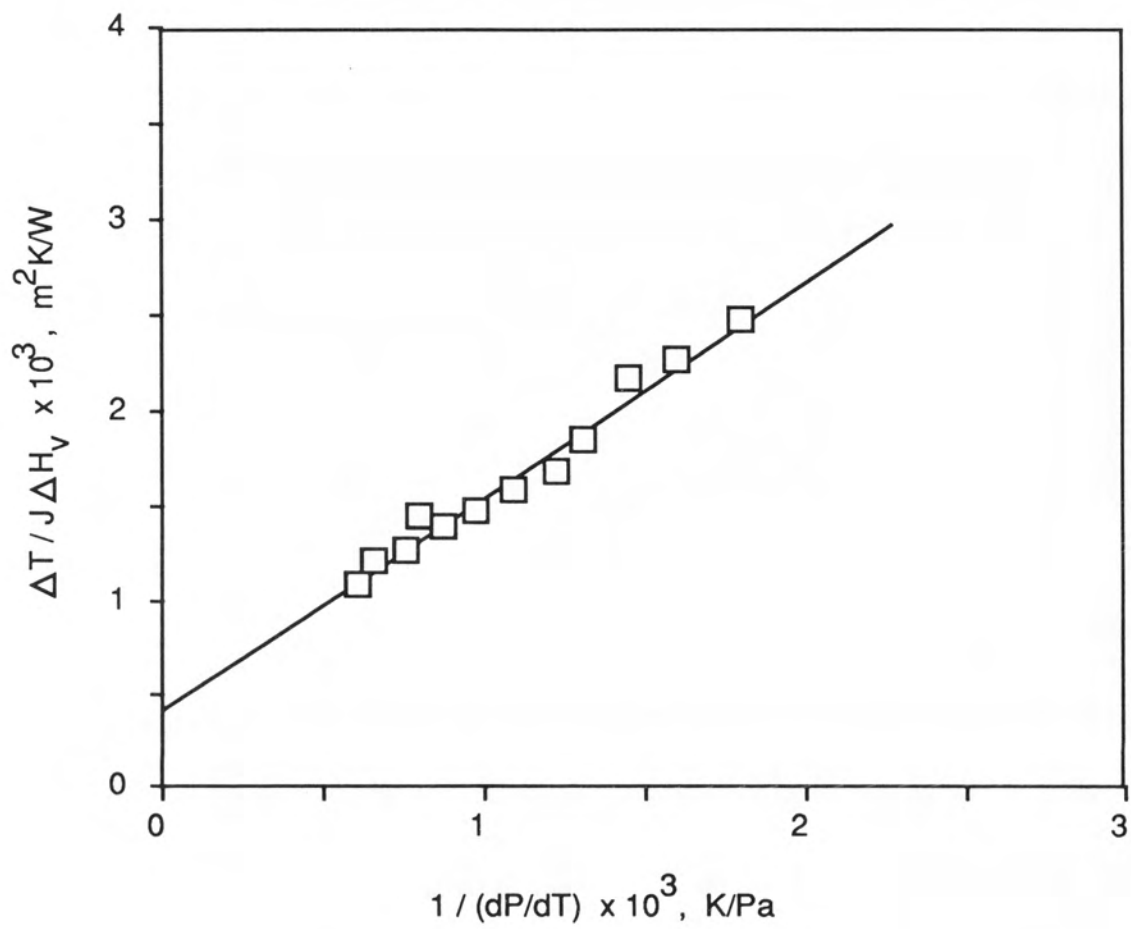
Figure 4.7 : Results for Enka 0.1 um membrane plotted according to equation (4.6).
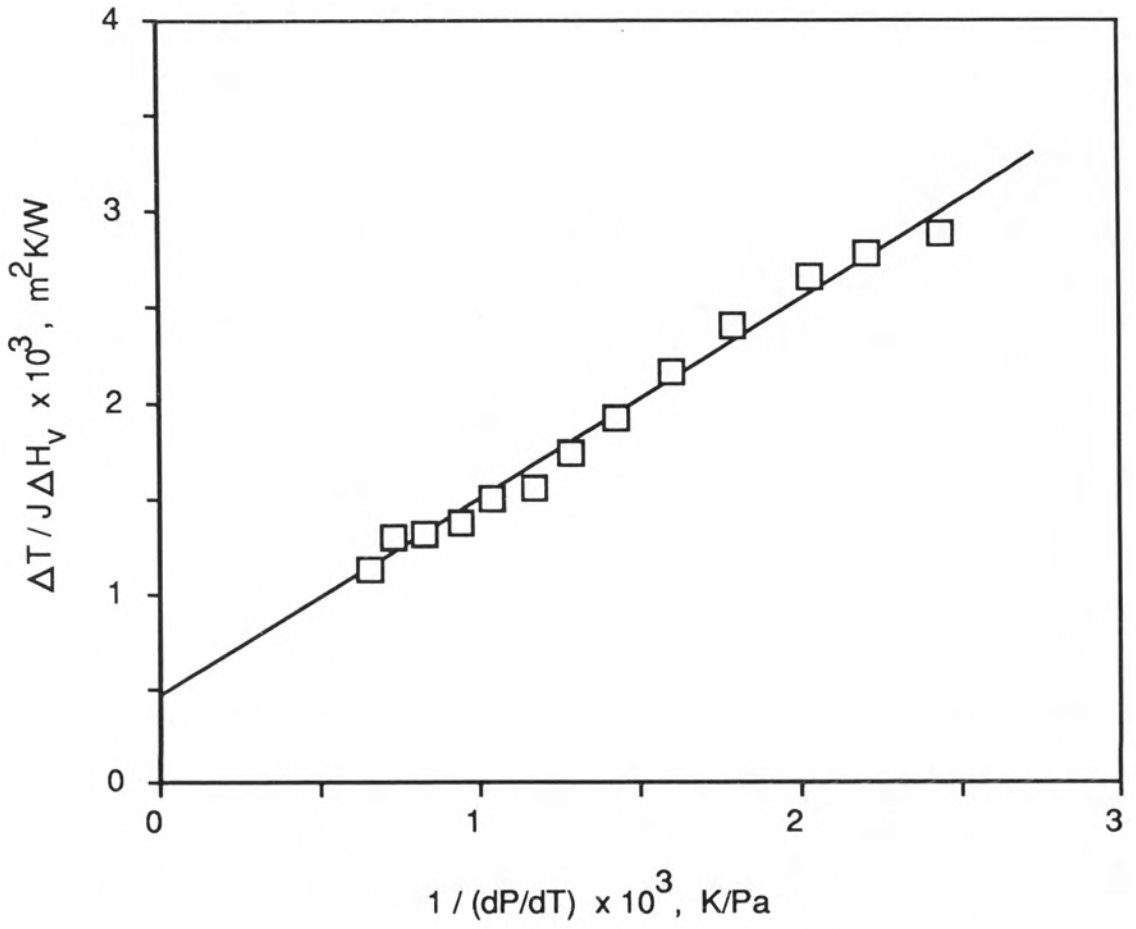
Figure 4.8 : Results for Enka 0.2 um membrane plotted according to equation (4.6).
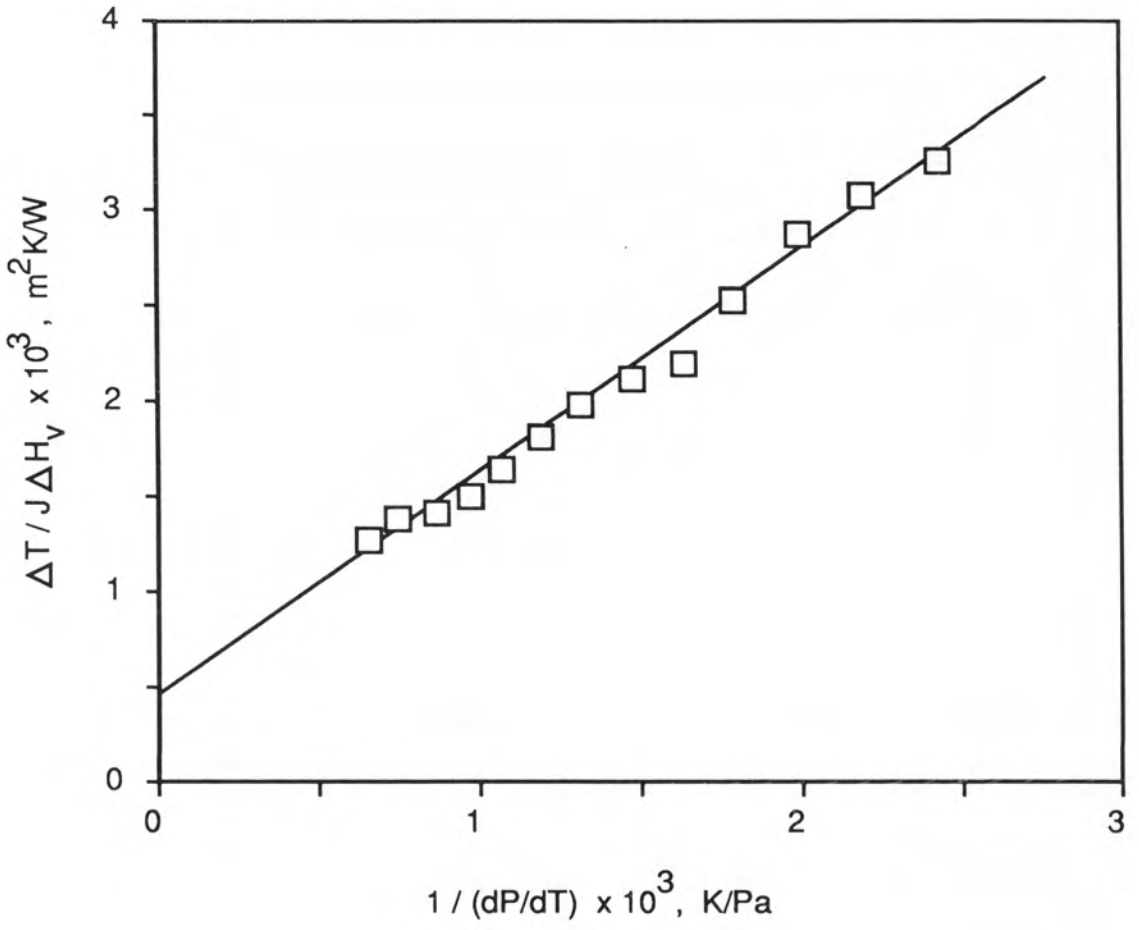
Figure 4.9 : Results for Durapore 0.45 um membrane plotted according to equation (4.6).

°C, and for trans-membrane temperature differences ranging from $\Delta T_m = 1$ to 10 °C. The experimental scatter in the three graphs is mainly due to the simplified mass transfer relationship (equation (4.1)) used in deriving equation (4.6). From the slopes and intercepts in figures 4.7 to 4.9, the film heat transfer coeffcients, h, and membrane mass transfer coefficients, C, were determined for each system. The mass transfer coefficients were multiplied by $(dP/dT)\Delta H_v$ evaluated at 60 and 80 °C, to give the vapour heat transfer coefficient, h_v, at these two temperatures. These results are summarised in Table 4.3.

Table 4.3: Heat Transfer Parameters for Three MD Systems

Membrane	Enka 0.1	Enka 0.2	Durapore
Membrane Conductivity k W/mK	0.052	0.052	0.077
Conduction Heat transfer Coefficient, h_c W/m^{2}K	520	370	700
Mass Transfer Coefficient $C \times 10^7$ kg/m^{2}sPa	4.5	4.3	4.8
Vapour Heat Transfer Co- efficient, h_v W/m^{2}K @ 60°C	1000	960	1070
" " " 80°C	2080	1990	2220
Overall Film Heat Transfer Coefficient, h W/m^{2}K	2440	2380	2490
Heat Loss by Conduction $h_c/(h_c + h_v)$ @ 60°C	0.34	0.28	0.40
" " 80°C	0.20	0.16	0.24
Temperature Polarisation Coefficient, TPC @ 60°C	0.62	0.64	0.58
" " " 80°C	0.48	0.50	0.46

The conduction heat transfer coefficient, h_c, was determined from a separate experiment as described above. For a dry air-filled Enka 0.1 μm polypropylene membrane, h_c was measured as 520 W/m^{2}K, which compares favourably with the value of 540 W/m^{2}K predicted from equation (4.5). A more detailed discussion of membrane conduction was given in section 2.1.2. On this basis it was assumed that membrane conductivities could be predicted from equation (4.5) for any MD system with reasonable accuracy. Calculated results for membrane conduction heat transfer coefficients for the three membranes are included in Table 4.3.

Two important heat transfer parameters can be calculated from the three MD heat transfer coefficients in Table 4.3. These are the fractional heat transfer by conduction, and the temperature polarisation coefficient. The fractional heat transfer by conduction, or heat loss by conduction, is simply the conduction heat transfer coefficient divided by the sum of the conduction and vapour heat transfer coefficients. The temperature polarisation coefficient, TPC, is calculated using equation (4.8). Each of these parameters calculated at both 60 and 80 °C is included in Table 4.3.

The results in Table 4.3 warrant some discussion, as they reflect all of the major heat transfer concepts relevant to MD. The first entry in Table 4.3 is the thermal conductivity of the gas filled membrane. The two Enka membranes have the same calculated conductivity as they are each 75% porous polypropylene. Their conduction heat transfer coefficients differ, however, due to their different thicknesses (see Table 4.2). The Durapore membrane has a higher thermal conductivity due to the higher conductivity of PVDF (see section 2.1.2).

The membrane mass transfer coefficients for the three membranes are

similar, despite the difference in pore sizes. As the systems were not
deaerated, pore size has only a small effect on flux, with molecular
diffusion through stationary air being the main resistance to flux (this
will be fully explained in chapter 6). Accordingly, the membrane
thickness has the major influence on the mass transfer coefficient. The
vapour heat transfer coefficient is calculated from the mass transfer
coefficient by multiplication with ΔH_v and dP/dT. Table 4.3 reports
values of h_v at 60 and 80 °C. The higher values at 80 °C reflect the
higher value of dP/dT, which increases exponentially with temperature.
This means that for constant trans-membrane temperature difference, ΔT_m,
the mass flux (and hence vapour heat flux) increases with increasing
average temperature.

The overall film heat transfer coefficients are approximately equal for
the three systems. This is expected, as the film heat transfer
coefficient is a property of the apparatus, which was the same for all
experiments. A value of $h = 2400$ W/m^{2}K suggests that good heat transfer
was achieved.

Table 4.3 reports values for the heat loss by conduction at 60 and 80
°C. These values quantify the fraction of the total heat being supplied
to the membrane that is lost by conduction across the membrane. It can
be seen that the heat loss is high at 60 °C and moderate at 80 °C. This
variation reflects the fact that h_v increases with temperature, while h_c
is essentially constant. The results in Table 4.3 suggest that heat loss
by conduction can be minimised by operating at high temperatures. An
alternative approach to reducing heat loss will be discussed in
chapter 6.

The final entry in Table 4.3 is the temperature polarisation coefficient

evaluated at 60 and 80 °C. Again, the variation of TPC with temperature reflects the temperature dependence of h_v. The values shown suggest that below 50 °C, these systems may become mass transfer limited, that is TPC > 0.7 ($h_v \ll h$). Conversely, above 90 °C, the systems may become heat transfer limited, that is TPC < 0.4 ($h \ll h_v$).

The values of the three heat transfer coefficients, h, h_v and h_c, shown in Table 4.3 are typical of those observed in MD, however the range of these coefficients can be quite large. For example, h_c may be only 100 W/m^2K for thick membranes or gas-gap devices, or may be greater than 1500 for thin or low porosity membranes. The value of h_v may be only 500 for thick aerated membranes, air gap devices and low temperature systems, or may be up to 15000 for deaerated high temperature systems. The value of h typically lies between 500 and 5000 W/m^2K, depending on the fluid dynamics, remembering that h has contributions from both the feed and permeate film heat transfer coefficients.

4.5 CONCLUSIONS

The major conclusion from this study on heat transfer in membrane distillation is that the overall film heat transfer coefficient, h, is a crucial parameter controlling MD performance. The benefit of high temperature operation can not be realised unless there is adequate film heat transfer. The components of h, coming from the feed and permeate film heat transfer coefficients (and in some sheet membrane cases, cooling and heating water coefficients), can be maximised through module design. The benefits of high turbulence and small flow cross-sections have been demonstrated, with tubular and hollow fibre membranes showing the most potential. Hollow fibres with laminar flow have the advantage that h is independent of flow rate. A design target of h = 2000 W/m^2K is

reasonable, however in extreme cases, h = 5000 W/m^{2}K may be achieved.

Heat loss by conduction across the membrane has been shown to be an important consideration, accounting for 10 to 40 % of the total heat input. The conduction heat transfer coefficient, h_c, can be calculated from the polymer and gas conductivities using equation (4.5). The fractional heat loss by conduction can be reduced by high temperature operation.

4.6 NOTATION

A   Flow cross-section [m^2]

b   Half channel height [m]

C   Membrane mass transfer constant [kg m^{-2} s^{-1} Pa^{-1}]

C_p Heat capacity [J kg^{-1} K^{-1}]

d_h Hydraulic diameter [m]

h   (Overall film) Heat transfer coefficient [W m^{-2} K^{-1}]

ΔH_v Latent heat of vaporisation [J kg^{-1}]

J .   Mass flux through membrane [kg m^{-2} s^{-1}]

k   Thermal conductivity [W m^{-1} K^{-1}]

L   Length [m]

M   Gas molecular weight [kg mol^{-1}]

n   Number (of tubes in shell and tube module) [-]

Nu   Nusselt number = hX/k [-]

p   Wetted perimeter [m]

P   Water vapour pressure [Pa]

ΔP Water vapour pressure drop across membrane [Pa]

Pr   Prandtl number = $C_p \mu$/k [-]

Q"   Heat flux [W m^{-2}]

r   radius [m]

R   Gas constant [J mol^{-1} K^{-1}]

Re   Reynolds number = $\rho vX/\mu$ [-]

T   Temperature [K,°C]

TPC   Temperature polarisation coefficient [-]

v   Velocity [m s^{-1}]

X   Characteristic dimension [m]

α Module shell side void fraction [-]

δ Membrane thickness [m]

ϵ Membrane porosity [-]

μ Viscosity [Pa s]

ρ Density [kg m^{-3}]

χ Membrane tortuosity [-]

ω Angular velocity [rad s^{-1}]

Subscripts

c   Conduction

f   Feed

g.   Gas

i   Individual

m   Membrane

o   Outside

p   Permeate

s   Shell (of module)

v   Vapour

4.7 REFERENCES

[4.1] Holman, J.P., "Heat Transfer", 5th ed., McGraw-Hill, 1981.

[4.2] Bird, R.B., Stewart, W.E. and Lightfoot, E.N., "Transport
       Phenomena", Wiley & Sons, New York, 1960.

[4.3] Shah, A.K. and London, A.L., "Laminar Flow: Forced Convection in
       Ducts", Academic Press, New York, 1978.

[4.4] Yang, M-C. and Cussler, E.L., "Designing Hollow-Fibre
       Contactors", A.I.Ch.E. Journal, 32(11) (1986) 1910-1916.

[4.5] Colton, C.K. and Smith, K.A., AICHE Journal, 18 (1972) 958.

[4.6] Hanbury, W.T. and Hodgkiess, T., "Membrane Distillation - An
       Assessment", Desalination 56 (1985) 287-297.

Chapter 5

Gas
Permeation
in
Microporous
Membranes

CHAPTER 5: GAS PERMEATION IN MICROPOROUS MEMBRANES

This chapter on gas permeation is the first of two chapters relating to mass transfer within MD membranes. This topic has been divided into two sections as there are two different water vapour permeation regimes encountered in MD. In the case where the membrane pores are substantially filled with air, the controlling flux mechanism is molecular diffusion through a stagnant gas film. This topic will be addressed in chapter 6. This chapter is concerned with vapour or gas flux through MD membranes without a stagnant species, where the flux is controlled by the porous membrane structure.

The permeability of MD membranes to water vapour cannot be measured directly by MD experiments due to the difficulty in achieving total deaeration, and the uncertainty in estimating the interfacial temperatures (and hence vapour pressures). Also it is not practical to conduct gas permeation experiments with water vapour as the gas, due to possible condensation within the apparatus. In this study, the permeability of MD membranes to water vapour was estimated by conducting gas permeation experiments with other gases. A theoretical model was then applied to the gas permeation results, allowing prediction of the permeation parameters for water vapour.

Relevance to MD suggested that gas permeation experiments be conducted using microporous membranes, subatmospheric gas pressures, and gases with molecular weights both higher and lower than water. The membranes tested were made from a variety of materials, with pore sizes ranging from 0.1 to 0.45 μm. The gases used were He, CH_4, N_2, air and CO_2. Gas fluxes were measured for pressure differences between 0 and 50 kPa, and average pressures between 10 and 90 kPa. The results were correlated by

a novel two parameter semi-empirical relationship which has the advantage of simplicity when compared to the multiparameter models found in the gas permeation literature. This relationship was found to be a useful engineering equation which may be generally applicable to gas permeation through microporous structures.

5.1 THEORY

A theoretical study of gas permeation through microporous structures usually begins with a comparison of the mean free path of the gas, λ, and the mean pore size of the structure. If the mean free path of the gas is much less than the pore size, then the dominant flux mechanism is viscous or Poiseuille flow. If the mean free path is much greater than the pore size, then Knudsen diffusion is the dominant mechanism. The mean free path of nitrogen at 50 kPa and 25°C is 0.13 μm, compared to pore sizes of 0.1 to 0.5 μm for microporous membranes. Clearly gas permeation in this case falls in the transition region between Knudsen and Poiseuille flow.

A third mechanism encountered in gas permeation is surface diffusion, whereby gas molecules adsorb on the membrane walls and diffuse under a pressure gradient. This mechanism is not likely to be dominant for non-condensible gases at low pressures and ambient temperatures, nor is it expected for water vapour permeation through hydrophobic materials.

Many models and equations describing the transition region between Knudsen diffusion and Poiseuille flow have been developed. The more noteworthy of these are discussed briefly below. Some are rigorous derivations from kinetic theory, most were derived for flow through straight capillaries, and many contain one or more adjustable

parameters, as well as requiring detailed knowledge of the membrane porosity, pore size and tortuosity. The main impediment to their use is their complexity and the need to accurately know the membrane properties. The emphasis in this work was to develop a semi-empirical relationship capable of correlating a range of permeation data with parameters having recognisable physical significance.

A general non-mechanistic flux equation for gas permeation through porous structures is

$$J = K \frac{\Delta P}{\delta} \qquad\qquad (5.1)$$

where K is the permeability of the porous material, and is independent of thickness. In general, however, K is a variable depending on pore geometry, gas pressure, temperature and gaseous species. The determination of K under any given conditions requires an understanding of the various permeation mechanisms.

Knudsen diffusion is a gas flux mechanism whereby gas molecules under a pressure gradient pass across a porous structure by a series of molecule/wall collisions. For gas permeation through an isotropic, microporous membrane the Knudsen diffusion equation may be written [5.1]

$$J_K = \frac{2}{3} \frac{r\epsilon}{\chi} \left\{ \frac{8RT}{\pi M} \right\}^{\frac{1}{2}} \frac{M}{RT} \frac{\Delta P}{\delta}$$

$$= K_K \, \Delta P/\delta \qquad\qquad (5.2)$$

where $(8RT/\pi M)^{\frac{1}{2}}$ is the mean molecular speed.

The Poiseuille flow model describes viscous flow of a gas through a porous structure. For a microporous membrane, the Poiseuille flow

equation may be written

$$J_P = \frac{1}{8} \frac{r^2 \epsilon}{\chi} \frac{1}{\eta} \frac{MP}{RT} \frac{\Delta P}{\delta}$$

$$= K_P \, \Delta P / \delta \tag{5.3}$$

Most attempts at describing the Knudsen/Poiseuille transition region involve a combination of equations (5.2) and (5.3). For example, Weber (in Schneider, [5.2]) in 1954 proposed the addition of the two permeabilities, K_K and K_P, with the Knudsen permeability being multiplied by $\{\pi/4+\lambda/2r\} / \{1+\lambda/2r\}$, to describe the transition region for flow along capillary tubes. Creutz [5.3] adopted a similar approach, including an adjustable parameter to fit the experimental data. Various authors have integrated these (and other) capillary equations over the range of pore sizes in a porous medium with reasonable success (for example Schneider [5.2]). This approach requires accurate knowledge of the pore size distribution, and involves a cumbersome numerical solution of the equations. The problem is further compounded by the ambiguous definition of "pore size". The pore size measured by particle rejection or bubble point or mercury intrusion will not be the same as that measured by gas permeation [5.4]. Equations (5.2) and (5.3) even suggest that the appropriate pore size is dependent on the gas permeation regime, due to the different dependence on r. Intuitively, Poiseuille flow depends on the mean hydraulic radius, while Knudsen diffusion depends on the mean distance between molecule/wall collisions.

A major contribution to the porous diffusion literature is the "Dusty Gas" model [5.5]. In this model the porous medium is visualised as a collection of uniformly distributed dust particles which are constrained to be stationary. By considering the dust particles as giant molecules, it is possible to derive Knudsen diffusion from multicomponent diffusion

theory. The model is extended to incorporate Poiseuille flow [5.6] by

the addition of an empirical term accounting for viscous effects. In

order to use the model, three parameters must be obtained from

experimental measurements.

A simple and effective alternative to these gas permeation models can be

proposed by inspection of the forms of equation (5.2) and (5.3). This

reveals that in Knudsen diffusion, $J \propto \Delta P$, while in Poiseuille flow,

$J \propto P \Delta P$. Thus the permeability is independent of pressure in the Knudsen

regime, and is proportional to pressure in the Poiseuille regime. It is

postulated that in the Knudsen/Poiseuille transition region, K depends

on P to varying extents, depending on the relative influence of the two

mechanisms. The following expression was proposed for the membrane

permeability,

$$K/\delta = a\wp^b$$

giving the flux

$$J = a\wp^b \; \Delta P \qquad\qquad (5.4)$$

$$0 \leq b \leq 1$$

where $\wp$ = dimensionless pressure = P/P_{ref}

          a = Membrane permeation constant

          b = fraction of permeability arising from viscous effects

            = 0 for Knudsen diffusion

            = 1 for Poiseuille flow

The membrane constant, **a**, is the permeability divided by the membrane

thickness evaluated at the reference pressure. The physical significance

of **a** is that it represents the proportionality constant between flux and

pressure drop at the reference pressure. Values of **a** allow comparison of

the flux performance of different membranes under the same conditions.

The exponent **b** lies between 0 and 1, and indicates the extent to which Poiseuille flow contributes to the permeability. The reference pressure, P_{ref}, is chosen as a typical or average pressure for the range of application. For example, when dealing with gas permeation at subatmospheric pressures, P_{ref} may be set at 50 kPa. The effect of equation (5.4) is to increase the permeability for pressures higher than P_{ref}, and decrease the permeability for lower pressures.

The form of equation (5.4) can be substantiated by manipulation of equations (5.2) and (5.3). Firstly, equation (5.3) can be rewritten replacing viscosity with the kinetic-molecular derivation [5.7]

$$\eta = \tfrac{1}{2} N M \bar{u} \lambda = \frac{1}{2} \frac{PM}{RT} \left\{ \frac{8RT}{\pi M} \right\}^{\tfrac{1}{2}} \lambda$$

giving

$$J_P = \frac{\pi}{32} \frac{r}{\lambda} \frac{r\epsilon}{\chi} \left\{ \frac{8RT}{\pi M} \right\}^{\tfrac{1}{2}} \frac{M}{RT} \frac{\Delta P}{\delta} \tag{5.5}$$

This expression for Poiseuille flow appears similar to the Knudsen diffusion expression in equation (5.2), except for the geometric constants, and the r/λ term. A linear addition of the Knudsen and Poiseuille permeabilities gives

$$K = M \bar{u} (A + B/\lambda) \tag{5.6}$$

where $A = 2r\epsilon/3\chi RT$

$B = \pi r^2 \epsilon/32\chi RT$

$\bar{u} = (8RT/\pi M)^{\tfrac{1}{2}}$

At constant temperature, A and B are constants for any given membrane. Values calculated for A and B from membrane specifications may not be directly applicable to experimental results, due to the different meanings of pore size and tortuosity in the two mechanisms, however linear shifts in A and B do not invalidate the form of equation (5.6).

The mean free path of a gas, λ, is a function of the pressure

$$\lambda = L/P \qquad\qquad (5.7)$$

where L is the mean free path of the gas at unit pressure, and is dependent on the collision diameter of the gas molecule [5.7].

Recognising that a equals K/δ evaluated at P_{ref}, equations (5.6) and (5.7) give

$$a = M\,\bar{u}\,(A + BP_{ref}/L)\,/\,\delta \qquad\qquad (5.8)$$

In equation (5.4), b is defined as the Poiseuille permeability divided by the total permeability at the reference pressure. From equations (5.6) and (5.7)

$$b = (M\,\bar{u}\,B/\lambda)/(M\,\bar{u}\,(A + B/\lambda))$$

$$= (BP_{ref}/L)/(A + BP_{ref}/L) \qquad\qquad (5.9)$$

Equation (5.6) can be expressed in terms of **a** and **b**, giving

$$K/\delta = a\,(1 + b(P - P_{ref})/P_{ref})$$

$$= a\,(1 + b(P - 1)) \qquad\qquad (5.10)$$

$$\approx a\,P^{b} \qquad\qquad (5.4)$$

In the above derivation, three different expressions are given for K, in equations (5.4), (5.6) and (5.10). Equation (5.6) is a linear addition of the Knudsen and Poiseuille permeabilities, however it is not particularly useful as an engineering equation since it requires knowledge of the membrane properties r, ϵ and χ, and calculation of the gas properties $\bar{u}$ and λ. Equation (5.10) re-expresses equation (5.6) in terms of the more tangible parameters **a** and **b**, and equation (5.4) is an

approximation of equation (5.10). Equations (5.4) and (5.10) are equivalent for all values of $\mathcal{P}$ when b=0 or b=1, and for all values of b when $P=P_{ref}$. For other values, the two equations agree with reasonable accuracy provided P and P_{ref} do not differ by more than a factor of 3. Although equation (5.4) was used very successfully in this study, equation (5.10) may be more accurate in some situations, for example when pressures vary over a wide range. Also the linear relationship in equation (5.10) may simplify the mathematics in some analyses.

Other authors [5.1] have used the equation $K = a' + b'P$ to describe the Knudsen/Poiseuille transition. This is equivalent to equation (5.6), and has a disadvantage as an engineering equation, as a' and b' are dependent on each other. In equation (5.4), a is the membrane permeability, and b is a measure of the operating regime, whereas a' and b' are each components of the permeability and operating regime.

5.2 GAS PERMEATION

5.2.1 Experimental

A series of gas permeation experiments was conducted to test the efficacy of equation (5.4). The apparatus is shown in figure 5.1. Experiments were conducted with Millipore, Durapore, Gore-Tex and Enka membranes with pore sizes ranging from 0.1 to 0.45 μm. The gases used were He, CH_4, N_2, air, and CO_2. For a given membrane and gas, fluxes were measured for a range of pressures and pressure drops, with $10 \leq P \leq 90$ kPa, and $0 \leq \Delta P \leq 50$ kPa. Pressure drops were adjusted for the pressure loss across the membrane support. Gas fluxes were measured by a volumetric flow meter, operated at a pressure of 105 kPa.
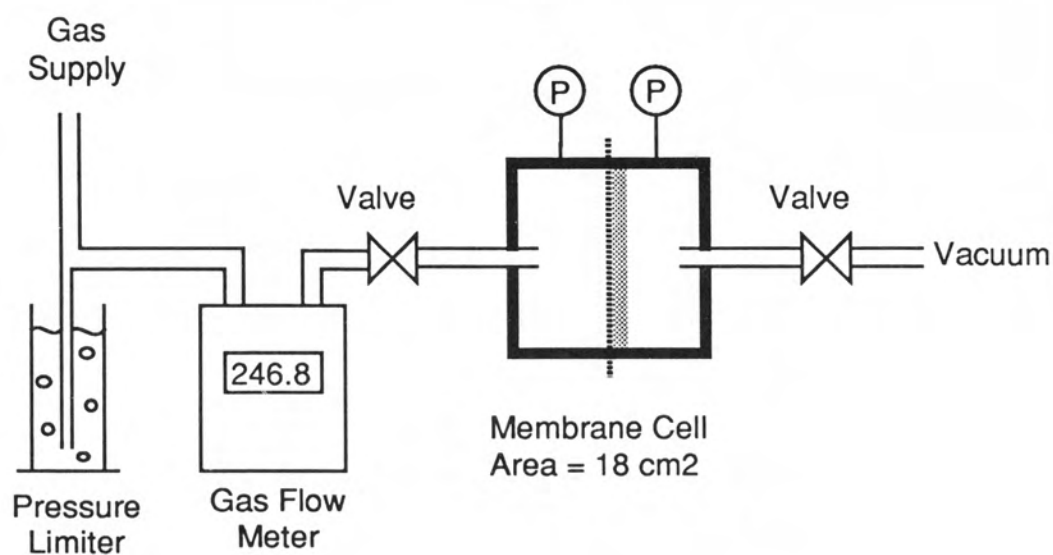
Figure 5.1 : Experimental gas permeation apparatus.

5.2.2 Results and Discussion

Initial experiments were conducted with air and a Durapore 0.45 μm PVDF

membrane, to compare the applicability of equations (5.2), (5.3), and

(5.4). (N.B. A partial separation of nitrogen and oxygen may be expected

in Knudsen diffusion.) To test the Knudsen and Poiseuille equations,

fluxes were plotted against ΔP and $P\Delta P$ respectively, as shown in figures

5.2(a) and 5.2(b). Knudsen diffusion under-predicts the fluxes at higher

pressures, while Poiseuille flow over-predicts. The proposed model,

equation (5.4), was tested by finding the value of the exponent, b, that

gave the best correlation of J vs. $\wp^b\Delta P$, with P_{ref}=50kPa.   The

correlation achieved with an exponent of b=0.34 was excellent, with

R^2=0.9950, as shown in figure 5.2(c).

Figure 5.3 shows the relationship between correlation coefficient and

exponent for this system, displaying the relatively poor correlations

achieved using Knudsen diffusion (b=0) and Poiseuille flow (b=1). It is

also apparent that good correlation is observed over a relatively broad

range of b values. For this system a b value anywhere between 0.24 and

0.44 gives a correlation greater than R^2=0.99. This facility makes

equation (5.4) useful as a predictive equation, as moderate errors in

predicting b can be tolerated without loss of accuracy. For example,

when studying a new system the permeability parameter a can be measured

by a single experiment, and a rough estimate of b can be used to

estimate permeabilities at other pressures. The values of a and b can

then be updated as more data points become available. A wide tolerance

on b also implies that the Knudsen diffusion equation may be used

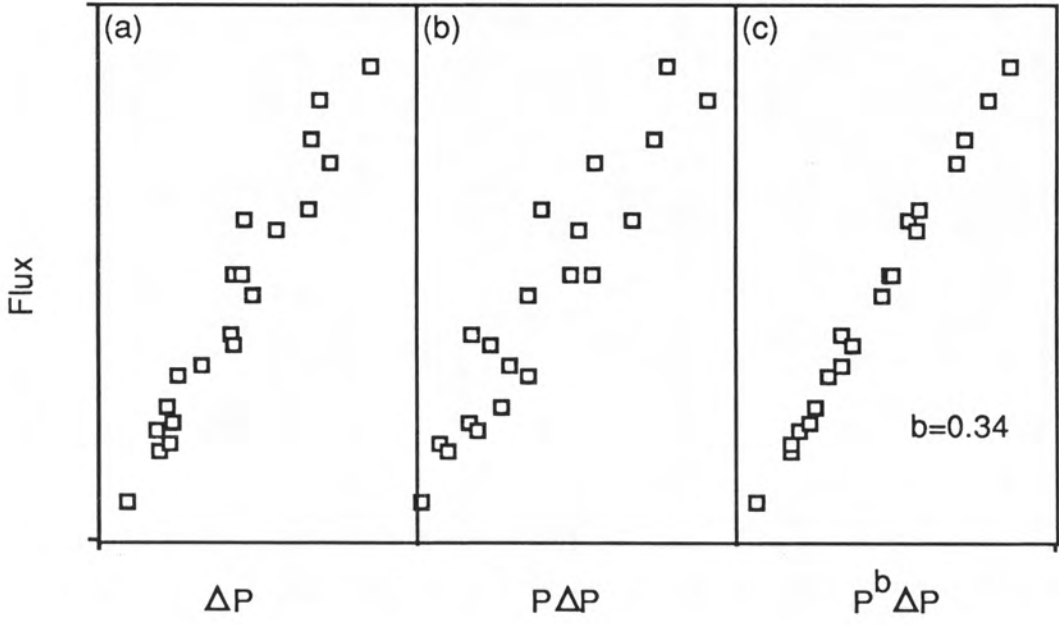provided b<0.1, and Poiseuille flow used if b>0.9.

Figure 5.2 : Normalised flux plotted according to
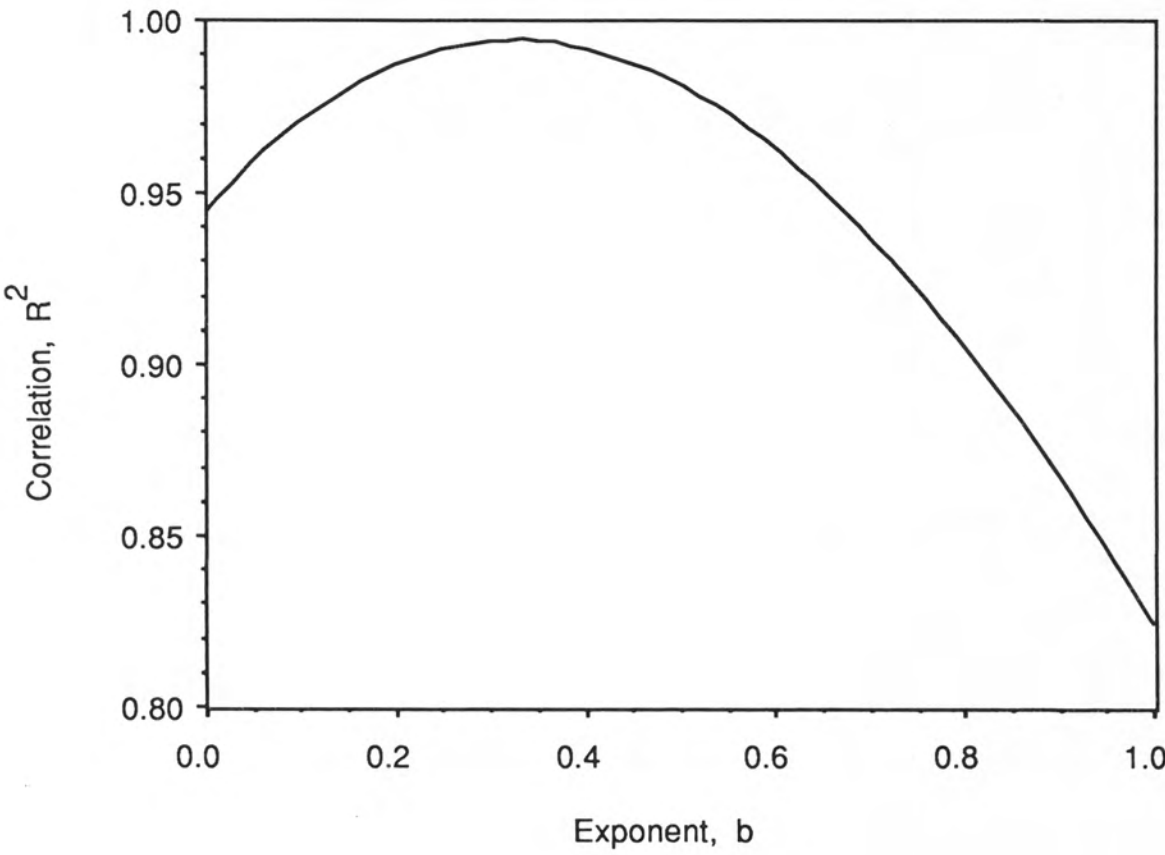(a) Knudsen diffusion, (b) Poiseuille flow, (c) Equation (5.4).

Figure 5.3 : Correlation achieved with equation (5.4) for different values of exponent b.

Gas permeation experiments were conducted with various microporous

membranes and gases, as shown in Table 5.1. The parameters reported

Table 5.1: Summary of Gas Permeation Results

Run	Membrane	Pore μm	Gas	$a \times 10^6$ kg/m^{2}sPa	$K \times 10^{10}$ s	b	R^2
1	Durapore HVHP	0.45	Air	6.25	6.88	0.34	0.9950
2	Durapore GVHP	0.22	Air	3.40	3.74	0.23	0.9975
3	Enka polyprop.	0.20	Air	2.71	3.79	0.20	0.9981
4	Enka polyprop.	0.10	Air	2.18	2.18	0.10	0.9986
5	Millipore GSWP	0.22	N_2	2.90	3.19	0.35	0.9996
6	Millipore GSWP	0.22	CO_2	4.73	5.20	0.51	0.9972
7	Millipore HAWP	0.45	N_2	6.66	7.33	0.41	0.9982
8	" " 2×thick	0.45	N_2	3.60	7.92	0.38	0.9944
9	Millipore HAWP	0.45	CO_2	10.97	12.07	0.52	0.9909
10	Millipore HAWP	0.45	He	0.77	0.85	0.13	0.9802
11	Gore-Tex PTFE	0.45	N_2	11.65	6.99	0.24	0.9978
12	Durapore HVHP	0.45	CO_2	8.55	9.41	0.57	0.9992
13	Durapore HVHP	0.45	N_2	5.46	6.01	0.54	0.9982
14	Durapore HVHP	0.45	CH_4	5.14	5.65	0.46	0.9982
15	Durapore HVHP	0.45	He	1.47	1.62	0.26	0.9972

in Table 5.1 are the membrane constant, a, the permeability, K ($=a\times\delta$),

the exponent b, and the correlation coefficient R^2. The high degree of

correlation observed in all the systems studied strongly supports the

form of equation (5.4). From the results with different membranes and

gases, several trends can be seen in the permeation parameters.

Runs 1, 2, 3, and 4 were conducted with the same gas, but different pore

size membranes. As expected, the permeability, K, increases with

increasing pore size. The exponent, b, also increases with pore size,

indicating the shift towards Poiseuille flow. These trends in K and b are shown in figure 5.4. (Note, when comparing membranes of different thicknesses, K values reflect the permeability of the porous structure, while a values reflect the membrane performance.) For Run 3, the permeability, K, was the same as for Run 2, however the membrane constant, a, was 25% lower, reflecting the greater thickness of the Enka membrane.

Runs 5 and 6 were conducted with the same membrane but different gases. It can be seen that the permeability increases with molecular weight, as predicted by both mechanisms. The exponent also increases with increasing molecular weight (decreasing mean free path) as expected. These trends, which are supported in later runs with different membranes, are displayed in figures 5.5 and 5.6. Results for the Durapore membrane are fitted approximately by dashed lines.

Runs 7 and 8 were conducted with the same membrane and gas, however in Run 8 two thicknesses of membrane were used. It can be seen that both the permeability and the exponent are virtually independent of membrane thickness.

Runs 7, 11 and 13 were conducted with the same gas, but different membranes with the same rated pore size. The three measured permeabilities were 7.33, 6.99, and 6.01×10^{-10} s respectively, which shows reasonable agreement for the three different membrane types. For the Gore-Tex membrane, however, the membrane constant, a, is roughly double that of the other membranes, due to decreased thickness. Thus, in service, the Gore-Tex membrane would provide substantially higher fluxes. The exponents for the three membranes vary by a factor of two (0.24 to 0.54), reflecting the different pore structures. This
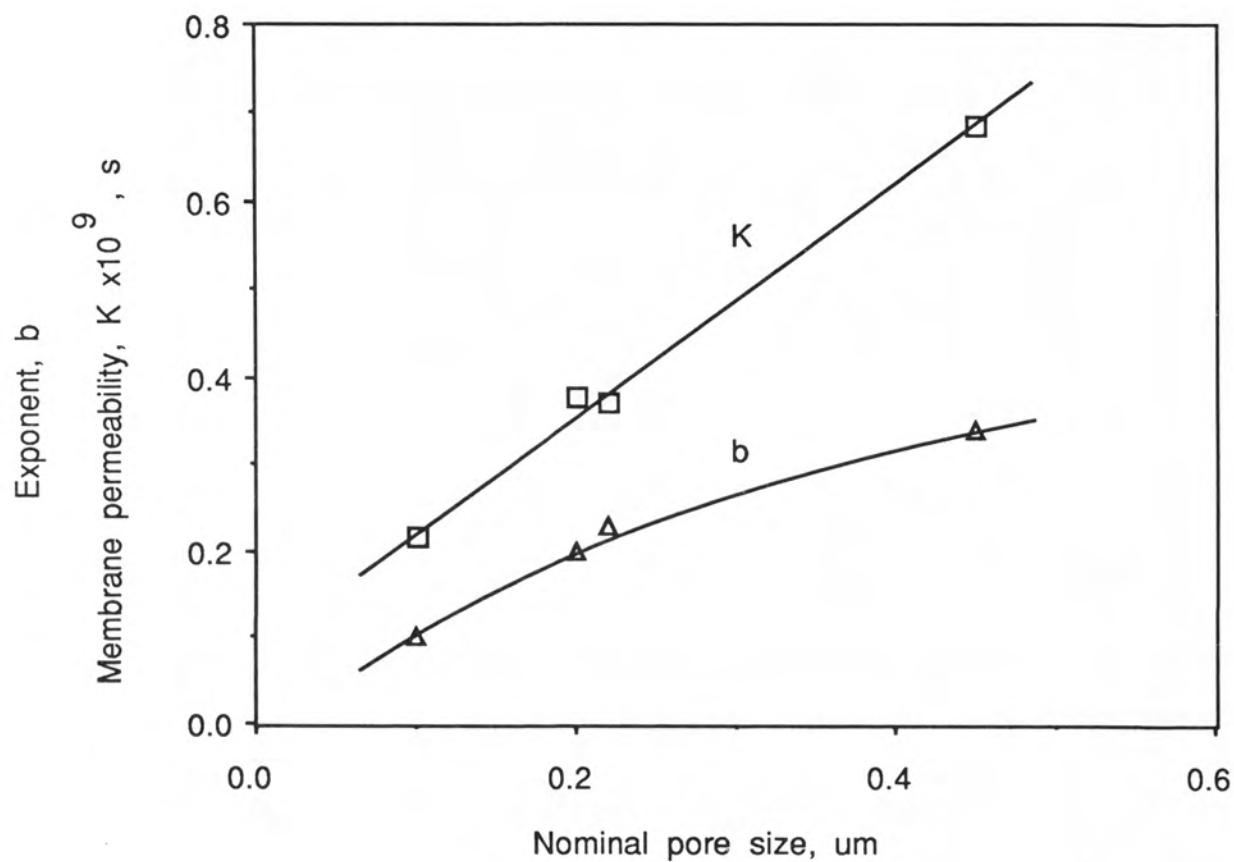
Figure 5.4 : Variation of permeability, K, and exponent, b, with pore size for air permeation through four membranes.

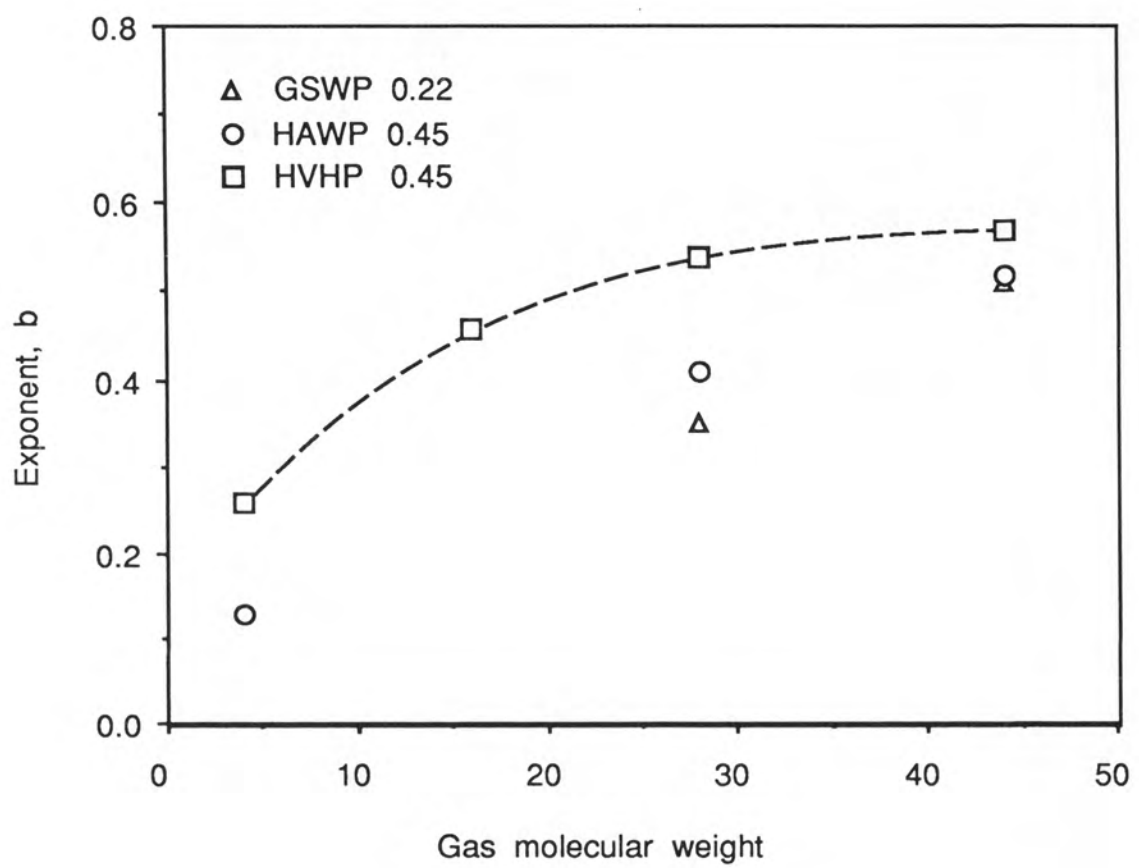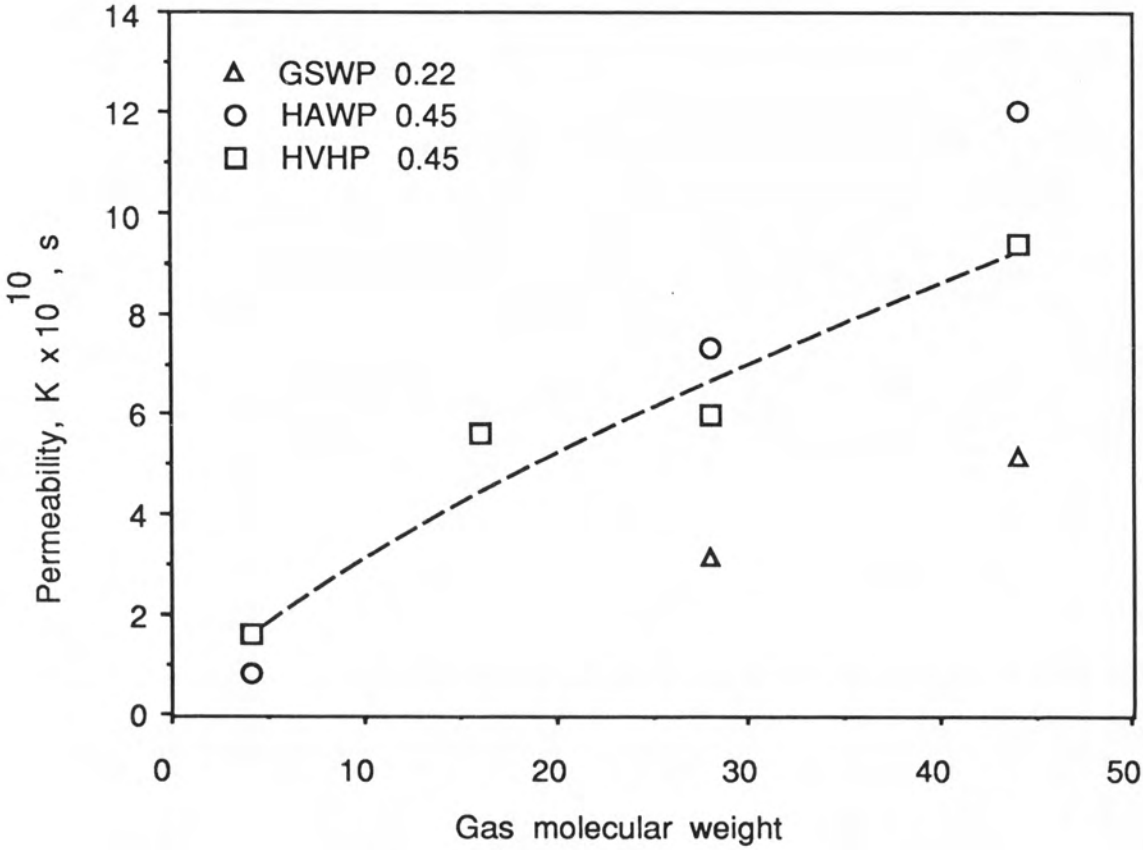Figure 5.5 : Variation of exponent, b, with molecular weight for three Millipore membranes.

Figure 5.6 : Variation of permeability, K, with molecular weight for three Millipore membranes.

emphasizes the need to measure the permeability parameters, as theoretical predictions would not yield such discrepancies. The fact that the three permeabilities are similar, yet the exponents differ, may provide useful information on the pore size distribution and pore shape of the different membranes. It is recommended that this phenomenon be investigated in future work.

Although equation (5.4) was formulated with the aim of predicting water vapour fluxes in MD, the results in Table 5.1 suggest that the equation may enjoy widespread use as an engineering equation for gas permeation in the Knudsen/Poiseuille transition region. The scope of application may be extended beyond this study to incorporate higher pressures and other porous materials, provided the gases are non-adsorbing, and the gas pressures do not vary by more than an order of magnitude.

5.3 WATER VAPOUR PERMEATION

The results for the various systems summarised in Table 5.1 have shown the merit of equation (5.4) as a gas permeation equation. The limitation of equation (5.4) is that the parameters **a** and **b** must be determined experimentally. The aim of this study was to describe the flux of water vapour through deaerated membrane distillation membranes. The parameters **a** and **b** cannot be determined directly from MD experiments, as the water vapour pressures on either side of the membrane are not known accurately, and it is difficult to totally deaerate the membrane. Neither is it convenient to conduct gas permeation experiments with water vapour, due to condensation within the apparatus. Hence the parameters **a** and **b** for water vapour were determined from the measured parameters for other gases.

For the Durapore 0.45 μm PVDF membrane, gas permeation experiments were conducted with CO_2, N_2, CH_4 and He in runs 12, 13, 14 and 15 respectively. The results obtained were used to estimate a and b for water vapour permeation through the Durapore membrane. (Note, results from run 1 with air were not included in this analysis, as the membrane used was from a different batch.) As a first approximation, results for the Durapore membrane shown in figures 5.5 and 5.6 (dashed lines) were used to estimate a ($=K/\delta$) and b for a molecular weight of 18 g/mol (water). This yielded a $= 4.4 \times 10^{-6}$ kg/m^{2}sPa, and b $= 0.47$. This interpolation based on molecular weight, however, is only approximate, as other gas properties such as the collision diameter are relevant [5.7].

More accurate estimates of a and b can be obtained by the use of equation (5.6), which expresses the permeability in terms of the membrane parameters A and B, and the gas parameters M, $\bar{u}$ and λ. As A and B are independent of the gas species, they can be evaluated from the results for one gas, and used to estimate a and b for another gas. (Note, having evaluated A and B, equation (5.6) can be used directly for predicting water vapour flux, however it has the disadvantage of expressing the permeability in terms of the gas properies $\bar{u}$ and λ.)

For each experimental point in runs 12, 13, 14 and 15, K was calculated from equation (5.1), and for each gas, $\bar{u}$ was calculated from equation (5.6). The mean free path at unit pressure, L, was calculated for each gas from viscosity data [5.8] using equation (5.5). For each experimental point, λ was then calculated from the average pressure using equation (5.7).

For the various gases and operating conditions, $K/M\bar{u}$ was plotted against

$1/\lambda$, as shown in figure 5.7. The intercept and slope of figure 5.7 gave $A = 2.2 \times 10^{-11}$ mol/m^{2}Pa and $B = 3.1 \times 10^{-18}$ mol/mPa for the Durapore membrane. The degree of overlapping of the points in figure 5.7 displays the fact that A and B are properties of the membrane and independent of the gas. This means that the values of A and B for the Durapore membrane can be used to calculate a and b for other gases using equations (5.8) and (5.9) and an appropriate reference pressure.

For the permeation of water vapour in MD, a reference pressure of 25 kPa was used, giving reasonable accuracy of equation (5.4) over the range 8 to 75 kPa (40 to 90°C). For the Durapore 0.45 μm PVDF membrane, a and b were calculated from A and B as $a = 3.7 \times 10^{-6}$ kg/m^{2}sPa and b = 0.43. In other words, water vapour fluxes through a deaerated Durapore 0.45 membrane may be described by the equation $J = 3.7 \times 10^{-6} (P/25000)^{0.43} \Delta P$.

The same procedure was used to estimate a and b for water vapour for an Enka 0.2 μm polypropylene membrane, based on the air permeation results of Run 3. The permeation results plotted according to equation (5.6) are shown in figure 5.8. The clusters of points in figure 5.8 represent experiments with the same average pressure, but different pressure drops. From the intercept and slope of figure 5.8, $A = 1.7 \times 10^{-11}$ mol/m^{2}Pa and $B = 7.1 \times 10^{-19}$ mol/mPa. Again using a reference pressure of 25 kPa, this gives $a = 1.6 \times 10^{-6}$ kg/m^{2}sPa and b = 0.19. The lower value of b for the Enka 0.2 μm membrane reflects the smaller pore size, and hence greater tendency towards Knudsen diffusion. The Durapore 0.45 μm and Enka 0.2 μm membranes were used exclusively in the deaeration study in chapter 6, with the results supporting the estimated parameters.

The above procedure would be greatly simplified if the membrane
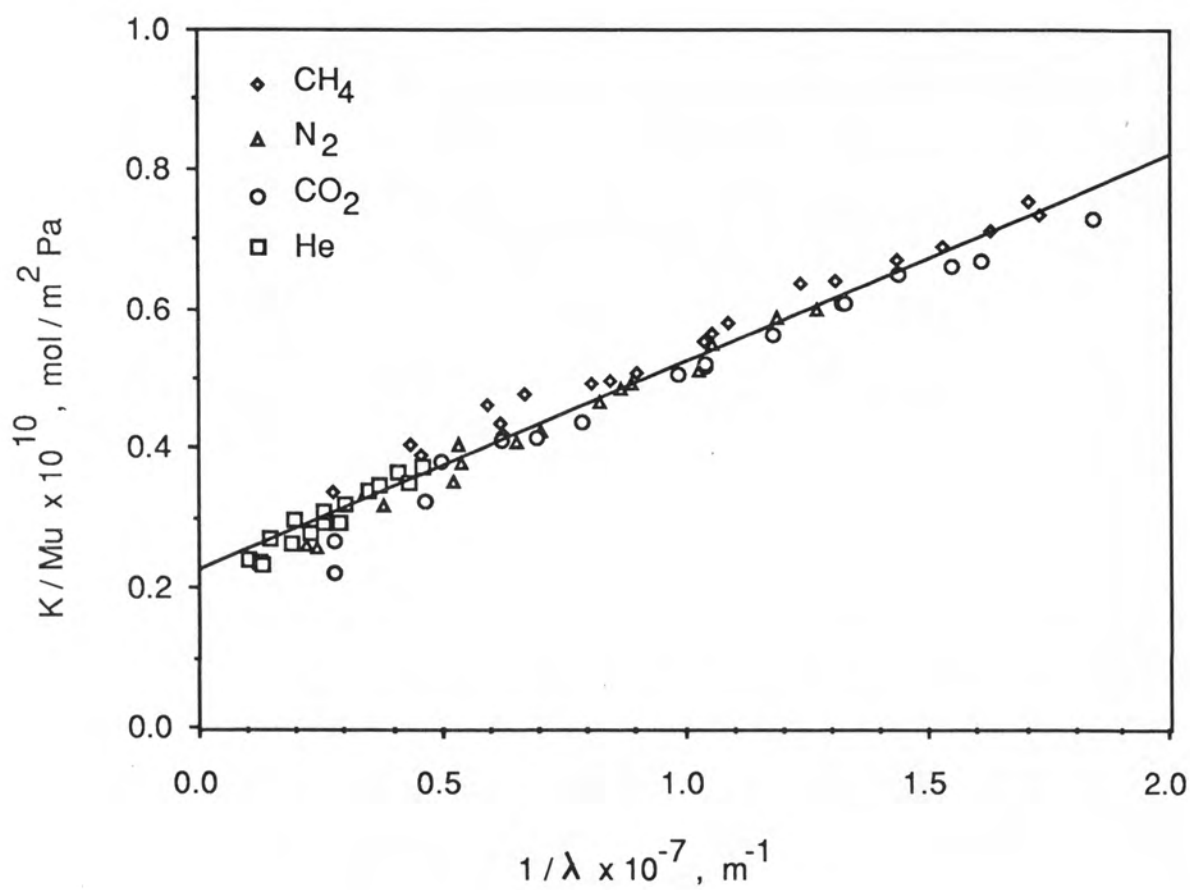
Figure 5.7 : Results from runs 12, 13, 14 and 15 plotted according to equation (5.6).
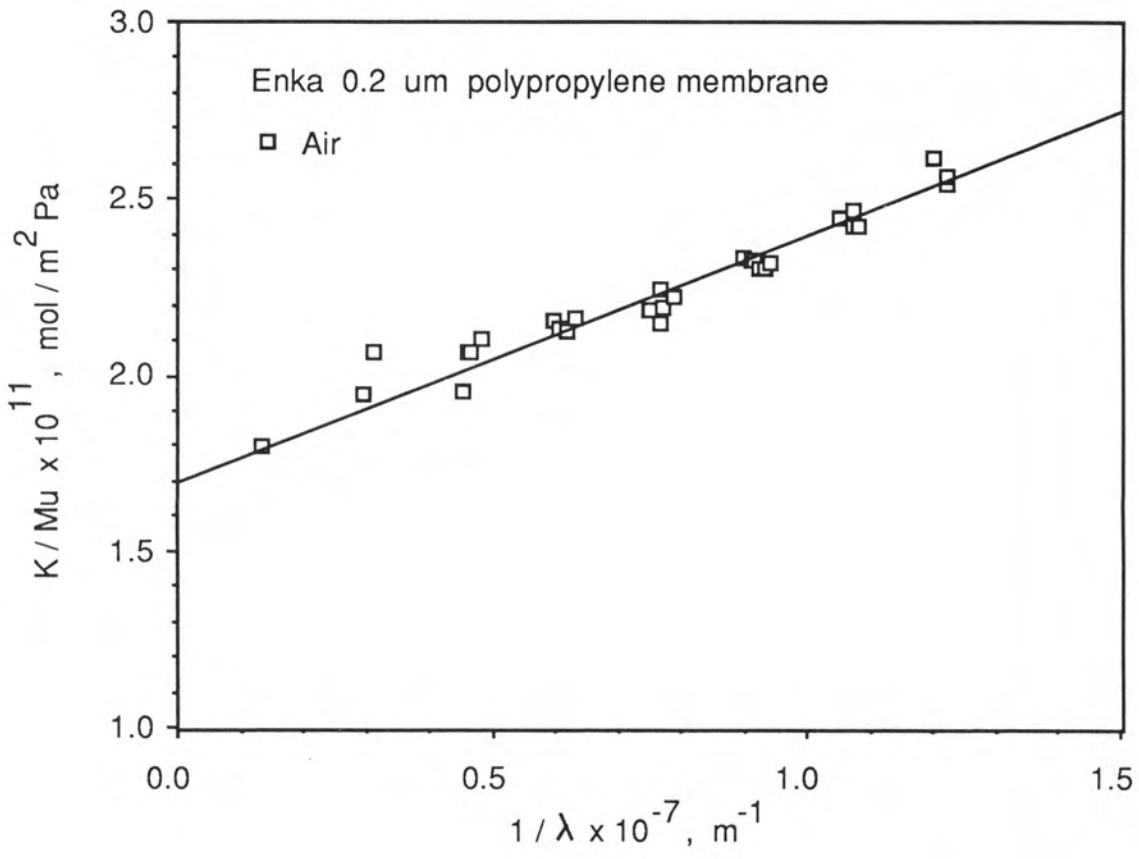
Figure 5.8 : Results from run 3 plotted according to equation (5.6).

parameters A and B could be estimated from membrane specifications rather than measured from gas permeation experiments. Table 5.2 compares

Table 5.2:   Comparison of Calculated and Measured Parameters A and B.

Equation (5.6) Parameters	A	B
Durapore 0.45 μm PVDF Calculated using r = 0.23 μm*	2.3×10^{-11}	7.5×10^{-19}
Measured from figure 5.7	2.2×10^{-11}	3.1×10^{-18}
Enka 0.2 μm Polypropylene Calculated using r = 0.1 μm*	1.0×10^{-11}	1.5×10^{-19}
Measured from figure 5.8	1.7×10^{-11}	7.1×10^{-19}

* ϵ=0.75, χ=2.

the values of A and B estimated from equation (5.6) using the manufacturers specifications with those measured experimentally. While the estimated and measured values of A show reasonable agreement (using a tortuosity of χ=2), the estimated values of B do not agree with those taken from figures 5.7 and 5.8. This does not mean that the results in figures 5.7 and 5.8 contradict equation (5.6). To the contrary, the linearity of the two figures supports the form of equation (5.6), justifying the linear addition of the Knudsen and Poiseuille permeabilities. The discrepancy between the predicted and measured values of B is most probably due to the use of an inappropriate pore size. For example, the appropriate pore dimension in Knudsen diffusion is the mean distance between molecule/wall collisions, while in Poiseuille flow the appropriate dimension is the mean hydraulic pore radius. The ramification of this is that the membrane parameters, A and B, cannot be estimated accurately from the membrane specifications, and must be determined experimentally.

5.4 CONCLUSIONS

This study of gas permeation in the Knudsen/Poiseuille transition region was conducted to investigate water vapour flux through totally deaerated MD membranes. The mass transfer equation $J = a\bar{P}^b\Delta P$ was formulated as an alternative to the more complex models in the gas permeation literature. The permeation parameter **a** is the membrane mass transfer constant $(J/\Delta P)$ measured at some reference pressure, while **b** indicates the extent to which Poiseiulle flow contributes to the flux. The equation was tested using various membranes and gases at subatmospheric pressures, giving excellent correlations in all cases. The simplicity and accuracy of the proposed equation makes it favourable over more rigorous models as an engineering equation for gas permeation.

The results from permeation experiments with other gases were used to predict the permeation parameters for water vapour through two different MD membranes. For a Durapore 0.45 μm PVDF membrane, $a = 3.7 \times 10^{-6}$ kg/m^{2}sPa and $b = 0.43$, and for an Enka 0.2 μm polypropylene membrane, $a = 1.6 \times 10^{-6}$ kg/m^{2}sPa and $b = 0.19$. These values were used successfully in the modelling of MD fluxes, the details of which are given in chapter 6.

5.5 ACKNOWLEDGEMENTS

5.6 NOTATION

a   Membrane permeability constant $[kg\ m^{-2}\ s^{-1}\ Pa^{-1}]$

A   Defined in equation (5.6)

b   Exponent defined in equation (5.4) [-]

B   Defined in equation (5.6)

J   Mass flux through membrane $[kg\ m^{-2}\ s^{-1}]$

K   Membrane permeability [s]

L   Mean free path at unit pressure [m Pa]

M   Gas molecular weight $[kg\ mol^{-1}]$

N   Gas density $[mol\ m^{-3}]$

P   Average gas pressure within membrane [Pa]

P_{ref} Reference pressure [Pa]

ΔP   Pressure drop across membrane [Pa]

℘   Dimensionless pressure = P/P_{ref} [-]

r   Membrane pore radius [m]

R   Gas constant $[J\ mol^{-1}\ K^{-1}]$

R^2 Correlation coefficient

T   Temperature [K]

ū   Mean molecular speed $[m\ s^{-1}]$

δ   Membrane thickness [m]

ε   Membrane porosity [-]

η   Gas viscosity [Pa s]

λ   Mean free path of gas [m]

χ   Membrane tortuosity [-]

Subscripts

K   Knudsen

P   Poiseuille

5.7 REFERENCES

[5.1] Present, R.D., "The Kinetic Theory of Gases", McGraw-Hill, 1958.

[5.2] Schneider, P., "Permeation of Simple Gases through a Porous Medium", Collection Czech. Chem. Commun., 40 (1975) 3114-3122.

[5.3] Creutz, E., "The Permeability Minimum and the Viscosity of Gases at Low Pressure", Nuc. Science and Eng., 53 (1974) 107-109.

[5.4] Kamide, K, and Manabe, S., "Characterization Technique of Straight-Through Porous Membrane", in Cooper, A.R., (ed.), "Ultrafiltration Membranes and Applications", Plenum, N.Y., 1980.

[5.5] Evans, R.B., Watson, G.M., Mason, E.A., "Gaseous Diffusion in Porous Media at Uniform Pressure", J. Chem. Phys., 35(6) (1961) 2076-2083.

[5.6] Evans, R.B., Watson, G.M., Mason, E.A., "Gaseous Diffusion in Porous Media. II. Effect of Pressure Gradient", J. Chem. Phys., 36(7) (1962) 1894-1902.

[5.7] Barrow, G.M., "Physical Chemistry", 2nd ed., McGraw-Hill, 1966.

[5.8] Perry, R.H. and Chilton, C.H., "Chemical Engineers' Handbook", 5th ed., McGraw-Hill, 1974.

Chapter 6

Mass
Transfer
in
MD
Membranes

CHAPTER 6: MASS TRANSFER IN MD MEMBRANES

Gas phase mass transfer in MD relates to water vapour permeation through membrane pores containing various levels of entrapped air. The previous chapter dealt with gas permeation through microporous membranes, leading to an equation predicting water vapour flux through deaerated MD membranes. This chapter extends the theory to describe fluxes for both deaerated and aerated MD systems.

The partial pressure of air within the membrane pores can be reduced by either deaerating the feed (and/or permeate) or by reducing the pressure of the liquids bounding the membrane. Previous work by Schofield [6.1] and Schneider and van Gassel [6.2] showed flux increases of 20 - 50 % by deaeration. These results were confirmed in this study. Examination of the results from a theoretical perspective showed this flux enhancement to be the result of a complex interaction between increased membrane permeability and worsened temperature polarisation. The results also showed that deaeration can lead to a reduction in the heat loss by conduction across the membrane.

6.1 THEORY

Air trapped within MD membranes can be considered as a stationary film, as its ability to exit through the condensing interface is limited by its solubility. The solubility of air in water is of the order of 10 ppm, implying that the flux of air is many orders of magnitude lower than that of water. Accordingly, the air establishes a pressure gradient opposing the flux of water vapour. In section 2.2, it was shown that molecular diffusion in the context of MD can be described by the equation

$$J = \frac{1}{P_a} \frac{\epsilon}{\chi\delta} \frac{DP'M}{RT} \Delta P$$

$$\equiv \frac{d}{P_a} \Delta P \qquad\qquad (6.1)$$

where P_a is the average pressure of air within the membrane, P' is the total gas pressure (air plus water vapour), ΔP is the water vapour pressure drop, and **d** accounts for the diffusion coefficient and membrane geometry. The parameter **d** is essentially constant, as the product of D and P' is a constant. The temperature dependence of **d** can be ignored as most MD systems operate within a narrow range of average membrane temperatures (typically 310 to 350 K).

Equation (6.1) is not sufficient to model MD fluxes under all conditions, as it predicts infinite flux for a totally deaerated membrane. Clearly this is not the case. Chapter 5 detailed the development of a novel semi-empirical equation suited to the description of water vapour flux through a deaerated membrane. The equation, based on a combination of Knudsen diffusion and Poiseuille (viscous) flow, is

$$J = a\wp^b \Delta P \qquad\qquad (6.2)$$

The parameters **a** and **b** were measured for a variety of gases and membranes, allowing their estimation for water vapour flux through the MD membranes used in this study (see chapter 5).

In this analysis, equations (6.1) and (6.2) were combined by assuming that the two mechanisms are independent. Thus the overall resistance in an MD membrane is equal to the membrane resistance plus the molecular diffusion resistance, giving

$$J = \left\{ \frac{1}{a \wp^b} + \frac{P_a}{d} \right\}^{-1} \Delta P \qquad (6.3)$$

In order to use equation (6.3), heat transfer theory must be used to relate the vapour pressures to the bulk liquid temperatures. The heat transfer theory presented in chapter 2 is summarised below,

The heat transfer equations governing heat flows in and around the membrane are

$$Q''_v = J \ \Delta H_v = h_v \ \Delta T_m \qquad (6.4)$$

$$Q''_c = (k_m/\delta) \ \Delta T_m = h_c \ \Delta T_m \qquad (6.5)$$

$$Q'' = Q''_v + Q''_c \qquad (6.6)$$

$$Q'' = h_f \ \Delta T_f = h_p \ \Delta T_p \qquad (6.7)$$

From equations (6.3) and (6.4), the vapour heat transfer coefficient can be written

$$h_v = \Delta H_v \frac{dP}{dT} \left\{ \frac{1}{a \wp^b} + \frac{P_a}{d} \right\}^{-1} \qquad (6.8)$$

where dP/dT is the slope of the vapour pressure curve evaluated at the average membrane temperature, and is approximately equal to $\Delta P/\Delta T_m$. The membrane conductivity, k_m, in equation (6.5) can be estimated from the solid and gas conductivities, using

$$k_m = \epsilon k_g + (1-\epsilon)k_s \qquad (6.9)$$

with a typical value being k_m=0.05 W/mK (chapter 4). The feed and permeate film heat transfer coefficients, h_f and h_p, can be estimated from heat transfer theory if the fluid dynamics are well defined, or may be measured experimentally.

For the symmetrical apparatus used in this study, the feed and permeate film heat transfer coefficients were equal, allowing their combination in an overall film heat transfer coefficient, $h = h_f/2$. This symmetry somewhat simplified the interpretation of results, as the average membrane temperature was equal to the average of the hot and cold bulk temperatures. In general, however, this simplification does not apply.

Solving equations (6.4) to (6.7), the flux may be written in terms of the bulk feed and permeate temperatures,

$$J = \frac{h_v}{\Delta H_v} \frac{h}{h_v + h_c + h} (T_f - T_p) \tag{6.10}$$

$$\text{where} \quad h = (1/h_f + 1/h_p)^{-1}$$

$$h_v = \Delta H_v \frac{dP}{dT} \left\{ \frac{1}{a \wp^b} + \frac{P_a}{d} \right\}^{-1}$$

$$h_c = (\epsilon k_g + (1-\epsilon)k_s) / \delta$$

Equation (6.10) simply states that flux = permeability × driving force, where h_v is the heat transfer equivalent of the membrane permeability, $(T_f - T_p)$ is the overall driving force, and ΔH_v converts the mass flux to a heat flux. The remaining term in equation (6.10) is an expression for the temperature polarisation coefficient, TPC, where

$$TPC \equiv \frac{\Delta T_m}{(T_f - T_p)} = \frac{h}{h_v + h_c + h} \tag{6.11}$$

The temperature polarisation coefficient reflects the fraction of the overall driving force, $(T_f - T_p)$, that contributes to the membrane driving force, ΔT_m.

Equation (6.10) can be rearranged to give a relationship between the inverse of flux, $1/J$, and the average partial pressure of air, P_a.

$$1/J = \frac{\Delta H_v}{h \, \Delta T_b} \frac{h_v + h_c + h}{h_v}$$

$$= \frac{\Delta H_v}{h \, \Delta T_b} \left\{ 1 + \frac{h_c + h}{\Delta H_v \, dP/dT} \left(\frac{1}{a \wp^b} + \frac{P_a}{d} \right) \right\}$$

$$= \left\{ \frac{\Delta H_v \, dP/dT \, a \wp^b + h + h_c}{h \, \Delta T_b \, dP/dT \, a \wp^b} \right\} + \left\{ \frac{h + h_c}{d \, h \, \Delta T_b \, dP/dT} \right\} P_a \qquad (6.12)$$

Equation (6.12) shows that a plot of $1/J$ versus P_a should be linear. Furthermore, for a system where a, b, and h_c are known, equation (6.12) can be used to determine h and d. For fixed feed and permeate temperatures, ΔT_b is constant, and for the symmetrical apparatus, dP/dT is constant, being a function of the average membrane temperature (see section 2.1). If fluxes for various partial pressures of air are plotted according to equation (6.12), h can be calculated from the intercept, and d can be calculated from the slope.

Equation (6.10) is similar to the equation used in chapter 4, with the addition of three parameters describing membrane mass transfer. In all there are five parameters which must be known or estimated in order to use equation (6.10). These are discussed below in order of their importance.

The film heat transfer coefficient, h, is the most important parameter governing MD. Provided the membrane selection is reasonable, the flux will be mainly determined by h. Methods of predicting and measuring h, or its components h_f and h_p, were given in chapter 4.

The molecular diffusion parameter, d, is the major parameter controlling the membrane permeability. It can be estimated from the air-water binary

diffusion coefficient and the membrane porosity and tortuosity using equation (6.1). In this work, a tortuousity of $\chi=2$ yielded good agreement between measured and predicted fluxes.

The gas permeation parameters **a** and **b** become important in deaerated MD systems. For the membranes used in this chapter, **a** and **b** were determined in chapter 5.

The membrane conductivity, k_m, is the fifth parameter needed to describe MD heat and mass transfer. This can be estimated with reasonable certainty from equation (6.9), as was detailed in chapter 4.

6.2 EXPERIMENTAL

An experimental program was conducted to study flux enhancement by deaeration, and to validate the heat and mass transfer theories. As the focus of attention was the membrane permeability at various air partial pressures, experiments were conducted with water as the feed. This avoided solution effects such as concentration polarisation and vapour pressure reduction. The experimental apparatus is shown in Figure 6.1.

The sheet membrane cell used in this study was described fully in chapter 3. Basically it is a jacketted cell where heating and cooling water control the temperature of the feed and permeate films. The feed and permeate lines were connected to a central reservoir, ensuring that the pressure was the same on either side of the membrane. Permeate flux was measured by meniscus rise in a graduated tube. The reservoir pressure was varied over a range of sub-atmospheric pressures to control the maximum gas pressure within the membrane. It was assumed that the
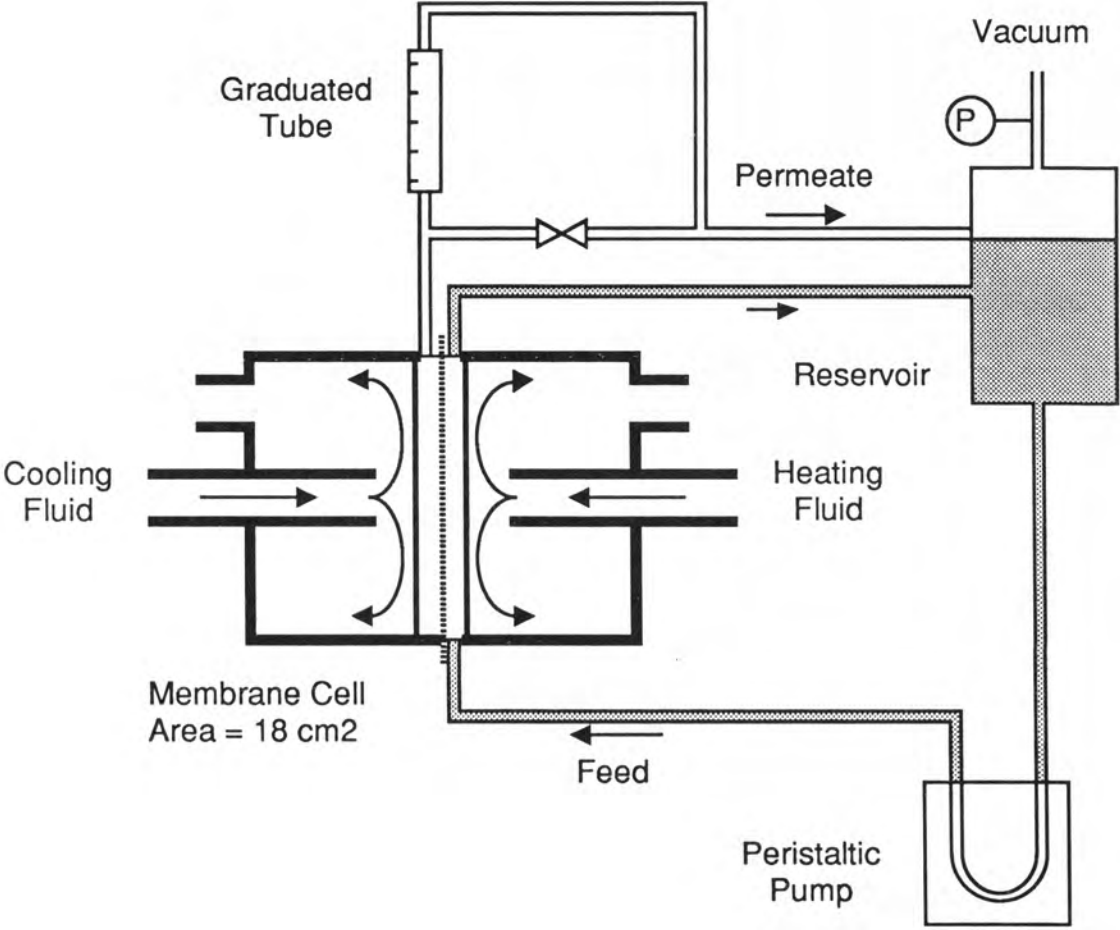
Figure 6.1 : Deaerated membrane distillation apparatus.

average partial pressure of air within the membrane was equal to the liquid pressure minus the water vapour pressure evaluated at the average membrane temperature. The symmetry of the apparatus meant that the average membrane temperature was equal to the average of the heating and cooling fluid temperatures.

Initially, problems were encountered with flux stability and reproducibility, especially at high fluxes. Increasing the thickness of the hydrophilic spacers between the membrane and the heat transfer surfaces rectified this problem, however the penalty was a decrease in flux (lower film heat transfer coefficients). It appears that at high fluxes, the resistance to flow of the spacer material was significant. With film thicknesses of around 0.5 mm, steady state fluxes were observed after several minutes, and were reproducible.

Experiments were conducted with a range of temperatures between 25 and 90 °C, with temperature differences between 10 and 55 °C. Air pressures were varied between 10 and 90 kPa. Experiments were conducted with a Durapore 0.45 μm PVDF membrane, using two different film thicknesses (i.e. two different film heat transfer coefficients), and with an Enka 0.2 μm polypropylene membrane. Note, the feed and permeate temperatures used for theoretical purposes are actually the heating and cooling water temperatures.

6.3 RESULTS AND DISCUSSION

6.3.1 Experimental Results

Results for the Durapore membrane with two different film thicknesses, and for the Enka membrane are shown in figures 6.2, 6.3 and 6.4. The
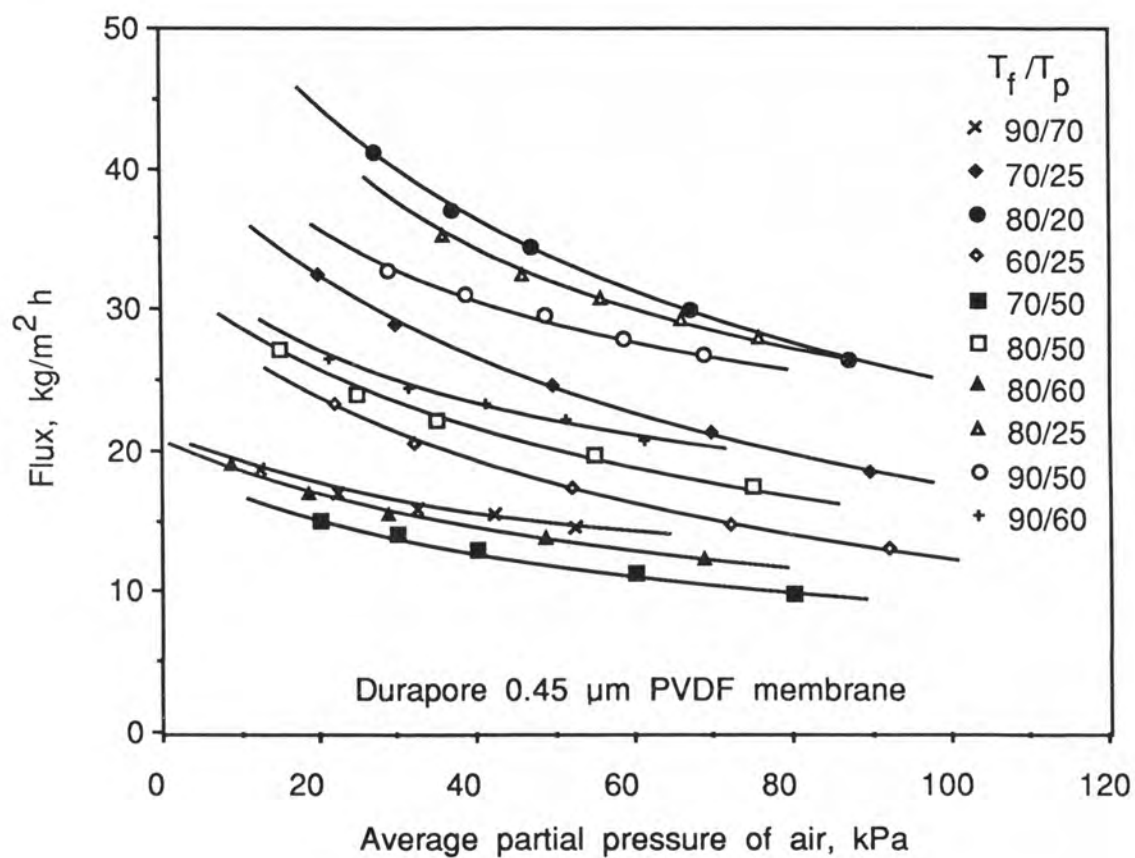
Figure 6.2 : Effect of deaeration on flux for various heating and cooling water temperatures, T_f and T_p.
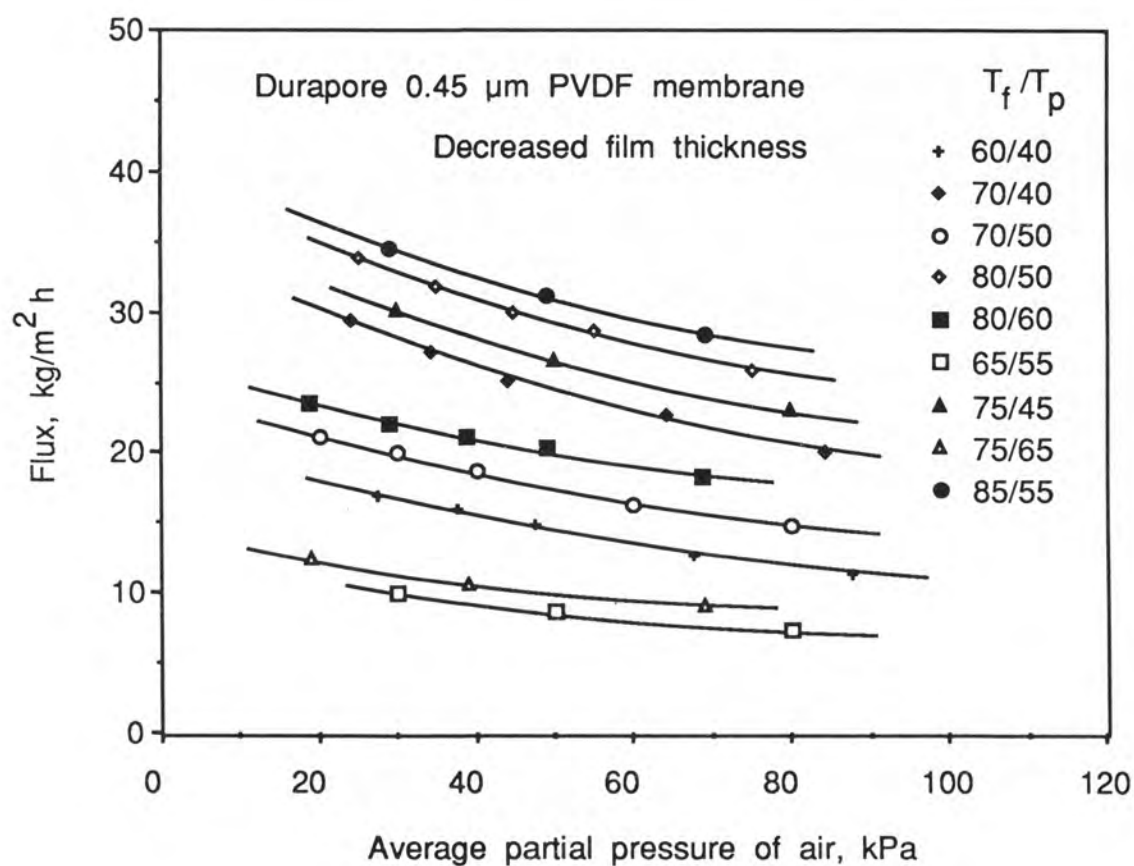
Figure 6.3 : Effect of deaeration on flux at various temperatures with increased film heat transfer coefficient.
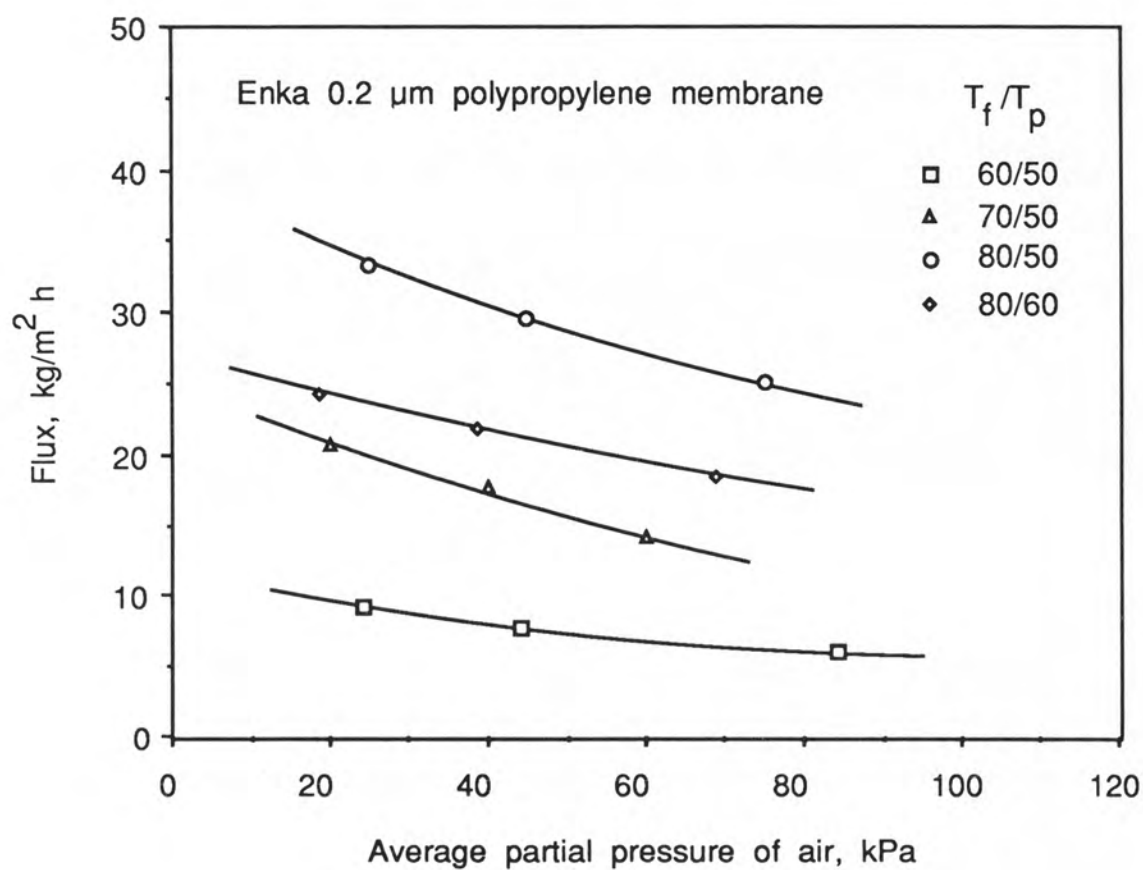
Figure 6.4 : Effect of deaeration on flux at various temperatures for Enka membrane.

flux increases observed with deaeration were in the range 20 to 80%, which is consistent with previous observations [6.1,6.2]. The curves fitted to these figures show that the relationship between J and P_a is not straightforward. For example, in figure 6.4, the curves for T_f/T_p = 80/60 and 70/50 have significantly different slopes. The flux increase with deaeration from P_a = 70 to 20 kPa is 60% for the 70/50 case, but only 30% for the 80/60 case. This reflects the fact that the higher temperature case would have a higher value of h_v (chapter 4), making it more heat transfer limited. Thus the response to increased membrane permeability would be less.

From figures 6.2 to 6.4, it is apparent that lower levels of air were achieved in the laboratory for the cases with lower temperature differences. At high temperature differences, the vapour pressure in the feed film is substantially higher than the average vapour pressure within the membrane. Thus flashing may occur within the feed film, while there is still a substantial pressure of air within the membrane. Flashing was observed by the presence of vapour in the feed return line. Results where flashing occurred were ignored, as the feed film heat transfer coefficient is greatly effected by the presence of a vapour phase in the feed film.

The results in figures 6.2, 6.3 and 6.4 were plotted according to equation (6.12), as shown in figures 6.5, 6.6 and 6.7. The linearity observed in all cases supports the theory. Values of h for the three systems were calculated from the various intercepts, and d was calculated from the slopes. The results are summarised in Table 6.1. Also shown in Table 6.1 are the values of the three parameters needed to solve equation (6.12). These were determined in chapters 4 and 5.
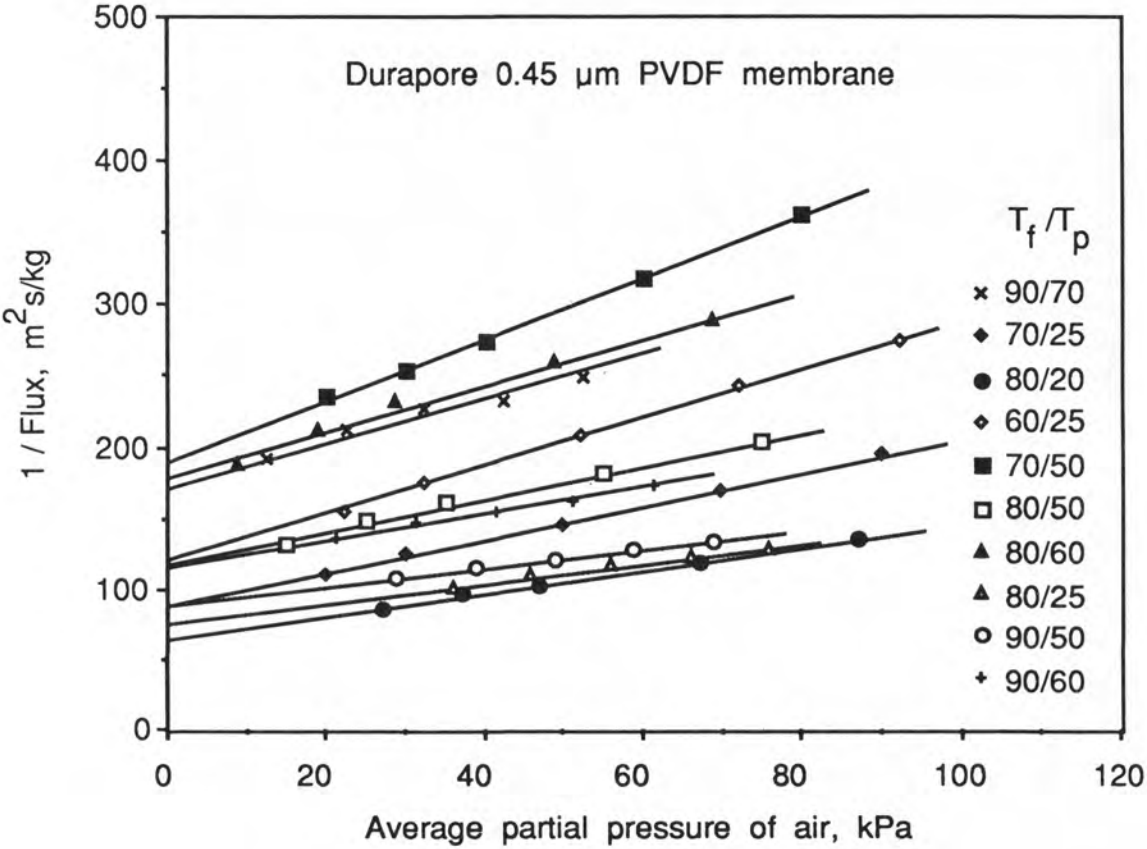
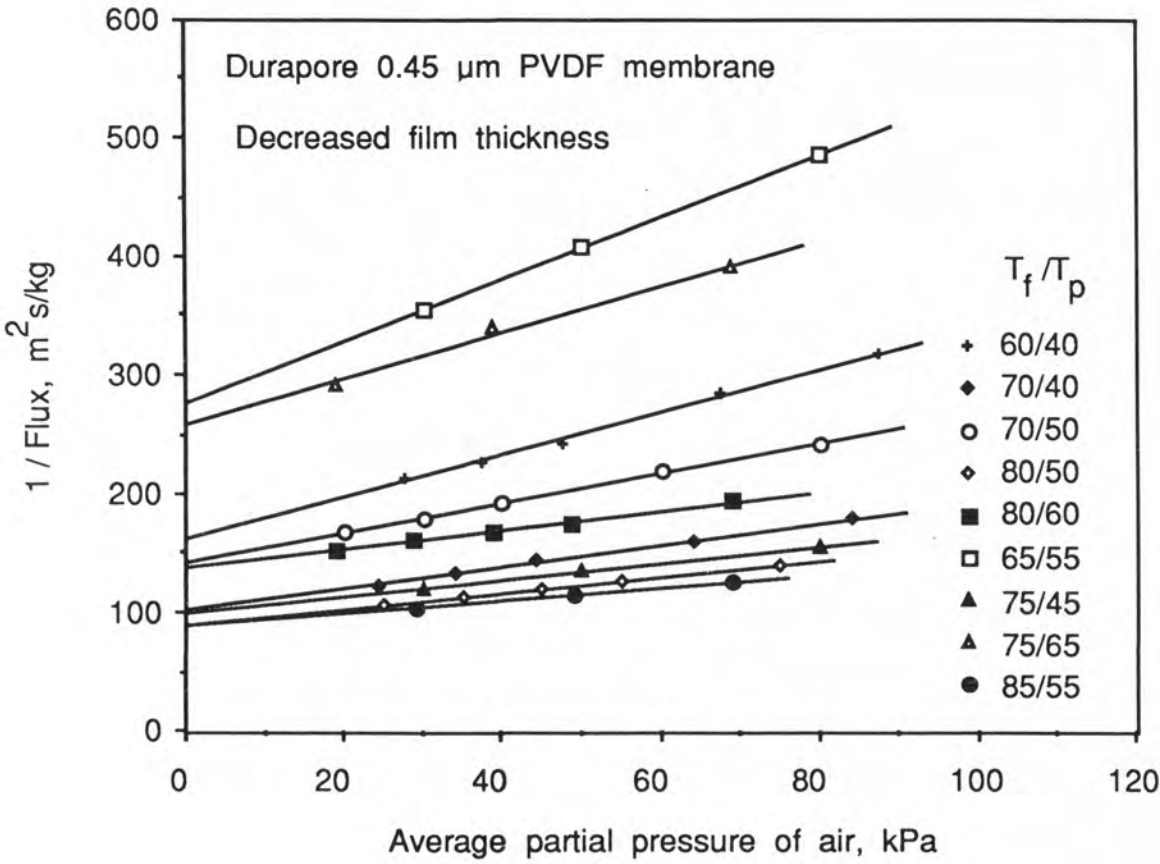Figure 6.5 : Results from figure 6.2 plotted according to equation (6.12)

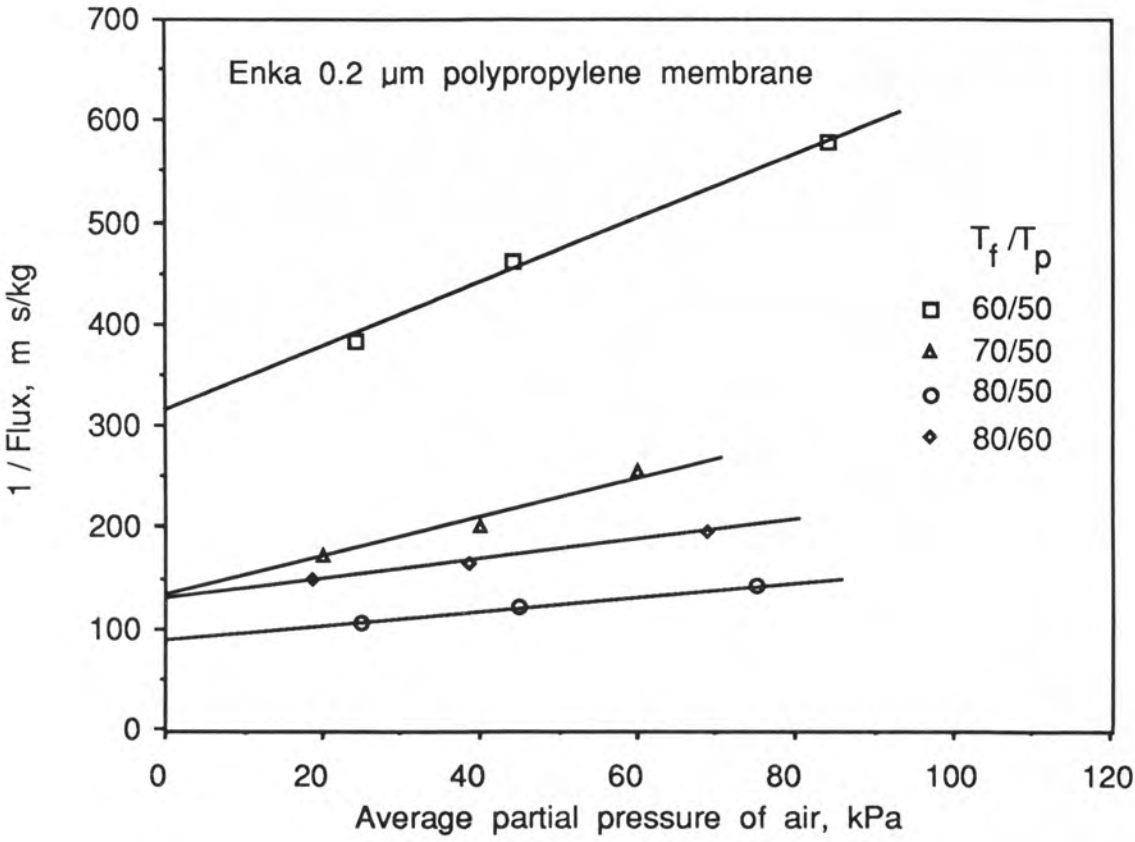Figure 6.6 : Results from figure 6.3 plotted according to equation (6.12)

Figure 6.7 : Results from figure 6.4 plotted according to equation (6.12)

Table 6.1: Five Heat and Mass Transfer Parameters for the Three

Experimental Systems in Figures 6.2, 6.3 and 6.4.

Membrane	$a \times 10^6$ kg/m^{2}sPa	b	h_c W/m^{2}K	h W/m^{2}K	d kg/m^{2}s
PVDF 0.45 μm	3.7	0.43	700	760 $\pm$ 50	0.056 $\pm$ 0.010
PVDF 0.45 μm	3.7	0.43	700	1020 $\pm$ 30	0.069 $\pm$ 0.006
ENKA 0.20 μm	1.6	0.19	370	1210 $\pm$ 20	0.052 $\pm$ 0.002

The values of h shown in Table 6.1 suggest that temperature polarisation was significant in the experimental system (the need for increased film thickness was discussed in section 6.2). An accurate value of h could not be calculated from heat transfer theory due to the unknown thermal resistance of the spacer material, and the complexity of the fluid dynamics in the jets of recirculating heating and cooling water.

The results in Table 6.1 show that there was a large uncertainty in the measurement of d for the Durapore membrane. This is partly due to the errors in the slopes of the lines fitted to figures 6.5 and 6.6. Errors would also be expected for the results in figure 6.5 where very high temperature differences were used. Here, the assumption that the average membrane temperature was equal to the average of the heating and cooling water temperatures may lead to errors in T_m of several degrees.

An average value of d for the Durapore membrane was taken as d = 0.063 kg/m^{2}s. This agrees with equation (6.1) (based on DP' = 3.35 m^{2}Pa/s at 60 °C [6.3]) using a tortuosity of χ = 2.4 and a porosity of ϵ = 0.75. The value of d = 0.052 kg/m^{2}s for the Enka membrane agrees with equation

(6.1) using $\chi = 2.2$ and $\epsilon = 0.75$.

Using a value of $d = 0.063$ kg/m^{2}s for the Durapore membrane, and $d = 0.052$ kg/m^{2}s for the Enka membrane, along with the other parameter values given in Table 6.1, fluxes were calculated for all experimental results using equation (6.10). The results are shown in figures 6.8, 6.9 and 6.10. It can be seen that equation (6.10), with appropriate parameters, is able to describe fluxes for the complete range of temperatures and air pressures used in this study. On this basis, the model was used to extrapolate the results to a wider range of conditions, particularly increased heat transfer coefficients.

6.3.2 Assessment of Parameters Controlling Performance

The theory presented in section 6.1 was used to assess the importance of the various parameters controlling MD. The obvious focal point was the optimisation of both flux and energy efficiency. The effect of deaeration on MD performance was shown to be complex, and some interesting conclusions were reached concerning heat loss by conduction across the membrane. The temperature polarisation coefficient, TPC, was found to be a useful tool for evaluating MD processes, and in the final analysis, it was found that the membrane need not limit the process in most applications.

Equation (6.10) was used to extrapolate the results for the Durapore membrane to higher film heat transfer coefficients. The results are shown in figure 6.11. It can be seen that to realise the full benefit of deaeration, the film heat transfer coefficients must be maximised. The values of h shown in figure 6.11 range from 500 W/m^{2}K to 5000 W/m^{2}K.
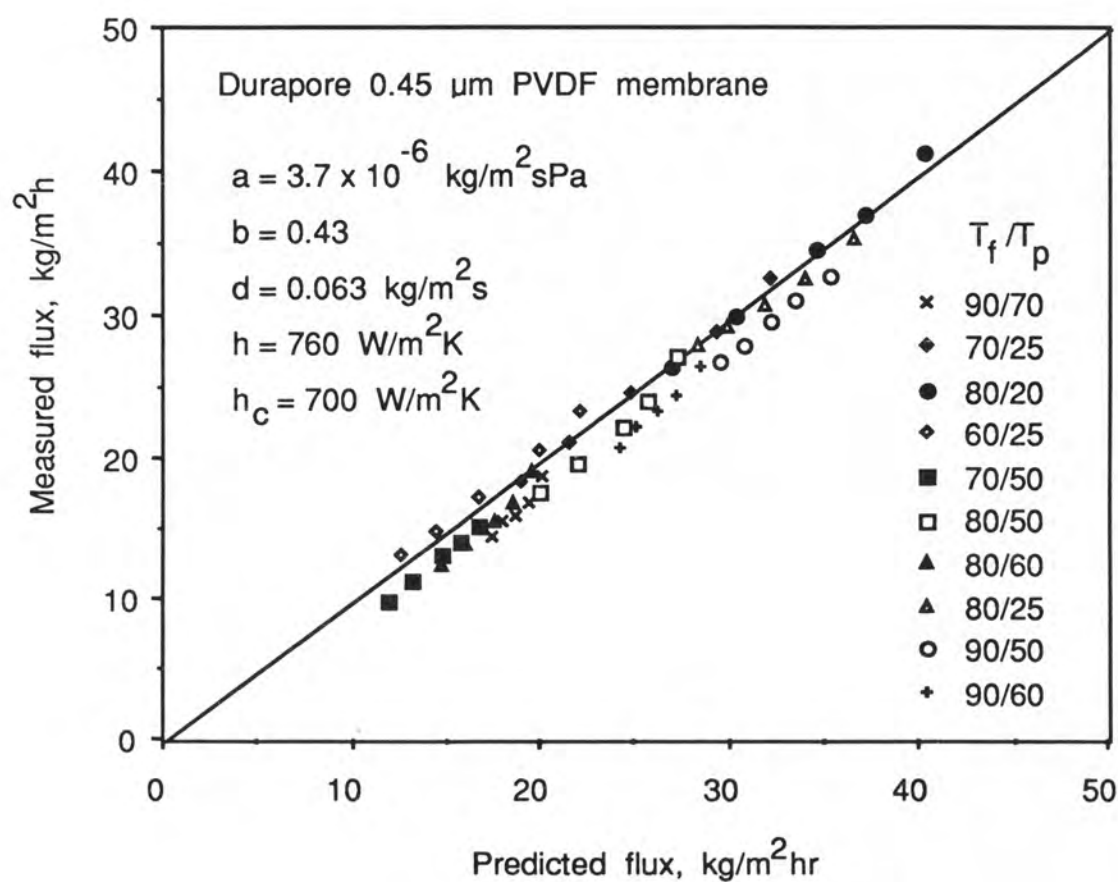
Figure 6.8 : Measured versus predicted flux for the results in figure 6.2.
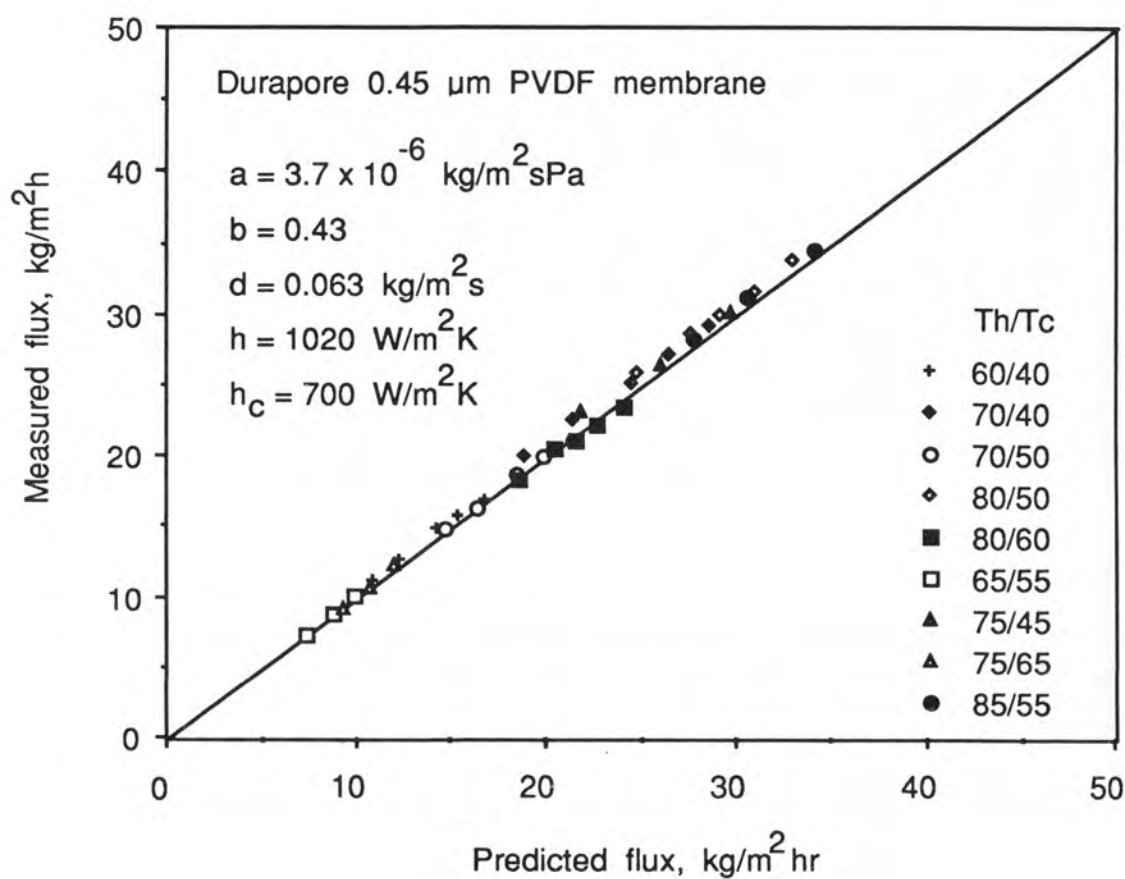
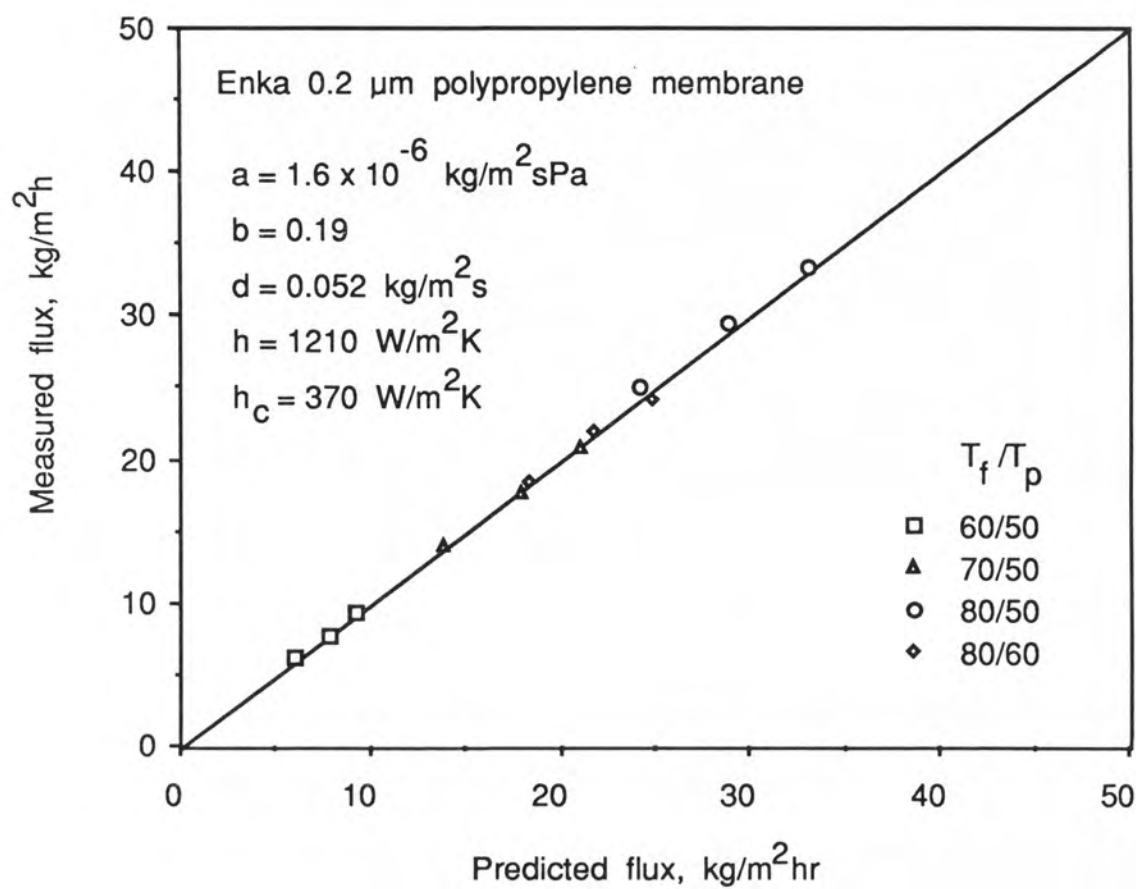Figure 6.9 : Measured versus predicted flux for the results in figure 6.3.

Figure 6.10 : Measured versus predicted flux for the results in figure 6.4.
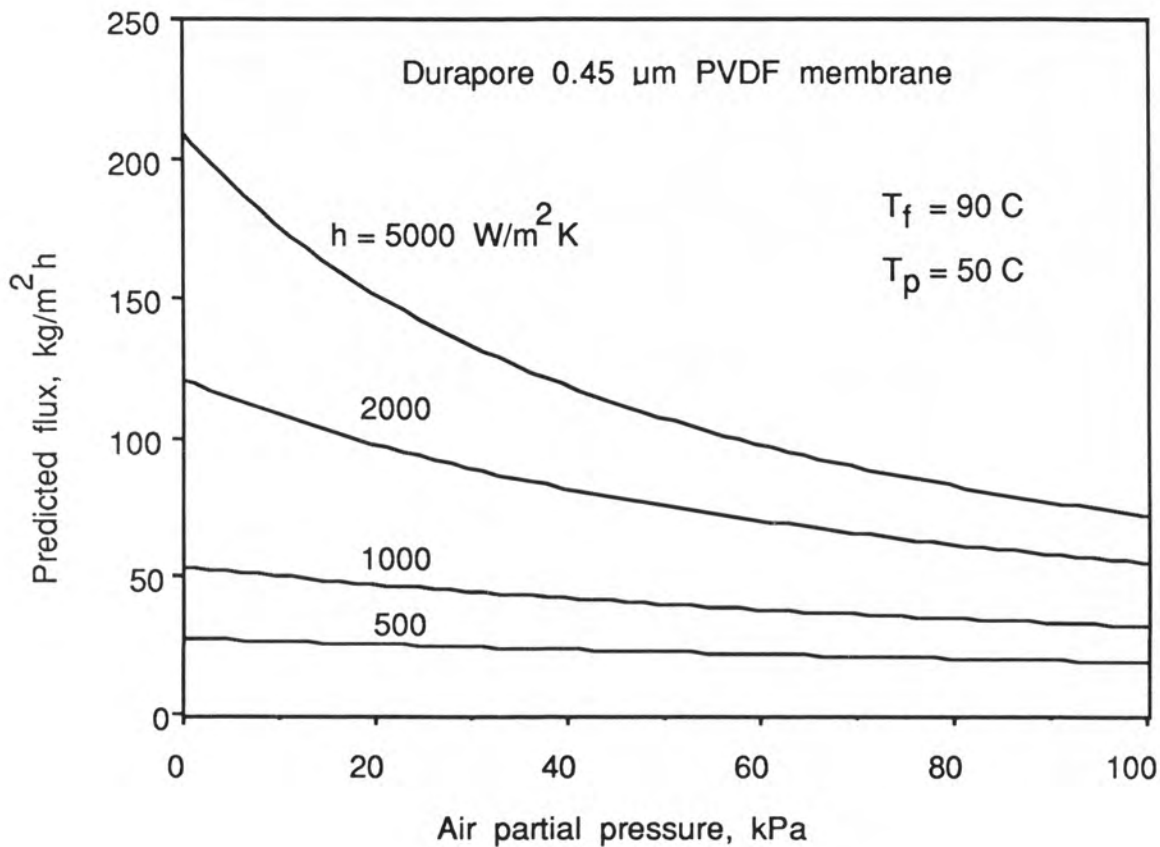
Figure 6.11 : Predicted fluxes for a 0.45 um MD membrane for various air pressures and film heat transfer coefficients.

This lower value is typical of a poorly designed system, while the higher value represents a maximum. In most applications, a heat transfer coefficient of 2000 W/m^{2}K is a realistic target.

For the curve representing h = 2000 W/m^{2}K in figure 6.11, J, h_v, and ΔT_m were calculated for the range of air pressures, as shown in figure 6.12. Under these conditions, the flux increases by 2-fold with deaeration. However to achieve this flux increase, the membrane permeability (which is proportional to h_v) has increased by 6-fold. The increase in flux results in worse temperature polarisation, and a subsequent 3-fold decrease in ΔT_m. At partial pressures of air below 20 kPa, the system becomes heat transfer limited, as h_v is in the range 6000 to 12000 W/m^{2}K (note, in chapter 4 a realistic maximum value of h was identified as 5000 W/m^{2}K).

Figure 6.11 identifies a realistic maximum flux for MD. In a deaerated system, the process is heat transfer limied, hence if the film heat transfer coefficient is maximised, so is the flux. The temperatures used in figure 6.11 can be considered as typical of a system designed for high flux. Hence the fluxes of 150 to 200 kg/m^{2}hr predicted at maximum heat transfer represent realistic maximum fluxes for MD.

MD in its basic form is an energy intensive process. Accordingly, efforts have been made in the past to minimise the heat loss by conduction across the membrane. Typically, the heat loss amounts to 20 to 40 % of the total heat input. To improve the energy efficiency, the ratio h_c/h_v must be decreased. One strategy has been to increase the thickness of the membrane, thus lowering h_c. Inspection of equation (6.10), however, reveals that both h_c and h_v are inversely proportional to the membrane thickness, δ (as a and d are inversely proportional
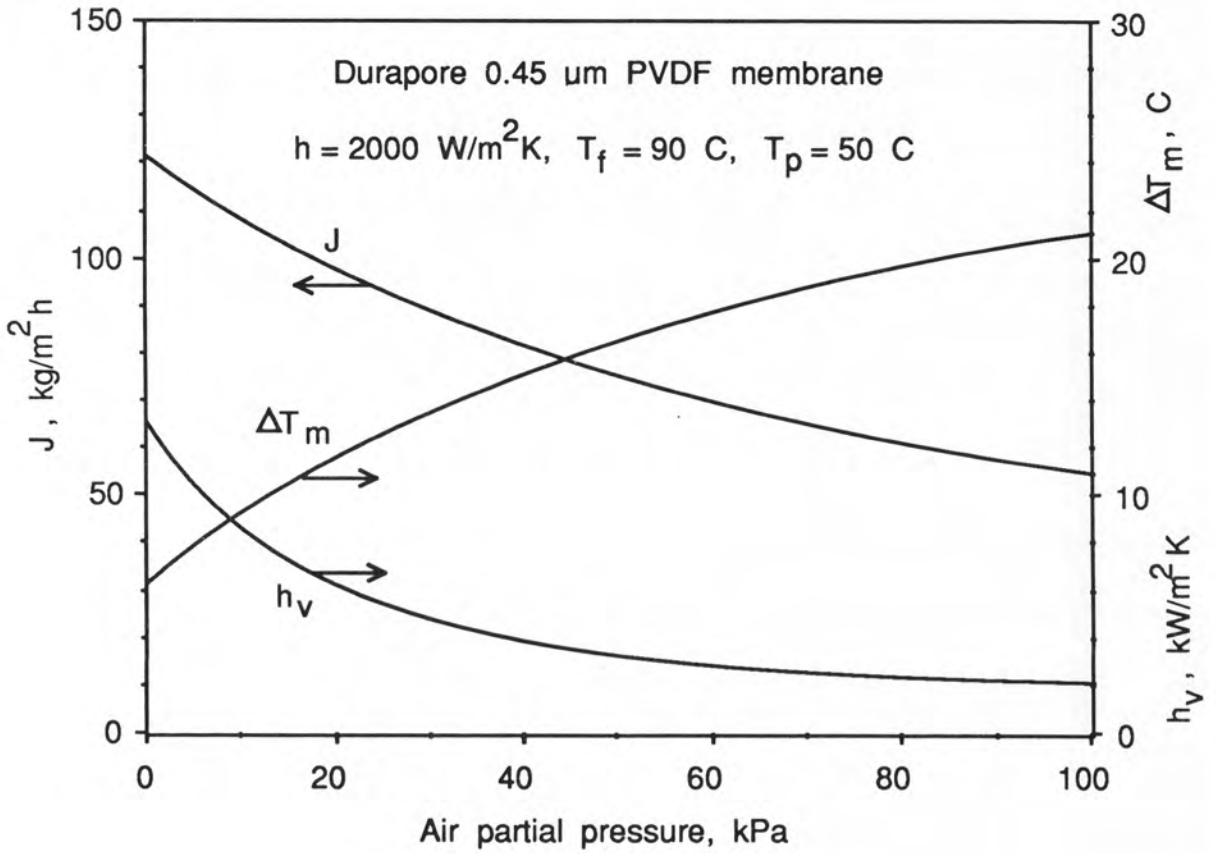
Figure 6.12 : Effect of deaeration on flux, J, vapour heat transfer coefficient, h_v, and membrane temperature difference, ΔT_m.

to δ). Thus manipulating the membrane thickness has no effect on the relative heat loss.

Another technique that has been used to minimise heat loss by conduction involves maintaining an air gap between the membrane and a condensing surface [6.4,6.5]. This concept was discussed in chapter 1. The air gap acts as an insulating layer, however as with the thicker membranes, the air gap also reduces flux by increasing the water vapour diffusion path. (Note, equation (6.10) cannot be directly applied due to the occurrence of convective transport in the air gap.) The air gap approach can reduce heat loss, although the penalty is reduced flux.

This study has shown that deaeration is a preferable technique for reducing heat loss by conduction. Unlike the other techniques aimed at decreasing the h_c/h_v ratio by reducing h_c, deaeration achieves this by increasing h_v. Figure 6.12 showed that deaeration can increase h_v by 6-fold with no corresponding change in h_c. For the same system, figure 6.13 shows how the fractional heat loss by conduction decreases with decreasing air pressure, with heat losses of less than 10% being calculated. Hence if flux is increased by deaeration, there is the added bonus of reduced heat loss by conduction.

Deaeration can be achieved by two simple techniques. If the feed and/or permeate are deaerated prior to entering the module, the partial pressure of air in the membrane will decrease due to equilibrium considerations as described by Henry's law. (Note, this will increase the pressure difference across the liquid/gas interface, thus increasing the driving force for liquid to enter the membrane pores.) The second technique for deaerating is by lowering the pressure of the feed and/or permeate, as was done in this experimental study. This limits the gas
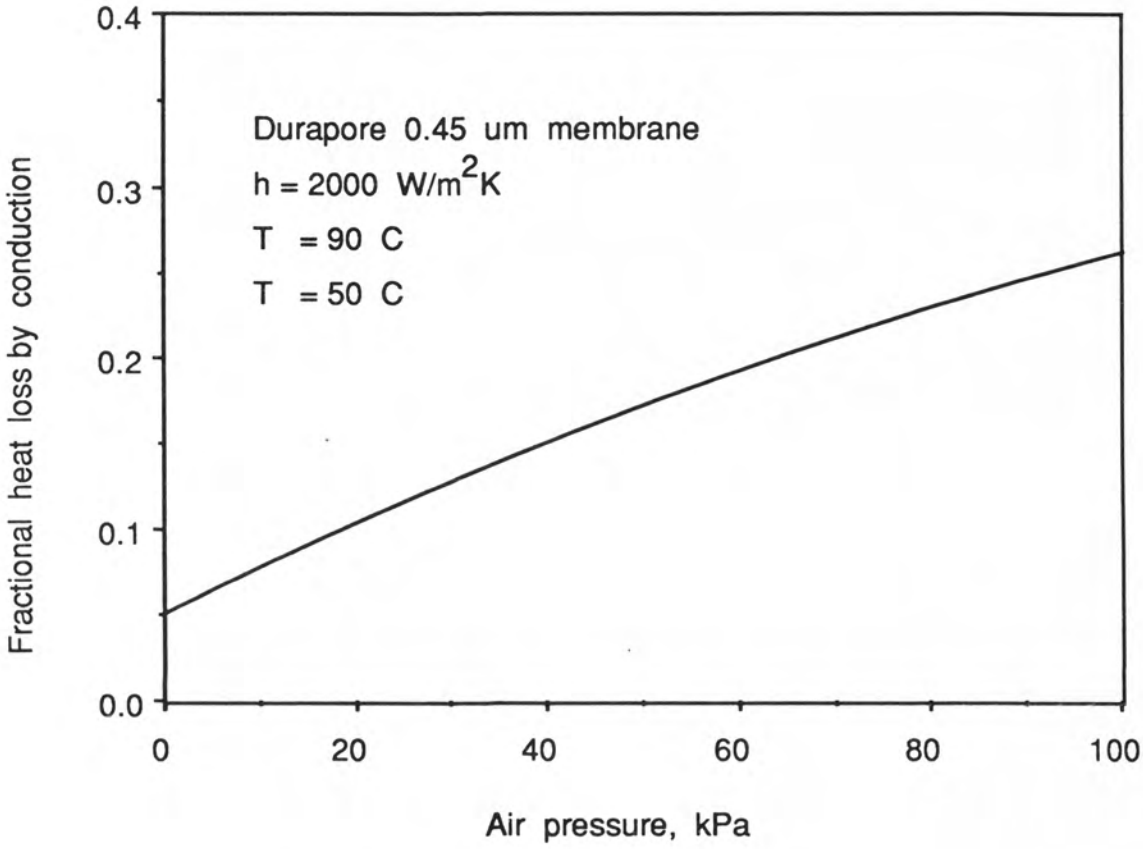
Figure 6.13 : Fractional heat loss by conduction for various partial pressures of air.

pressure within the membrane pores. For example if the liquid pressure is 10 kPa higher than the interfacial vapour pressure, then the air partial pressure at the interace is limited to 10 kPa. This method of deaerating lowers the interfacial pressure difference, hence reducing the tendency for membrane wetting. In practice, this may be achieved by placing the module in the suction line to the pumps, or by operating the system with a barometric leg (i.e. locating the pumps on a lower level to satisfy net positive suction head requirements).(N.B. Schneider and van Gassel [6.2] achieved deaeration by pulling a vacuum directly on the membrane pore space in a specially designed module. This method would be impractical in an industrial situation.)

Equation (6.11) expresses the temperature polarisation coefficient as a ratio of heat transfer coefficients, giving new significance to TPC values. The TPC lies between 0 and $h/\{h+h_c\}$ (typically 0.8), and reveals whether the process is limited by mass transfer or heat transfer. In general, if TPC < 0.3, the process is heat transfer limited (i.e. $h \ll h_v$), while if TPC > 0.6, mass transfer is limiting. An MD process will be heat transfer limited if the module design does not give adequate heat transfer to the membrane surfaces. Conversely, the process will be mass transfer limited if the membrane permeability is too low.

An important result has come from the theoretical modelling of MD systems. While aerated MD systems are often mass transfer limited (TPC>0.6), deaerated systems were seldom found to be so. Even using extreme film heat transfer coefficients ($h=5000W/m^2K$), deaerated systems rarely had TPC>0.6. This is also illustrated in figure 6.12, where at low pressures of air, h_v is in the range 6000 to 12000 W/m^2K, which is substantially higher than the maximum achievable h. The implications of this are important. If systems are designed for deaerated operation,

either by operating at low liquid pressures, or by deaerating the feed, there is little scope for improvement by developing special MD membranes. Attention would be better focussed on designing MD modules that provide high heat transfer coefficients on both sides of the membrane.

6.4 CONCLUSIONS

This study has seen the development of a combined heat and mass transfer theory capable of describing MD fluxes over a wide range of temperatures and air pressures. The two major parameters are the film heat transfer coefficient, h, and the molecular diffusion parameter, d. At low pressures of air, two additional parameters, a and b, are needed to describe the combined Knudsen/Poiseuille flow through the porous membrane. The model has been used to successfully describe experimental fluxes for two different membranes with varying film heat transfer coefficients.

The heat and mass transfer model has revealed that the modest flux increases observed with deaeration are a result of greatly increased membrane permeability, but worsened temperature polarisation. The full benefits of deaeration can only be realised with very high film heat transfer coefficients. Associated with the flux increase with deaeration is a drop in the fraction of heat lost by conduction across the membrane. Thus deaeration may be preferable to the "gas-gap" approach to minimising heat loss. Also, deaeration by reducing liquid pressures may reduce the tendency for membrane wetting. The permeability of a 0.45 μm Durapore membrane is sufficiently high, when deaerated, that the MD process will always be heat transfer limited. This means that there is little to be gained by developing membranes specifically for MD, and

attention would be better focussed on improving module heat transfer.

Extrapolation from experimental results has identified a realistic maximum flux for MD. At feed and permeate temperatures of 90 and 50 °C, the flux for a totally deaerated Durapore 0.45 μm membrane with the maximum heat transfer coefficient of h — 5000 W/m^{2}K is around 200 kg/m^{2}h.

6.5 NOTATION

a   Membrane permeability constant [kg m^{-2} s^{-1} Pa^{-1}]

b   Exponent defined in chapter 5 [-]

d   Membrane molecular diffusion constant [kg m^{-2} s^{-1}]

D   Diffusion coefficient [m^2 s^{-1}]

h   Heat transfer coefficient [W m^{-2} K^{-1}]

ΔH_v Latent heat of vaporisation [J kg^{-1}]

J   Mass flux through membrane [kg m^{-2} s^{-1}]

k   Thermal conductivity [W m^{-1} K^{-1}]

M   Gas molecular weight [kg mol^{-1}]

P   Average gas pressure within membrane [Pa]

P'   Total gas pressure [Pa]

ΔP Water vapour pressure drop across membrane [Pa]

$\wp$ Dimensionless pressure — P/P_{ref} [-]

Q"   Heat flux [W m^{-2}]

R   Gas constant [J mol^{-1} K]

T   Temperature [K,°C]

TPC   Temperature polarisation coefficient [-]

δ Membrane thickness [m]

ϵ Membrane porosity [-]

χ Membrane tortuosity [-]

Subscripts

a   Air

c   Conduction

f   Feed

m   Membrane

p   Permeate

v   Vapour

6.6 REFERENCES

[6.1] Schofield, R.W., "Membrane Distillation", B.E. Thesis (1984), School of Chem Eng and Ind Chem, University of NSW, Australia.

[6.2] Schneider, K., van Gassel, T.S., "Membrandestillation", Chem.Ing. Tech., 56 (1984) 514-521.

[6.3] Sherwood, T.K., Pigford, R.L., and Wilke, C.R., "Mass Transfer", McGraw-Hill, New York, 1975.

[6.4] Jönsson, A.-S., Wimmerstedt, R. and Harrysson, A.-C., "Membrane Distillation - A Theoretical Study of Evaporation Through Micro-porous Membranes", Desalination, 56 (1985) 237-250.

[6.5] Andersson, S.-I., Kjellander, N., and Rodesjo, B., "Design and Field Tests of a New Membrane Distillation Desalination Process", Desalination, 56 (1985) 345-354.

Chapter 7

Solute
Effects
in
Membrane
Distillation

CHAPTER 7: SOLUTE EFFECTS IN MEMBRANE DISTILLATION

In most membrane processes, the concentration of solute in the feed dictates the system performance. This was not found to be the case in MD under most conditions. This chapter examines the effects that solute has on flux and performance through vapour pressure reduction and changes in transport properties. Experiments were conducted with turbulent flow in a cross flow sheet membrane cell, and computer modelling was used to interpret results.

Previous work by Franken [7.1] has investigated solute mass transfer when the feed contains volatile organics (ethanol). This study is limited to non-volatile solutes, which is appropriate for most applications. Experiments were conducted with salt and sugar solutions, using Durapore 0.45 μm PVDF membranes. A detailed theoretical analysis was conducted for the salt case.

7.1 THEORY

7.1.1 General MD Theory

In chapters 4 and 6, the heat and mass transfer equations were presented for the simplified case when the film heat transfer coefficients are equal on either side of the membrane. This simplified case does not apply here. In chapter 4, experimental results were modelled with reasonable accuracy using the simple mass flux equation

$$J = C (P_f - P_p) \qquad\qquad (7.1)$$

A more elaborate flux equation was used in chapter 6 for the prediction of fluxes in deaerated systems. As experiments conducted in this study

of solute effects were aerated, equation (7.1) was adequate.

The vapour pressures in equation (7.1) can be calculated, for the case where there is no solute present, from the interfacial temperatures using the Antoine equation

$$P° = \exp (23.238 - 3841/(T - 45)) \tag{7.2}$$

where T is in degrees Kelvin, and P° indicates pure water. The effect of solute on vapour pressure will be discussed below.

From equation (2.17), the interfacial temperatures, T_{fm} and T_{pm}, are a function of the feed and permeate bulk temperatures, and the four heat transfer coefficients.

$$T_{fm} = T_f - (T_f - T_p) \frac{1/h_f}{1/(h_v+h_c) + 1/h_f + 1/h_p} \tag{7.3}$$

$$T_{pm} = T_p + (T_f - T_p) \frac{1/h_p}{1/(h_v+h_c) + 1/h_f + 1/h_p} \tag{7.4}$$

In equations (7.3) and (7.4), T_f and T_p are experimental conditions. The conduction heat transfer coefficient, h_c, was determined for the Durapore membrane (chapter 4) as $h_c = 700$ W/m^{2}K. The feed film heat transfer coefficient for turbulent flow can be calculated from the Seider-Tate equation (chapter 4)

$$h_f = Nu \; k/d_h$$

$$= 0.023 \; Re^{0.8} \; Pr^{0.33} \; (\mu/\mu_m)^{0.14} \; k/d_h \tag{7.5}$$

where d_h is the hydraulic diameter of the feed channel. The vapour heat transfer coefficient, h_v, is a measure of the membrane permeability, and can be calculated from

$$h_v = J \, \Delta H_v \,/\, (T_{fm} - T_{pm}) \tag{7.6}$$

Equations (7.1) to (7.6) can be solved iteratively (in reverse order) to estimate flux for a pure water feed. Details of computer modelling and iterative solutions are given in Appendix C. The two parameters that are not calculated are C and h_p. In this analysis, these parameters were estimated from the results in chapter 4, and adjusted to fit the experimental results.

7.1.2 Solute Effects

One of the effects that feed solute has in MD is to reduce the vapour pressure at the evaporating surface. Vapour pressure reduction is a colligative property, and for dilute solutions obeys Raoult's law [7.2]

$$P_f = (1-x_m) \, P_f^\circ \tag{7.7}$$

where x_m is the mole fraction of solute at the evaporating surface, and P_{fm}° is the vapour pressure of pure water at that temperature. Vapour pressure reduction by solute means that if the trans-membrane temperature difference is less than a threshold temperature, ΔT_{th}, then flux will be from the permeate to the feed. The threshold temperature was derived in chapter 2, giving

$$\Delta T_{th} = \frac{RT^2}{M\Delta H_v} \, \frac{x}{1-x} \tag{7.8}$$

As an example, for a 1 M (6 wt%) NaCl solution at 60 °C, equation (7.8) predicts $\Delta T_{th} = 0.4$ °C. Thus the threshold temperature difference only becomes important at high concentrations and low driving forces.

For concentrated solutions, equation (7.7) does not hold, and vapour

pressures must be determined from experimental results or published
data. The conventional way of relating the vapour pressure of a solution
to the vapour pressure of the solvent at the same temperature is via an
activity coefficient, which for aqueous solutions of non-volatile
solutes may be defined as [7.3]

$$\gamma = \frac{P}{(1-x)\ P^\circ} \tag{7.9}$$

The above equations express concentrations in terms of the mole fraction
of solute, x. It is often more convenient to express concentrations as
molarities or mass fractions. The following two equations can be used to
convert units.

$$x = \frac{c}{c + \rho_w/M_w\ (1 - c\ M_s/\rho_s)} \tag{7.10}$$

$$x = \frac{W}{W + M_s/M_w\ (1 - W)} \tag{7.11}$$

where c is the concentration in moles/litre, W is the weight fraction of
solute, M is the molecular weight, ρ is the density, and the subscripts
s and w refer to solute and water respectively.

As with other membrane processes, concentration polarisation results in
the membrane wall (or interfacial) concentration being higher than the
bulk concentration. This is brought about by bulk flow of the permeating
species to the membrane surface, inducing an opposing concentration
gradient of the retained species. The usual expression for concentration
polarisation, based on the film model (using MD notation), is [7.4]

$$c_{fm} = c_f\ \exp(\ J/\rho_w k_s\ ) \tag{7.12}$$

where k_s is the solute mass transfer coefficient in the feed, and c_{fm}

and c_f are the concentrations of solute at the interface and in the bulk feed respectively. Equation (7.12) allows x to be calculated at the interfacial concentration by using $c=c_{fm}$ in equation (7.10). The solute mass transfer coefficient can be estimated via an appropriate correlation, such as the Dittus/Boelter equation

$$k_s = 0.023 \ Re^{0.8} \ Sc^{0.33} \ D/d_h \tag{7.13}$$

where D is the diffusion coefficient, d_h is the hydraulic diameter of the channel, and Re and Sc are the dimensionless Reynolds and Schmidt numbers respectively.

The presence of solute in the feed also alters the fluid dynamics through density and viscosity, and influences heat transfer through thermal conductivity and heat capacity. In some situations, the effect of these transport properties on flux is greater than the effect of vapour pressure reduction. The variation of transport properties with concentration depends on the solute. The properties of sodium chloride (salt) and sucrose (sugar) solutions are detailed below.

7.1.3 Sodium Chloride Solutions

As desalination is a major application for MD, it was appropriate that salt solutions form a major part of this study on solute effects. In order to analyse the experimental results, tabulated data from the literature have been used to evaluate the properties of salt solutions at various concentrations and temperatures. The data have been correlated by the simple equations presented below.

The activity coefficients for salt solutions at various concentrations were calculated from data measured at 30 °C [7.5] and 100 °C [7.6],

revealing only a minor dependence on temperature. For concentrations ranging from zero to saturation, the activity coefficient can be approximated by the expression

$$\gamma = 1 - 0.5\,x - 10\,x^2 \tag{7.14}$$

with an error of less than 2%. Figure 7.1 shows the variation of vapour pressure with salt concentration at 80 °C. The values predicted by equation (7.7) are shown for comparison, displaying the deviation from ideality at high concentrations.

Variations in the transport properties with concentration effect the film heat transfer coefficient in equation (7.5). Transport properties were determined for salt solutions for temperatures ranging from 50 to 90 °C. Density and heat capacity were found to be only slightly temperature dependent [7.7], and over the temperature range of interest, can be approximated by the equations

$$\rho = 980 + 1950\,x \tag{7.15}$$

$$C_p = 4180 - 8370\,x \tag{7.16}$$

where ρ is the density of salt solution [kg/m^3], and C_p is the heat capacity [J/kgK]. Viscosity and thermal conductivity were found to be both temperature and concentration dependent [7.7,7.8]. Despite the strong dependence of viscosity on both temperature and concentration, a linear relationship gives reasonable accuracy over the range of interest. The approximations for viscosity, μ [Pa s] and thermal conductivity, k [W/mK] are

$$\mu = (8.7\times10^{-4} - 6.3\times10^{-6}\,T)(1 + 12.9\,x) \tag{7.17}$$

$$k = (0.608 + 7.46\times10^{-4}\,T)(1 - 0.98\,x) \tag{7.18}$$
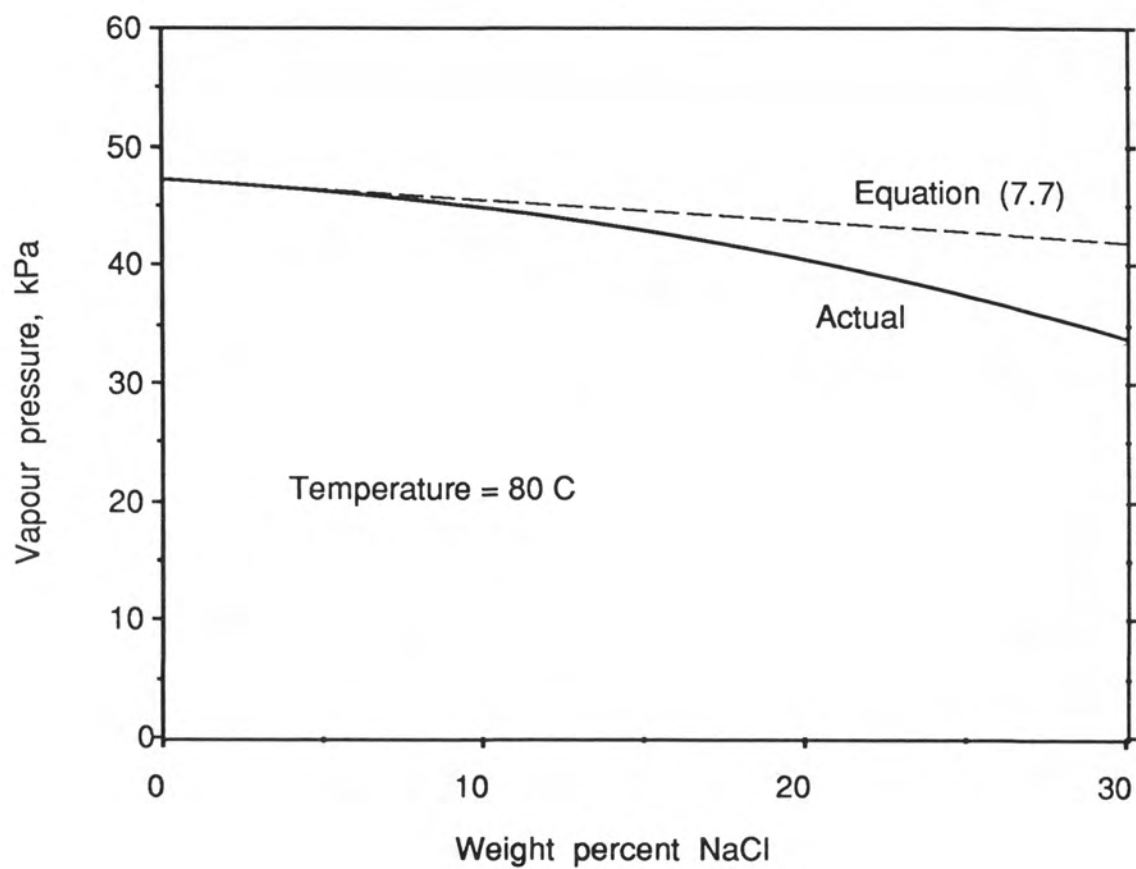
Figure 7.1 : Reduction of vapour pressure with solute concentration.

where T is the temperature in °C. Equations (7.15) to (7.18) are accurate to ±4% over the full range of salt concentrations, and for temperatures between 50 and 90 °C.

7.1.4 Sucrose Solutions

Sugar solutions were chosen as a typical MD application with a high molecular weight solute. In section 7.3, it is shown that the two major contributing factors to flux reduction for salt solutions are vapour pressure reduction and viscosity. For sugar solutions, however, the effect of vapour pressure reduction is far less than for salt. Vapour pressure reduction is ideally a colligative property, hence the effect decreases with increasing molecular weight at constant mass fraction. Experiments were conducted at sugar concentrations of 15 wt% (x=0.0173) and 30 wt% (x=0.0411). At these concentrations, the vapour pressure reduction is less than 3% (i.e. P/P°>0.97) [7.9], implying that the contribution to flux reduction is minimal. The viscosity, μ [Pas], of sugar solutions [7.10] was approximated by the relationship

$$\mu = (1.03 - 0.009\ T)(1 + 180\ x^{1.5}) \tag{7.19}$$

where T is in °C. This equation is accurate to within 5% over the range $50 \le T \le 80$ °C and $0 \le W \le 0.3$. It is shown in section 7.3 that viscosity effects alone can describe the flux reduction observed for sugar solutions.

7.2 EXPERIMENTAL

The flat sheet membrane module used in this study was described in chapter 3, and is shown in figure 7.2. Basically, it is a cross-flow cell with a heat transfer plate separating the permeate and cooling
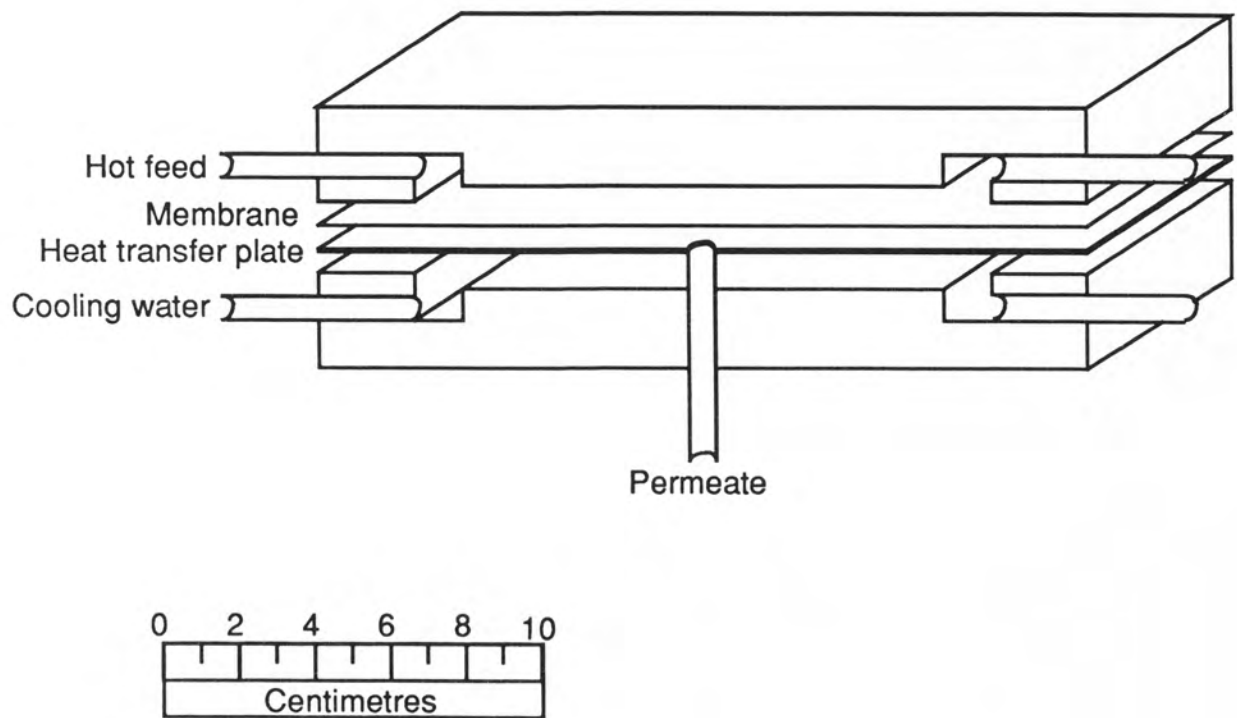
Figure 7.2 : Cross flow MD cell.

water. The feed channel was 114 mm long, 25 mm wide and 1.5 mm thick, having a hydraulic diameter of d_h = 2.83 mm. This resulted in turbulent flow at most of the feed rates used. The feed solution was preheated in a thermostatted bath, and the permeate flow rate was measured by meniscus rise in a graduated tube, as shown in figure 7.3. Flowrate, temperatures and pressures were monitored around the module as shown. At the feed flow rates used, the temperature drop of the feed was less than 2 °C, allowing an average feed temperature to be used in calculations.

Experiments were conducted with NaCl and sucrose solutions at various feed flow rates, temperatures and concentrations. Experiments were also conducted with water for comparison. Millipore Durapore 0.45 μm PVDF membranes were used exclusively in this study, as they had been well characterised in chapters 4, 5 and 6.

7.3 RESULTS AND DISCUSSION

7.3.1 Experimental Results

Experiments with NaCl were conducted at concentrations of 0, 2.5 M (14 wt%, x=0.047) and 5 M (25 wt%, x=0.095). The feed flow rates used were 1.0 and 2.0 l/min (0.45 and 0.9 m/s) and feed temperatures were 61, 71, and 81 °C. The cooling water temperature was maintained at 21 °C for all experiments. The results for salt solutions are shown in figures 7.4 and 7.5, for the two different flow rates.

At a feed velocity of 0.45 m/s, laminar flow was observed at the high concentration, with Reynolds numbers in the range 1400 to 1900. All other conditions were turbulent. At the higher feed velocity, Reynolds
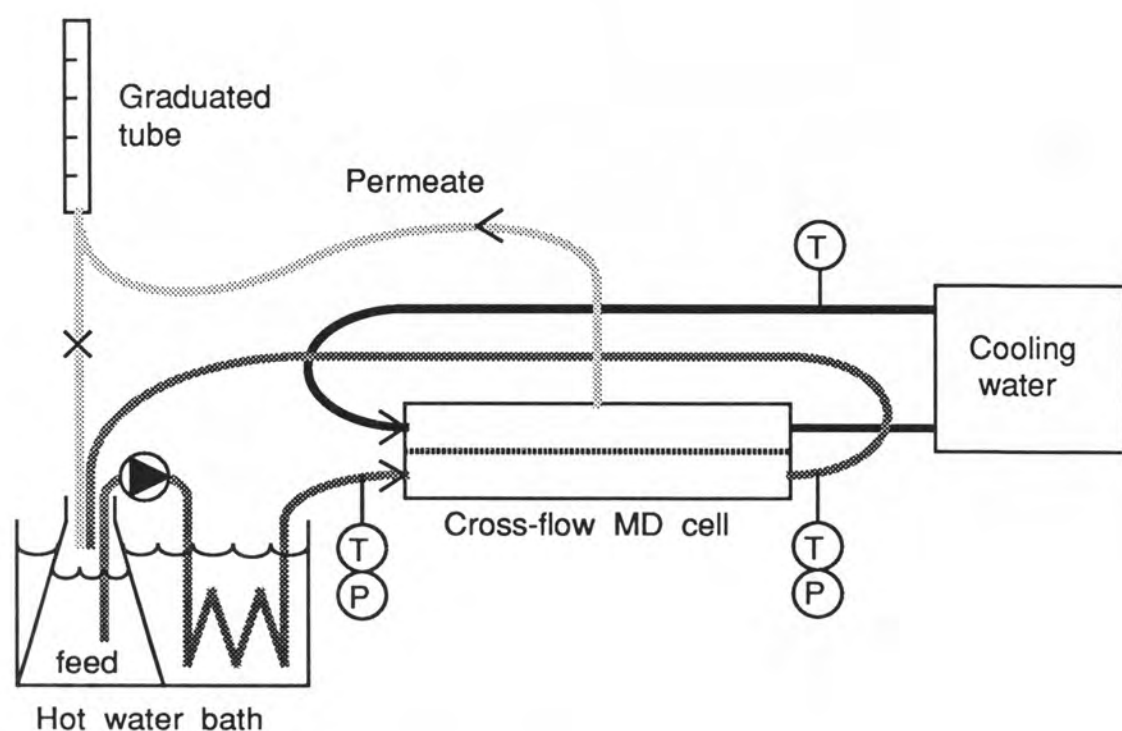
Figure 7.3 : Cross-flow apparatus for studying solute effects in Membrane Distillation

Figure 7.4 : Flux for various feed temperatures for three different salt concentrations.
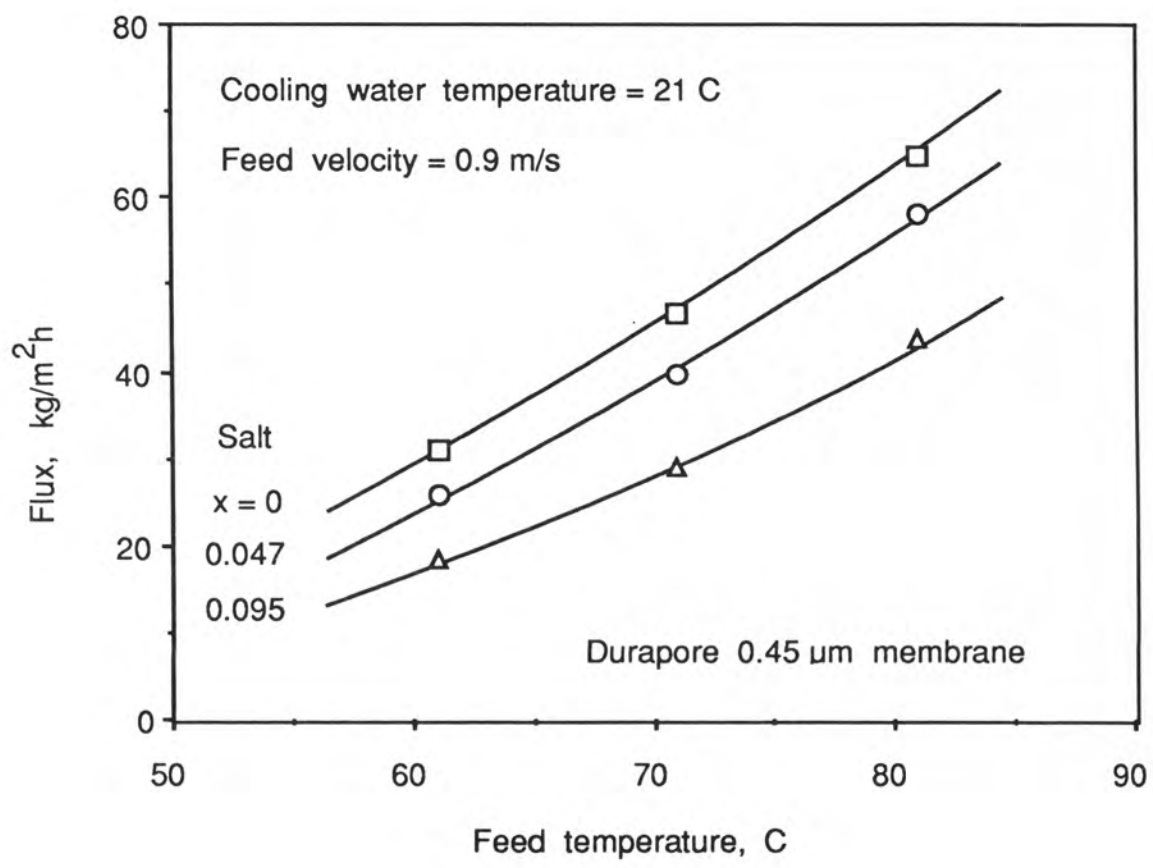
Figure 7.5 : Flux for various feed temperatures for three different salt concentrations.

numbers were 2700 to 3700 for the high concentration, and 5100 to 6900 for water.

The main observation from figures 7.4 and 7.5 is that flux is not greatly affected by the presence of solute. Even at a concentration of x=0.095, which is close to saturation, the flux is only reduced by around 40%. For applications such as desalinating sea water, the concentrations used would be around x=0.01, suggesting that fluxes would be above 90% of those observed with pure water feed.

Another observation from figures 7.4 and 7.5 is that the flux reduction from x=0 to x=0.047 is less than the reduction from x=0.047 to x=0.095. This reflects the decrease in activity coefficient with concentration, as indicated in figure 7.1.

Experiments were also conducted with salt solutions saturated at the feed temperature, resulting in some interesting observations. As flux proceeded, a layer of precipitated salt crystals formed on the membrane surface. This greatly reduced the film heat transfer coefficient, and flux decayed rapidly. At the conclusion of the experiment, the salt scale could be removed in sheets, revealing that the membrane had become internally wet in discrete locations covering around 5% of the membrane area. Membrane wetting and fouling will be discussed briefly in section 7.3.3.

Experiments with sugar were conducted at concentrations of 0, 15 wt% (x=0.017) and 30 wt% (x=0.041) with the same flow rates and temperatures used for salt. The results for sugar solutions for two different feed flow rates are shown in figures 7.6 and 7.7. As with the salt experiments, the flux reduction with concentration is small. Comparing
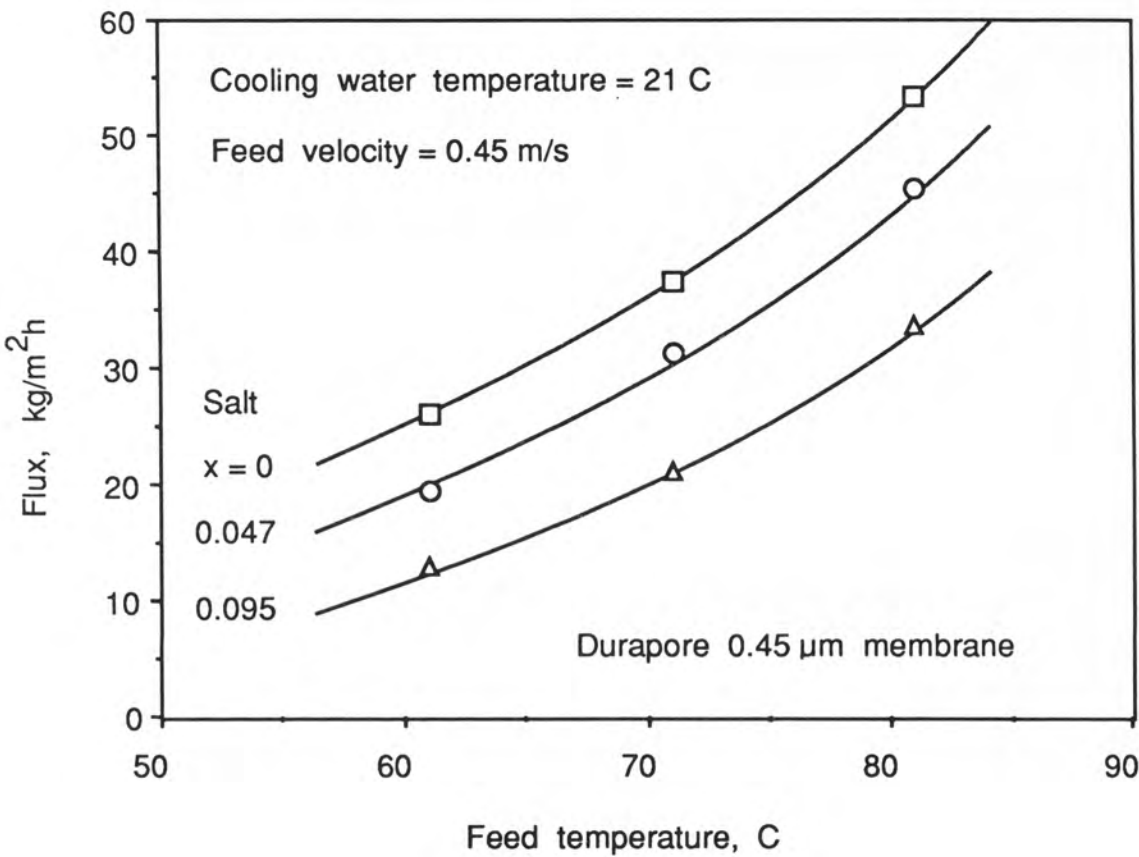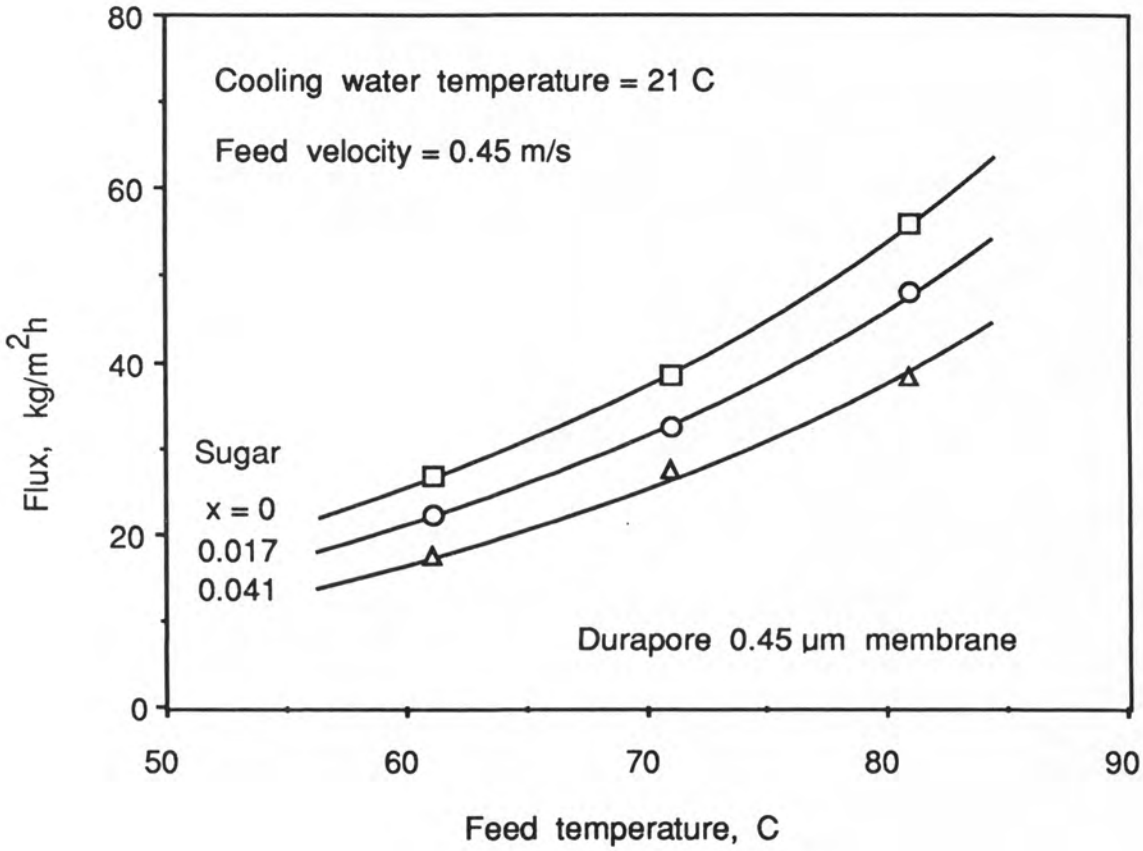
Figure 7.6 : Flux for various feed temperatures for three different sugar concentrations.
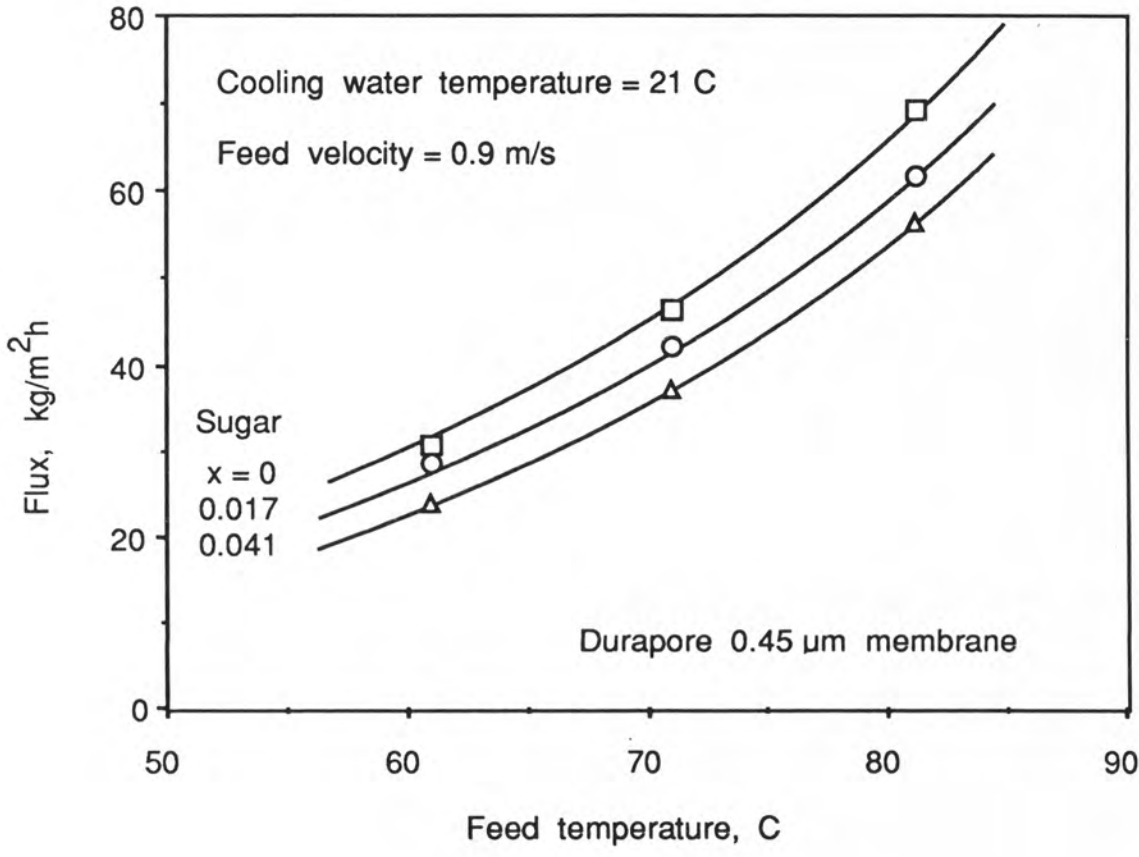
Figure 7.7 : Flux for various feed temperatures for three different sugar concentrations.

figures 7.5 and 7.7, it is apparent that the flux reduction caused by 30 wt% sugar is less than that caused by 25 wt% salt. This is mainly due to the higher molecular weight of sugar. For the same weight fraction, the mole fraction, x, for sugar will be less, resulting in less vapour pressure reduction. This will be discussed further in the following section.

7.3.2 Theoretical Modelling

An appreciation of the flux reductions observed can be gained by modelling the system to determine which solution properties have the greatest effect. For example, in some situations, vapour pressure reduction may be the major cause of flux reduction, while in other situations, increased viscosity may have a greater effect through increased boundary layer thickness. The equations presented in section 7.1 were incorporated into a computer model of the experimental system. Details of computer modelling are given in Appendix C. The parameters C and h_p were estimated from chapter 4 results as $C=5\times10^{-7}$ kg/m^2sPa and $h_p=3000$ W/m^2K, however better agreement was achieved using $C=5.9\times10^{-7}$ and $h_p=4000$. Figures 7.8 and 7.9 show the model predictions for the results in figures 7.4 and 7.5. While there is some discrepancy between the predicted and experimental results, the model does predict the major trends with temperature and concentration.

The theoretical model was used to determine the relative importance of the various solute factors affecting flux. For example, consider the experimental result for pure water at 81 °C and a feed velocity of 0.9 m/s, as shown in figure 7.9. For the 5 M salt solution under the same conditions, the flux was decreased by 32%. In other words, the flux
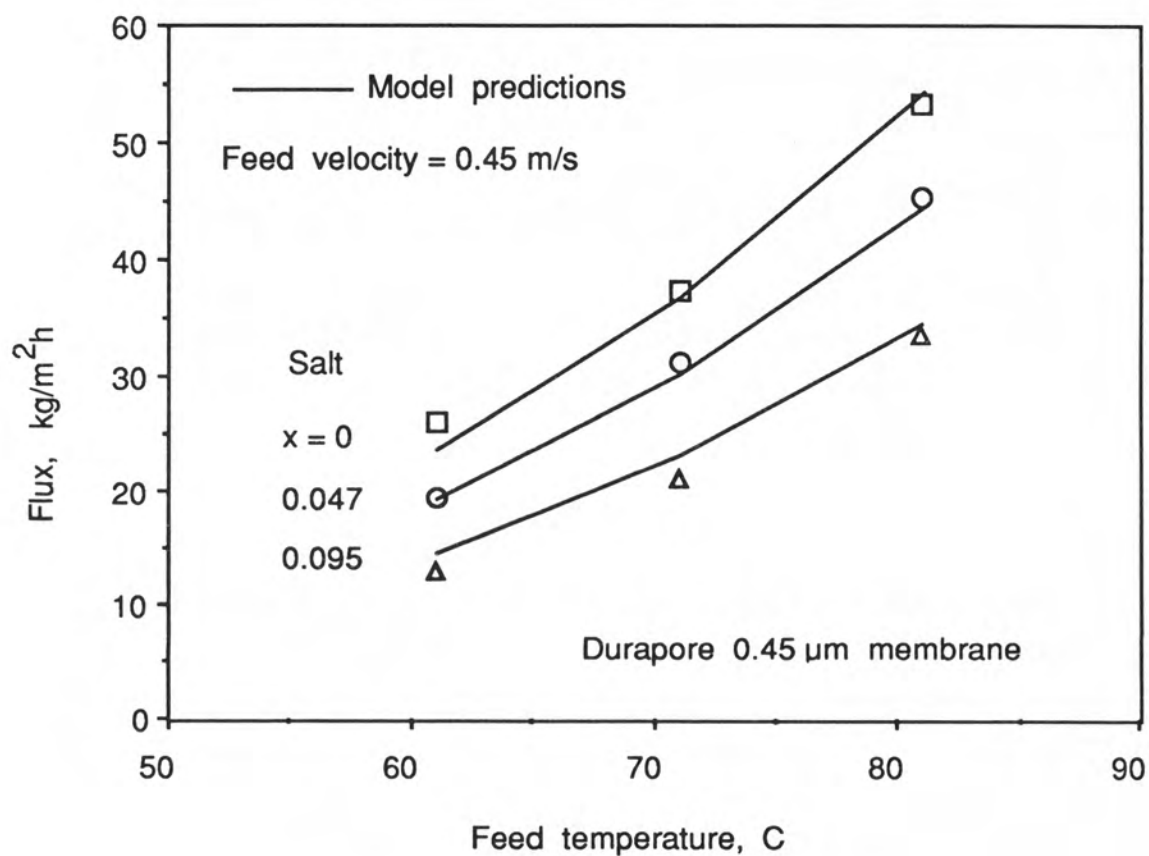
Figure 7.8 : Model predictions for results in Figure 7.4.
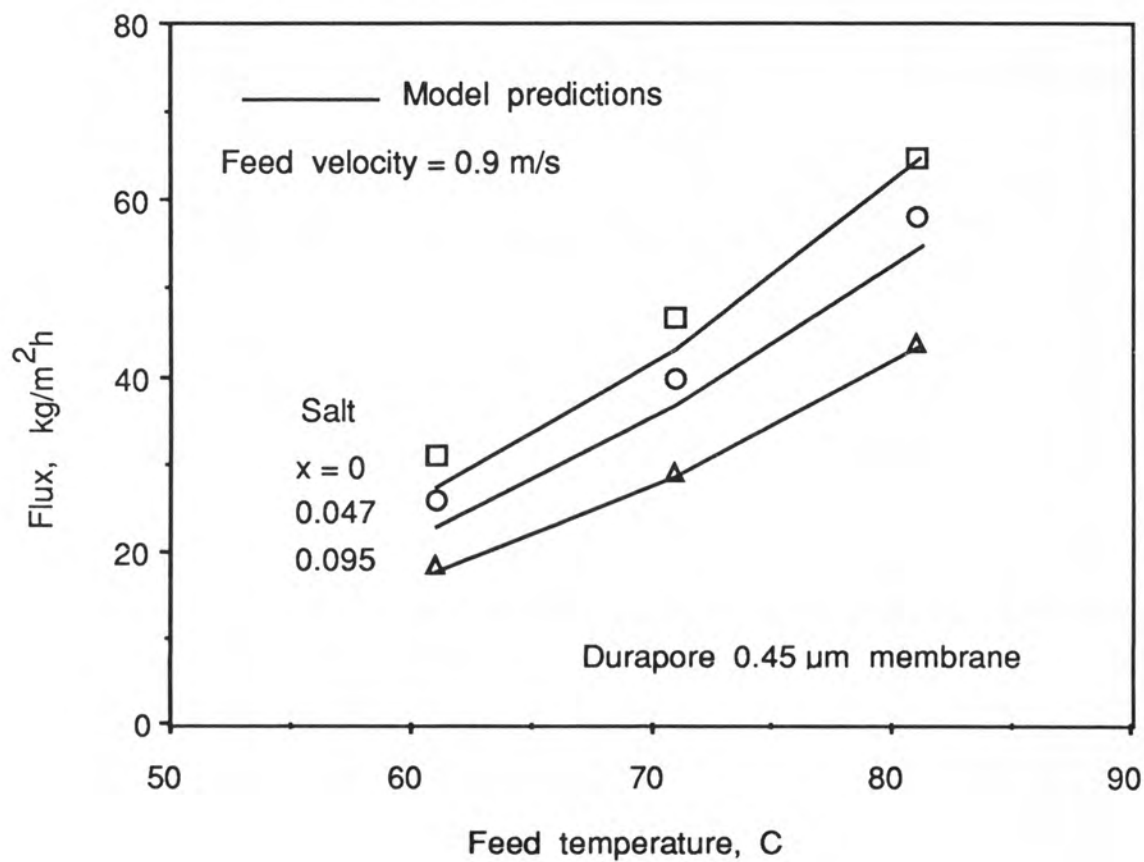
Figure 7.9 : Model predictions for results in Figure 7.5.

relative to water was 0.68. The relative flux predicted from the theory was also 0.68, showing excellent agreement in this case. This calculated value of 0.68 is the result of accounting for vapour pressure reduction, concentration polarisation, and changes in viscosity, density, thermal conductivity and heat capacity. The relative importance of these factors was determined by comparing the fluxes predicted when only accounting for specific factors. For example, if only viscosity is considered, the predicted relative flux is 0.89, showing that roughly one third of the flux reduction in this case is caused by the change in viscosity.

Table 7.1 summarises the results obtained from this parametric study. Values (relative to water) were estimated for $P/P°$ (vapour pressure reduction), c_{fm}/c_f (concentration polarisation), μ, ρ, k and C_p. These values were used to calculate the effects on Reynolds number, Re, Prandtl number, Pr, Nusselt number, Nu, solute mass transfer coefficient, k_s, film heat transfer coefficient, h_f, vapour heat transfer coefficient, h_v and flux, J. The cases examined were: (1) vapour pressure reduction (including concentration polarisation); (2) viscosity; (3) density; (4) thermal conductivity; (5) heat capacity; (6) all factors except concentration polarisation; and (7) all factors. These seven cases are discussed separately below.

Column 1 in table 7.1 gives the results for vapour pressure reduction and concentration polarisation. From the theory it was estimated that the wall concentration was 10% higher than the bulk concentration (c_{fm}/c_f=1.10) and that the vapour pressure was 75% of that for pure water. As expected, this has no effect on Re, Pr, Nu, k_s, and h_f, as these heat and mass transfer parameters are dependent on fluid properties. The vapour heat transfer coefficient, h_v, is reduced by 30 %, reflecting a decrease in $\Delta P_m/\Delta T_m$. The flux relative to water was

Table 7.1: Factors influencing flux reduction for 5 M NaCl feed at 81°C.

Theoretical considerations								
All parameters								
All except concentration polarisation								
Heat capacity								
Thermal conductivity								
Density								
Viscosity								
Vapour pressure reduction								
	Column	1	2	3	4	5	6	7
Estimated parameters relative to water	$P/P°$	0.75					0.78	0.75
	μ		2.33				2.33	2.33
	ρ			1.18			1.18	1.18
	k				0.93		0.93	0.93
	C_p					0.78	0.78	0.78
	c_{fm}/c_f	1.10						1.10
Calculated parameters relative to water	Re	1	0.43	1.18	1	1	0.52	0.52
	Pr	1	2.33	1	1.07	0.78	1.98	1.99
	Nu	1	0.67	1.14	1.03	0.94	0.74	0.74
	k_s	1	0.67	1.08	1	1	0.73	0.74
	h_f	1	0.67	1.14	0.96	0.94	0.69	0.68
	h_v	0.70	0.92	1.03	0.99	0.99	0.68	0.64
	J	0.76	0.89	1.04	0.99	0.99	0.71	0.68

calculated as 0.76, which when compared to the experimental result of 0.68, indicates that vapour pressure reduction is the major cause of flux reduction in this case.

Column 2 gives the results obtained accounting for viscosity effects only. The relative viscosity was estimated as 2.33. This causes a reduction in the Reynolds number (decreased turbulence) and an increase in the Prandtl number (increased convective heat transfer). The combined effect is a 33% reduction in the Nusselt number, and hence also in the

film heat transfer coefficient, h_f. The solute mass transfer coefficient, k_s, is decreased by approximately the same amount as the film heat transfer coefficient, as would be expected using the heat transfer/mass transfer analogy. The vapour heat transfer coefficient, h_v, is reduced by 8% due to worsened temperature polarisation on the feed side. This has the effect of lowering the average membrane temperature, which reduces $\Delta P_m / \Delta T_m$ and hence h_v. The nett result is that viscosity effects reduce the flux by 11%, making viscosity the second most important factor in flux reduction.

The effect of density on flux reduction is shown in column 3. An 18% increase in the density results in a 14% increase in the film heat transfer coefficient, through the Reynolds number. The nett result is a 4% increase in flux. Density is the only factor for salt solutions that results in a flux increase.

The effects of thermal conductivity (column 4) and heat capacity (column 5) are to reduce the film heat transfer coefficient by around 5% each, resulting in negligible reductions in flux.

Column 6 shows the results obtained from considering all factors except concentration polarisation. The results show a relative flux of 0.71, compared to the value 0.68 obtained when including concentration polarisation (column 7). In other words, concentration polarisation only leads to a 3% reduction in flux in this case. This is an important result, as concentration polarisation is a major cause of flux reduction in other membrane processes such as ultrafiltration. The combined effect of high transfer coefficients and low to moderate fluxes reduces the effect of concentration polarisation in MD.

Column 7 in table 7.1 gives the estimated and calculated parameters for the case where all factors are considered. The calculated relative flux of 0.68 agrees with the measured value. The 32% flux reduction is the result of a 36% decrease in h_v and a 32 % decrease in h_f. In other words, the contributions of vapour phase mass transfer and liquid film heat transfer are approximately equal. The overall relative flux of 0.68 can be obtained by multiplying the individual relative fluxes in columns 1 to 5.

The analysis of results at other temperatures and flow rates showed that in some cases, the effect of viscosity (column 2) was almost as great as that of vapour pressure reduction (column 1). This would be expected for systems that are heat transfer limited, as viscosity effects the film heat transfer coefficient, while vapour pressure reduction effects the vapour heat transfer coefficient. Figure 7.10 compares the relative effects of viscosity (column 2), vapour pressure reduction (column 1) and all factors (column 7) for five different experimental conditions.

The result on the left of figure 7.10 has the least contribution from viscosity effects, while the result on the right has almost equal contributions from viscosity and vapour pressure reduction. The relative effect of viscosity over vapour pressure reduction increases from left to right, as the process becomes more heat transfer limited, that is at higher temperatures and lower flow rates. The result on the right is for a lower concentration, and displays the fact that vapour pressure reduction is not linear with salt concentration. For this case (c=2.5 M), $P/P°=0.92$, whereas for the case in table 7.1 (c=5 M), $P/P°=0.75$.

For the case where sugar is the solute, the relative effects of viscosity and vapour pressure reduction are different. In section 7.1.4
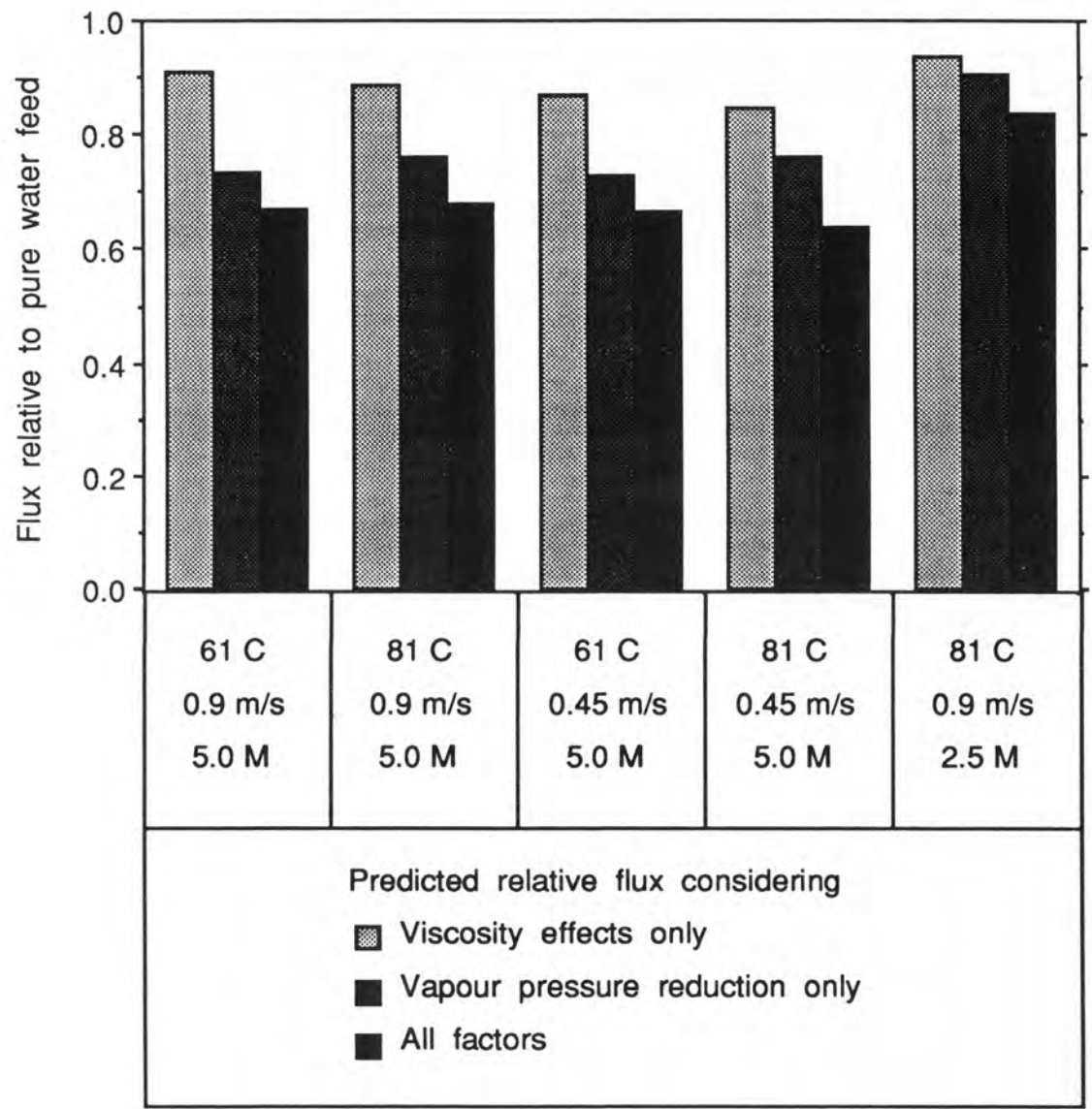
Figure 7.10 : Relative effects of viscosity and vapour pressure reduction on flux reduction for various feed temperatures, flow rates and concentrations.

it was revealed that the vapour pressure reduction for a 30 wt% sugar
solution is less than 3% (c.f. 29% reduction for a 30 wt% salt
solution). The viscosities for 30 wt% sugar and salt solutions, however,
are approximately equal. Thus it would be expected that viscosity
effects are the major cause of flux reduction for sugar solutions. The
computer model for the salt experiments was modified for the sugar case.
The membrane mass transfer coefficient had to be increased slightly to
$C = 6.3 \times 10^{-7}$ kg/m^{2}sPa (c.f. 5.9×10^{-7} for salt experiments). This may
have been due to the use of a different membrane sample. The model
results, considering only viscosity effects, are compared to the
experimental results in figure 7.11. It can be seen that viscosity
effects alone can explain the flux reduction for sugar solutions. Even
at higher concentrations, where vapour pressure would be significant,
viscosity effects would be expected to dominate.

The results presented above have shown that for a turbulent cross flow
system, the flux reduction brought about by solute in the feed is small
at moderate concentrations (<10wt%). The flux reduction is predominantly
caused by vapour pressure reduction and increased viscosity (decreased
film heat transfer). The heat transfer theory presented in chapter 4
suggests that the situation may be better in laminar flow hollow fibre
systems. In laminar flow, the film heat transfer coefficient is not
dependent on viscosity, being only dependent on thermal conductivity.
From table 7.1 it can be seen that thermal conductivity has only a small
effect on flux. An increase in viscosity will result in decreased flow
rate at constant pressure drop, however heat transfer is also
independent of flow rate in fully developed laminar flow (see chapter
4). Thus viscosity effects would be minimal in a hollow fibre system.

As laminar hollow fibre systems have similar heat transfer coefficients
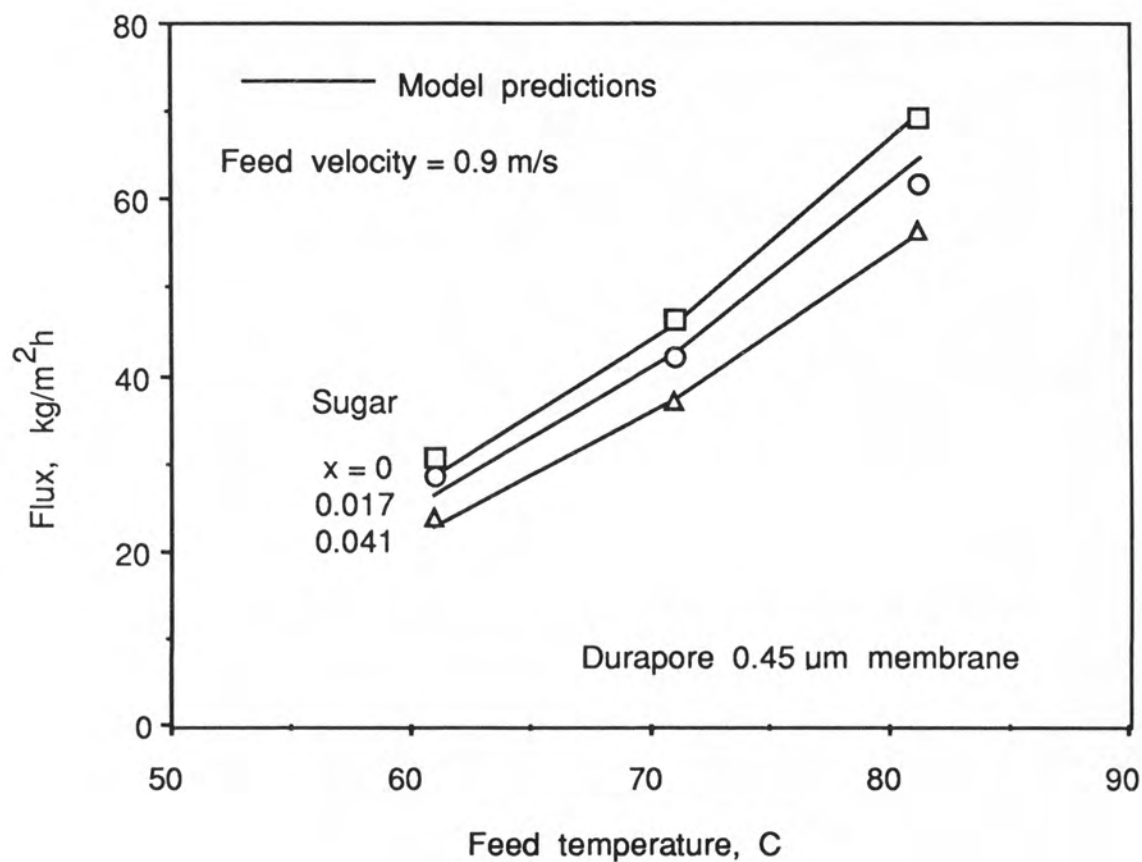
Figure 7.11 : Fluxes from figure 7.7 showing model predictions considering viscosity effects only.

to turbulent systems, it is expected that they should also have similar
solute mass transfer coefficients. This indicates that concentration
polarisation should be no worse in laminar systems than it was in this
study. Thus for hollow fibre systems, the only major factor reducing the
flux would be vapour pressure reduction, which cannot be avoided. These
considerations are supported in chapter 8, where pilot plant studies are
conducted using hollow fibre MD modules.

7.3.3 Membrane fouling and wetting

The theory of capillary wetting in MD was introduced in chapter 2. The
two solution properties that prevent wetting of the membrane are the
surface tension and the contact angle. Although the problem of membrane
wetting has not been specifically addressed in this study, some
observations have been made that warrant attention.

Firstly, it was mentioned above that when operating with saturated
solutions, a salt scale formed on the membrane, and discrete wet patches
(translucent patches which could be described as pin holes) were
observed. The total area of these wet patches was estimated as 5% of the
membrane area. After drying of the membrane, continued operation
resulted in the same patches becoming wet. A possible explanation for
this phenomenon is given below.

The presence of a large surface pore or imperfection can allow partial
penetration of the feed into the membrane. Within this valley or well,
concentration polarisation will result in localised high concentrations.
At supersaturated concentrations, as may exist at the evaporating
surface, salt may precipitate at the solid/liquid/gas interface. This
would render the pore walls hydrophilic, allowing gradual encroachment

into the pores. As penetration into the membrane increased, localised concentration polarisation would lead to higher levels of supersaturation, and hence the propagation of wetting across the membrane. If the membrane is not thoroughly rinsed prior to drying, precipitated solute within the membrane will allow wetting to reoccur.

Another observation was made regarding contact angle effects. At the conclusion of several experiments, wet patches of membrane were observed in the shape of finger prints (allowing identification of the perpetrator). At high feed concentrations, wetting had propagated right across the membrane, while at lower concentrations only partial wetting had occurred. This is consistent with the concept of propagation of wetting discussed above. It is believed that finger prints leave surface active agents on the membrane which change the contact angle at the gas/ liquid interface, facilitating wetting. This emphasises the need to avoid surfactants when handling MD membranes.

It is recommended that the topic of wetting be the focus of further study.

7.4 CONCLUSIONS

The major conclusion from this study is that the presence of solute in low to moderate concentrations does not have a large effect on flux. Even at concentrations of 25 to 30 wt%, the flux reduction is less than 50%.

The major cause of flux reduction in salt solutions is vapour pressure reduction. For the system studied, this accounted for 50 to 80% of the total flux reduction. Viscosity was found to be the second major factor

in flux reduction for salt solutions, as increased viscosity leads to increased boundary layer thickness, and hence a lower film heat transfer coefficient on the feed side. For sugar solutions, viscosity effects alone accounted for flux reduction for concentrations up to 30 wt%. Other transport properties were found to have only a minor effect on flux.

Based on the results for the turbulent cross flow cell, laminar flow hollow fibre systems were identified as having minimal flux reduction by solute, as they are not sensitive to viscosity effects.

7.5 ACKNOWLEDGEMENT

I would like to thank Mr Richard Macoun for his assistance with cross flow MD experiments and data retrieval.

7.6 NOTATION

b   Channel height [m]

c   Concentration [mol l^{-1}]

C   Membrane mass transfer constant [kg m^{-2} s^{-1} Pa^{-1}]

C_p Heat capacity [J kg^{-1} K^{-1}]

D   Diffusion coefficient [m^2 s^{-1}]

d_h Hydraulic diameter [m]

h   Heat transfer coefficient [W m^{-2} K^{-1}]

ΔH_v Latent heat of vaporisation [J kg^{-1}]

J   Mass flux through membrane [kg m^{-2} s^{-1}]

k   Thermal conductivity [W m^{-1} K^{-1}]

k_s Solute mass transfer coefficient [m s^{-1}]

M   Gas molecular weight [kg mol^{-1}]

Nu   Nusselt number = hX/k [-]

P   Water vapour pressure [Pa]

P°   Vapour pressure of pure water [Pa]

Pr   Prandtl number = $C_p\mu/k$ [-]

R   Gas constant [J mol^{-1} K^{-1}]

Re   Reynolds number = $\rho vX/\mu$ [-]

Sc   Schmidt number = $\mu/\rho D$ [-]

T   Temperature [K,°C]

v   Fluid velocity [m s^{-1}]

W   Weight fraction solute [-]

x   Mole fraction solute [-]

X   Characteristic length [m]

γ Activity coefficient [-]

μ Viscosity [Pa s]

ρ Density [kg m^{-3}]

Subscripts

c   Conduction

f   Feed

m   Membrane

p   Permeate

s   solute

th   threshold

v   Vapour

w   water

7.7   REFERENCES

[7.1]   Franken, A.C.M., "Membrane Distillation - A New Approach Using

        Composite Membranes", Ph.D. Thesis (1988), University of Twente,

        The Netherlands.

[7.2]   Barrow, G.M., "Physical Chemistry", 2nd ed., McGraw-Hill, 1966.

[7.3]   Smith, J.M., and van Ness, H.C., "Introduction to Chemical Engineering Thermodynamics", 3rd ed., McGraw-Hill, 1975.

[7.4]   Porter, M.C., "Concentration Polarisation with Membrane Ultrafiltration", Ind. Eng. Chem. Prod. Res. Develop., 11(3) (1972) 234-248.

[7.5]   Olynyk, P. and Gordon, A.K., "The Vapour Pressure of Aqueous Solutions of Sodium Chloride at 20, 25 and 30° for Concentrations from 2 Molal to Saturation", J. Am. Chem. Soc. 65 (1943) 224-226.

[7.6]   Weast, R.C. (ed.), "Handbook of Chemistry and Physics", 57th ed., CRC Press, Cleveland, Ohio.

[7.7]   Perry, R.H. and Chilton, C.H., "Chemical Engineers' Handbook", 5th ed., McGraw-Hill, 1974.

[7.8]   Peters, M.S. and Timmerhaus, K.D., "Plant Design and Economics for Chemical Engineers", 3rd ed., McGraw-Hill, 1981.

[7.9]   Hoynak, P.X. and Bollenback, G.N. "This is Liquid Sugar", Refined Syrups and Sugars Inc., New York, 1955.

[7.10] Pancoast, H.M. and Junk, W.R., "Handbook of Sugars", 2nd ed., AVI Publishing Co. Inc., Connecticut, 1980.

Chapter 8

Pilot
Plant
Study

CHAPTER 8: PILOT PLANT STUDY

A pilot plant study was conducted to investigate process aspects of MD. The laboratory scale pilot plant was constructed based on a module containing 1 m^2 of membrane area, this being a typical size for commercial modules. As membrane processes are modular in nature, scale up is essentially linear. The data gathered from this study have been used to make projections for the operation of full scale MD plants.

MD pilot plant studies have been conducted in other centres around the world over the past decade, as discussed in chapter 1. Gore-tex [8.1], in the United States, studied their spiral-wound system during the early 1980's, but have since abandoned the technology. Enka [8.2], in West Germany, have done extensive studies on their turbulent flow tubular membrane system incorporating heat recovery. They have developed the technology to the commercial stage, but have had limited success marketing their system. The Swedish National Company [8.3] are currently conducting pilot plant studies on their gas-gap sheet membrane system utilising the waste heat from diesel powered electricity generators. None of these studies has lead to a wide spread industrial acceptance of MD.

This pilot plant study differs from these previous studies in that it is based on the use of hollow fibre membranes with laminar flow of both feed and permeate. The results presented in chapter 4 suggest that this configuration provides better heat transfer than the three systems mentioned above, particularly at low flow rates, and the results from chapter 7 indicate that solute effects will be minimised.

During the course of this pilot plant study, MD was proposed as a possible technology for the dewatering of "red water", a waste product from the manufacture of trinitrotoluene (TNT). A large section of this study was devoted to this application, under the support of the Australian Department of Defence.

8.1 PILOT PLANT DESIGN

A membrane distillation pilot plant was designed, based on a counter-current hollow fibre MD module. A flow diagram for the pilot plant is shown in figure 8.1 and a photograph is included in Appendix A, figure A.4. Under normal conditions, the plant operated as follows. The feed solution was stored in an elevated reservoir, pumped through a heat exchanger to achieve the desired feed temperature, passed through the tube side of the MD module, where the sensible heat was consumed as latent heat of vaporisation, and returned to the reservoir. Heating water was supplied to the heat exchanger from a recirculated thermostatted water bath. The permeate was stored in an elevated reservoir, pumped counter-currently through the shell side of the MD module, where it absorbed the latent heat of vaporisation, cooled in the heat exchanger and returned to the reservoir. Some of the heat from the permeate was used to preheat the feed, while the remainder was removed by recirculated thermostatted cooling water. The permeate could be returned to the feed reservoir under gravity flow, to allow extended steady state operation.

Feed and permeate flow rates were measured by rotameter before returning to their respective reservoirs. Pressures and temperatures were monitored for all streams entering and leaving the MD module. Reservoir levels were monitored by sight glasses, allowing flux measurement. Flow
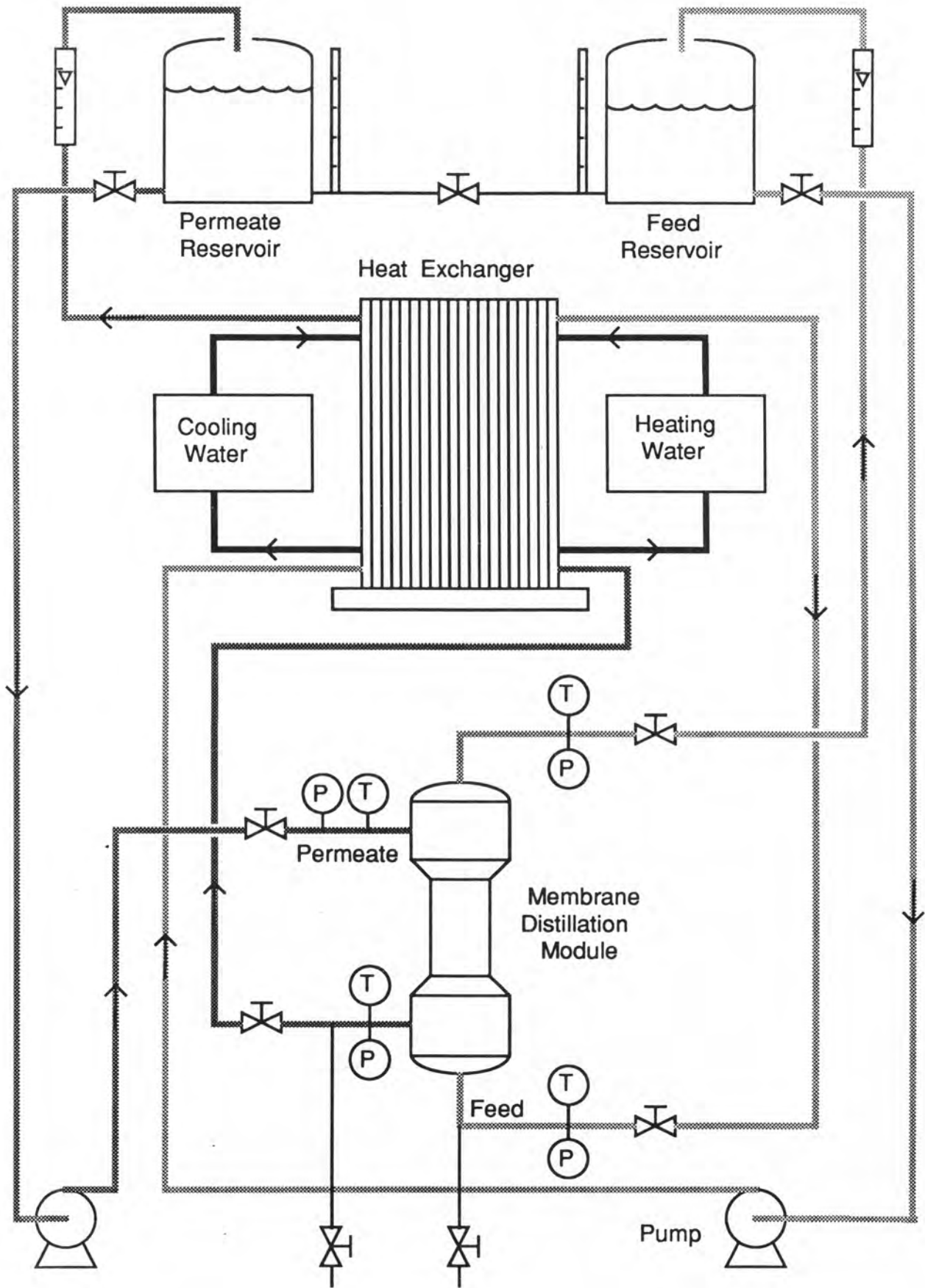
Figure 8.1 : Membrane distillation pilot plant.

rates and pressures were controlled by valves around the MD module. Feed and permeate temperatures were controlled by means of the heating and cooling water temperatures.

Specifications for the major pilot plant items are given below.

Membrane Distillation Modules

Two different MD modules were used in this study. Module I, which was used for the bulk of the study, was a modified version of a shell-and-tube microfiltration module constructed by Memtec Limited, Australia. A cross-section of a shell and tube module is shown in figure 8.2. Module II was constructed in-house, the major difference being reduced shell side voidage and less membrane area. The benefits of reducing shell side voidage were discussed in chapter 4. Details of the two modules are given below, and photographs are included in Appendix A, figure A.5.

Hollow Fibre Membranes
_____

Material: Polypropylene
Pore size: 0.2 μm
Porosity: 0.7
Diameter: 0.3mm i.d., 0.6mm o.d.

	Module I	Module II
Shell material:	Polyvinyl Chloride	Glass
Potting compound:	Urethane	Silicone rubber
Fibre length:	400 mm (exposed)	170 mm (exposed)
Number:	~2000	~1100
Area:	~0.7 m^2	~0.17 m^2
Shell side voidage:	~0.6	~0.5

The materials for module I limited its operating temperature to 70 °C.
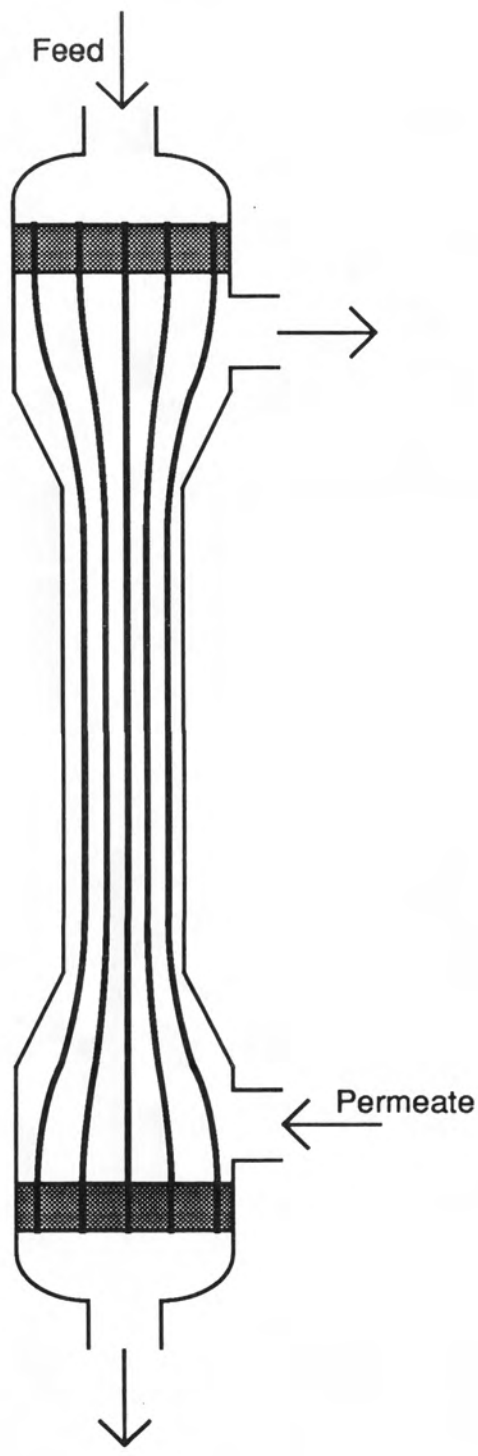
Figure 8.2 : Shell and tube module

Heat Exchanger

An APV™ plate and frame heat exchanger performed the duty of three exchangers, as shown in figure 8.3. At one end, heat was exchanged between the permeate and the cooling water. At the other end, the feed was heated by the heating water. The centre of the exchanger transfered heat from the hot permeate to the incoming feed.

Plate and Frame Heat Exchanger

Material: Stainless steel
Number of plates: 50
Area per plate: 0.02 m^2

Heating Unit

The heating unit provided thermostatted heating water to the heat exchanger. It consisted of an insulated bath, a 1.2 kW Thermomix™ recirculating immersion heater, and two additional 1 kW immersion heaters manually controlled by a Variac™ auto-transformer.

Hot Water Bath

Volume: 18 litre
Heating fluid: Water
Heating capacity: 3.2 kW
Recirculation rate: 10 l/min

Cooling Unit

The cooling unit provided thermostatted cooling water to the heat exchanger. It consisted of an FTS™ RC-100 recirculating cooler and DMC-2 controller.
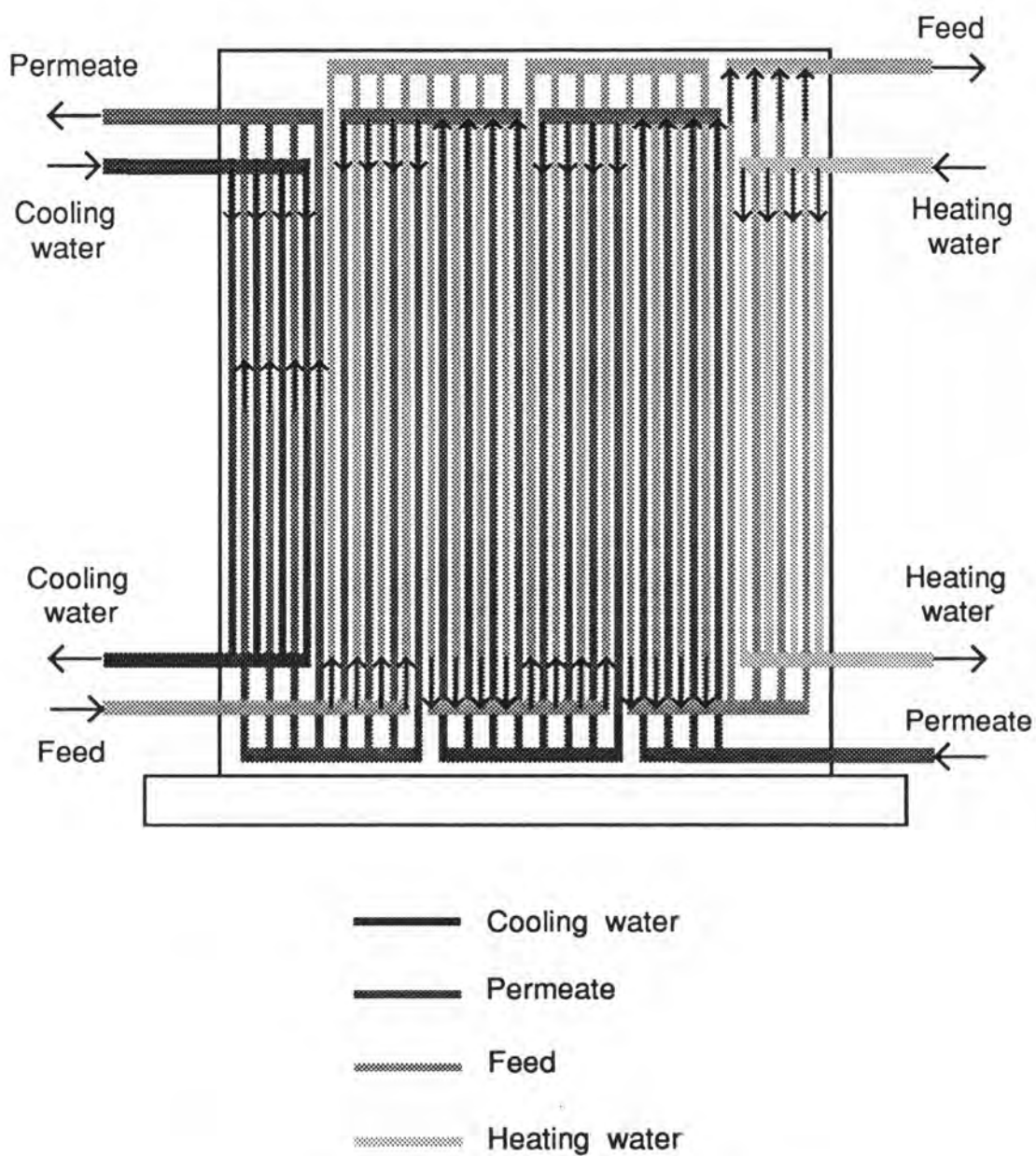
Figure 8.3 : Plate and frame heat exchanger.

Refrigeration Unit
_____

Volume: 9 litre

Cooling fluid: Water

Cooling capacity: 4.4 kW @ 30°C

Recirculation rate: 15 l/min

Pumps

Both the feed and permeate were recirculated by Iwaki™ MD-30RZ magnetically driven centrifugal pumps.

Pumps
_____

Maximum flow: 15 l/min

Maximum pressure: 80 kPa

Wetted material: Polypropylene

Temperature Indicators

Temperatures at the MD module inlets and outlets were monitored by a Jenko™ 767-Pt digital thermometer with platinum resistance immersion probes.

Digital thermometer
_____

Temperature range: -150 to 500 °C

Accuracy: 0.2 °C

Resolution: 0.1 °C

Sundry Items

Information regarding pressure, flow rate, and reservoir level monitoring, as well as plumbing specifications are given below.

Miscellaneous Items
───────────────────

Pressure gauges: Bell Instruments™ 0-160 kPa

Rotameters: GEC™ metric 18E 0-10 l/min

Reservoir level sight glass: Resolution 1 mm (30 ml)

Reservoir volumes: 10 litre

Piping: Vinidex™ 15 mm UPVC pressure pipe

Tubing: Nylex™ 20 mm reinforced tube

Valves: 15 mm PVC ball valves and diaphragm valves

8.2   EXPERIMENTAL PROGRAM

8.2.1   Fundamental Study

The first study conducted with the pilot plant was to display the capability of module I. Using distilled water as the feed, temperatures and flow rates were varied over the full range achievable with the equipment. From this study it was evident that module I was oversized for the pumping and heating capacity of the pilot plant, however the range of operating conditions achieved was sufficient to fully characterise the system.

For module I with distilled water as the feed, the effects of feed flow rate and feed temperature on flux are shown in figure 8.4. For each change in conditions, one hour was allowed to attain steady state, and two flux measurements were taken 30 minutes apart to ensure stability. Due to the limitations on pumping rate and heat input of the equipment, these results do not cover the complete practical range of feed flow rates and temperatures. It is expected that feed temperatures of 80 - 85°C with flow rates of 6 - 8 l/min should result in fluxes of 15 - 20 kg/m^{2}h. A computer model was developed to extrapolate from the lab results to more realistic operating conditions. Details of this model are given in Appendix C.
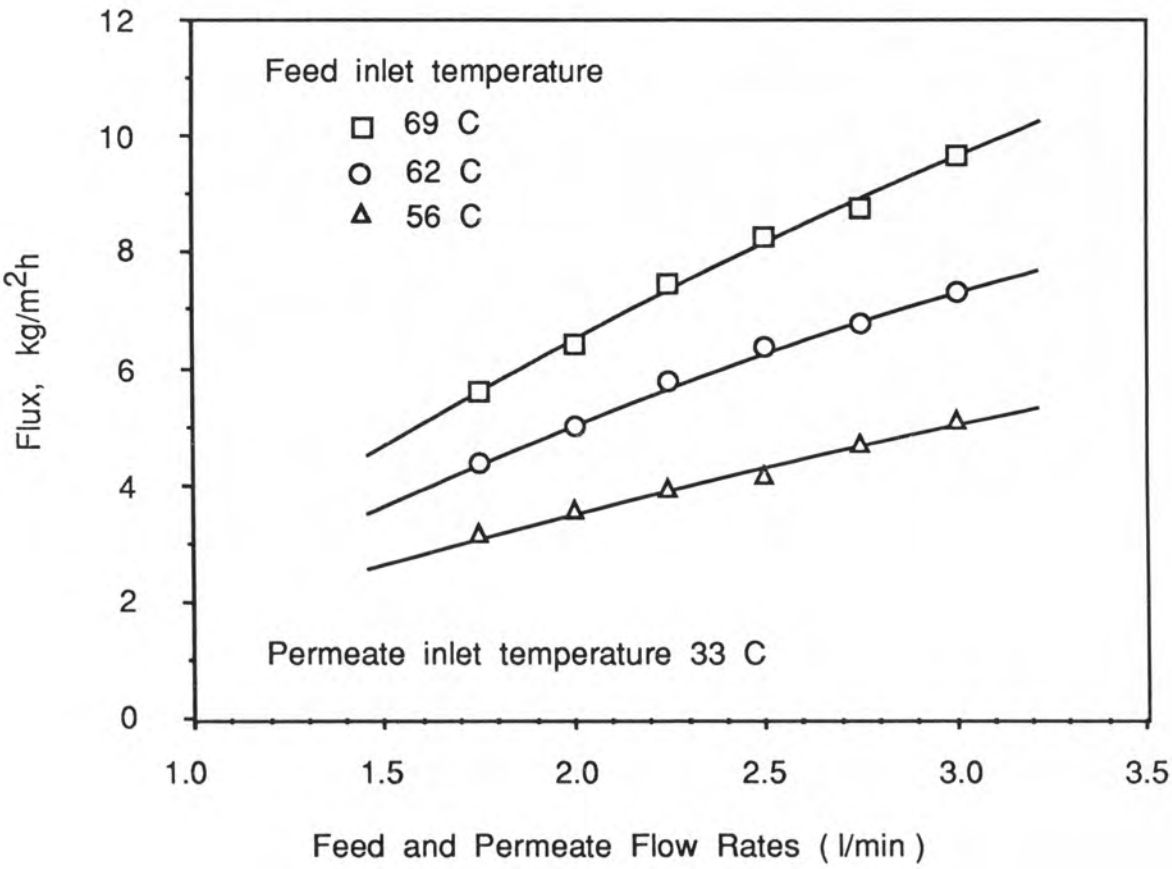
Figure 8.4 : Fluxes for module I with distilled
water feed

From figure 8.4, it can be seen that flux increases with both feed temperature and flow rate, as would be expected. The significance of feed flow rate as a process variable will be discussed in section 8.3. From the results in chapter 7, the fluxes observed here with distilled water feed are indicative of the fluxes expected in most applications.

8.2.2 Applications

Many applications have been identified for MD, the majority of which involve removing water from solutions containing salts or other non-volatile solutes. In the preliminary stages of this study, tests were done on salt water, sugar solutions etc., and the adequacy of the technology was easily displayed [8.4]. In other research establishments, work has been done on the MD of solutions containing dissolved solids [8.5] and dissolved organics [8.6] and commercial units are being tested for the desalination of sea water [8.3]. In the early stages of this study, the concentration of fruit juices was seen as a possible new application for MD. Preliminary tests, however, revealed some short-comings in this application, including the loss of some flavour, and the discoloration of the juice concentrate. Prompted by the Australian Department of Defence, a possible application was seen in the dewatering of "red water", an effluent from the manufacture of TNT.

Red water is a complex mixture of salts and medium/low volatility organics (benzene/toluene derivatives). It is produced in large quantities and must be incinerated to dispose of the harmful organics. As red water is ~95% water, there would be great energy savings if the bulk of the water could be removed prior to incineration. Due to the complex nature of the solution, there was no ideal technology suited to this task. Initial tests with MD, however, were encouraging, and red

water was chosen as the major application to be studied in this project. (Note, MD is not ideal for this application as the major component, water, is removed through the membrane.)

Pilot plant trials were conducted using both red water and salt water as feed. The major objective was to display the technical feasibility of the process, and to examine the compatability of the membrane and module materials with the feed solutions.

Effluent Dewatering

Before red water was tested in the pilot plant, laboratory scale experiments were conducted with sheet membranes, using the apparatus from chapter 4. The first test for the MD of red water was to remove 90% of the water from a red water feed, collecting the permeate as 9 successive fractions. The 10th fraction was the remaining concentrate. The feed, concentrate and permeate fractions were then analysed for conductance to indicate salt levels, and for UV absorbance to indicate levels of organics. The results from this test are shown in Table 8.1.

These results indicate that 90% of the water can be removed from red water with the loss of less than 1% of the organics, and less than 0.5% of the salts. The permeate purity that can be obtained may be even higher than this, as small areas of wet membrane were observed after the experiment. Such wetting of the membrane allows diffusion of the solute into the permeate. The occurrence of wetting is a complex phenomenon depending on the temperatures, pressures and types of solute used. In an industrial situation, wetting can be combatted by periodic cleaning and drying of the membranes.

Table 8.1: Permeate Purity for the Dewatering of Red Water.

Membrane	-	Millipore 0.22 μm PVDF flat sheet
Conditions	-	$T_f = 70°C$ $T_p = 20°C$
Duration	-	3 Hours

SAMPLE	CONDUCTANCE μS cm^{-1}	ABSORBANCE $\lambda = 250$ nm
Red water diluted/100	190	3.24
Permeate Fraction #1	55.5	1.54
" " #2	36.5	2.68
" " #3	29.9	2.66
" " #4	31.5	2.56
" " #5	77.0	2.38
" " #6	42.5	2.18
" " #7	21.9	1.96
" " #8	20.9	1.82
" " #9	70.4	2.18
Concentrate Fraction #10	81000	

Further lab-scale experiments were conducted to gauge the performance of MD as a process, with interest centered on fluxes achieved under varying conditions. The major parameters considered were feed concentration, time, temperature and membrane type.

Figure 8.5 shows the effect of permeate removal on water vapour flux using a Millipore 0.22 μm PVDF membrane. The results show that up to 90% of the water can be removed with the flux declining by only 35%. Such a result would not be attainable with other processes such as reverse osmosis. The level of flux reduction for these sheet membrane experiments is similar to that observed in chapter 7 with salt and sugar solutions.
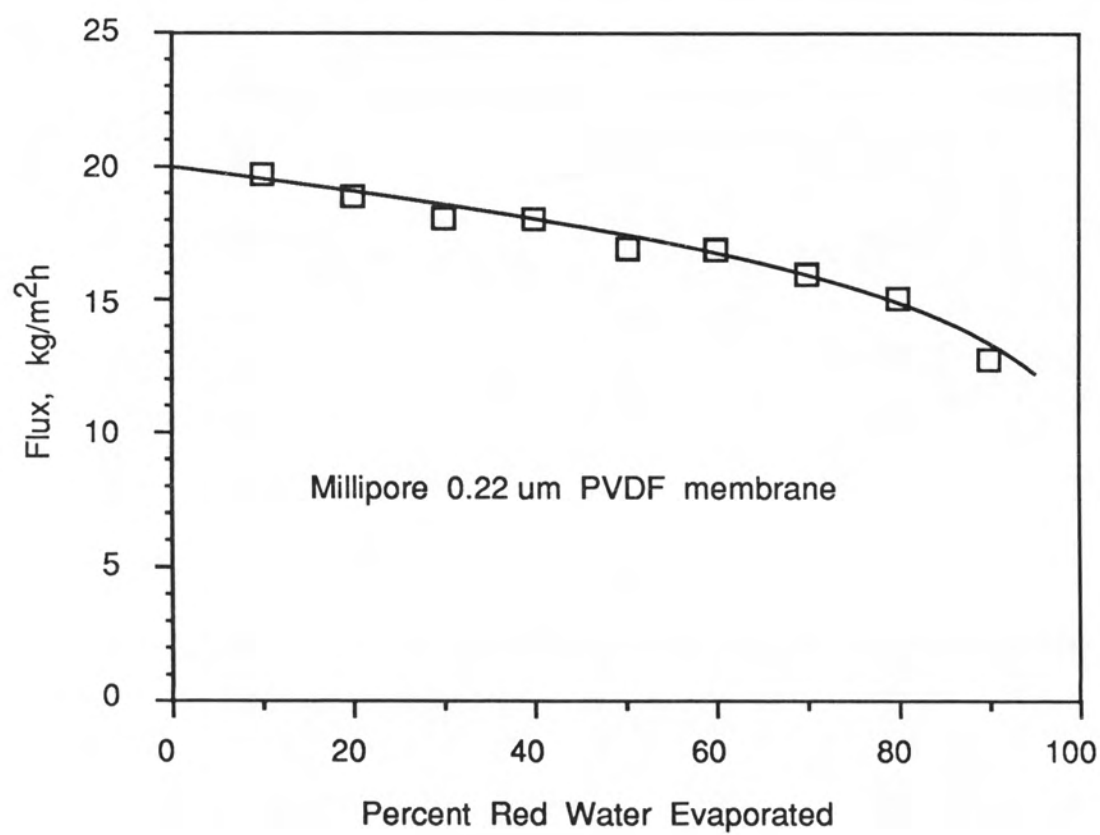
Figure 8.5 : Effect of red water concentration on flux.

Figure 8.6 shows the effect of time on flux for various concentrations of red water using an ENKA 0.2 μm polypropylene membrane. The results show that even at four times the initial concentration (i.e. 75% water removed), the flux decline in MD is slow. Partial wetting of the membrane was observed after extended operation.

Figure 8.7 shows the effect of heating water temperature on flux for an ENKA 0.2 μm membrane. The results are similar to those obtained with distilled water, and display the rewards for operating at higher temperatures.

Module I

Having displayed the suitability of MD for the dewatering of red water on a laboratory scale, attention was focussed on the pilot plant. For red water, an important initial test was to observe the flux stability to determine if membrane fouling and/or wetting would be a major problem. This was accomplished by operating the pilot plant in a steady state mode, with continuous recycle of the permeate back into the feed reservoir, thus keeping the feed concentration constant. Figure 8.8 shows the results for fluxes measured over a three day period. The results show only a minor decrease in flux over this time span, indicating that membrane fouling and wetting are not a major concern under these conditions.

As a measure of the performance of MD for the concentration of red water, the conductivity of the permeate was measured throughout this test. The results are shown in Table 8.2. Also shown are the equivalent concentrations of NaCl corresponding to the various conductances, based on the conductance of dilute salt solutions being 2.16 μS/cm.ppm. [8.7].
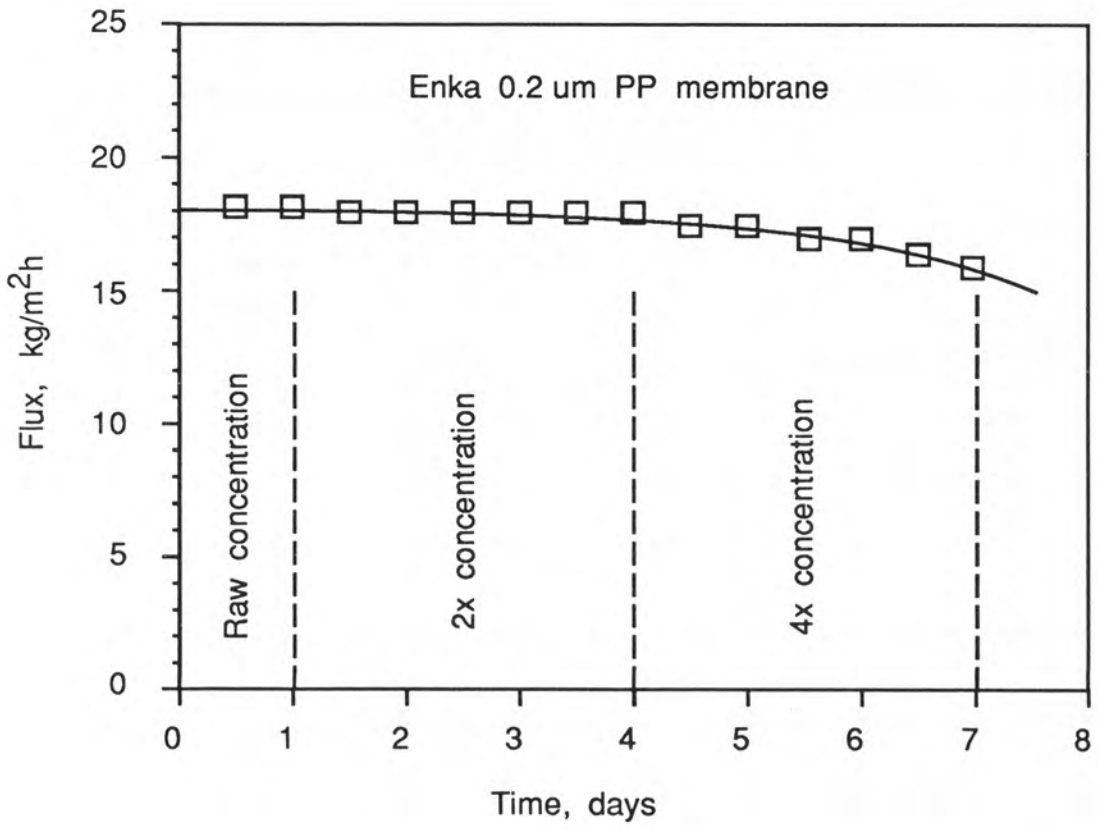
Figure 8.6 : Effect of time on flux for three red water
concentrations.
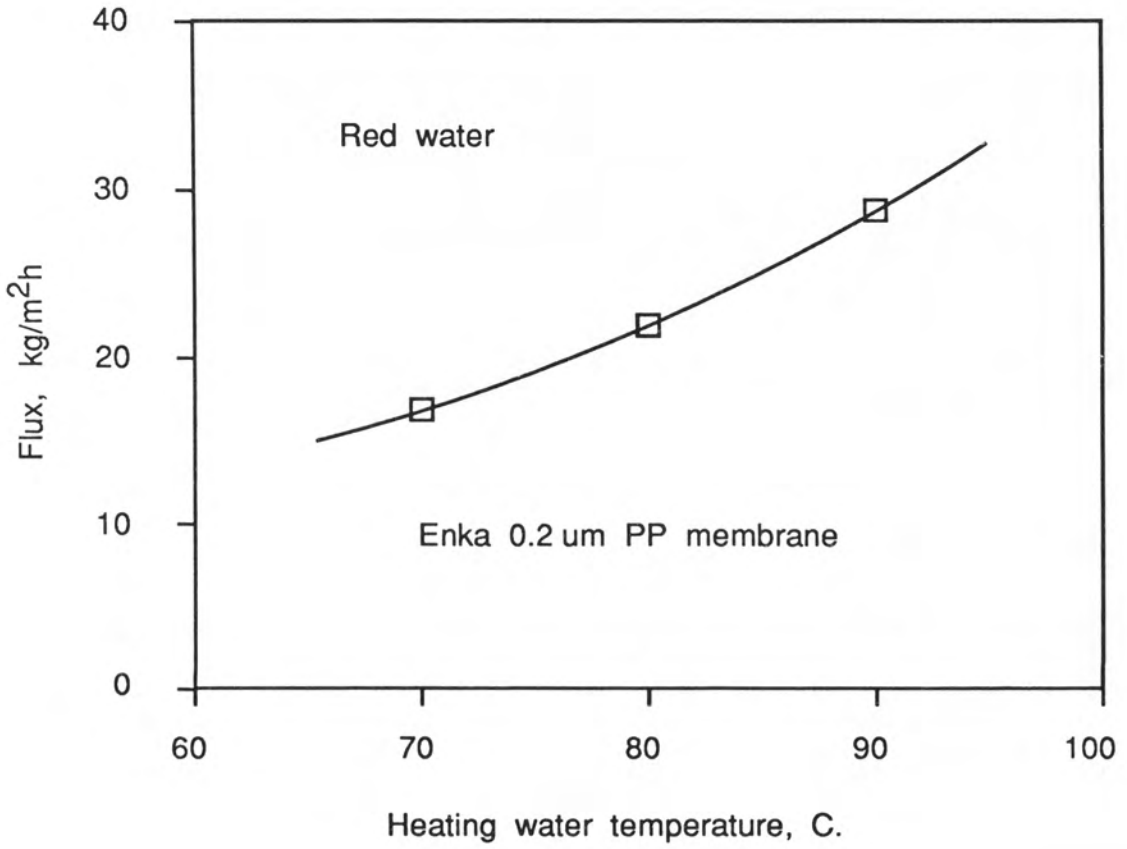
Figure 8.7 : Effect of heating water temperature
on flux.
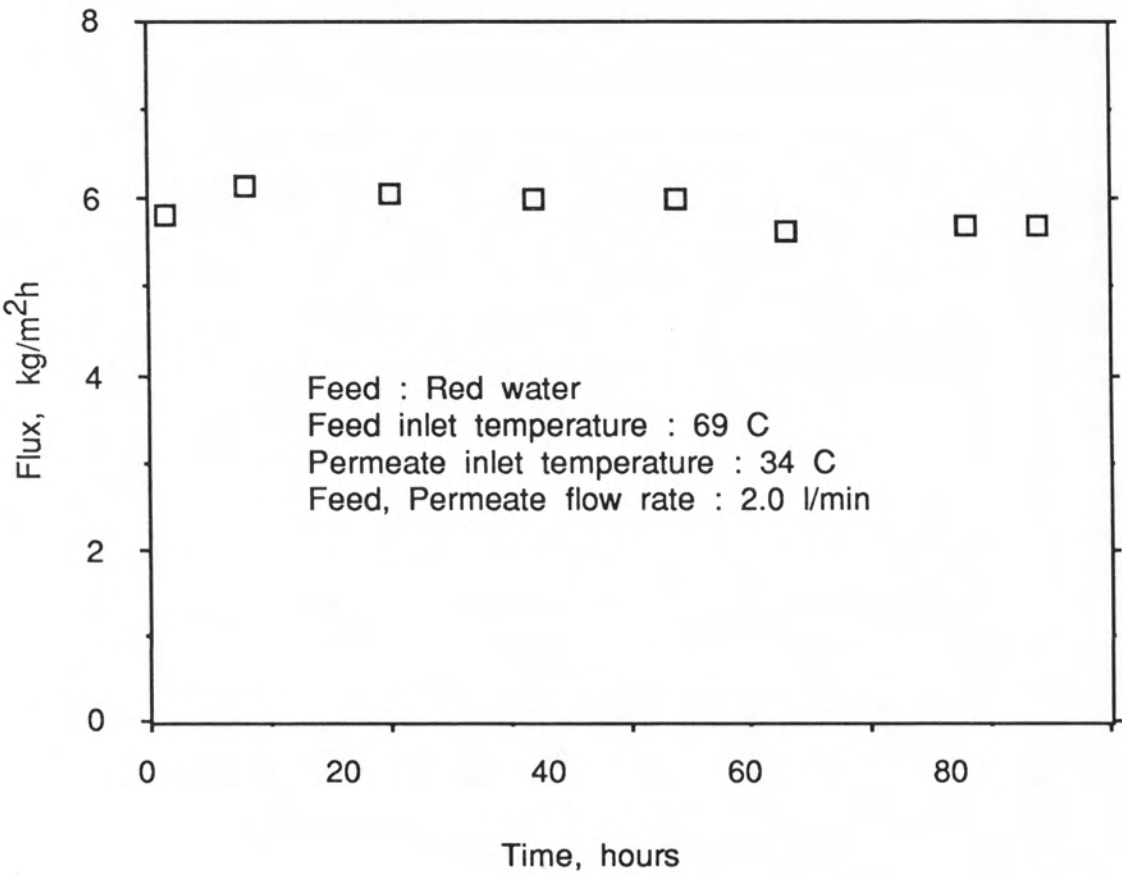
Figure 8.8 : Module 1 performance with red water feed.

The equivalent NaCl concentration in the permeate was less than 30 ppm corresponding to a rejection of salts greater than 99.6%. Analysis of the permeate by the Department of Defence revealed 2,4 dinitro-toluene concentrations ranging from 30-70 ppm. This volatile organic must be removed from the permeate by an alternative technology such as adsorption.

Table 8.2:   Flux and Permeate Purity for the Dewatering of Red Water using Module I.

Feed: Red water			
Feed inlet temperature: 69 °C			
Permeate inlet temperature: 34 °C			
Feed, permeate flow rates: 2.0 l/min			
Time hours	Flux kg/m^{2}h	Conductance μS/cm	Equivalent NaCl conc., ppm.
1.3	5.8	46	21
8	6.2	46	21
20	6.1	53	25
32	6.1	53	25
44	6.0	54	25
53	5.7	58	27
68	5.7	60	28
74	5.7	60	28
Feed diluted/100		190	88

A second major test for the red water application was to study the effects of red water concentration on flux and flux stability. In this test, the pilot plant was run at steady state for a period of time and then permeate was collected to increase the feed concentration, followed by further steady state operation, and so on. The results are shown in figure 8.9.

fig 8.9
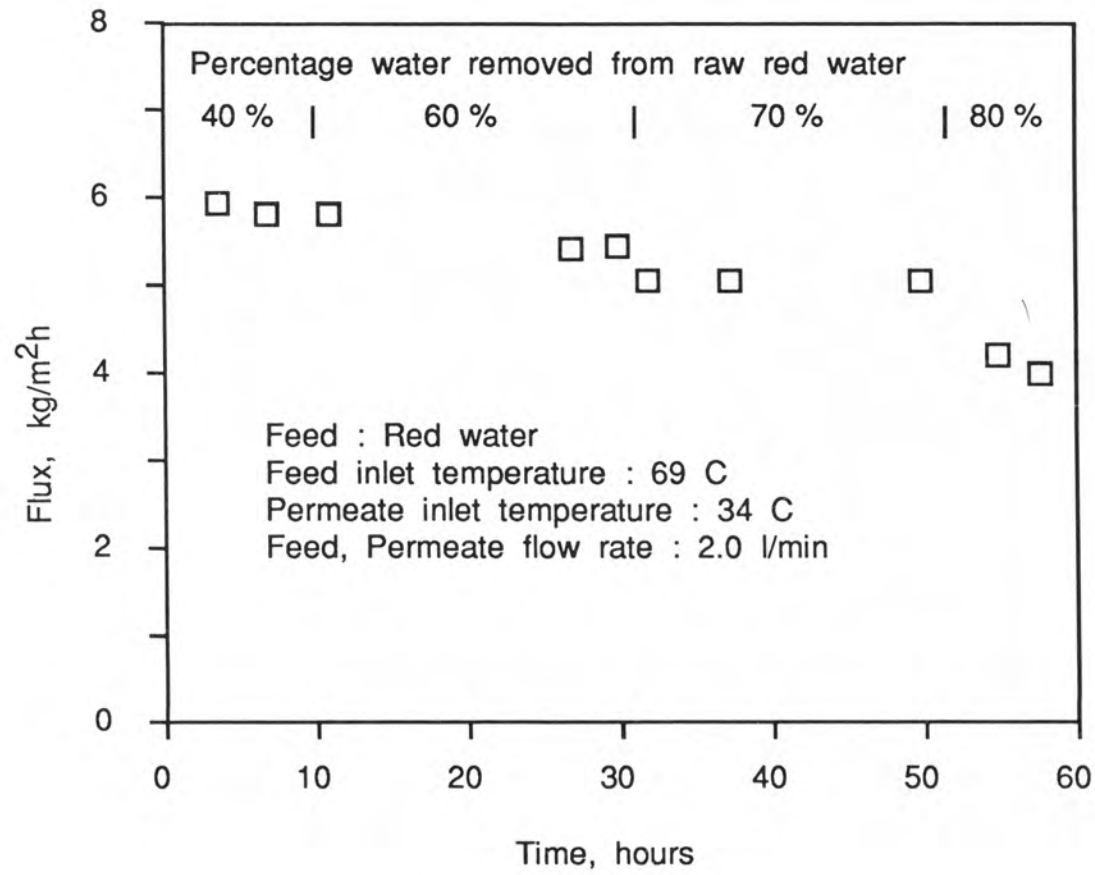
Figure 8.9 : Effect of red water concentration on
flux and flux decline.

These results show that flux decreases with increasing feed concentration as would be expected due to the solute effects discussed in chapter 7. The magnitude of the flux decline also indicates possible fouling of membranes and heat transfer surfaces at high concentrations. The flux decline for a 5-fold concentration of the feed was around 30%. A much larger decline would be expected from alternative membrane processes such as reverse osmosis. These results indicate that an MD process for the treatment of red water would have to include a periodic cleaning procedure.

Desalination

The suitability of MD for the desalination of salt water was tested over a five day period using a steady state feed concentration of 25,000 ppm (2.5 wt %) NaCl. The results are shown in Table 8.3. From permeate conductivity measurements, the degree of contamination of the permeate was around 0.5% of the feed concentration (99.5% rejection). The degree of flux decline indicates that some fouling and/or wetting has occurred, and this is supported by the increasing conductivity measurements. It should be noted that the membranes used in this study had already been used for the red water study, and may have maintained some residual fouling. Theoretically, the rejection of salt should be 100%. In an industrial context, periodic cleaning and drying of the membrane should result in a full recovery of the initial flux and permeate purity.

A major observation from both the red water and desalination studies concerns the flux reduction caused by the presence of solute in the feed (disregarding the flux decline with time due to fouling/wetting). For both applications, with the exception of red water at high concentrations, the flux was within 10% of that achieved with distilled

Table 8.3: Flux and Permeate Purity for the Desalination
of Salt Water using Module I.

Feed: Salt water, 2.5 wt%

Feed inlet temperature: 69 °C

Permeate inlet temperature: 34 °C

Feed, permeate flow rates: 2.5 l/min

Time hours	Flux kg/m^{2}h	Conductance μS/cm	Equivalent NaCl conc., ppm.
3	6.9	113	52
6	6.9		
15	7.2	117	54
38	7.2	155	72
46	7.0	195	90
61	6.9		
72	6.8	246	114
85	6.5	277	128
109	6.5	297	138
Feed		33000	25000

water feed at the same operating conditions. This implies that the sizing of MD equipment is not strongly dependent on the feedstock, as was found in chapter 7.

One final experiment with module I was to examine the effect of feed and permeate pressures on flux. The pilot plant was temporarily modified so that the MD module was situated in the suction line to the pumps. In other words, both the feed and permeate were flowing through the module at subatmospheric pressures. The suction head requirements of the pumps limited the flow rates to 2 l/min. At this flow rate, with feed and permeate inlet temperatures of 60 and 24 °C respectively, the flux was 6.7 kg/m^{2}h. With the pumps returned to their usual position, these

operating conditions were duplicated giving a flux of 5.1 kg/m^{2}h. Thus decreasing the liquid pressures resulted in a 30 % increase in flux. This is consistent with the flux increases observed in chapter 6 with partial deaeration. Greater flux increases would be expected for totally deaerated systems, particularly for modules with high film heat transfer coefficients.

8.2.3 Improved Module Design

An improved MD module was constructed, the specifications for which were given in section 8.1. Module II was constructed with a lower shell side voidage to increase the film heat transfer coefficient on the shell side, and had substantially less membrane area making it better suited to the pilot plant heating and pumping capacities. As with module I, a fundamental study was conducted using distilled water as the feed, to measure the variation of flux with feed temperature and flow rate. The results are shown in figure 8.10 along with comparative results from module I (note that module II had approximately half the number of fibres of module I, hence the comparative flow rates are halved).

From figure 8.10 it can be seen that module II produced twice the flux of module I under similar conditions. This is predominantly due to the increased heat transfer coefficient on the shell side, achieved by reducing the shell side voidage from 0.6 for module I to 0.5 for module II. The shorter fibre length also contributes to increased flux. It is recommended that an improved pilot plant be constructed to continue the study of module II performance.

With the knowledge that the sizing of MD equipment is not strongly dependent on the feed stock, module II results were used for scale-up
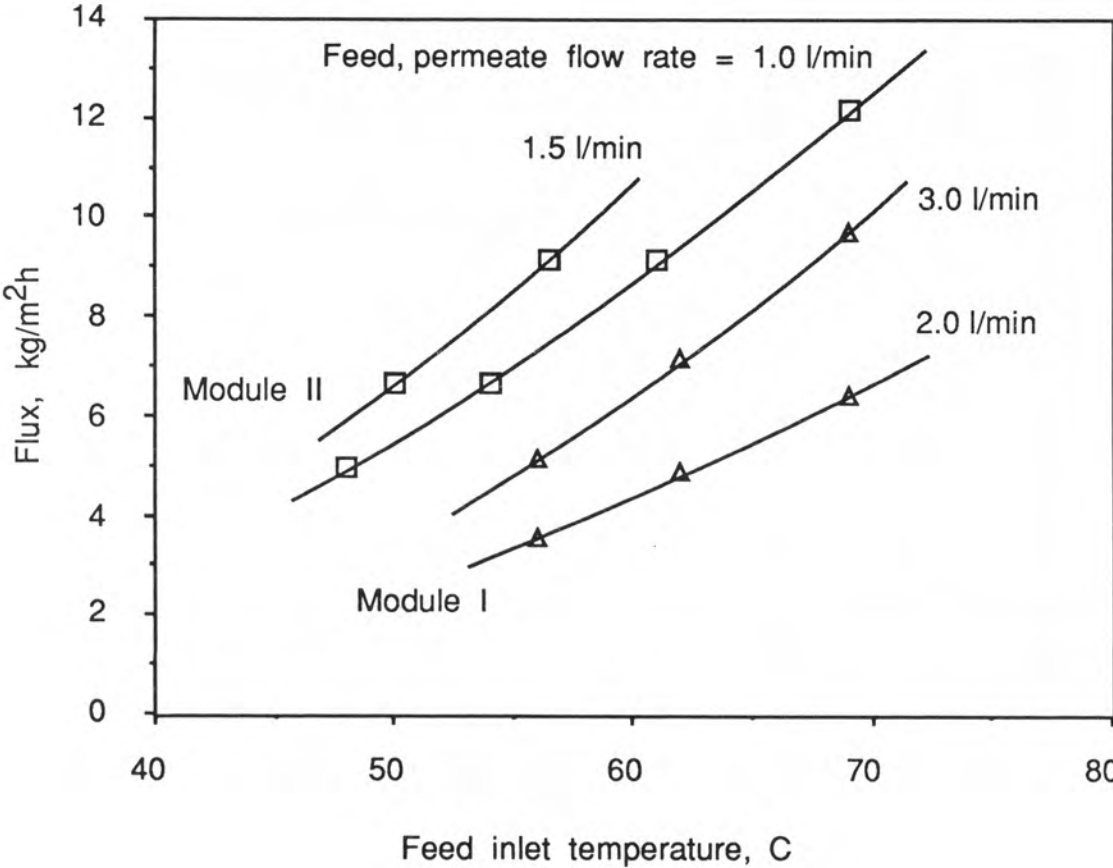
Figure 8.10 : Comparison of modules I and II with
distilled water feed.

purposes, as detailed in the following section. It is anticipated that future module designs will result in even higher fluxes. In chapter 3, details were given of a laboratory scale hollow fibre module designed primarily for studying the effects of shell side voidage. Preliminary results with low shell side voidages (less than 0.5) have yielded fluxes in excess of 90 kg/m^2h under deaerated conditions with a feed temperature of 90 °C. It is suggested that work continue in this important area of module design.

8.3 DESIGN AND DEVELOPMENT

The knowledge gained from the theory and experimental program has been used to make some economic projections for MD. The performance data from the pilot plant study have been used to assess the likely performance of MD in various industrial situations. A computer model based primarily on the performance of module II has been used to predict MD performances under a range of operating conditions, leading to cost analyses for various applications. The design procedure was based on results obtained for the MD of distilled water, recognising that the presence of solute in the feed only decreases the flux slightly.

The major consideration when designing an MD process is the energy cost. The bulk of the energy requirement is to provide the latent heat of vaporisation, with pumping and control only consuming a small fraction of the total energy input. Thus the bulk of the energy requirement is in the form of thermal energy. This opens up energy sources such as low pressure steam, industrial waste heat, and solar energy. The energy source, or more importantly energy cost, determines whether emphasis is placed on minimising the membrane area or maximising the energy recovery. These considerations are discussed below.

Several strategies are available for recovering the latent heat of vaporisation in MD. The simplest of these involves the use of hollow fibre shell-and-tube MD modules as were used in this pilot plant study. A simplified flow diagram for this energy recovery concept is shown in figure 8.11. The feed enters the module hot, and exits cool and slightly concentrated. Cold distilled water enters countercurrently and exits warm, having absorbed the latent heat. This warm permeate then partially reheats the recycled cool feed. A conventional heat exchanger is used for this task. The amount of energy recovered depends on the axial temperature drop along the MD module, ΔT_{MDax}, as well as the ΔT across the membrane and across the heat exchanger. The heat recovery factor, Z, can be calculated from

$$Z = \Delta T_{MDax} / (\Delta T_{MD} + \Delta T_{HX}) \qquad\qquad (8.1)$$

which for the example in figure 8.11 is $Z = (80 - 40) / (5 + 5) = 4$. This value indicates that heat passing across the membrane is used four times in this process, making it almost equivalent to 4-effect evaporation. Another way of expressing the energy efficiency is in terms of the fractional energy recovery, Y, where

$$Y = (\Delta T_{MDax} - \Delta T_{MD} - \Delta T_{HX}) / \Delta T_{MDax}$$

$$= 1-1/Z \qquad\qquad (8.2)$$

which for this example is $Y = (40 - 5 - 5) / 40 = 0.75$. This means that of the total energy passing across the membrane, 3/4 is recovered in the heat exchanger. It should be emphasized that not all of the energy passing from feed to permeate is latent heat, and that heat is lost by
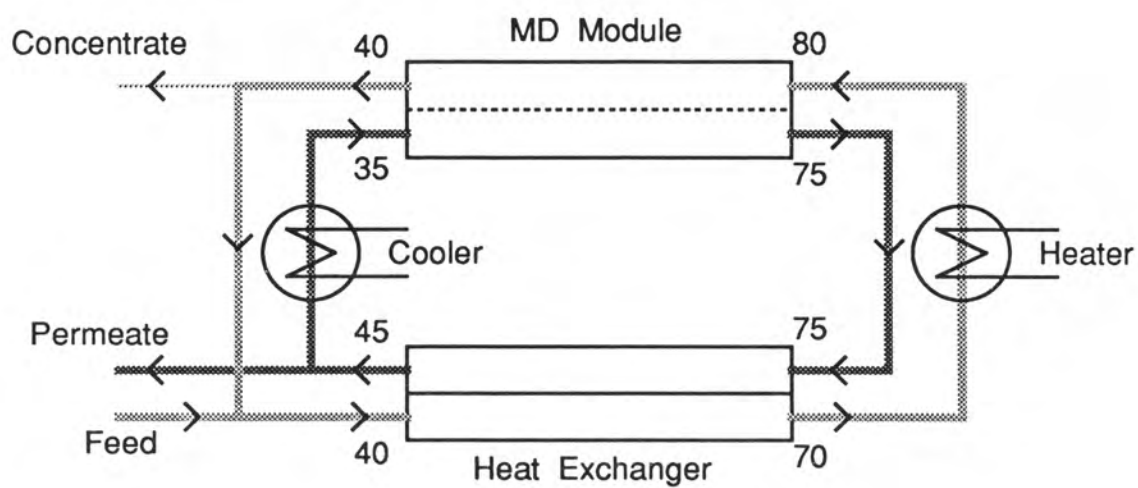
Figure 8.11 : MD with energy recovery.

conduction across the membrane, somewhat reducing the energy efficiency.

The process shown in figure 8.11 can be modified by replacing the heat exchanger with a heat pump. A heat pump uses a compression cycle to transfer heat from a low temperature to a higher temperature. In this context, a heat pump would allow the recovery of all of the latent heat. The energy required to operate the heat pump (usually electrical energy) depends on the temperatures of the streams [8.8] and in this application would be typically 20 to 30 % of the heat being recovered. Thus, with the use of a heat pump, an MD process can be operated with 70% energy recovery even when the feed and permeate exit temperatures do not overlap. The added complexity and cost of including a heat pump in the process precludes the use of heat pumps except perhaps in large scale facilities.

The choice of operating conditions in an MD process depends on the degree of energy recovery required. A computer model was developed to extrapolate from the pilot plant results to a more complete range of operating conditions. Details of the computer model are given in Appendix C. Basically, the model used an iterative approach to solve the transport equations at the feed and permeate temperatures at various positions along the module.

Having estimated the film heat transfer coefficients for module II (chapter 4), the conductivity of the membrane (chapter 4), and the approximate mass transfer characteristics of the membrane (chapter 6), minor adjustments were made to the parameters so that the model results matched the experimental results for module II. The major parameters for the model were h_f = 9000 W/m^{2}K, h_p = 5000 W/m^{2}K, d = 0.041 kg/m^{2}s, a = 2.4 × 10^{-6} kg/m^{2}sPa, b = 0.19 and h_c = 330 W/m^{2}K. (Additional

details are given in Appendix C.) Figure 8.12 shows the model calculations for module II compared with the experimental results. It is important to note that the overall film heat transfer coefficient for this system is h = 3200 W/m^{2}K, which is approaching the identified maximum (see chapter 4) of h = 5000 W/m^{2}K.

It was found that the same mass transfer parameters, with appropriate heat transfer parameters, could also describe the results obtained for module I to within 10%, giving credibility to the theoretical model.

Based on the design of module II, the model was used to predict performances for a range of feed temperatures and flow rates. A sample computer output is shown in Table 8.4.

Table 8.4: Sample Output from the Computer Model Based on Module II.

	Tfi	Tpi	Pf	Pp	
	60	30	120	120	
Flow	Flux	Y	Qloss	Tfo	Tpo
2.0	12.92557	-0.33673	0.302680	45.02186	44.97815
1.6	11.43910	-0.10566	0.304313	43.37712	46.62059
1.2	9.603721	0.126360	0.306303	41.31943	48.67992
0.8	7.277320	0.359712	0.308823	38.66226	51.33770
0.4	4.221101	0.595010	0.312106	35.08879	54.91120

Table 8.4 shows the performance of module II with a feed inlet temperature of 60 °C, a counter-current permeate inlet temperature of 30 °C, and feed and permeate inlet pressures of 120 kPa. For five different feed (and permeate) flow rates [l/min], the model has calculated the
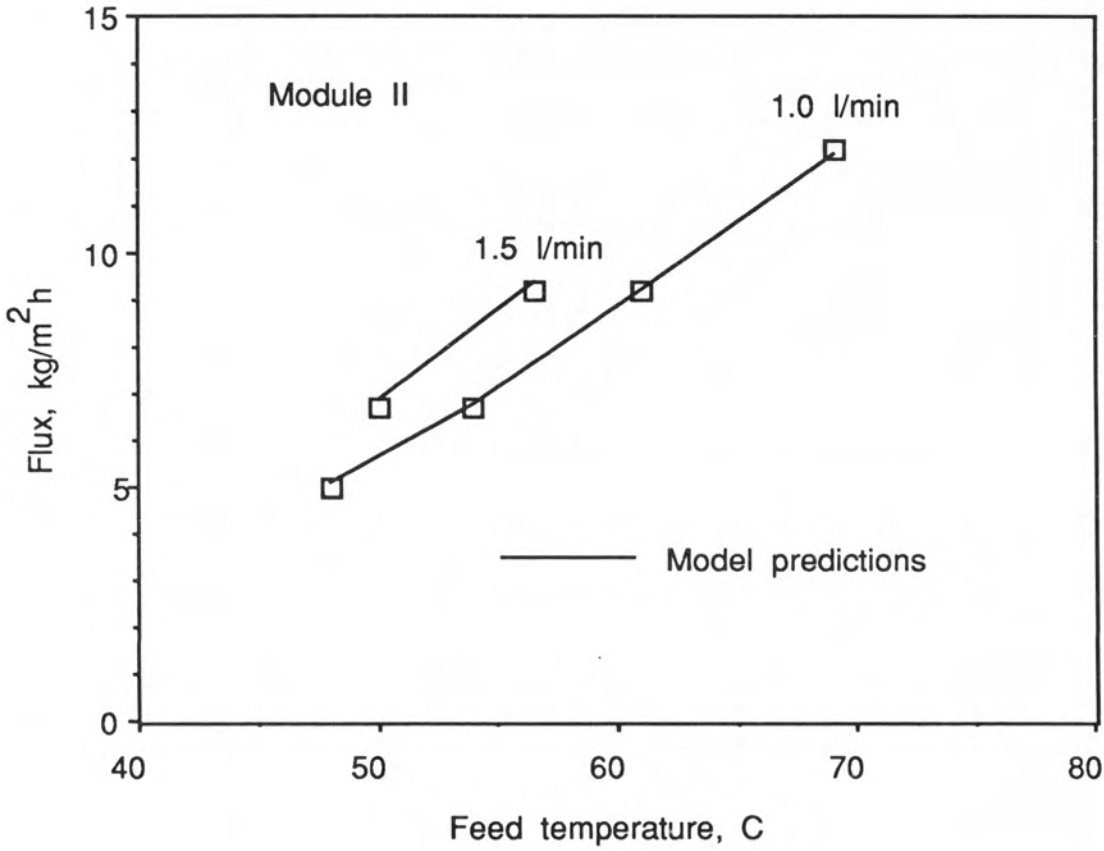
Figure 8.12 : Experimental results and model predictions for Module II.

flux [kg/m^{2}h], the heat recovery factor, Y, the fraction of heat lost by conduction, Q_{loss}, the feed outlet temperature, T_{fo}, and the permeate outlet temperature, T_{po}. It can be seen that higher flow rates give higher fluxes, higher feed outlet temperatures, and lower permeate outlet temperatures, while the heat loss by conduction is almost constant. The heat recovery factor (based on ΔT_{HX} = 5 °C) is negative for the two highest flow rates, indicating that no heat can be recovered under these conditions. Table 8.4 shows that increased heat recovery is at the expense of flux. High heat recovery factors can only be obtained at low flow rates, which in turn result in low fluxes. In an economic optimisation, a trade off must be reached between energy recovery and flux.

Figure 8.13 shows the calculated flux and temperature profiles along the module at the indicated operating conditions. As the feed and permeate flow rates are equal, the bulk temperature difference is constant, however the membrane temperature difference varies. This is due to increased temperature polarisation at higher temperatures, as was discussed in chapter 4. The flux for this case varies by a factor of 2 along the module, indicating effective use of the entire membrane area.

Simulations were conducted to examine the effects of feed temperature and pressure on performance. Figure 8.14 shows the effect of feed temperature on flux for various flow rates. As expected, flux increases with increasing feed temperature. At a permeate inlet temperature of 30 °C, the flux at a feed temperature of 80 °C is approximately double that at 60 °C for all flow rates. Figure 8.15 shows the effect of feed (and permeate) inlet pressure on flux. At a feed temperature of 70 °C, the flux may be increased by around 30% by dropping the inlet pressures from 120 kPa to 60 kPa. This is due to the lowering of the pressure of air
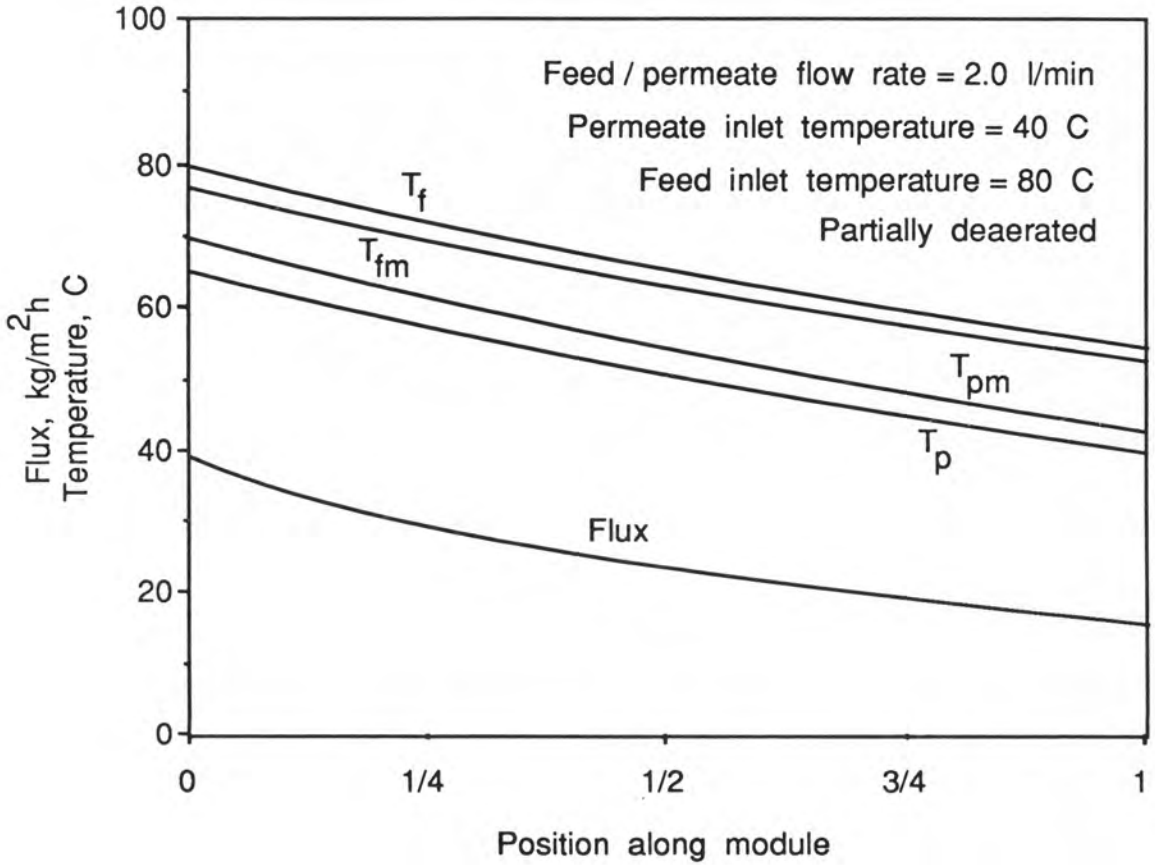
Figure 8.13 : Flux and temperature profiles from simulation of Module II performance.
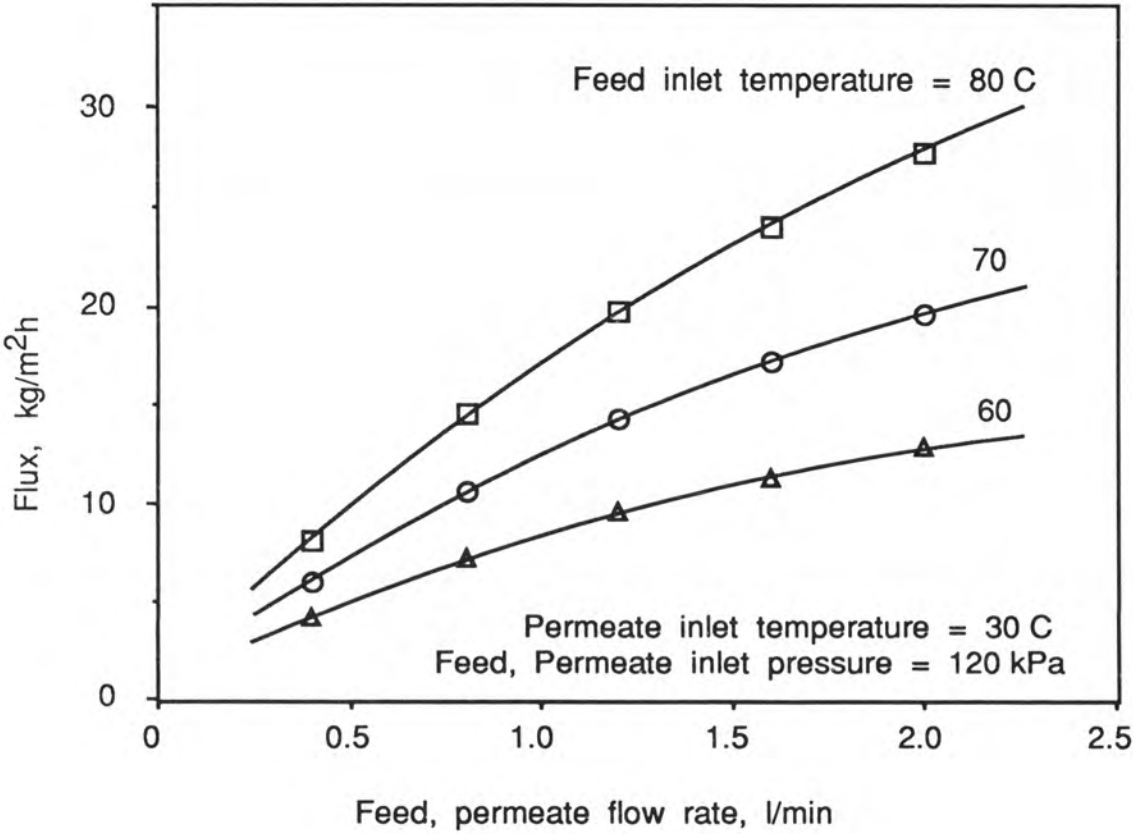
Figure 8.14 : Predicted module II fluxes for various
feed temperatures and flow rates.
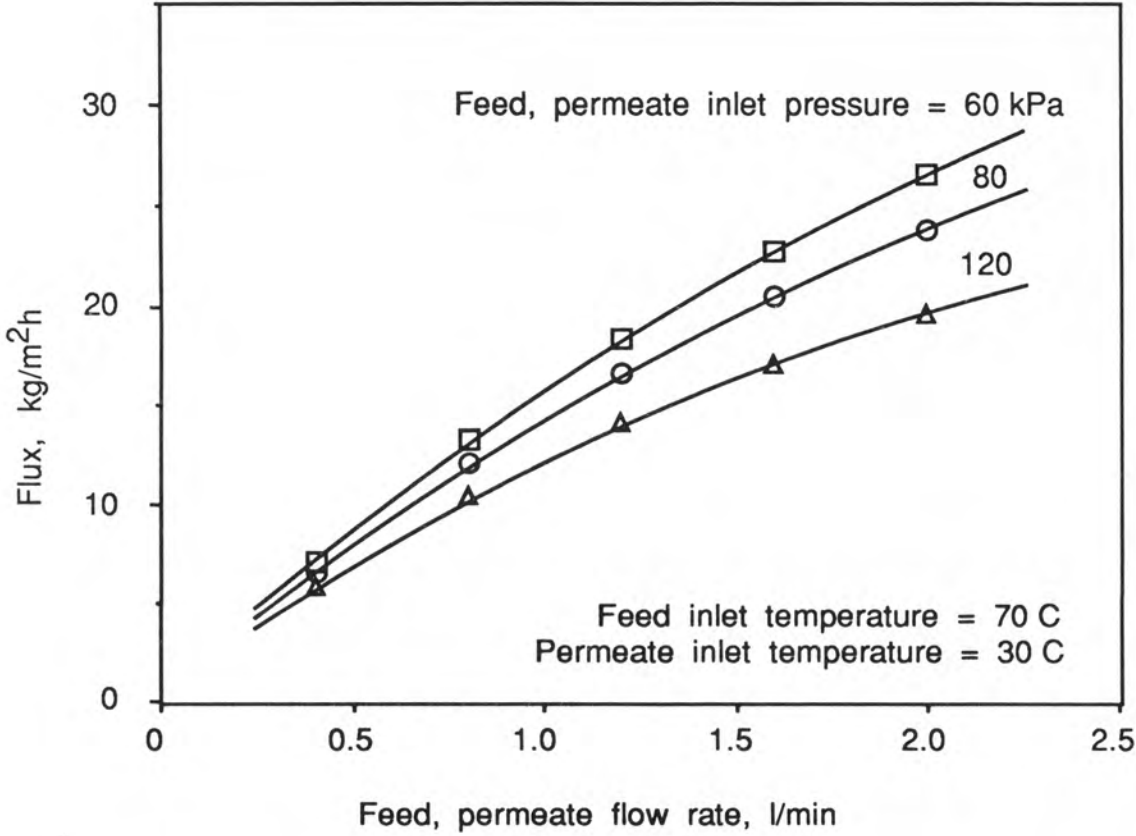
Figure 8.15 : Predicted module II fluxes for various
pressures and flow rates.

within the membrane, as was discussed in chapter 6. Figure 8.16 shows how the heat loss by conduction varies with feed temperature and pressure. The results show that heat loss is reduced by both increasing temperature (chapter 4) and decreasing pressure (chapter 6). Heat loss by conduction can be very important when energy costs are high.

Figure 8.17 gives a graphic display of the trade off between flux and energy recovery. Note that for flow rates above 3 l/min, no energy recovery is possible as the permeate outlet temperature does not exceed the feed outlet temperature. For module II, performance can be changed from high flux to high energy recovery simply by changing the flow rate. This is an important result in favour of using hollow fibre membranes with laminar flow rather than tubular membranes with turbulant flow. This concept is described below.

In chapter 4 it was shown that a tubular membrane must be operated with the highest possible feed and permeate velocities (high turbulence) to maximise the film heat transfer coefficients, as $h \propto v^{0.8}$. The membrane length is then chosen to result in either high axial temperature drop (high energy recovery, long tubes) or high flux. Performance cannot be changed from high flux to high energy recovery by reducing the flow rate without a corresponding loss in film heat transfer coefficient. In the extreme case, flow may even become laminar, resulting in unacceptably low heat transfer. With hollow fibre systems, however, high film heat transfer coefficients are achieved by small cross flow areas, and in fully developed laminar flow, h is independent of flow rate (chapter 4). This is supported by the fact that the performance of module II was modelled over the experimental range of conditions with constant feed and permeate film heat transfer coefficients of 9000 and 5000 $W/m^2 K$ respectively. Thus for hollow fibre laminar systems, flow rate is a
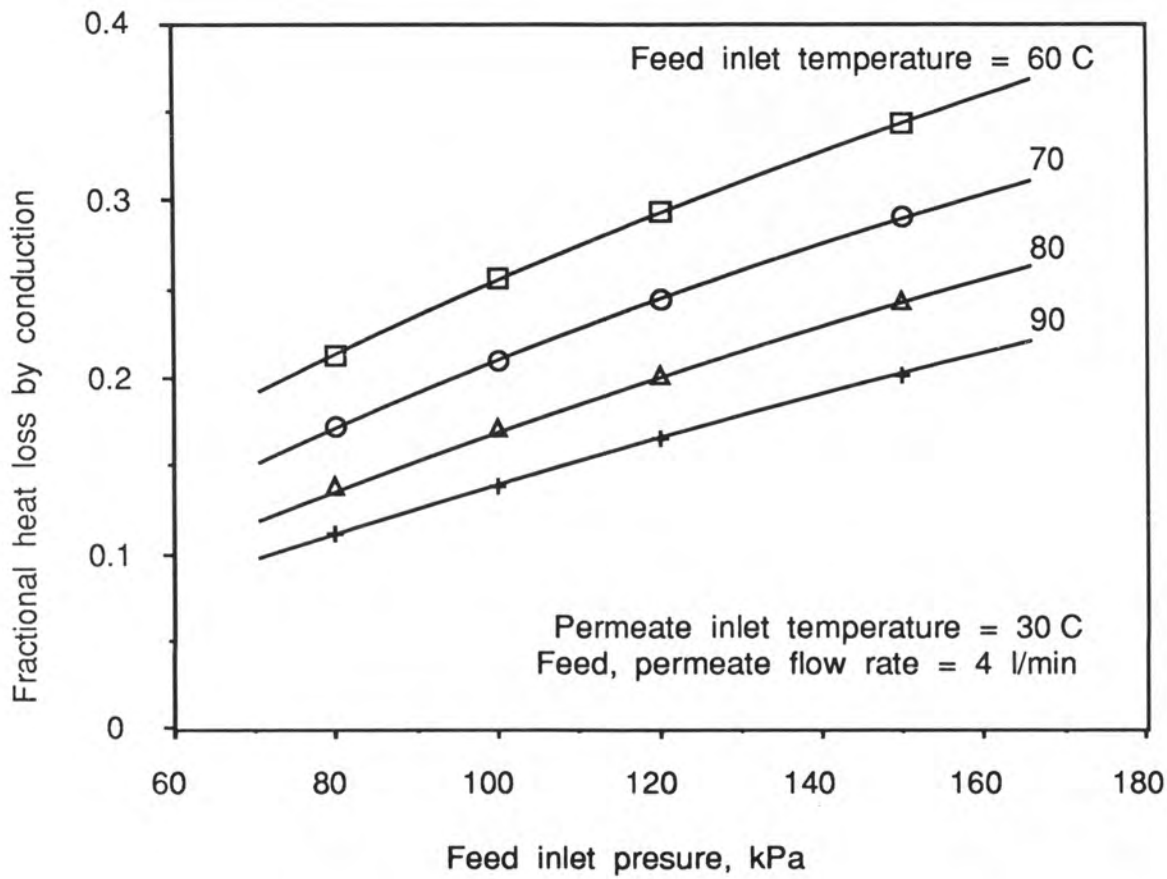
Figure 8.16 : Effect of feed temperature and pressure
on fractional heat loss by conduction.
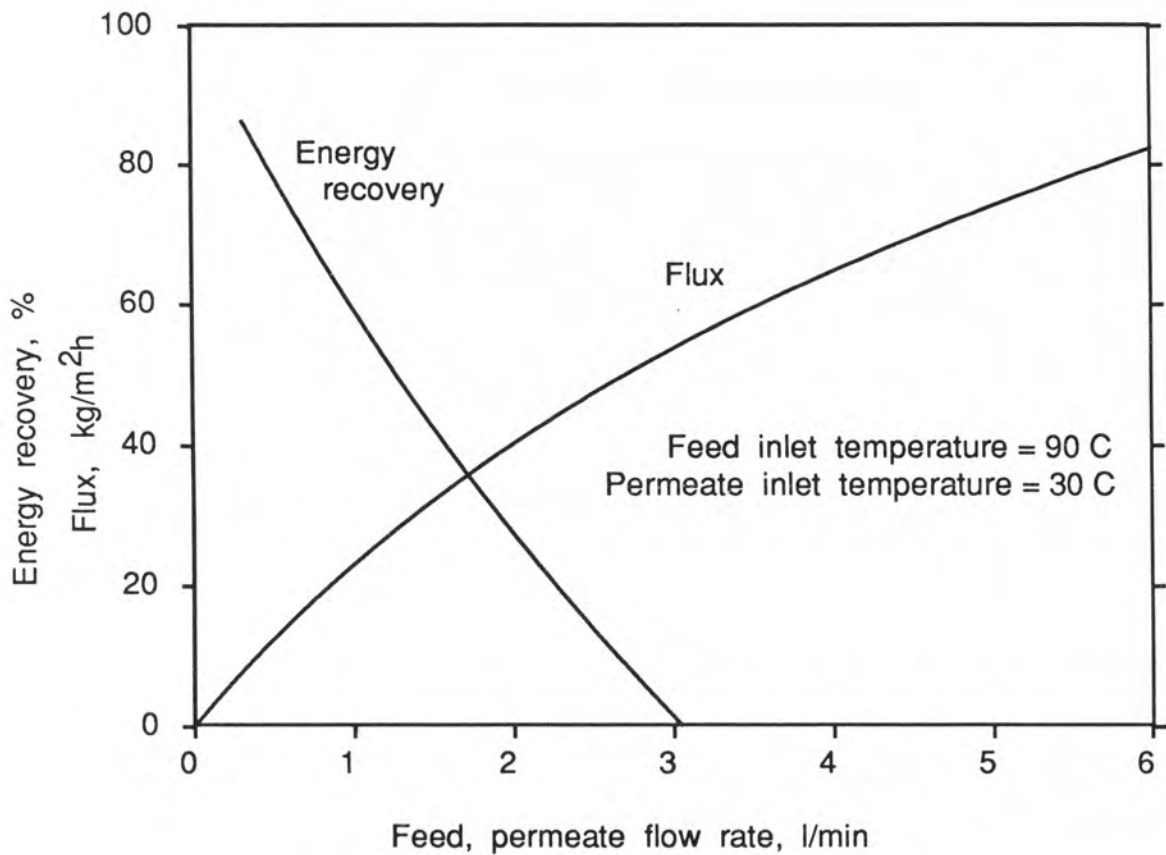
Figure 8.17 : Flux and energy recovery as a function of feed, permeate flow rate.

process variable which can be used to alter the balance between flux and energy recovery, for example to compensate for changes in energy costs and feed temperatures.

An economic discussion of MD processes is very much dependent on the energy source and scale of operation. For example, a small scale facility (say 50 kg/h distilled water) may be operated using the waste heat from a diesel powered electricity generator, thus having virtually no energy cost. In such a system, no energy recovery is required and the system is optimised when the membrane area is minimised. However for large scale production (say 5000 kg/hr), the energy cost may be such that the major plant cost is the heat exchange equipment for energy recovery. In general an MD module optimisation is required for each individual application.

As a guide line for cost estimates, typical extrapolated results for module II performance are given in Table 8.5. For any given application,

Table 8.5: Design Fluxes for Hollow Fibre MD Modules.

Flux, kg/m^{2}h	Feed Temperature	
	90°C	70°C
Design flux with no energy recovery	80-90	20-30
Design flux with 60% energy recovery	20-30	5-10
Design membrane module purchase cost - $200 - $400/m^2		

the appropriate flux in Table 8.5 can be used to estimate the membrane area and cost, enabling an approximate cost analysis for the process.

Note that if energy is recovered by means of a heat pump, the design
flux is that listed for no energy recovery.

A preliminary cost analysis has also been done on a smaller scale plant
utilising solar energy [8.9]. For a 50 kg/h plant, the capital cost
would be $10,000 - $15,000, with a production cost of $10 to $15/m^3 (or
1 to 1.5 cent/litre). The solar-driven MD unit production cost may be
somewhat more costly than alternative technologies such as reverse
osmosis, however the equipment would be virtually independent of
electrical power supply and the degree of feed pretreatment would be
minimal. Thus the system could be attractive for arid-zone rural areas,
where only brackish water is available. The process has shown sufficient
merit to justify continued study.

8.4   CONTINUING PILOT PLANT STUDY

This   pilot   plant   study   culminated in recommendations for the
construction of an improved pilot plant to allow the study of solar
powered MD. The major proposed modifications are discussed below.

Heating/cooling

The heating and cooling water facilities for the pilot plant were
sufficient to produce 5 kg/h of permeate. This is reasonable for a
laboratory scale pilot plant. This pilot plant used a plate and frame
heat exchanger to heat the feed, cool the permeate, and recover latent
heat. However under most operating conditions, the amount of latent heat
recovered was negligible. While the concept of recovering latent heat is
valid in an industrial context, it proved to be unnecessary and
undesireable in the pilot plant study. It is proposed that the next

pilot plant use submerged coils in the heating and cooling water baths
to heat the feed and cool the permeate, and no attempt be made to
recover latent heat. Using ethylene glycol in the cooling bath at say 5
°C, and a suitable oil in the heating bath at say 110 °C, adequate heat
transfer rates should be obtained with a reasonable heat transfer area.

MD modules

For the study of solar powered MD, the most likely operating conditions
are medium feed temperatures (~70 °C) and high heat recovery, or low
feed/permeate approach temperatures. The results in section 8.3 suggest
expected fluxes of 5 - 20 kg/m^{2}h. Based on a permeate production rate of
5 kg/h (latent heat requirement of 3.3 kW), this gives a membrane area
of 0.25 m^2. It is proposed that a module similar to module II be
constructed, however with greater emphasis on reduced shell side voidage
(note that the fibres must be sufficiently splayed at the module ends to
allow fluid access to the entire tube bundle). In commercial modules it
is favourable to use long fibres, however in parametric studies it is
favourable to use short fibres, allowing a wider range of conditions to
be studied. The fibre length of 0.17 m used in module II seems
reasonable for future work. Both modules used in this study contained
0.2 μm polypropylene fibres with an inside diameter of 0.3 mm, and an
outside diameter of 0.6 mm. The study of heat transfer in chapter 4
suggested that these fibre dimensions result in good heat transfer. It
is proposed that the same membranes be used in future modules, however
that experiments also be conducted with fibres of other dimensions. A
tubular membrane apparatus has already been constructed for examining
various tubular membranes and shell side voidages, the details of which
were given in chapter 3.

Pumping

The virtues of deaerated MD were expounded in chapter 6, and were
supported in this pilot plant study. The simplest way to achieve partial
deaeration is to operate with suction of the feed and permeate through
the MD module. It is proposed that the next pilot plant allows the
option of operating with the feed and permeate under either pressure or
suction. This can be achieved through appropriate plumbing, and by
placing the pumps on a lower level to the module, thus satisfying
suction head requirements. The pumps used in this study should be
replaced by stainless steel pumps designed for high suction.

Plumbing

This pilot plant used PVC pipes for the bulk of the plumbing. This
choice was appropriate as the shell of module I was made of PVC. The
maximum operating temperature for PVC piping at low pressures is ~70 °C.
It is proposed that the next pilot plant be constructed using insulated
stainless steel tubing. At flow rates of around 2 l/min, an appropriate
tube diameter is 10 mm (3/8 inch). For convenience, the tubes entering
and leaving the module should be flexible, allowing easy replacement of
modules. The feed and permeate reservoirs should also be made of
stainless steel, with graduated sight glasses to monitor the levels. All
valves and fittings should be stainless steel.

Process monitoring

The temperature monitoring equipment for this study was more than
adequate, and may be directly incorporated into the next pilot plant.
The same applies to the rotameters for measuring feed and permeate flow

rates. The pressure gauges, however, must cover the range -100 to 200 kPa gauge pressure.

8.5 CONCLUSIONS

This pilot plant study has confirmed many of the conclusions made from the laboratory studies reported in chapters 4, 6 and 7, such as the benefits of high temperature operation and deaeration. More importantly, though, it has given some important information for transforming the laboratory experiments into an industrial process. The major conclusions from this study are listed below.

1: MD is a suitable process for both the dewatering of red water and the desalination of salt water. In both applications, there may be a need for periodic cleaning and drying of the membranes to combat wetting.

2: The sizing of MD equipment is not strongly dependent on the feedstock. Membrane area requirements for most applications can be estimated from fluxes achieved with distilled water feed.

3: Shell side voidage is an important factor in heat transfer and hence flux in hollow fibre MD modules. A reduction in the shell side voidage from 0.6 for module I to 0.5 for module II resulted in a significant flux increase.

4: MD modules based on small diameter fibres with laminar flow of the feed and permeate can deliver both high fluxes and high energy recoveries. With a feed temperature of 90 °C, hollow fibre modules can deliver fluxes of up to 90 kg/m^{2}h with no energy recovery, or 30 kg/m^{2}h

with 60 % energy recovery.

5: For hollow fibre MD systems, the feed/permeate flow rate is a process variable that can be used to compensate for variations in energy supply and feed temperture. This is not the case for tubular systems in turbulent flow.

8.6 ACKNOWLEDGEMENT

I would like to thank Mr. S.P. Vaughan for his assistance with the construction of the pilot plant, and its operation during the study of module I.

8.7 REFERENCES

[8.1] Gore, D.W., "Gore-Tex Membrane Distillation", Proc. 10th Ann. Conv. Water Supply Improvement Assoc., Honolulu, July 25-29, 1982.

[8.2] Schneider, K., van Gassel, T.S., "Membrandestillation", Chem.Ing. Tech., 56 (1984) 514-521.

[8.3] Andersson, S.-I., Kjellander, N., and Rodesjö, B., "Design and Field Tests of a New Membrane Distillation Desalination Process", Desalination, 56 (1985) 345-354.

[8.4] Schofield, R.W., "Membrane Distillation", B.E. Thesis (1984), School of Chem Eng and Ind Chem, University of NSW, Australia.

[8.5]   Drioli,   E.,   Wu,   Y.,   and Calabro, V., "Membrane Distillation in

the Treatment of Aqueous Solutions",   J.   Mem.   Sci.,   33   (1987)

277- 284.

[8.6]   Franken,   A.C.M.,   "Membrane   Distillation - A New Approach Using

Composite Membranes", Ph.D. Thesis (1988), University of   Twente,

The Netherlands.

[8.7]   Weast, R.C. (ed.), "Handbook of Chemistry and Physics", 57th ed.,

CRC Press, Cleveland, Ohio.

[8.8]   Smith, J.M.,   and van Ness,   H.C.,   "Introduction to Chemical

Engineering Thermodynamics", 3rd ed., McGraw-Hill, 1975.

[8.9]   Fane,   A.G.,   Private   Communication   -   Report   on Rural Credits

(Australia) Project, 1986.

Chapter 9

Conclusions
and
Recommendations

CHAPTER 9: CONCLUSIONS AND RECOMMENDATIONS

9.1 CONCLUSIONS

At the time of commencement of this study, a need was seen for a detailed fundamental study of heat and mass transfer in MD. This study has resulted in theory capable of describing the performance of direct contact MD systems with non-volatile solutes over the full range of expected operating conditions. All major facets of this theory have been supported with experimental results. The major conclusions from this study are summarised below, with reference to the appropriate chapters.

The major conclusion from chapter 4 is that the overall film heat transfer coefficient, h, is a crucial parameter controlling MD performance. The components of h, coming from the feed and permeate film heat transfer coefficients, can be maximised through module design. The benefits of high turbulence and small flow cross-sections were demonstrated, with tubular and hollow fibre membranes showing the most potential. Hollow fibre membranes with laminar flow have the advantage that the heat transfer coefficient is essentially independent of flow rate. For shell and tube modules, shell side film heat transfer coefficients were shown to increase markedly with decreasing shell side voidage. A design target of h $= 2000$ W/m^{2}K was shown to be reasonable, while a realistic maximum was identified as h $= 5000$ W/m^{2}K.

Heat loss by conduction across the membrane was shown to be an important consideration, consuming between 10 and 40 % of the total heat input for the system. The conduction heat transfer coefficient, h_c, can be calculated from the polymer and gas conductivities using equation (4.5). The fractional heat loss by conduction was found to decrease with

increasing operating temperature.

In chapter 5, gas permeation in the Knudsen/Poiseuille transition region was successfully described by the semi-empirical mass transfer equation $J = a\wp^b \Delta P$. This equation was tested for a range of membranes and gases, and found to be an effective alternative to the more complex models in the gas permeation literature. The permeation parameter **a** is the membrane mass transfer constant $(J/\Delta P)$ measured at some reference pressure, $\wp$ is the dimensionless pressure, and **b** indicates the extent to which Poiseiulle flow contributes to the flux. The results from permeation experiments with various gases were used to estimate the permeation parameters for water vapour, allowing prediction of MD fluxes under totally deaerated conditions

In chapter 6, this gas permeation model was extended to account for the presence of air within MD membranes by including a molecular diffusion parameter, d. This lead to the development of a combined heat and mass transfer theory capable of describing MD fluxes over the normal range of operating temperatures and for various levels of deaeration. The model was tested experimentally with two different membranes and different film heat transfer coefficients. The major parameters influencing performance were found to be the film heat transfer coefficient, h, and the molecular diffusion parameter, d. The gas permeation parameters, **a** and **b**, became important at low partial pressures of air.

The combined heat and mass transfer model revealed that the modest experimental flux increases observed with deaeration were the result of greatly increased membrane permeability, but worsened temperature polarisation. A significant flux increase with deaeration can only be achieved with very high film heat transfer coefficients. Deaeration

resulted not only in increased flux, but also in a drop in the fraction
of heat lost by conduction across the membrane. Heat losses of less than
10% were calculated for deaerated systems. It was also seen that if
deaeration is achieved by reducing the feed and permeate pressures, this
may reduce the tendency for membrane wetting. Deaeration was found to
increase the membrane permeability to the extent that the process is
film heat transfer limited. Thus when the film heat transfer coefficient
is maximised, so too is the flux. This means that there is little to be
gained by developing membranes specifically for MD, and attention would
be better focussed on improving module heat transfer. A realistic
maximum flux for MD was identified as 200 kg/m^{2}h.

In chapter 7 it was found that the presence of solute in the feed at low
to moderate concentrations does not have a large effect on flux. Even at
concentrations of 25 to 30 wt%, the flux reduction is less than 50%. For
the turbulent flow experimental system, the major cause of flux
reduction for salt solutions was found to be vapour pressure reduction.
It was also found that increased viscosity has a significant effect
through increased boundary layer thickness (decreased film heat transfer
coefficient). For sugar solutions, flux reduction was explained by
viscosity effects alone, with vapour pressure reduction being
negligible. Other transport properties were found to play only a minor
role in flux reduction. Laminar flow systems were identified as having
minimal flux reduction by solute, as they are not sensitive to the
viscosity effects.

Chapter 8 detailed a pilot plant study based on hollow fibre MD modules,
with external heat recovery from the permeate to the incoming feed. This
study confirmed many of the conclusions made from the laboratory studies
reported in chapters 4, 6 and 7, such as the benefits of high

temperature operation and deaeration. MD was shown to be a suitable process for both the dewatering of an effluent, "red water", and the desalination of salt water. In both applications, the need was seen for periodic cleaning and drying of the membranes. Fluxes for both applications were close to those observed for a pure water feed. Thus the sizing of MD equipment is not strongly dependent on the feedstock.

Important conclusions were drawn from the pilot plant study regarding system performance. Shell side voidage was confirmed as being an important factor in heat transfer and hence flux in hollow fibre MD modules. A reduction in the shell side voidage from 0.6 to 0.5 was shown to increase flux significantly. It was found that MD modules based on small diameter fibres with laminar flow of the feed and permeate can deliver high fluxes at high flow rates, and high energy recoveries at low flow rates. With a feed temperature of 90 °C, hollow fibre modules can deliver fluxes of up to 90 kg/m^2h with no energy recovery, or 30 kg/m^2h with 60 % energy recovery. For hollow fibre MD systems, the feed/permeate flow rate is a process variable that can be used to compensate for variations in energy supply and feed temperture. This is not the case for tubular systems in turbulent flow, where a reduction in flow rate leads to a substantial drop in film heat transfer.

The conclusions above suggested that the best system for direct contact MD is a hollow fibre system with laminar flow of the feed and permeate, deaerated by reducing the feed and permeate pressures. This system maximises all of the desireable features of direct contact MD, while minimising the undesireable features. The deaeration results in high membrane permeabilities, making the system heat transfer limited. As closely packed fibres can yield overall film heat transfer coefficients close to the identified maximum of h=5000 W/m^2K, the system

is close to optimum. Deaeration can reduce the heat loss by conduction to less than 10%, while reducng the tendency for membrane wetting. Flux reduction caused by the presence of solute in the feed is minimised, as only vapour pressure reduction (which cannot be avoided) has an effect. Feed and permeate flow rates can be varied without decreasing the near optimum heat transfer coefficients, thus providing flexibility of operation. Latent heat can be recovered if desired through external heat exchange, or high fluxes can be obtained by increasing flow rates.

9.2 RECOMMENDATIONS

The main recommendation from this study is that experimental and pilot plant studies continue, in an effort to optimise hollow fibre module design. The parameters that must be considered are fibre inside and outside diameter, fibre length and shell side voidage. Modules must be designed that can house a large number of closely packed fibres, while providing even flow distribution on the shell side.

Continued work is also recommended in the following areas:

Applications

Many potential applications have been identified for MD. For MD to be truly competitive, however, an inexpensive source of thermal energy must be available. Hence applications must be found where the need for pure water (or concentration of solutions) coincides with an available energy source. For example, the need for potable water in arid areas can be coupled with solar energy.

Wetting and Fouling

The occurrence of membrane wetting in MD has not been studied in detail. While the cost of periodic cleaning and drying of MD membranes would not be prohibitive, an understanding of the wetting phenomenon may reduce the frequency of this procedure, making the process more attractive. Appropriate membrane modifications may also expand the range of solutions that can be processed by MD. The effects of long term operation and membrane fouling must also be studied for the various proposed applications.

Gas Permeation

The model $J = a \wp^b \Delta P$ developed in chapter 5 has shown merit as a gas permeation equation for the Knudsen/Poiseuille transition region. Work in this area could be extended to investigate other porous media, and a wider range of gases. Also the fact that materials with the same permeability can have different measured values of b may provide some information on pore size distribution and pore shape. Thus the analysis of gas permeation results with the model may be a useful technique for characterising porous materials.

Appendices

APPENDIX A. PHOTOGRAPHS
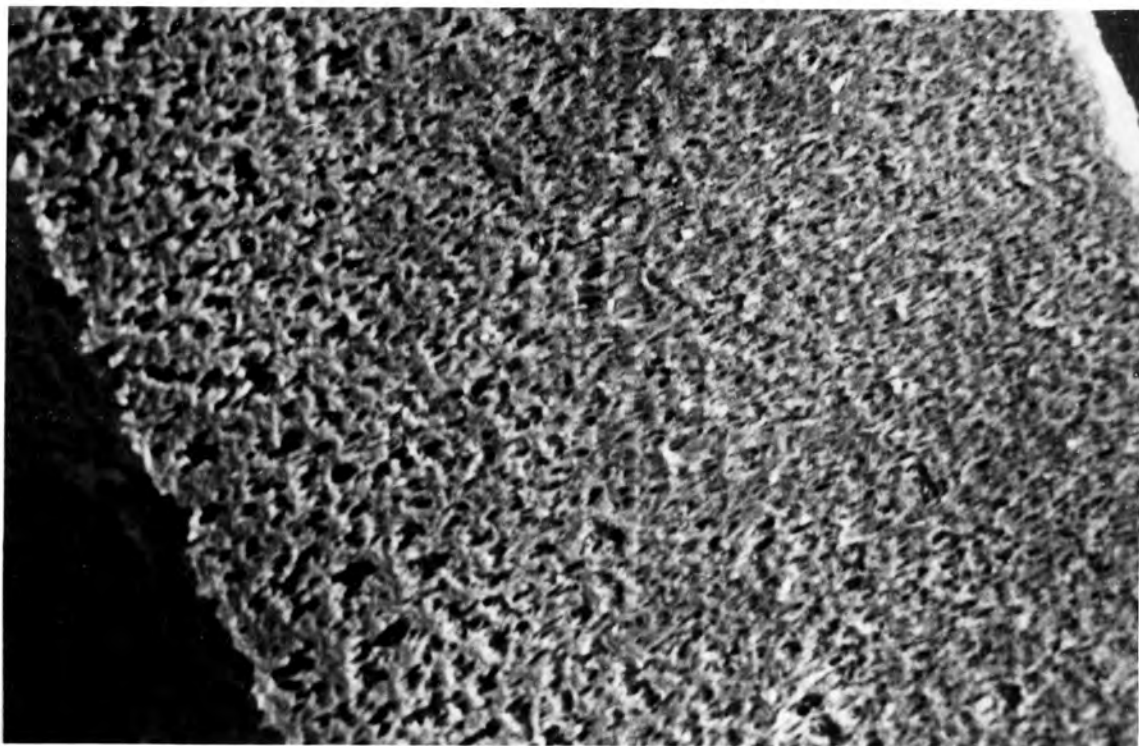
Figure A.1: Cross section of 0.2 μm polypropylene membrane
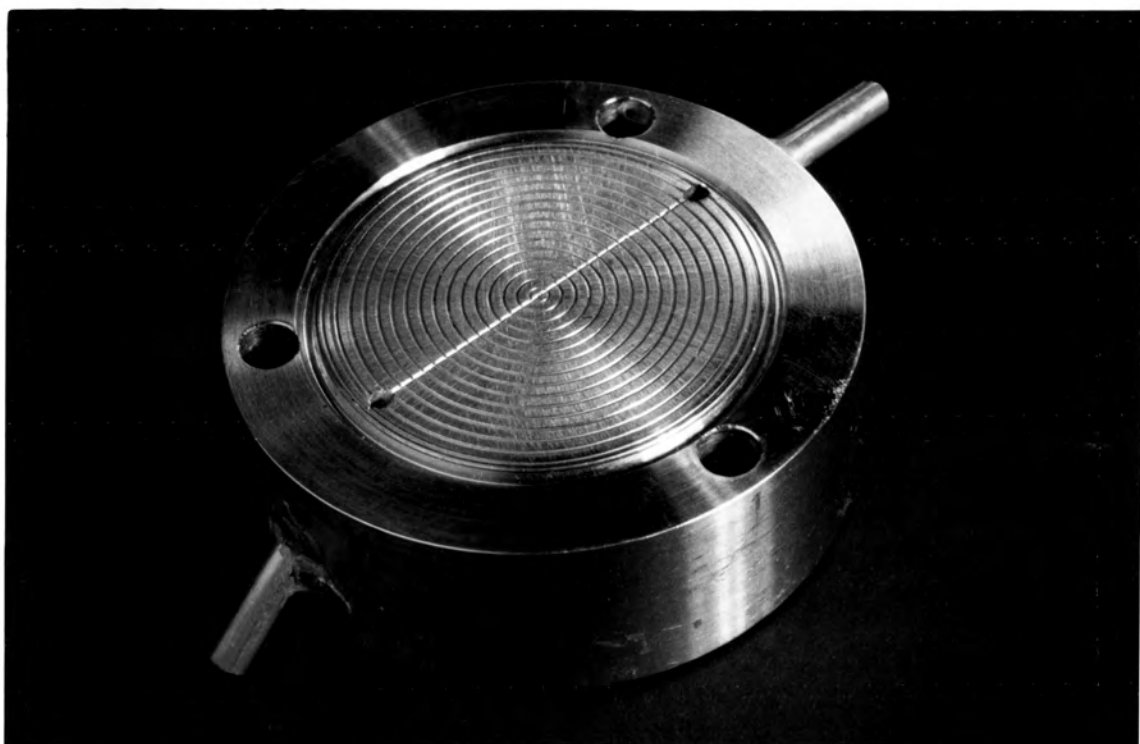
Figure A.2: Jacketted sheet membrane cell
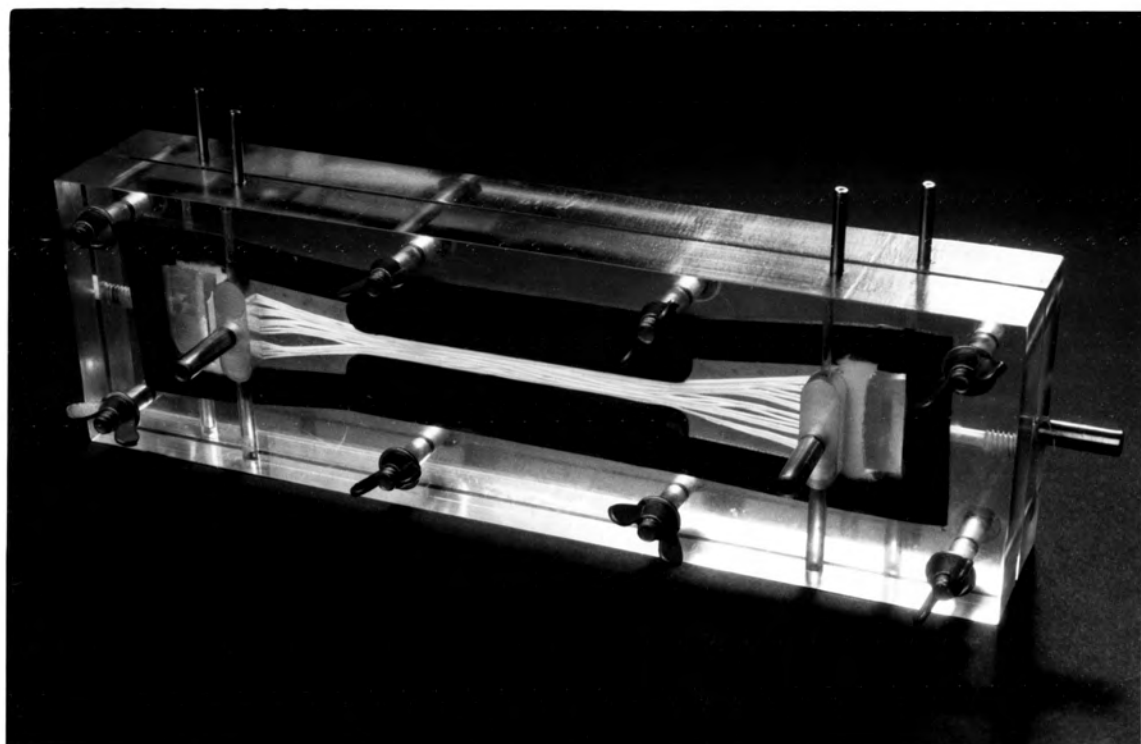
Figure A.3: Laboratory scale hollow fibre membrane cell
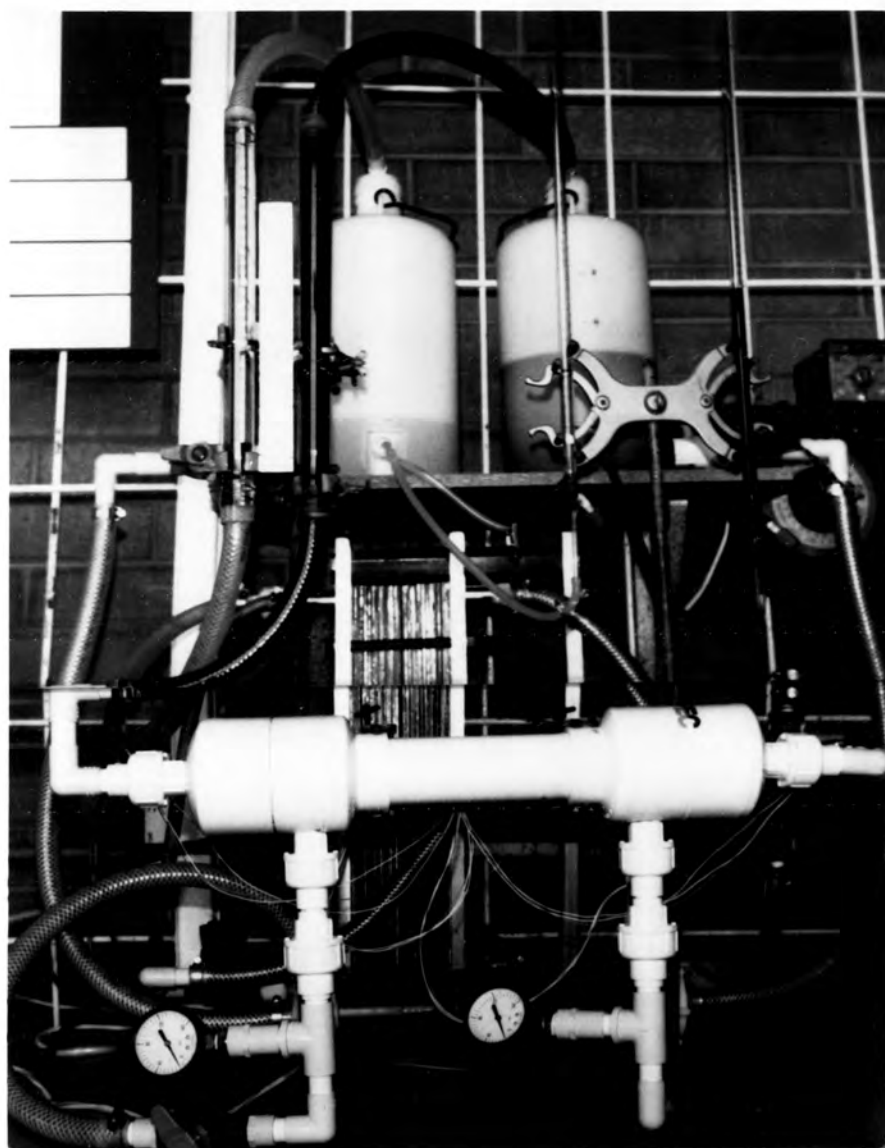
Figure A.4: Pilot Plant
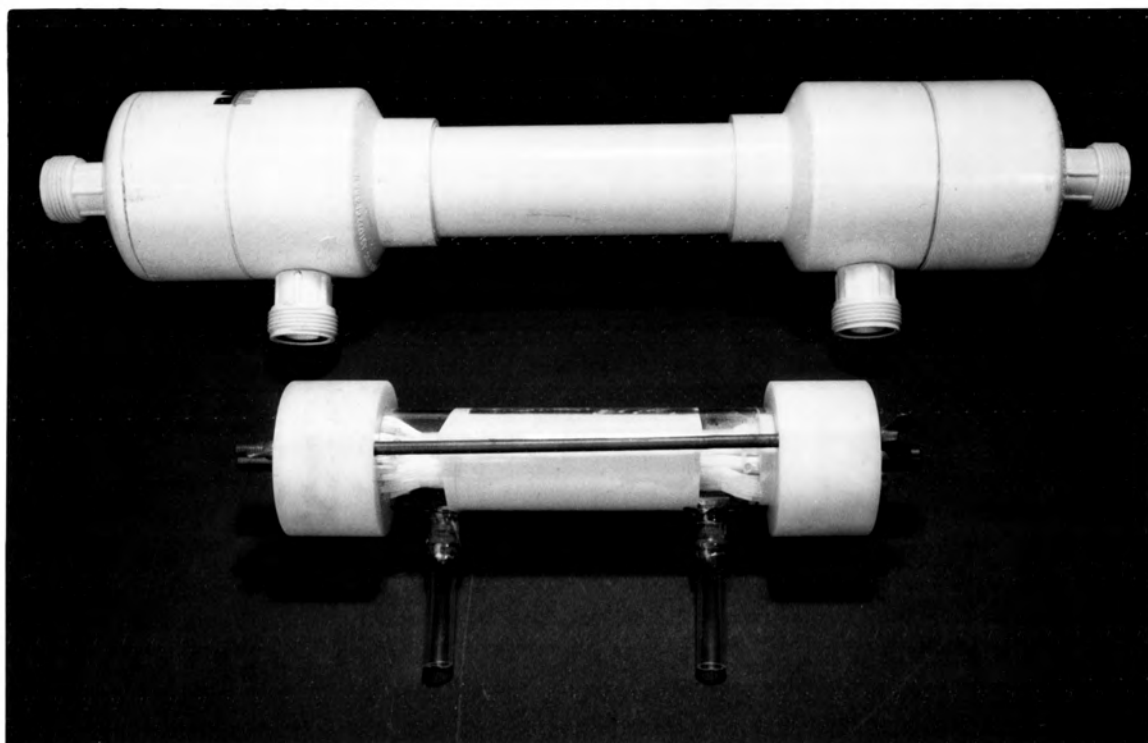
Figure A.5: Pilot plant hollow fibre MD modules I (top) and II (bottom)

APPENDIX B.   TERMINOLOGY FOR MEMBRANE DISTILLATION

At the "Workshop on Membrane Distillation" in Rome, Italy, May 1986, a committee (which included the author of this thesis) was formed for the purpose of standardising concepts and nomenclature in the field of Membrane Distillation. The report from this committee, prepared by A.C.M. Franken and S. Ripperger, is reproduced here without alteration. Wherever possible, the guidelines of this report have been adhered to in this thesis.

1. Introduction

One of the subjects of the 'Round Table' at the 'Workshop on Membrane Distillation' in Rome on 5 May 1986 was nomenclature. The best example for the need of a more uniform language is the name of the process itself. In Rome the following names were used by the authors present: membrane distillation, Trans Membrane Distillation, thermo-pervaporation, pervaporation and membrane evaporation.

At this workshop a committee was formed with the task of preparing a terminology for membrane distillation. The committee consists of the following members:

V. Calabro	Universita della Calabria	Calabria	I
A.C.M. Franken	Twente University	Enschede	NL
S. Kimura	University of Tokyo	Tokyo	J
S. Ripperger	Enka (Membrana)	Wuppertal	D
G. Sarti	Universita di Bologna	Bologna	I
R. Schofield	Univ. of New South Wales	Kensington	AUS

In this document terms, definitions and symbols, which are used in the field of membrane distillation, are defined. The basis for this document is formed by the terminology for pressure driven membrane operations [1]; wherever this is relevant the terms in this document are defined in the same way.

2. Name of the membrane operation

The most suitable name for this operation is **membrane distillation.** This name has the advantage that it is already used by most authors, that it has no commercial ties with a company and that it cannot be confused with other membrane processes.

For the same reasons as mentioned above, the names Trans Membrane Distillation (the commercial name for the Enka process), pervaporation and thermo-pervaporation (already used for other membrane operations [2]) should not be used. Introducing a new name, like membrane evaporation, has the disadvantage that both author and reader will have adjustment problems, that may result in an even greater confusion of tongues.

The name pervaporation is often used by Japanese authors for two different processes: the process of membrane distillation and the process of pervaporation. In our opinion an essential difference exists between these processes.

According to our definition (see chapter 3a), membrane distillation is a process in which the membrane itself has **no influence** on the vapour-liquid-equilibrium of the liquids to be separated. On the other hand, pervaporation is a process in which liquid diffuses through a membrane and evaporates at the permeate side of the membrane. The separation characteristics of the pervaporation process are determined by sorption into and diffusion through the membrane.

3. Description of the membrane operation

a. Characteristics of membrane distillation

The name 'membrane distillation' should be applied for membrane operations having the following characteristics:

- the membrane should be **porous**
- the membrane should **not be wetted** by the process liquids
- **no capillary condensation** should take place inside the pores of the membrane
- only **vapour** should be transported through the pores of the porous membrane
- the membrane must not alter the **vapour-liquid equilibrium** of the different components in the process liquids
- at least **one side** of the membrane should be in **direct contact** with the process liquid
- for each component the driving force of this membrane operation is a **partial pressure gradient** in the vapour phase.

b. Different embodiments of membrane distillation

Many different embodiments of membrane distillation can be found in literature. For instance, Enka uses a membrane operation in which the liquid on both sides of the membrane is in direct contact with the membrane (3), whereas on the other hand the Swedish National Development Company uses a system in which the vapour is condensed against a cooling-plate (4).

For the different embodiments of membrane distillation the following terms are defined:

- **direct-contact membrane distillation** for a system in which the liquid on both sides of the membrane is in **direct contact** with the

membrane and in which the liquid on the downstream side is used as the **condensing medium** (figure 1).

$T_{F,IN}$ $T_{P,OUT}$

MEMBRANE

$T_{F,OUT}$ $T_{P,IN}$
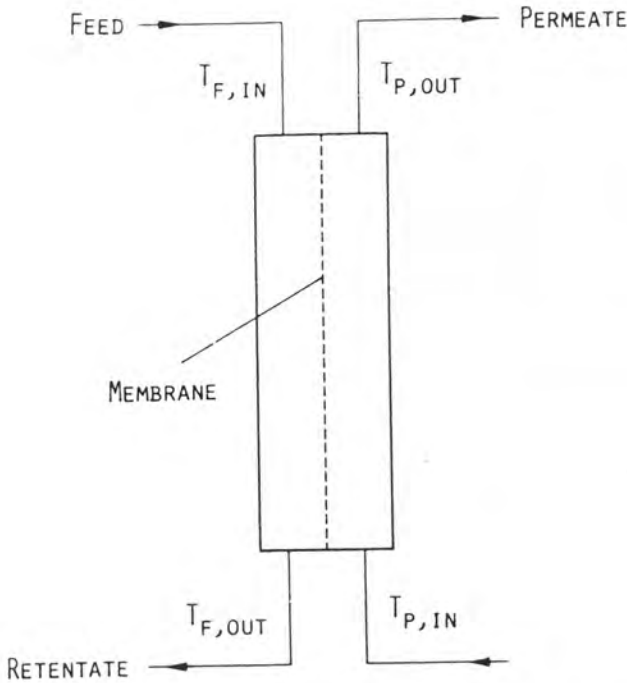
Figure 1: Direct-contact membrane distillation

gas-gap membrane distillation for a system in which the vapour on the downstream side is condensed against a **cooling surface** and in which the condensed liquid on the downstream side **does not have to be** in contact with the membrane (figure 2). In this configuration the condensation of the permeate takes place **inside** the module.

AIR GAP

MEMBRANE

HEATEXCHANGING SURFACE

FEED

COOLING FLUID
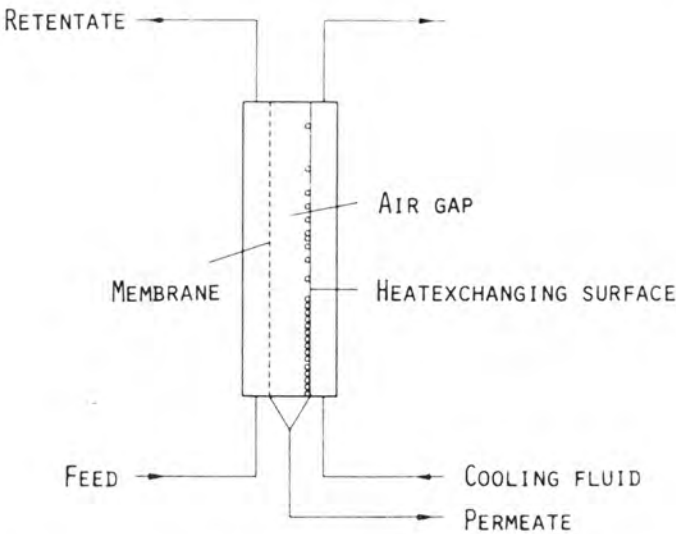
PERMEATE

Figure 2: Gas-gap membrane distillation

- <u>low pressure membrane distillation:</u> in this system a low **pressure** is applied **downstream** and the condensation of the permeate takes place **outside** the module. An other term that can be used in this case is: 'vacuum membrane distillation', but this term is in fact more limiting than low pressure membrane distillation.
- <u>sweeping gas membrane distillation:</u> in this system a **sweeping gas** (e.g. nitrogen) is applied **downstream** and the condensation of the permeate takes place **outside** the module.

Note: If the term 'membrane distillation' is used without any further specification, then this term applies to the 'direct-contact'-system. To avoid complications, it is better to use the full term 'direct-contact membrane distillation'.

Example: the system of Enka should be called 'direct-contact membrane distillation' and the system of the Swedish National Development Company should be called 'gas-gap membrane distillation'.

4. Membrane characteristics

The membranes, used in membrane distillation, should be characterized by the following membrane (performance) parameters:

a. (polymer) material

b. thickness of the membrane

c. porosity of the membrane

d. nominal pore size

e. liquid-entry-pressure of water

a. (polymer) material

The material of which the membrane is made is the most important parameter. At this moment membranes for membrane distillation are all made of polymers, but as one should not exclude other type of materials the term polymer is placed between brackets.

b. thickness of the membrane

This parameter is of importance because it gives information on both the mechanical strength of the membrane and the fluxes to be expected.

c. porosity of the membrane

The porosity of the membrane is defined as the volume of the pores devided by the total volume of the membrane; the symbol for the porosity is ε. A method for the determination of the porosity of (hydrophobic) membranes is suggested in appendix 1.

d. nominal pore size

Nominal pore size is important as it can lead to a first approximation of the fluxes to be expected. 'Nominal' pore size is a blanket term incompassing pore sizes estimated from bubble-point tests, gas permeation experiments, or any other convenient technique, and is usually quoted by the membrane manu-facturer. Despite the approximate nature of nominal pore size, it conveys useful information, which can be used to make an approximate calculation of the fluxes to be expected.

e. liquid-entry-pressure of water

The liquid-entry-pressure of water (sometimes faulty called 'wetting pres-sure') is the pressure (Pa) that must be applied onto pure water before it penetrates into a non-wetted (dry) membrane; the symbol for the liquid-entry-pressure of water is LEP_w. A method for the determination of LEP_w of hydro-phobic membranes is suggested in appendix 1.

These five characteristics are suggested, because they give a visual (a,b) and mechanical (a,b,c) picture of the membrane, while indicating the suitabi-lity for membrane distillation (e) and the fluxes to be expected (b,c,d).

As additional information the following membrane characteristics can be given:
    f. IPA bubble point
    g. maximum pore size
    h. pore size distribution
    i. pore size morphology
    j. temperature stability
    k. chemical resistance

f. IPA bubble point

The IPA (isopropylalcohol) bubble point can be measured according to a standard test method as described in ASTM F-316. This method employs a proce-

dure for determining the maximum pore size and the pore size distribution of a membrane filter by measuring the initial bubble point and gas flow versus pressure through a liquid wet filter. The only difference between the 'IPA bubble point method' and ASTM F-316 is that IPA is used as the wetting liquid instead of water.

g. maximum pore size

The maximum pore size can be calculated by substituting the IPA bubble point pressure into the following formula:

$$\text{pore size} = \frac{4.B.\gamma}{p}$$

in which B: pore size morphology constant

γ: surface tension of IPA

p: bubble point pressure

The pore size morphology constant B is 1 for a circular pore and less than 1 for an elliptical or irregular-shaped pore (7). Because most pores are not circular, the use of the terms 'pore diameter' and 'pore radius' is misleading. Unless membranes with circular pores are used, the term **'pore size'** is recommended.

Note: because the 'pore size morphology constant B' is not known in most cases, it is recommended that the 'IPA bubble point pressure' is given next to the value of the maximum pore size.

h. pore size distribution

The pore size distribution can be measured by means of the standard test method as described in ASTM F-316. A short description of this method is given in point 4f.

i. pore size morphology

The pore size morphology is closely related to the calculation of the 'maximum pore size' (point 4g) through the 'pore size morphology constant B'. Therefore, it should be given if the pores are, for instance circular, elliptical or rectangular.

j. temperature stability

The long term stability of a membrane to extreme temperatures should be given here.

k. chemical resistance

The chemical resistance to solvents, acids and bases is important, especially if the membranes have to be cleaned.

5. Process characteristics

The efficiency of a membrane distillation operation can be characterized in many different ways and depends on many different parameters, such as membrane characteristics, module design, hydrodynamic conditions, temperature level, etcetera.

The following parameters are defined to characterize a membrane distillation operation and a membrane distillation process:

    a. evaporation efficiency EE

    b. process efficiency PE

    c. concentration factor CF

    d. temperature polarization coefficient TPC

a. evaporation efficiency EE

This parameter is defined to characterize the efficiency of a membrane distillation operation. The evaporation efficiency EE is defined as:

$$EE = \frac{\text{part of the heat which contributes to evaporation}}{\text{total heat input in the module}}$$

Besides evaporation also a certain heat transfer due to conduction takes place. Therefore, EE is always lower than 1. The value of EE can be calculated very easily. The 'part of the heat which contributes to evaporation' can be calculated by multiplying the measured flux J by the heat of evaporation ΔH_{vap} and the membrane area A. The 'total heat input into the module' can be calculated from a measurement of the caloric value of the incoming and the outgoing feed stream.

b. process efficiency PE

This parameter is used to characterize the efficiency of a membrane distillation process (N.B. this is a process in which the membrane distillation operation is the most important unit operation). The process efficiency PE is defined as:

$$PE = \frac{\text{heat which contributes to the evaporation of the distillate}}{\text{total heat input of the process}}$$

If the process only consists of a membrane distillation operation then the evaporation efficiency EE is equal to the process efficiency PE. In most cases a heat recovery is advantageously. An example of a membrane distillation process with heat recovery is given in figure 3.
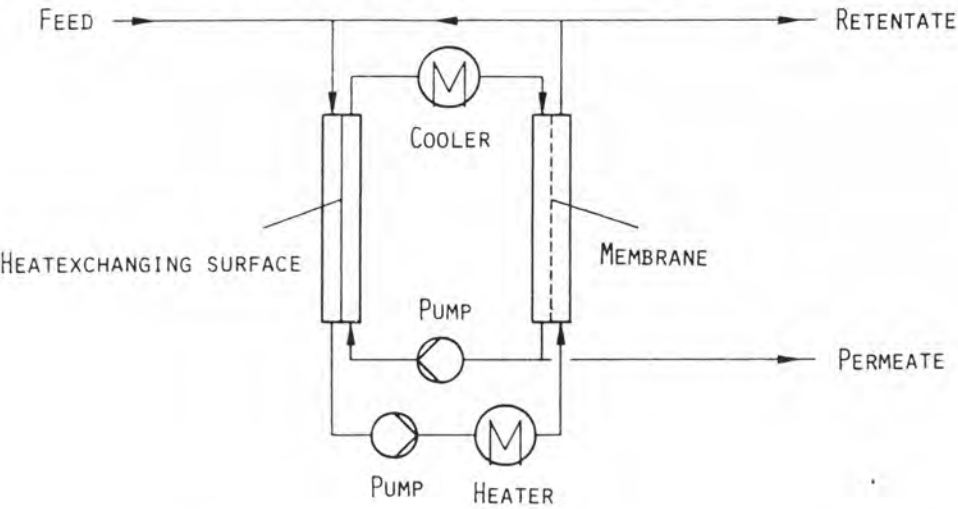
Figure 3: Membrane distillation process with heat recovery

c. concentration factor CF

The concentration factor CF is defined as the degree of increasing the concentration of a component in a membrane operation. CF can be calculated dividing the concentration of the retentate by the concentration of the feed. In formula: $CF = C_r/C_f$. This term is defined in the same way as for pressure driven membrane operations (1).

Due to the low concentration of the solution by one passage of a membrane distillation module, the solution has to be circulated if a concentration of the feed is required (this situation is shown in figure 4).
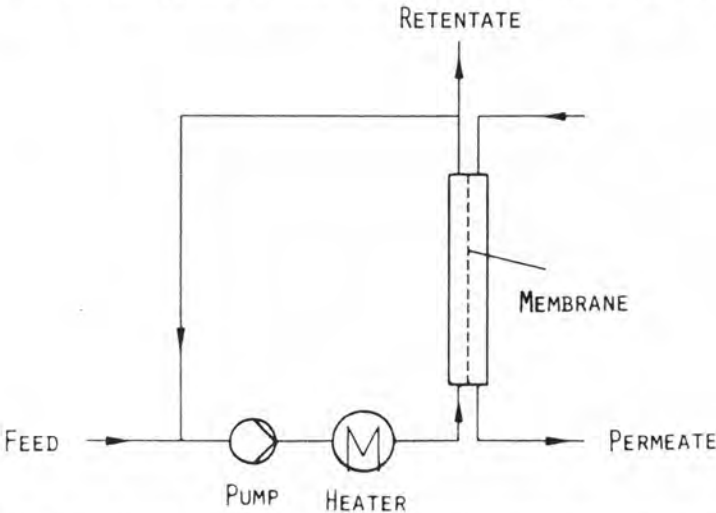
Figure 4: Membrane distillation process with recirculation of the feed

d. temperature polarization coefficient TPC

Another phenomenon which occurs in a membrane distillation operation is 'temperature polarization'. Although this term has several disadvantages (its effect cannot be measured directly and the term itself is physically not correct), it is used very often in scientific literature. The value of TPC is given by the temperature difference between the evaporation surface and the condensation surface divided by the temperature difference between the bulk of the feed and the bulk of the permeate.

For direct contact membrane distillation the evaporation surface is formed by the feed-membrane interface and the condensation surface is formed by the permeate-membrane interface. In formula:

$$\text{TPC} = \frac{T_{fm} - T_{pm}}{T_{fb} - T_{pb}}$$

It must be stated again that the temperatures at the evaporation (respectively condensation) surface cannot be measured directly. In fact they can only be calculated in special cases when the hydrodynamic conditions on both sides of the membrane are known.

6. Definitions

In this chapter a summary is given of the terms that are used in membrane distillation. Whereever this is relevant, the terms are defined in the same way as for pressure driven processes (1).

Bubble point pressure: pressure at which a continuous stream of gas bubbles is pressed through a liquid wet filter.

Bulk temperature T_b: temperature that exists in the bulk phase; in practice this temperature is equal to the measured temperature.

Circulation loop: a section of a membrane plant containing one or more circulation pumps ensuring adequate cross-flow velocity of the fluid over the membrane (an example is given in figure 4).

Concentration factor CF: the degree of increasing the concentration of a
component in a membrane operation; $CF = C_r/C_f$.

Cross-flow velocity u: the velocity of a fluid flowing parallel to the
membrane (also called: tangential velocity).

Direct-contact membrane distillation: see chapter 3b.

Evaporation efficiency EE: see chapter 5a.

Feed: the fluid entering a membrane module or plant.

Flux J: amount of permeate, or of any component in the permeate, that is
transported through a membrane per unit of membrane area and per unit
of time.

Fouling: the deposition of material on the membrane surface and/or in its
pores, leading to a change in the membrane performance.

Gas-gap membrane distillation: see chapter 3b.

Liquid-entry-pressure LEP: pressure at which the liquid penetrates into a
porous membrane (old term to be replaced: 'wetting pressure').

Module: the smallest practical unit containing one or more membranes and
supporting structures (old terms to be replaced: permeator, membrane
element).

Permeate: the portion of the feed passing through the membrane. Distillate
can also be used as a term to describe the 'permeate' of membrane dis-
tillation, but it is better to use 'permeate' because it is commonly
used in membrane literature.

Pore size: openings in a membrane; this term is prefered to 'pore diameter'
and 'pore radius', because all pore shapes can be described by this
term.

Porosity: the porosity is defined as the volume of gas that is trapped inside a membrane divided by the total volume of the membrane; a practical definition is given in the appendix 1: 'Determination of membrane characteristics'.

Process efficiency PE: see chapter 5b.

Retentate: the portion of the feed not passing through the membrane (old term: concentrate).

Retention: the ability of a membrane to hinder a component from passing through it or to retain a component in the fluid.

Retention coefficient R: the degree of separation of a certain component from the solvent by the membrane under defined operating conditions; $R = 1 - C_p/C_r$. This term should be used if a solution of a solute (e.g. salt) in a solvent (e.g. water) is treated by membrane distillation.

Selectivity α: this term is to be defined as:

$$\alpha = \frac{(wt\%\ A\ /\ wt\%\ B)\ in\ permeate}{(wt\%\ A\ /\ wt\%\ B)\ in\ feed}$$

This term should be used as both components in the membrane distillation system are volatile.

Tangential velocity u: see 'cross-flow velocity'.

Temperature polarization coefficient TPC: see chapter 5.

7. Symbols and units

It is very difficult to define symbols in such a way that both author and reader are pleased with it. The discussions between the members of the nomenclature committee concentrated on the point of the symbols. The discussions about the definition of symbols took about 80% of our discussion time, indicating the difficulty of this matter.

To define the symbols the committee has used the following starting-points:

1. the symbols must be logic and clear to both author and reader.
2. the symbols must be in agreement with the existing membrane literature. The report on the terminology for pressure driven membrane operations (1) is used as a basis for the definition of the symbols.
3. the symbols must be in agreement with the literature on heat transfer. The symbols used in the English literature are used as a basis.

The committee realizes that not everyone will be fully satisfied with the way we defined the symbols for membrane distillation. Nevertheless, we hope that the people working in the field of membrane distillation will use these symbols in their publications.

a. Use of symbols

In this document only those symbols are given which are most frequently used in membane distillation literature. The use of these symbols is strongly recommended.

Latin symbols

A	Membrane area	m^2
C	Concentration	kg/m^3
CF	Concentration factor	--
C_p	Heat capacity	J/kg.K
D	Diffusion coefficient	m^2/s
d	Pore Size	m
EE	Evaporation efficiency	--
ΔH_c	Latent heat of condensation	J/kg
ΔH_{vap}	Latent heat of vaporization	J/kg
h	Heat transfer coefficient	W/m^2K
J	Flux	
	mass flux	kg/m^2s
	molar flux	$kmol/m^2s$
	volume flux	m^3/m^2s
	gas flux	Nm^2/m^2s
k	Thermal conductivity	W/m.K
LEP	Liquid Entry Pressure	Pa

l	Thickness of the air gap	m
M	Molecular weight	Dalton
P	Pressure	Pa
PE	Process efficiency	--
Q	Heat transfer rate	W
Q''	Heat flux	W/m^2
R	Retention coefficient	--
R	Universal gas constant	J/mol.K
T	Temperature	K
TPC	Temperature Polarization Coefficient	--
t	Time	s
U	Overall heat transfer coefficient	$W/m^2 K$
u	Cross-flow velocity	m/s
V	Volume	m^3
w	Weight fraction	--
x	Molar fraction	--

Greek symbols

α	Selectivity	--
γ	Surface tension	N/m
Δ	Difference	--
δ	Membrane thickness	μm
ε	Membrane porosity	--
η	Gas viscosity	Pa.s
μ	Liquid viscosity	Pa.s
π	Osmotic pressure	Pa
ρ	Density	kg/m^3
χ	Membrane pore tortuosity	--

Subscripts:

av	Average
b	Bulk
f	Feed
i,j	Index
l	Liquid
m	Membrane

o	Initial, zero
p	Permeate
s	Solute
t	Time
v	Vapour
w	Water

b. use of units

A general rule for the use of units is, that the unit should be as **standard** as possible. This means that in principle SI-units or related units should be used. For instance, the membrane thickness can be given in micrometers instead of meters.

The units which are recommended are given in the 'List of symbols' above.

8. Literature:

1. V. Gekas; 'Terminology for pressure driven membrane processes'.
2. P. Aptel et al.; J. Membr. Sc. 1 (1976) 271.
3. K. Schneider & T.J. van Gassel; Chem. Ing. Tech. 56 (1984) 514.
4. Swedish National Development Company; prospect about membrane distillation.
5. W.L. Gore et al.; European Patent EP 88315.
6. I. Cabasso et al.; J. Appl. Pol. Sc. 18 (1974) 2117.
7. R.A. Cotton et al. in 'Membrane filtration; Application, Techniques and Problems' (editor: B.J. Dutka), page 19-39; Marcel Dekker Inc., New York-Basel.

Appendix 1:

Determination of membrane characteristics

ad 4b. porosity of the membrane:

The porosity of the membrane is defined as the volume of the pores devided by the total volume of the membrane. The porosity can be measured by making use of a pyknometer, a balance, IPA and water. In this method use is made of the fact that IPA (isopropyl alcohol) penetrates into the pores of the membrane and water does not penetrate into the pores of the membrane.

First, the **density of the polymer material** is calculated using the following formula:

$$\rho_{pol} = \frac{\rho_{IPA} \cdot wt3}{wt1 + wt3 - wt2},$$

in which wt1: weight of the pyknometer with IPA

wt2: weight of the pyknometer with IPA and membrane

wt3: dry weight of the membrane.

In the same way the **density of the membrane** can be calculated according to the following formula:

$$\rho_m = \frac{\rho_w \cdot wt3}{wt1 + wt3 - wt2},$$

in which wt1: weight of the pyknometer with water

wt2: weight of the pyknometer with water and membrane

wt3: dry weight of the membrane.

The porosity of the membrane can be calculated by the following formula:

$$\epsilon = 1 - \frac{\rho_m}{\rho_{pol}}.$$

ad 4c. determination of LEP_w:

The following procedure is suggested for the determination of the liquid-entry-pressure of water. The apparatus for this measurement is shown
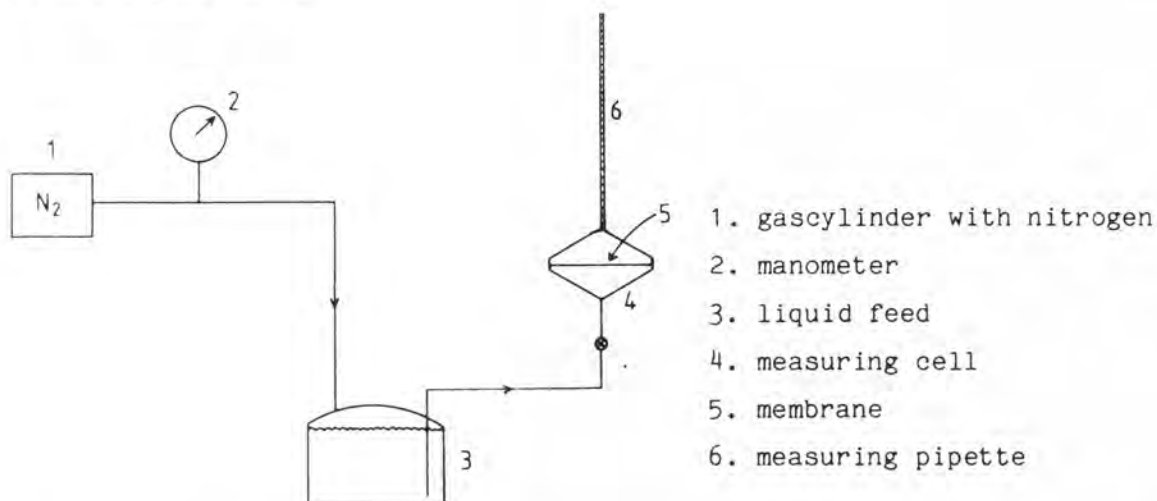
in the figure below.

1. gascylinder with nitrogen
2. manometer
3. liquid feed
4. measuring cell
5. membrane
6. measuring pipette

Figure 5: Apparatus for the determination of the liquid-entry-pressure

Measuring procedure:

The dry hydrophobic membrane 5 is placed into the measuring cell 4 and the reservoir 3 is filled with the liquid feed mixture (in this case water). The half-cell which forms the permeate side of the membrane is also filled water. By means of a gascylinder, filled with nitrogen, a slight pressure is applied to the system in order to remove all the gas at the feed side of the membrane. The pressure which is used to remove the gas should of course be lower than the liquid-entry-pressure. During the de-gasification of the feed a continuous stream of gas bubbles passes through the membrane. As soon as this stream of gas bubbles stops, there is no more gas in the feed compartment. After the de-gasification of the permeate side the measurement can be started.

During the measurement the pressure is raised stepwise (with 0.1 bar). At each installed pressure one should watch whether a flux through the membrane occurs. The minimum pressure at which a (continuous) flux is observed is called 'liquid-entry-pressure'.

APPENDIX C.   COMPUTER MODELLING

At various stages throughout this study, particularly in chapters 7 and 8, computer models were needed to solve the heat and mass transfer equations. A complete description of all models used is not warranted, however details of the approach used are given below. The basic flow diagram for iterative solution of the transport equations is shown in figure C.1.

The 10 equations referred to in the flow diagram are listed below.

$$h_v = J \, \Delta H_v \, / \, (T_{fm} - T_{pm}) \tag{C.1}$$

$$T_{fm} = T_f - (T_f - T_p) \frac{1/h_f}{1/(h_v+h_c) + 1/h_f + 1/h_p} \tag{C.2}$$

$$T_{pm} = T_p + (T_f - T_p) \frac{1/h_p}{1/(h_v+h_c) + 1/h_f + 1/h_p} \tag{C.3}$$

$$P = \exp(23.238 - 3841/(T - 45)) \tag{C.4}$$

$$c_{fm} = c_f \exp(J/\rho_w k_s) \tag{C.5}$$

$$x = \frac{c}{c + \rho_w/M_w (1 - c \, M_s/\rho_s)} \tag{C.6}$$

$$P_f = \gamma \, (1-x_m) \, P_f^\circ \tag{C.7}$$

$$P_a = P_{liq} - (P_f + P_p)/2 \tag{C.8}$$

$$C = \left\{ \frac{1}{C\varphi^b} + \frac{P_a}{d} \right\}^{-1} \tag{C.9}$$
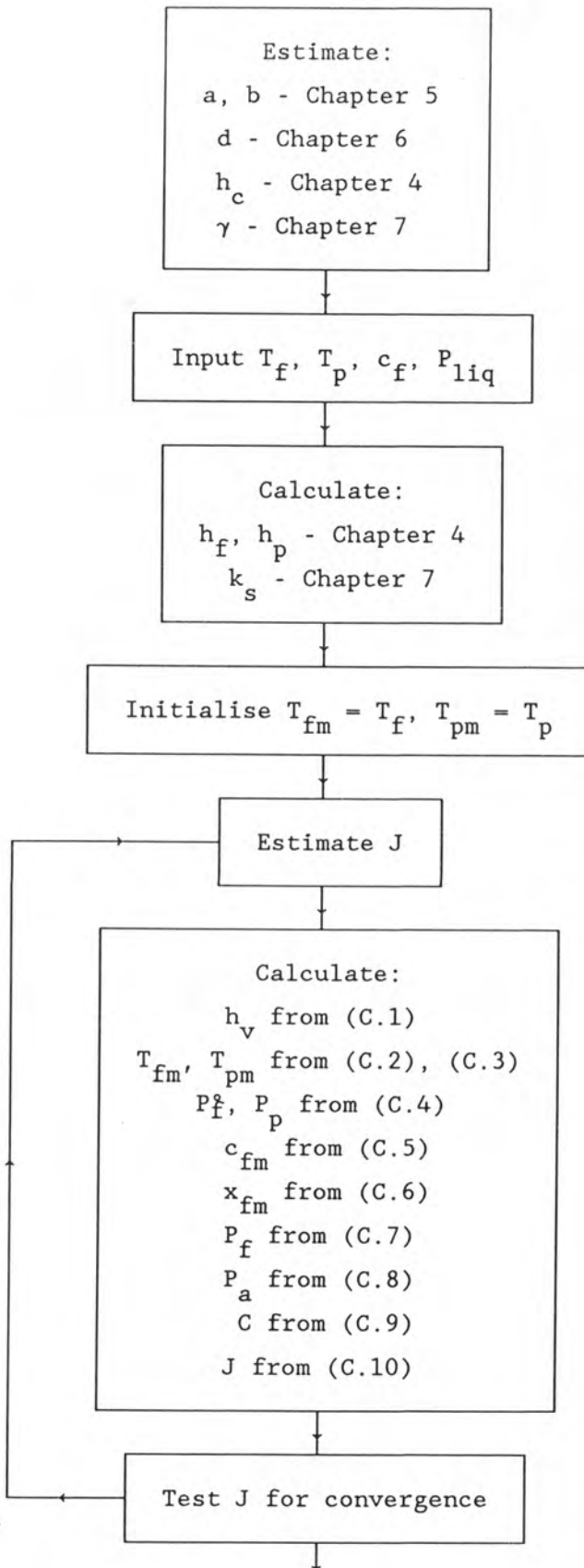
$$J = C \, (P_f - P_p) \tag{C.10}$$

Figure C.1: Flow Diagram for Computer Model

For modelling of module performances (chapter 8), the above flow diagram must be solved incrementally along the length of the module, using mass and energy balances to calculate variations in the flow diagram inputs. For this case, h_f, h_p and k_s will depend on module design, flow dynamics and liquid properties.

In this study, Lotus 1-2-3 spreadsheets were developed for most computer simulations. As an example, the spreadsheet for modelling module II performance in chapter 8 is discussed below, with reference to Outputs 1 and 2.

Output 1 shows the input section of the spreadsheet. While most of the entries are self-explanitory, many require some explanation. These are annotated below. For calculation purposes, the membrane fibres were divided into a number of increments[1]. The membrane conductivity[2], and the feed and permeate film heat transfer coefficients[3,4] were estimated from chapter 4. The membrane mass transfer characteristics, a[5], b[6], and d[7], were estimated using the theory from chapters 5 and 6. The membrane thickness[8], mass flow rate per fibre and fluid velocity[9] were calculated from the appropriate membrane and process inputs. An area correction factor[10] was applied to the membrane permeability to account for the fact that the average area for permeation within the membrane is greater than the inside area, on which all transport equations are based. The activity coefficient[11] for water at the evaporating surface was calculated from the theory of chapter 7. Having set up the spreadsheet for a particular module geometry, the process variables[12] can then be varied to examine the performance. The major process variables are the feed and permeate inlet conditions[12] for temperature, flow rate, pressure and concentration.

Output 1:

Membrane	Inputs:		Calculations:		Stream inlets:[12]	
pore, um	0.2		Increments	20[1]	Tf, C	70
porosity	0.75		a, kg/m2sPa	0.000002[5]	Tp, C	30
i.d., mm	0.3		a*1000	0.0024	Ff, l/min	2
o.d., mm	0.6		b	0.19[6]	Fp, l/min	2
length, m	0.17		d, kg/m2s	0.040666[7]	Pf, kPa	80
number	1100		km/d, W/m2K	333.3333	Pp, kPa	110
km, W/mK	0.05[2]		delta, m	0.00015[8]	Cf, g/l	100
hf, W/m2K	9000[3]		A/fibre	0.000008		
hp, W/m2K	5000[4]		Aav/Ai	1.4[10]		
			m, kg/s/fibre	0.000030	Results:	
Soln. properties:			V, m/s	0.428917[9]	J, kg/m2h	21.4210[13]
Rho, kg/m3	977.12				Tf, out	47.7464[14]
Mu, Pa.s	0.000409		Dimensionless No.s		Tp, out	52.2954[15]
Cp, J/kgK	4184.24		Sc	296.5229	Pf, out	67.0384[16]
k, W/mK	0.66128		Pr	2.593103	Pp, out	93.2942[17]
D, m2/s	0.000000		Re	306.7993	Y	-0.0202[18]
Gamma	0.971[11]				Qloss	0.22054[19]
Hvap, J/kg	2337630		Mass transfer coeff.			
M, kg/mol	0.058		ks	0.008656		
Rho,solute	2370					

Also included in Output 1 is a summary of the major program results. These are the flux[13], the feed and permeate outlet temperatures[14,15] and pressures[16,17], the fractional heat recovery[18] and the fractional heat loss by conduction[19]. Lotus has a built-in facility for generating tables of outputs for various inputs, a sample of which was given in Table 8.4.

Output 2 details the main calculation section of the spread sheet. For each membrane fibre increment, the flow diagram above is solved iteratively (spreadsheet column). This is necessary as the flux[20] is a function of the interfacial temperatures[21,22] and vice versa. A simultaneous iteration along the fibre (across the spreadsheet) ensures that the permeate temperature in the Nth increment matches the permeate input temperature specified in Output 1. This is accomplished by adjusting the permeate temperature in increment 1[23]. The calculated values for the first 7 increments are shown on Output 2(a). The column of calculation headings is defined in Output 2(b), and for illustrative purposes, the Lotus equations for increment 2 are shown in Output 2(c). Typically, the spreadsheet required 10-30 recalculations to converge.

Output 2(a)

N	1	2	3	4	5	6	7
Tfeed	70	68.47664	67.00745	65.58885	64.21757	62.89060	61.60517
Tperm	[23]52.28815	50.76480	49.29561	47.87701	46.50573	45.17876	43.89333
Cfeed	100	100.0222	100.0548	100.0973	100.1494	100.2105	100.2805
T fm	[21]67.38202	65.95111	64.56827	63.23043	61.93478	60.67871	59.45985
T pm	[22]57.00051	55.31075	53.68613	52.12217	50.61476	49.16015	47.75491
Qc	3460.505	3546.786	3627.378	3702.754	3773.339	3839.520	3901.646
C fm	100.1017	100.0970	100.0927	100.0886	100.0848	100.0813	100.0779
x fm	0.031724	0.031722	0.031721	0.031720	0.031718	0.031717	0.031716
VP fo	27847.55	26139.46	24573.90	23135.67	21811.51	20589.79	19460.34
VP f	26182.15	24576.24	23104.35	21752.16	20507.20	19358.56	18296.67
VP p	17341.03	16001.67	14798.13	13713.36	12732.83	11844.11	11036.51
Pfeed	79469.10	78925.03	78367.98	77798.13	77215.63	76620.64	76013.29
Pperm	93289.73	94012.87	94753.59	95511.77	96287.34	97080.23	97890.40
Jprev	0.008600	0.008207	0.007840	0.007497	0.007176	0.006874	0.006591
P a	57707.50	58636.07	59416.74	60065.37	60595.61	61019.30	61346.70
C	0.000000	0.000000	0.000000	0.000000	0.000000	0.000000	0.000000
J	[20]0.008603	0.008209	0.007842	0.007499	0.007177	0.006876	0.006593
Qv	20647.32	19703.79	18822.55	17998.38	17226.59	16502.97	15823.69
J,kg/m2h	30.97098	29.55569	28.23382	26.99757	25.83989	24.75446	23.73554
x feed	0.031691	0.031691	0.031691	0.031691	0.031691	0.031691	0.031691
Wt% feed	9.539910	9.539910	9.539910	9.539910	9.539910	9.539910	9.539910
Mu,f	0.000409	0.000419	0.000430	0.000439	0.000449	0.000459	0.000468
Mu,p	0.000544	0.000558	0.000571	0.000585	0.000598	0.000612	0.000625
dP,f	530.8995	544.0706	557.0539	569.8632	582.5113	595.0105	607.3725
dP,p	705.5315	723.2306	740.8109	758.2903	775.6860	793.0151	810.2940

Output 2(b)

N	Increment
Tfeed	Feed temperature
Tperm	Permeate temperature
Cfeed	Feed concentration
T fm	Feed temperature at membrane interface
T pm	Permeate temperature at membrane interface
Qc	Heat transfer by conduction
C fm	Feed concentration at membrane interface
x fm	Mole fraction of solute at interface
VP fo	Vapour pressure of water at evaporating surface
VP f	Vapour pressure of solution at evaporating surface
VP p	Vapour pressure of water at condensing surface
Pfeed	Pressure of feed stream
Pperm	Pressure of permeate stream
Jprev	Flux calculation during previous iteration (for feedback)
P a	Air pressure within membrane
C	Membrane mass transfer coefficient
J	Flux, $kg/m^2 s$
Qv	Heat transfer by evaporation
J,kg/m2h	Flux in conventional units
x feed	Mole fraction solute in feed
Wt% feed	Feed concentration
Mu,f	Feed viscosity
Mu,p	Permeate viscosity
dP,f	Feed incremental pressure drop
dP,p	Permeate incremental pressure drop

Output 2(c)

N	2
Tfeed	@IF($Q$2=0,+$P$2-(A1-1)*($P$2-$P$3-$Q$4)/$M$2,+S2-(S19+S7)*$M
Tperm	@IF($Q$2=0,A2-$Q$4,+S3-(S19+S7)*$M$9/$M$11/$J$15)
Cfeed	+S4*(1+@SUM($S$18..A18)*$M$9/$M$11/$M$2)
T fm	@IF($Q$2=0,+A2-$Q$4/2+$Q$5/2,+A2-((0.5*A15+A18)/1.5*$J$19+A7)
T pm	@IF($Q$2=0,+A3+$Q$4/2-$Q$5/2,+A3+((0.5*A15+A18)/1.5*$J$19+A7)
Qc	@ABS($M$7*(A5-A6))
C fm	@IF(A4=0,0.1,@EXP(A18/$M$20/$J$13)*A4)
x fm	1/(1+55*$J$20*1000*(1/A8-1/$J$21))
VP fo	@EXP(23.238-3841/(A5+228))
VP f	+A10*(1-A9)*$J$18
VP p	@EXP(23.238-3841/(A6+228))
Pfeed	+S13-A25
Pperm	+S14+A26
Jprev	+A18
P a	@IF(A13>A14,A14-(A11+A12)/2,A13-(A11+A12)/2)
C	1/(1/$M$3/((A11+A12)/50000)^$M$5+A16/$M$6)*$M$10
J	@IF(A17*(A11-A12)>0,A17*(A11-A12),0)
Qv	+A18*2400000
J,kg/m2h	+A18*3600
x feed	1/(1+55*$J$20*1000*(1/A4-1/$J$21))
Wt% feed	1/(18/58*(1/A21-1)+1)*100
Mu,f	(23.73-10.64*@LOG(A2))*0.0001
Mu,p	(23.73-10.64*@LOG(A3))*0.0001
dP,f	+$P$4/60000*8*A23*$J$6/$M$2/3.142/($J$4/2000)^4/$J$7
dP,p	+$P$5/60000*8*A24*$J$6/$M$2/3.142/($J$4/2000)^4/$J$7